Lancaster University

Developing an Environmentally Friendly Diagnostic System for the Detection of Respiratory Diseases

by

Hejan Bozkurt

Biomedical and Life Sciences Department

Faculty of Health and Medicine

Under supervision of

Prof. Muhammad Munir

Dr. Leonie Unterholzner

This dissertation is submitted for the degree of
Doctor of Philosophy

Graduate College

November 2024

Dedication

To my mother, for always reminding me to eat, sleep, and believe in myself – even when I was too stubborn to listen. Your love, support, and encouragement have been the foundation of all my accomplishments. This is for you, with all my love and gratitude…

Declaration of Originality

I declare that this thesis entitled “Developing an Environmentally Friendly Diagnostic System for the Detection of Respiratory Diseases” is my own work and that, to the best of my knowledge and belief, it contains no material previously published or written by another person nor material which to a substantial extent has been accepted for the award of any other degree or diploma at any university or equivalent institution. Where applicable, any part of this thesis containing materials prepared jointly with other has been explicitly identified. Any views expressed in this thesis are those of the author and do not necessarily reflect the views of Lancaster University or any other institution.

Hejan Bozkurt

30 November 2024

List of Contents

List of Tables

List of Figures

List of Abbreviations

ACE2: angiotensin-converting enzyme 2

AdV: adenovirus

AOM: acute otitis media

AP: alkaline phosphatase

APC: antigen-presenting cell

ARDS: acute respiratory distress syndrome

ATP: adenosine triphosphate

AuNPs: gold nanoparticles

B3: backward outer primer

BHQ1: Black Hole Quencher 1

BIP: backward inner primer

BL: backward loop primer

bp: base pair

Bst: *Bacillus stearothermophilus*

CAP**:** community-acquired pneumonia

Cas: CRISPR-associated (genes)

cDNA: complementary DNA

CNS: central nervous system

COPD: chronic obstructive pulmonary disease

COVID-19: Coronavirus Disease 2019

CPE: cytopathic effects

CRISPR: Clustered Regularly Interspaced Short Palindromic Repeats

crRNA: CRISPR RNA

Ct: cycle threshold

DETECTR: DNA Endonuclease-targeted CRISPR Trans Reporter

DIG: digoxigenin

DNA: deoxyribonucleic acid

dNTP: deoxynucleotide triphosphate(s)

DSB: double-stranded break

DTT: dithiothreitol

E. coli: *Escherichia coli*

ELISA: enzyme-linked immunosorbent assay

EMIT: enzyme multiplied immunoassay technique

F3: forward outer primer

FAM: fluorescein amidites

FDA: Food and Drug Administration

FIP: forward inner primer

FITC: fluorescein isothiocyanate

FL: forward loop primer

GFP: green fluorescent protein

GI: gastrointestinal

HA: haemagglutinin

HBoV: human bocavirus

HCl: hydrochloric acid

HDR: homology-directed repair

HIA: haemagglutinin inhibition assay

HIV: human immunodeficiency virus

hMPV: human metapneumovirus

HPIV: human parainfluenza virus

HPV: human papillomavirus

HRP: horseradish peroxidase

HRV: human rhinovirus

HSV/VZ: herpes simplex virus/varicella-zoster

ICU: intensive care unit

IFN-γ: interferon-gamma

IgA: immunoglobulin A

IgG: immunoglobulin G

IgM: immunoglobulin M

IL-10: interleukin-10

IL-13: interleukin-13

IL-2: interleukin-2

IL-4: interleukin-4

IL-6: interleukin-6

ISH: in-situ hybridisation

LAMP: loop-mediated isothermal amplification

LB: lysogeny broth

LFD: lateral flow dipstick

LRI: lower respiratory tract infection

MEM: minimal essential medium

MERS-CoV: Middle East Respiratory Coronavirus

MgOAc: magnesium acetate

MHC: major histocompatibility complex

miRNA: microRNA

mRNA: messenger RNA

MRSA: methicillin-resistant *Staphylococcus aureus*

NA: neuraminidase

NALC: N-acetyl-L-cysteine

NHC: β-D-*N*4-hydroxycytidine

NHEJ: non-homologous end joining

NP: nasopharyngeal

NP: nucleoprotein

OP: oropharyngeal

ORF: open reading frame

PAM: protospacer adjacent motif

PBS: phosphate-buffered saline

PCR: polymerase chain reaction

PK: proteinase K

POCT: point-of-care testing

PRR: pattern recognition receptor

QD: quantum dot

RBC: red blood cell

RBD: receptor-binding domain

RCA: rolling-circle amplification

RDE: receptor-destroying enzyme

RdRP: RNA-dependent RNA polymerase

RNA: ribonucleic acid

RNase: ribonuclease

RNP: Cas9 ribonucleoprotein

RPA: recombinase polymerase amplification

RSV: respiratory syncytial virus

RT: reverse transcription/reverse transcriptase

SARS-CoV-2: Severe Acute Respiratory Syndrome Coronavirus 2

SEM: scanning electron microscopy

SERS: Surface Enhanced Raman Spectroscopy

sgRNA: single-guide RNA

SHERLOCK: Specific High Sensitivity Enzymatic Reporter Unlocking

SNP: single nucleotide polymorphism

SOC: super optimal broth with catabolite repression

SpCas9: *Streptococcus pyogenes* Cas9

SSB: single-stranded DNA binding protein

STI: sexually transmitted infection

Taq: *Thermus aquaticus*

TEM: transmission electron microscopy

Th1: T helper 1 cells

Th17: T helper 17 cells

Th2: T helper 2 cells

THF: tetrahydrofuran

TMB: 3,3',5,5'-tetramethlybenzidine

TMPRSS2: transmembrane serine protease

TNF-α: tumour necrosis factor alpha

tracrRNA: trans-activating CRISPR RNA

Tt: time-to-threshold

URI: upper respiratory tract infection

UTR: untranslated region

WBC: white blood cell

X-gal: 5-bromo-4-chloro-3-indolyl-β-d-galactopyranoside

Acknowledgements

Firstly, I would like to express my deepest appreciation to my supervisor, Prof. Muhammad Munir, for his unlimited guidance, support, and encouragement, which allowed me to keep going when things started getting more difficult during my PhD, helping me to finish this project smoothly.

I am also profoundly thankful to my secondary supervisor, Dr. Leonie Unterholzner, for her guidance and constructive feedback on my written work, which helped me improve my thesis writing skills.

I would also like to thank Dr. Mohammed Rohaim from Munir's Laboratory of Molecular Virology for his incredible knowledge, support, and technical help since the beginning of this project.

I am also thankful to the staff members and fellow PhD students of the BLS department for their constant assistance and friendship, which greatly contributed to the success of this research.

The most special thank you to my parents for their endless love and support during my PhD and my entire life. I have always been proud to be your daughter. To my maternal grandparents, your love and encouragement have always lifted me. I feel incredibly fortunate to be your granddaughter. To my one and only brother, thank you for always cheering me up when I needed motivation.

Lastly, to my loving partner, your constant support, patience, and understanding have been my anchor through the thick and thin of this journey. I could not have done this without you.

Thesis Abstract

Respiratory viruses are the most common infectious cause of morbidity and mortality in humans worldwide. Considering the events of the recent Coronavirus Disease 2019 (COVID-19) pandemic, there is an urgent need for rapid and accurate diagnostic methods to allow early disease detection and subsequent treatment. Although current gold standard testing methods, such as reverse transcription-quantitative polymerase chain reaction (RT-qPCR), are mainly accurate, they are limited by high costs, complex instrumentation, and slow turnaround times, particularly in low-resource settings. This thesis hypothesises that reverse transcription-recombinase polymerase amplification (RT-RPA), an isothermal amplification method, can offer a cost-effective, environmentally friendly alternative for detecting respiratory viruses with comparable diagnostic performance to RT-qPCR.

In order to evaluate this hypothesis, RT-RPA was developed and tested to detect SARS-CoV-2 and other respiratory viruses. Assay performance was compared with RT-qPCR and reverse transcription-loop-mediated isothermal amplification (RT-LAMP) across 140 clinical samples. RT-RPA demonstrated high sensitivity and specificity, particularly with fluorescence-based detection, though lateral flow detection (LFD) offered better portability. TOPO TA cloning and in vitro transcription were used to generate and validate synthetic viral RNA for assay development. Further evaluations showed that RT-RPA achieved faster detection times and comparable or superior sensitivity for multiple viral targets, including cases where RT-PCR failed to detect low viral loads. Despite a small number of false positives, particularly for respiratory syncytial virus B (RSV-B), RT-RPA maintained its strong diagnostic accuracy. Overall, this work supports using RT-RPA as a robust alternative to RT-qPCR, especially for point-of-care testing (POTC) in low-resource settings, highlighting its potential for broad application in respiratory virus diagnostics.

Chapter 1: General Introduction

1.1. Importance of Respiratory Viruses and Global Burden

Infections of the respiratory tract can be grouped based on their symptomatology and anatomic involvement, such as upper and lower respiratory infections (LRIs). Most upper respiratory infections (URIs) are caused by viral pathogens, although there are some cases involving bacteria (Dasaraju and Liu, 2014). Rhinovirus is the leading viral pathogen in URIs, causing a peak of common cold cases in the fall months. Other viruses include influenza virus, adenovirus (AdV), enterovirus, and respiratory syncytial virus (RSV) (Thomas and Bomar, 2022). Pathogens enter the respiratory tract by inhalation of infected droplets to invade the mucosa. Depending on the invading pathogen, they can cause epithelial destruction or loss of ciliary activity. Most URIs are benign, and severe complications are not very common. Influenza virus is an exception, which may lead to pneumonia, meningitis, sepsis, and bronchitis. Typical symptoms of URIs include cough, sore throat, runny nose, nasal congestion, headache, fever, and body aches. These symptoms usually start around 1 to 3 days after exposure and last 7 to 10 days, which can persist up to 3 weeks. Adults have 2 to 3 common cold cases, meanwhile children have up to 8 common cold cases per annum (Simasek and Blandino, 2007). URIs caused more than 20 million missed days of school and more than 20 million days of work lost worldwide, leading to a significant economic and social burden (Adams et al., 1999).

Patients may develop secondary URIs after catching common cold, such as sinusitis, pharyngitis, croup or laryngitis, and otitis media. Sinusitis is caused by the inflammation of one or more paranasal sinuses. Inflammation can be a result of either viral or bacterial infection, which impairs the ciliary activity of the epithelial lining of the sinuses. Bacterial sinusitis typically occurs after a viral URI. Bacteria can be introduced into the sinuses by coughing and nose blowing. Due to mucus hypersecretion caused by ciliary immobility, paranasal sinuses get blocked, preventing drainage and allowing secondary bacterial overgrowth. The mucus may be converted to

mucopurulent discharge upon bacterial multiplication in the sinus cavities. The pus starts irritating the mucosal lining to cause more oedema, epithelial destruction, and nasal obstruction. Therefore, the patients may experience pain, pressure, and tenderness over the area of the affected sinuses. Almost 90% of people with the common cold also experience sinusitis and its symptoms (Battisti et al., 2024). It is most common in children younger than 15 and adults aged 25 to 64 (Lemiengre et al., 2018). Even though complications associated with sinusitis are not very common, they can be severe in some cases, causing significant morbidity and mortality. Intracranial complications of sinusitis, such as focal collections (abscesses and empyemas), meningitis, encephalitis, and dural sinus thrombophlebitis, caused hospitalisation in 0.5% to 24% of patients (Clayman et al., 2021) with a 3% incidence in paediatric admissions (Lerner et al., 2021).

Pharyngitis is caused by the inflammation of the pharynx along with lymphoid tissues of the posterior pharynx and lateral pharyngeal bands. Inflammation can result from either viral or bacterial infection, where more severe cases are likely to be bacterial and may develop after a viral URI (Frost et al., 2018). Around 50% to 80% of pharyngitis cases are caused by a viral infection only, with rhinovirus being the most common pathogen, followed by AdVs, influenza viruses, coronaviruses, and parainfluenza viruses. These viruses enter the mucosal cells of the nasopharynx and oral cavity, causing inflammation, oedema, and hyperaemia of the mucous membranes and tonsils. This results in symptoms like sore throat, fever, body aches and difficulty in swallowing. Children with viral pharyngitis can also exhibit some other symptoms like mouth-breathing, vomiting, abdominal pain, and diarrhoea (Rotbart, 1998; Middleton, 1996).

Croup is inflammation and swelling of the throat, larynx, and large airways of the lungs. When children younger than 5 years old have this infection, it is known as croup. Meanwhile, the same infection is known as laryngitis in older children. Croup is one of the most common respiratory infections among young children. It affects around 5% of children during the second year of life (Cherry, 2008). Even though children between the ages of 6 months and 3 are the ones affected by croup the most, some cases are recorded in children as young as 3 months old. It rarely affects adults and elderly people

(Björnson and Johnson, 2008). Parainfluenza type 1 is the most common type of virus that causes croup (Hall and Hall, 2017; Segal et al., 2005; Marx et al., 1997). According to a study, parainfluenza virus type 1 causes approximately 40% of the cases, followed by parainfluenza virus types 2 and 3 (Rihkanen et al., 2008). Influenza A and B, as well as RSV, can also be the causative virus in rare cases (Hall and Hall, 2017). Human metapneumovirus (hMPV), AdV, and coronavirus may also cause some of the cases. Acute laryngitis was the primary diagnosis in hospitalised children aged 1 month to 14 with respiratory symptoms (Ji et al., 2009). Bacteria rarely cause acute laryngitis or can cause bacterial superinfection after an initial viral infection (Kivekäs and Rautiainen, 2018). Almost all cases of croup and acute laryngitis are caused by viruses. The most common symptoms of the disease include hoarseness due to inflammation of vocal cords, followed by possible aphonia and sore throat. Fever, swollen lymph nodes, and tender cervical lymphadenopathy may sometimes occur. Inflammatory oedema and mucus production may narrow the airways in the subglottic area, leading to airway obstruction, which can be fatal if left untreated.

Acute otitis media (AOM) is an infection of the middle ear which can be viral, bacterial, or both. The most common viral pathogens of AOM include RSV, coronavirus, influenza virus, AdV, hMPV, and human bocavirus (HBoV) (Ubukata et al., 2018; Ubukata et al., 2019; Protasova et al., 2017; Chonmaitree et al., 2008). AOM is the second most common diagnosis among children in the emergency department (Meherali et al., 2019) and the most common reason for prescribing antimicrobial drugs (Worral, 2008). It is more common in children than adults, and almost 80% of all children will experience this infection during their lifetime (Usonis et al., 2016; Schilder et al., 2016). It starts with inflammation triggered by a viral URI affecting the nose, nasopharynx, middle ear mucosa, and Eustachian tubes. Inflammation causes swelling in the narrowest part of Eustachian tubes, reducing ventilation. This generates negative pressure in the middle ear, resulting in a leakage from inflamed mucosa and accumulation of secretions. Other symptoms of AOM include earache, hearing loss, ear popping, ear fullness, dizziness, and fever.

Causative agents of LRIs can be either viral or bacterial pathogens. Viral pathogens are mainly responsible for bronchitis and bronchiolitis in adults and children. The most

common viruses that cause bronchitis include influenza viruses, rhinoviruses, AdVs, and human parainfluenza viruses (HPIVs) (Worrall, 2008). The pathogen enters the distal airway when inhaled or aspired. It starts multiplying in the epithelium to cause inflammation, leading to mucus hypersecretion and sometimes impaired lung function. Bronchiolitis mainly occurs in children less than a year old, followed by a decline during their second and third years. The symptoms of bronchiolitis include fever, rapid breathing, lower chest wall indrawing, and wheezing (Cherian et al., 1990). In severe bronchiolitis, inflammation and necrosis of the epithelium may block small airways, causing airway obstruction. RSV is the leading cause of bronchiolitis worldwide, which is known to cause up to 70% to 80% of lower respiratory cases through peak season, followed by parainfluenza virus type 1 and influenza virus causing some of the cases (Simoes, 1999; Stensballe et al., 2003).

Respiratory viruses are also known to cause chronic obstructive pulmonary disease (COPD), which affects 10% of the global population and is the third main cause of mortality worldwide (Barnes, 2007). According to a study, respiratory viral infections cause 50% of COPD acute exacerbations (Linden et al., 2019). Co-infection with a bacterial pathogen has been identified in 25% of the cases, which is often more severe (Sykes et al., 2007). In patients with COPD, host innate immunity is dysregulated against viral infections (Singanayagam et al., 2012). Increased numbers of natural killer T cells activate IL-13-producing macrophages in the lungs, causing airway inflammation (Holtzman et al., 2009). If this inflammation persists, alveolar destruction leads to reduced lung elasticity, chronic bronchitis, mucus hypersecretion and airflow obstruction (Hogg et al., 2004; Kim and Criner, 2013). Severe virus-associated exacerbations also promote increased levels of cytotoxic T cells, neutrophils, eosinophils, TNF-α and IL-6 in the sputum of COPD patients (Frickmann et al., 2012; Allie et al., 2017). Smoking is a significant contributing factor in COPD; the viruses cause more severe disease exacerbation due to weaker host immune response, faster loss of lung function and increased symptomatology in smoking COPD patients. Rhinovirus, influenza virus, RSV, parainfluenza virus, and seasonal coronavirus are the most frequently detected viruses in COPD, which may lead to epithelial barrier destruction, microvascular dilatation, oedema, and immune cell infiltration (Aghapour et al., 2018; Allie et al., 2017).

Community-acquired pneumonia (CAP) is a lung disease that causes the patient to get infected in a community setting. It is the second most common cause of hospitalisation and the most common infectious cause of mortality worldwide (Xu et al., 2016). Although the influenza virus is the major viral cause of CAP, other respiratory viruses like RSV, parainfluenza virus, and AdV can also cause the disease (Jain et al., 2015). Viral pathogens typically colonise the nasopharynx and then enter the lower respiratory tract of the patient, known as micro-aspiration. Invading viruses can trigger the host's pulmonary defence. If this defence can be avoided by a high number of viruses that can spread through the bloodstream or macro-aspiration, pneumonia will occur. Common symptoms of pneumonia include fever, dyspnea, chest pain, and weight loss. Pneumonia is the eighth major cause of mortality worldwide and the main cause of mortality among infectious diseases. The mortality rate can be as high as 23% for hospitalised patients requiring intensive care for severe pneumonia (Regunath and Oba, 2023).

Respiratory virus infections are known to cause severe illnesses that can further lead to acute respiratory failure, which can progress rapidly to acute respiratory distress syndrome (ARDS). ARDS is associated with severe damage to the lungs, often caused by sepsis, pneumonia, trauma, and pancreatitis. According to a study, approximately one-third of the hospitalised COVID-19 patients developed ARDS and nearly three-quarters of hospitalised COVID-19 patients already had ARDS (Tzotzos et al., 2020). A capillary membrane surrounding the alveoli starts leaking through the damaged walls of the alveolar sac and builds up, causing pulmonary oedema. Oedema impairs gas exchange with the capillaries in the lungs, preventing enough oxygen from being released into the bloodstream. This means less oxygen reaches the organs, causing hypoxia and even multiple organ failure in some cases. Elderly individuals or those with chronic conditions like obesity, diabetes mellitus, or respiratory or cardiovascular disease have a higher risk of infection. It is also common among COVID-19 patients to develop ARDS that is caused by pneumonia (Wu et al., 2020). ARDS in COVID-19 patients is associated with symptoms like fever, shortness of breath, chest pain, high blood pressure and cyanosis (Ghelichkhani and Esmaeili, 2020; Henry and Lippi, 2020). COVID-19 patients with ARDS may have high lung compliance, which is not the case in patients with classic ARDS (Li and Ma, 2020). This increases the possibility and duration of mechanical ventilation in COVID-19 patients with ARDS

(Bain et al., 2021).

1.2. Control Strategies

Respiratory viruses are commonly known to cause only milder diseases, even though they have the potential to cause epidemics in some cases. Around 10% to 15% of the world population is infected by influenza yearly (Jefferson et al., 2011). The attack rate caused by influenza can be as high as 50% during major epidemics. Around 8000 people contracted SARS-CoV, and 780 of them passed away during the 2003 SARS epidemic, causing a social and economic crisis (Bell and WHO Working Group, 2004). Epidemics can spread rapidly among closed populations, such as hospitals, nurseries, long-term care facilities, job training centres, boarding schools, dormitories, orphanages, and public swimming pools. In addition to COVID-19 pandemic caused by SARS-CoV-2, new avian H5N1 and H1N1 swine Influenza led to global anxiety due to the possibility of a pandemic in 2006 and 2009, respectively (WHO, 2010). When animal viruses mix genetically to produce a novel human virus through the process of antigenic shift, the potential of a new pandemic arises. The antigenic shift involves genetic assortment or mixing of genome segments from human, swine, and avian influenza viruses. For instance, this process often happens in domestic pigs in Southeast Asia, where animals and humans live in proximity (Webster, 2004; Bush, 2005; Greenfeld, 2006).

1.2.1. Preventative Measures

Even though the availability of antiviral drugs and vaccinations helps to interrupt the spread of respiratory viruses, the effectiveness of additional physical barriers should be addressed in reducing the spread of these viruses. Specific control measures must be applied in person to standard procedures to eliminate the transmission of viral respiratory infections. Indoor air quality can be improved by limiting crowds in communal spaces, using proper ventilation systems, and encouraging people with respiratory symptoms to sit away from other patients. Face masks should always be

available in hospitals and clinics to allow some protection from people with respiratory symptoms. People with chronic conditions have a higher risk of infection, so they must always wear the most protective mask or respirator. Encouraging hand hygiene by providing conveniently located sinks for hand washing along with their supplies (e.g. soap, disposable towels) and hand dispensers filled with alcohol-based hand sanitisers is necessary to reduce respiratory infections. If a patient is known to have an existing respiratory infection or is suspected to have one, they must be kept in a separate room until diagnosis. Selection of the diagnostic test depends on the suspected cause of the infection, such as the most prevalent respiratory viruses circulating in the community at that time. Healthcare personnel and hospital visitors must clean their hands after having contact with respiratory secretions. If a patient's test result is positive, they must be advised to quarantine until the symptoms disappear. In the case of positive asymptomatic patients, they still need to quarantine for a minimum of 7 to 10 days.

1.2.2. Antiviral Medications

A few antiviral drugs are currently approved for treating viral respiratory infections, mainly targeting influenza viruses. Amantadine and rimantadine are M2 inhibitors that interrupt the replication of Influenza A by blocking the viral M2 protein ion channel involved in host cell entrance (Bukrinskaya et al., 1982; Hay et al., 1985). Unfortunately, there is a risk of resistance upon using these drugs for various Influenza A strains, so they are not recommended very often for treating Influenza A infections (Fiore et al., 2011). Neuraminidase (NA) inhibitors can be used to treat Influenza A and B, which have a surface glycoprotein with NA activity. Viral NAs are necessary for influenza reproduction and facilitating viral budding from the host cell. NA inhibitors mimic sialic acid, which is required for the virus to invade host cells, block the active site of NA, and leave uncut sialic acid residues on the surface of host cells and influenza viral envelopes. Viral haemagglutinin (HA) binds to the uncut sialic acid residues, resulting in aggregation of the viruses at the host cell surface. This reduces the amount of progeny viruses released from infected cells, meaning they can no longer infect other host cells to cause further infection in the respiratory tract (Palese and Compans, 1976).

Laninamivir, Oseltamivir, Peramivir, Zanamivir and Ribavirin are typical examples of NA inhibitors that can be used to treat both Influenza A and B viruses. Replication of influenza virus in the respiratory tract peaks between 24 and 72 hours after disease onset; therefore, NA inhibitors are only effective during the viral replication stage and must be administered as early as possible.

There are two types of medication that can be used to treat COVID-19 patients in emergency cases. These are called Paxlovid (nirmatrelvir/ritonavir) and Lagevrio (malnupiravir), which are used for the treatment of mild to moderate COVID-19 (Hammond et al., 2022). Nirmatrelvir/ritonavir is a combination of two medications with distinct mechanisms of action. Nirmatrelvir is a peptidomimetic inhibitor of Mpro, which is the main protease of SARS-CoV-2. If Mpro is inhibited, the virus cannot process the polyprotein precursors required for viral replication. Ritonavir is a human immunodeficiency virus-1 (HIV-1) protease which can also inactivate human cytochrome CYP3A, the main human drug-metabolising enzyme. Considering that nirmatrelvir is also a human cytochrome CYP3A4 substrate, the metabolism of nirmatrelvir will be inhibited by ritonavir, resulting in an increased plasma concentration of nirmatrelvir so that nirmatrelvir can work better (Lam and Patel, 2022). This feature allows ritonavir to be used as a boosting agent for drugs with low oral bioavailability. Combining these medications is also significant in fighting against the major variants of SARS-CoV-2, including Omicron variants (Fishbane et al., 2022). However, there is a risk of resistance to using Paxlovid, which might be due to a possible escape mechanism (Lee et al., 2022).

Malnupiravir is a prodrug of β-D-*N*4-hydroxycytidine (NHC), a ribonucleoside with an antiviral activity against the SARS-CoV-2. It works by disrupting the normal function of the RNA-dependent RNA polymerase (RdRP) enzyme involved in viral replication. This causes the RdRP enzyme to make mistakes during viral genome replication. These mistakes affect the transcription of viral RNA into a complementary DNA (cDNA) template, followed by its translation into a functional protein. This reduces the ability of SARS-CoV-2 to replicate and cause a disease. However, according to a recent study, using Lagevrio might introduce some random genetic mutations in the virus that either cause further inhibition of the viral replication or the generation of dangerous new

variants (Focosi, 2022). Regardless, both Paxlovid and Lagevrio seemed to reduce the risk of hospitalisation, as well as mortality in non-hospitalised, unvaccinated adults with mild to moderate COVID-19 (Hammond et al., 2022; Bernal et al., 2022).

1.2.3. Vaccines Against Respiratory Viruses

Currently, there are three types of influenza vaccines used worldwide: inactivated influenza, live attenuated influenza, and recombinant HA vaccine (Nuwarda et al., 2021). Inactivated influenza vaccines kill the influenza virus or some parts of it. The virus is typically grown in embryonated chicken eggs or cultured cells of mammalian origin. Inactivation can be done by using chemical compounds (e.g. formaldehyde or β- propiolactone) or physical factors (e.g. heat or UV radiation) to destroy the viral genetic material (Kovpak et al., 2022). Therefore, inactivated viruses can no longer multiply; however, they maintain their integrity to be recognised by the host immune system to activate an adaptive immune response. The antigen present in the vaccine is taken up by an antigen-presenting cell (APC) and sent to a draining lymph node upon vaccination. The APC displays the antigen on its surface along with a major histocompatibility complex (MHC) molecule so that it can interact and activate T cells. Helper T cells then induce an antibody-mediated or cell-mediated immune response, developing antigen- specific adaptive response (Pollard and Bijker, 2021; Karch and Burkhard, 2016). This creates an immunological memory against the virus if the individual gets infected by the same virus so the immune system can respond quicker and more effectively (Vetter et al., 2018). Inactivated vaccines are more stable and safer than live attenuated vaccines, which also makes them more durable during transportation and storage (Pollard and Bijker, 2021; Clem, 2022). Additionally, inactivated vaccines cannot become virulent and cause disease, so they are safe for immunocompromised and pregnant individuals (Vetter et al., 2018; Plotkin et al., 2018). Unfortunately, inactivated viruses cannot trigger an immune response as strong as regular viruses. Therefore, multiple booster injections are required for an effective immune response (Hoft et al., 2017).

Live attenuated influenza vaccines use a weakened form of the virus to mimic natural infection without causing disease. Attenuated vaccines can be produced by introducing genetic mutations, like gene deletions or substitutions, to the virus so they become less

virulent in the host (Siegrist, 2024). Once it is administered nasally with one spray per nostril, the attenuated virus starts replicating in the mucosa to induce mucosal IgA antibodies, which protect the site of viral entry against the infection (Clements and Murphy, 1986; Wrammert et al., 2008; Mohn et al., 2016). Attenuated viruses cannot multiply sufficiently, so they are typically not infectious. However, they can still activate an immune response that is strong enough to protect against the infection until the immune system eliminates the virus. They can create a strong and long-lasting immune response by inducing killer cytotoxic T cells, helper T cells and antibody-producing B cells. Because these viruses are still somewhat active, a secondary mutation may cause the attenuated virus to become virulent in some cases. This may cause disease, especially in immunocompromised individuals.

Recombinant HA vaccines are produced by genetic engineering to introduce a small piece of the HA antigen into the body. This antigen is incorporated into a harmless carrier, such as a plasmid or a viral vector, which is taken up by the host cells. These vaccines work very similarly to the inactivated vaccines in fighting an infection. However, recombinant HA vaccine is less immunogenic, requiring three times more HA than inactivated vaccines to produce a similar number of antibodies (Cox et al., 2008). Because these vaccines do not involve the use of any eggs, they are a suitable option for people with egg allergies. There is also no risk of mutations from egg adaptation, unlike egg-based influenza vaccines, such as inactivated and live attenuated influenza vaccines (Grohskopf et al., 2018). Recombinant HA vaccines are also quicker to manufacture, so they may be more suitable for use during an influenza pandemic. It would be much safer than other influenza vaccines as no virus is used during the production of these vaccines (Treanor et al., 2001). Unfortunately, these vaccines can only be used in adults as they lack efficacy in children (Gutierrez and El Sahly, 2015; Wong and Webby, 2013).

Currently, the main types of COVID-19 vaccines available are messenger RNA (mRNA), viral vector, protein subunit, and inactivated whole-virus vaccines. The structural spike (S) protein of SARS-CoV-2 is one of the most immunogenic in promoting neutralising antibody response. Therefore, it is commonly present in COVID-19 vaccines. mRNA vaccines work by guiding cells to make S protein, which

is present on the surface of SARS-CoV-2. Once the number of S proteins being made starts increasing, they are displayed on the host cell surface. These trigger host immune cells to produce antibodies against the S protein. If the individual becomes infected with SARS-CoV-2, the antibodies help the immune system fight against the infection. The mRNA vaccine does not enter the cell's nucleus, where the DNA is present. Pfizer-BioNTech and Moderna COVID-19 vaccines are examples of the mRNA vaccine (McDonald, 2020).

Limitations of mRNA vaccines include short-lived protection, reduced efficacy towards variants of concern and the activation of Th17 immune responses. According to some studies, the number of IgGs produced against the S protein decreased 6 months after the second dose of the mRNA vaccine (Echaide et al., 2022; Mastroianni et al., 2022). Individuals with third and fourth doses have a significant increase in their IgG numbers compared to the individuals with two doses of injection. However, the number of IgG starts decreasing again 6 months after the booster dose (Canetti et al., 2022; Wand et al., 2023). Reduced protection within the population against SARS-CoV-2 is caused by the emergence of new variants, resulting in modification of mRNA vaccines. These vaccines can be easily modified by changing the immunogenic transgene to target variants. Pfizer-BioNTech and Moderna brought two bivalent vaccines to the market, which are called Comirnaty and Spikevax. These encode the S protein of the original variant together with BA.4-5 Omicron variants (Chalkias et al., 2022). Booster doses can provide enhanced protection against new Omicron subvariants, producing a higher number of Omicron-specific neutralising antibodies than monovalent vaccines (Winokur et al., 2023). Some other studies emphasised the production of a Th17-type T cell response during COVID-19 due to activating a pro-inflammatory cytokine cascade, also known as cytokine storm (Egwuagu, 2009; Trapnell et al., 2009). Th1 responses are responsible for gathering immune cells to the infection site and controlling the T cell cytotoxicity of infected cells. This is regulated by T cells, which mainly express IFN-γ and IL-2. Th2 responses are involved in antibody production and airway inflammation, which are observed in some respiratory cases. This is regulated by T cells mainly expressing IL-4 and IL-10 (Supriya et al., 2021). Th17-type T cell response causes a disruption in Th1-Th2 immunity, leading to exacerbation of the inflammation and pathogenesis of SARS-CoV-2 (Martonik et al., 2021; Lonberg, 2008).

Vector vaccines involve the use of viral vectors, which are recombinant viruses that encode antigens of interest in an unrelated modified virus. The viral vector guides cells to make copies of the viral S protein. Once the number of S proteins being made starts increasing, they are displayed on the host cell surface. These triggers host immune cells to produce antibodies against the S protein. If the individual becomes infected with SARS-CoV-2, the antibodies help the immune system fight against the infection. These vectors are modified by removing the virulence gene while maintaining the capacity to enter host cells. This allows them to deliver target genes without causing infection while mimicking the mechanism of viral infection. In the case of COVID-19, the viral vector carries the S gene of SARS-CoV-2 into the nucleus, which is transcribed into mRNA by DNA polymerase. mRNA then leaves the nucleus and moves into the cell plasma to bind to the ribosomes. Antigen proteins are made and released from the ribosomes, followed by antigen presentation on the host cells to induce the host immune response. Janssen/Johnson & Johnson, AstraZeneca and the University of Oxford all have a vector vaccine for COVID-19 (Soheili et al., 2023) AdVs are commonly used as a vector for the COVID-19 vaccine, as they can infect a wide range of host cells (Lee et al., 2017).

Long-term protection is available with this vaccine, even without the booster injections. Viral vectors can induce a strong and long-lasting cellular response, such as activating cytotoxic T cells to reduce the number of infected cells. Cytotoxic T cells multiply, differentiate and transform into effector T cells when triggered by antigens. Meanwhile, cell-mediated immunity induces macrophages and natural killer cells to eliminate intracellular pathogens (Deng et al., 2022). On the other hand, there is a risk of developing immunity against the viral vector itself when this type of vaccine is used. This causes a reduction in the efficiency of gene transfer or elimination of the transduced cells over a period. Sometimes, the immune system cannot differentiate between specific components of viral vectors and wild-type viruses. In that case, innate and adaptive immunities attack the viral vector. Pattern recognition receptors (PRRs), also known as innate immune receptors, detect viruses by recognising conserved molecular motifs. Viral capsids or specific structural proteins are foreign to the host immune system, so they can easily become the target of adaptive immune responses (Deng et al., 2022).

Protein subunit vaccines are only made from a few selected parts of the virus (e.g. a polysaccharide, nucleic acid, protein) that would best stimulate the host immune system (Bill, 2015). They are not as immunogenic as the other two vaccines, containing harmless S proteins. Once the immune system recognises the S protein, it produces antibodies and white blood cells (WBCs). The Novavax COVID-19 vaccine is an example of the protein subunit vaccine. The SARS-CoV-2 is made up of structural, non-structural, and accessory proteins. Three main structural proteins, which are S, membrane (M), and envelope (E), are found within the viral phospholipid bilayer and in the nucleocapsid (N) protein of the ribonucleoprotein core (Koupaei et al., 2022). S protein binds to the angiotensin-converting enzyme 2 (ACE2) receptor to induce host cell attachment and entry. S protein has two main subunits, which are S1 and S2. The S1 subunit is a C-terminal receptor-binding domain (RBD) that is responsible for detecting the ACE2 receptor. The S2 subunit is involved in membrane fusion to initiate the host cell entry. Antibodies bind to the S proteins to neutralise the virus, which is why the S protein is the main component used in COVID-19 vaccines. M protein is involved in the formation of the viral envelope. E protein plays a significant role in SARS-CoV-2 infectivity. N protein recognises the RNA and wraps it into a symmetrical helical structure (Currier et al., 2021). As only a few selected parts of the virus are used in this vaccine, it does not provide the full functionality and complexity of the virus antigen. Therefore, these vaccines may not be as strong as the others, leading to limited immune responses in some cases (Dong et al., 2020). This makes them suitable for immunocompromised individuals.

The United States Food and Drug Administration (FDA) has approved two RSV vaccines, Arexvy and Abrysvo, for individuals who are 60 and older with healthy immune systems. A single RSV vaccine can protect against RSV for at least two winter seasons. There is no vaccine currently licensed against RSV for individuals under 60. In healthy individuals aged 60 and older, one dose of Arexvy was 83% effective in preventing lung infections associated with RSV during the first RSV season. One dose of Arexvy was still 56% effective against any lung infections during the second RSV season. On the other hand, a single dose of Abrysvo was 89% effective for the first RSV season and continued its efficacy during the second RSV season. The data of this study showed that Abrysvo provided significant protection against RSV-associated lower

respiratory tract disease all around the second season, which strengthened its usage as a reliable vaccine for older adults aged 60 and over (Walsh and Gonzalo, 2023).

Besides influenza, SARS-CoV-2, and RSV, there is no effective vaccines against the other common respiratory viruses (Moscona, 2005). Scientists have tried to produce a live attenuated intranasal vaccine against parainfluenza viruses; however, they were unsuccessful due to attenuated strains maintaining the capacity to infect central neurons in the nasal cavity. Therefore, these vaccines could cause harmful effects on the central nervous system (CNS) (Mori et al., 1996). Rhinoviruses currently have no vaccines due to the large number of serotypes and the lack of cross-serotype protection (McLean, 2014). There is also no vaccine against the bocaviruses as they have always been detected in patients infected with other viruses. Therefore, scientists have never been entirely certain if the bocavirus was the primary virus causing the infection (Guido et al., 2016). Previously, live AdV vaccines were administered orally in enteric-coated capsules, which were only effective against serotypes 4 and 7. These vaccines were not allowed in civilian populations; they were only allowed in military populations due to a plethora of additional serotypes that caused severe diseases (Gray and Erdman, 2018). Even though AdVs currently have no existing vaccine, they can be used as a viral vector to produce vaccines against other respiratory viruses, such as AdV-based SARS-CoV-2 and AdV-based influenza vaccines (Chavda et al., 2023).

1.3. Common Respiratory Viruses

1.3.1. Adenoviruses

AdVs are non-enveloped, double-stranded DNA viruses from the *Adenoviridae* family. They are known to cause mild to severe infections in the upper and lower respiratory tract, such as common cold, bronchitis or pneumonia (Lynch et al., 2011; Ison, 2008; Sandkovsky et al., 2014). Therefore, the most common symptoms include a runny nose, fever, continuous cough, headache, and pink eye associated with conjunctivitis. Children who develop pneumonia from the virus may also suffer from chronic lung disease (Simões et al., 2019). In the case of severe intestinal infection, the AdVs can

cause intussusception, which is the intestinal blockage that occurs when a part of the intestine slides into the adjacent part of the intestine. This is more common in babies with the symptoms of vomiting, bloody stool, abdominal swelling, and knees flexed to the chest. In order to treat intestinal infections in children, drinking plenty of liquid is necessary to prevent severe dehydration, which may lead to emergency hospitalisation if left untreated. Hospitalised children are likely to be supported with intravenous fluids or nasogastric tube feeding; meanwhile, their electrolyte levels in the blood must be monitored continuously. Bronchodilators and other mechanical ventilation systems can be used for oxygen supplementation to the affected respiratory sites in children who are more heavily infected by the virus. AdVs can be easily detected from nasopharyngeal (NP) aspirates and blood or urine samples by using PCR (Lee et al., 2010). Carrying out real-time PCR of viral DNA in blood or urine samples is considered the diagnostic gold standard for AdV detection (Ison, 2006; Lankester et al., 2002; Erard et al., 2007).

1.3.2. Human Influenza Virus Infections

Human influenza viruses are enveloped, negative-sense, single-stranded RNA viruses from the *Orthomyxoviridae* family. There are four types of influenza viruses, indicated by the letters A, B, C, and D. Influenza A, B and C can infect humans, with the first two causing seasonal epidemics of respiratory diseases (Taubenberger and Morens, 2008). Influenza C virus infections cause very mild illness in humans, whereas Influenza D infections are currently known to cause illness in cattle. No human infections have been observed from this virus so far. Infections caused by the influenza viruses can spread in the population by respiratory droplet transmission. These can be symptomatic or asymptomatic infections ranging from mild common cold symptoms like runny nose, sore throat, fatigue, pneumonia, acute respiratory failure, or multi-organ failure in the most severe cases (Moghadami, 2017). Many influenza infections are accompanied by bacterial co-infection (Bardi et al., 2021). Carrying out viral culture is the diagnostic gold standard for most respiratory viruses, including influenza (Olsen et al., 1993; Winn and Koneman, 2006).

1.3.2.1. Influenza A Viruses

Influenza A viruses have zoonotic reservoirs, unlike Influenza B viruses, which can also spread from animals to humans. They are divided into subtypes based on the two main proteins on their surface: HA, with 18 different subtypes, and NA, with 11 different subtypes. They are the only influenza viruses that are known to cause pandemics. They consist of eight segments that enable them to undergo antigenic drift or antigenic shift. Antigenic drift can occur in Influenza A, B, and C, involving small mutations in the genes encoding these surface proteins. The surface proteins, HA and NA, are the antigens of influenza viruses, meaning they are typically recognised by the host immune system to initiate an immune response. Annual flu shots are prepared based on antigenic drift, targeting different HA and NA proteins on the virus. Another type of mutation is called antigenic shift, which only occurs in Influenza A. It is a significant major change in the virus that produces completely new HA or NA proteins. This change is likely to be an amino acid substitution in either of the surface proteins, which may provide a fitness advantage by helping the virus escape from the host's immune defences (Treanor, 2004). These changes could even lead to a new seasonal Influenza A subtype, which affects up to 10% of adults and 20% of children annually (WHO, 2014). The most widely known examples of antigenic shift include the 1889 Russian flu pandemic (H3N8) (Valleron et al., 2010), the 1918 Spanish flu (H1N1), the 1957 Asian flu (H2N2) (Xu et al., 2010), the 1968 Hong Kong flu (H3N2) (Lindsay et al., 1970) and the 2009 swine flu (H1N1) (Peteranderl et al., 2016). Pandemics cause significant mortality within a short period of time due to infected people having very little or no immunity against the newly emerged virus. For example, the 1918 Spanish flu and the 2009 swine flu pandemics were both caused by an H1N1 virus which infected nearly one-third of the world population, leading to the death of at least 40 million people in less than a year (Taubenberger and Morens, 2006).

1.3.2.2. Influenza B Viruses

Typically, Influenza B viruses can only spread from human to human, but a few studies

have identified Influenza B infection in seals (Zaraket et al., 2021; Krammer et al., 2018; Bodewes et al., 2013). These viruses are divided into two lineages named B/Yamagata and B/Victoria, where the latter changes more rapidly than the former (Zaraket et al., 2021). Even though they are also comprised of eight segments, like Influenza A viruses, they can only cause seasonal epidemics due to their slower mutation rate (Nobusawa and Sato, 2006). This does not stop them from being as contagious as Influenza A viruses, and in fact, they may even cause higher mortality rates in some populations like HIV patients (Sharma et al., 2019).

1.3.2.3. Influenza vs. Common Cold Viruses

Although influenza and common cold infections have very similar symptoms, these infections are caused by different viruses. The flu is caused exclusively by influenza viruses, whereas the common cold can be caused by different respiratory viruses (e.g. rhinoviruses, parainfluenza viruses, seasonal coronaviruses). Even though the symptoms of both infections are similar, the flu is generally more intense than the common cold in terms of symptoms and timing, as it begins more abruptly than slowly. Unlike severe influenza infections, common cold infections do not cause any serious health issues like pneumonia, bacterial co-infection, and emergency hospitalisation.

1.3.3. Respiratory Syncytial Viruses

RSVs are enveloped, negative-sense, single-stranded RNA viruses that belong to the family of *Paramyxoviridae*. They are the most important cause of lower respiratory diseases worldwide, especially in children. hMVPs are from the same family as syncytial and parainfluenza viruses, which are mostly known to infect children (van den Hoogen, 2001). Both hMPVs and RSVs are known to cause mild to severe respiratory symptoms like runny nose, sore throat, cough, and fever, leading to acute respiratory tract and lung infections in people of all ages, so they are almost indistinguishable from each other (Panda et al., 2014). Co-infection of hMVP with RSV has been observed to cause more severe symptoms. RSVs replicate within the epithelial lining of the nasopharynx and upper respiratory tract to initiate infection, gradually spreading to

small bronchioles or alveoli in the lower respiratory tract (Collins and Graham, 2008). Both viruses can be transmitted directly via contact with an infected human (Haas et al., 2013) or indirectly via air droplets (Grayson et al., 2016).

1.3.4. Human Parainfluenza Viruses

Human parainfluenza viruses (HPIVs) are enveloped, negative-sense, single-stranded RNA viruses that belong to the family of *Paramyxoviridae*. They are antigenically divided into four main types, as indicated by the numbers 1, 2, 3, and 4. These viruses can cause upper and lower respiratory diseases in both children and adults. Symptoms associated with upper respiratory diseases are fever, runny nose and continuous cough ranging from mild to moderate, whereas symptoms associated with lower respiratory diseases are croup, bronchitis, bronchiolitis, and pneumonia, which are more severe. Other symptoms may include sore throat, sneezing, wheezing, and ear pain. Each of these symptoms is associated with different types of HPIV. For example, HPIV-1 and HPIV-2 cause croup in children and other common cold symptoms. HPIV-3 is typically known to cause more severe respiratory infections like bronchitis, bronchiolitis and pneumonia. HPIV-4 is less common in the population and is known to cause milder to severe respiratory diseases. They can be transmitted via air droplets and personal contact like shaking hands or touching infected objects or surfaces (Burke et al., 2013)

1.3.5. Human Rhinoviruses

HRVs are non-enveloped, positive-sense, single-stranded RNA viruses that belong to the family of *Picornaviridae*. They account for over 50% of URIs among children, which are mainly asymptomatic infections (van Benten et al., 2003; Iwane et al., 2011). Symptomatic patients display common cold symptoms like rhinorrhoea, sore throat, coughing, and wheezing (Arruda et al., 1997). HRV infections are also associated with asthma and lower respiratory diseases such as pneumonia, bronchitis, and bronchiolitis, specifically in asthmatic patients (Saraya et al., 2014). They can cause acute otitis media (AOM) and rhinosinusitis in cases of bacterial co-infection **(**Pitkäranta et al., 1997). For

example, nearly 90% of children hospitalised with acute asthma attacks were tested to be HRV-positive (Bizzintino et al., 2010). A study identified detectable HRV in half of the 3 to 18-year-old hospitalised patients with wheezing (Heymann et al., 2004). Their infection rate can be as high as 8 to 12 times a year (Pappas et al., 2008). The HRVs can also be transmitted directly by human contact or indirectly by aerosols (Hendley and Gwaltney, 1988).

1.3.6. Human Bocaviruses

HBoVs are non-enveloped, single-stranded DNA viruses that belong to the family of *Parvoviridae*. These viruses mainly cause infection in children aged 6-24 months. However, they can also be present in adults and elderly with respiratory symptoms (Jartti et al., 2011). These symptoms include cough, fever, rhinitis, dyspnea, acute wheezing, and diarrhoea (Bastien et al., 2006; Kesebir et al., 2016; Fry et al., 2007). The virus has been observed in various biological samples like blood (Tozer et al., 2009), saliva (Martin et al., 2009), stool (Lee et al., 2007) and urine (Wang et al., 2010). Three additional HBoV subtypes were identified in human stool samples, which were subsequently named HBoV-2, HBoV-3, and HBoV-4 to differentiate them from the first isolated subtype, HBoV-1 (Kapoor et al., 2010). HBoV-1 has been primarily detected in the upper and lower respiratory tract, sometimes along with the gastrointestinal (GI) tract (Schildgen, 2013). HBoV pathogenicity needs to be fully understood due to a lack of experimental animal models, making it difficult to mimic the replication of the virus in vitro cell cultures (Huang et al., 2012). HBoV infections are usually accompanied by other viral or bacterial respiratory or gastroenteritis pathogens, such as AdV, rhinovirus, norovirus, and rotavirus (Lau et al., 2007; Campe et al., 2008; Regamey et al., 2007; Guido et al., 2011). Due to rare HBoV mono infections, a hypothesis was created that the virus may be a harmless passenger rather than a true pathogen (Chow and Esper, 2009).

1.3.7. Coronaviruses

Coronaviruses are enveloped, positive-sense, single-stranded RNA viruses with a ~30kb genome (McBride and Fielding, 2012). They are characterised by club-like spikes poking out from their surface. SARS-CoV-2 is made up of four main structural proteins, which are the N, E, M, and S proteins, playing important roles in its infectivity. These viruses are known to infect mammals and birds, causing upper respiratory disease in chickens and fatal respiratory infections in humans (Fehr and Perlman, 2015). They are the largest group of viruses that belong to several different families, including *Coronaviridae, Arteriviridae, Mesoniviridae*, and *Ronoviridae* (Fehr and Perlman, 2015). Coronaviruses from the *Coronaviridae* family are further subdivided into four genera: alpha (α), beta (β), delta (δ), and gamma (γ). Alpha and beta can only infect humans, whereas delta and gamma are responsible for bird infections. There are six other human coronaviruses besides SARS-CoV-2, which are 229E (α), NL63 (α), OC43 (β), HKU1 (β), as well as SARS-CoV (β) and Middle East Respiratory Coronavirus (MERS-CoV) (β) with the last two being highly pathogenic (Cui et al., 2019). Human coronaviruses 229E and OC43 are known to cause common cold and lower respiratory diseases in some cases (Liu et al., 2020). SARS-CoV was recorded to cause watery diarrhoea in 60% of infected patients (Hui and Zumla, 2019; Monaghan, 2016). People infected with MERS-CoV were observed to display flu-like symptoms that are similar to those in SARS-CoV and SARS-CoV-2, such as fever, dry cough, headache, fatigue, and even renal failure in more severe cases (Arabi et al., 2014; Gao et al., 2016). There was a SARS-CoV outbreak in 2003, followed by a MERS-CoV outbreak in 2012 that caused thousands of deaths (Liu et al., 2020; Otter et al., 2016).

1.4. Early Diagnostics for Respiratory Viral Infections

Viral specimens can be collected from different areas of the body, depending on the clinical symptoms and signs, as well as the pathogenesis of the suspected disease. Nasal or throat swabs are the most common specimens for suspected respiratory disease (CDC, 2024). Swabs should be swirled in a small screw-capped bottle containing a virus transport medium. The medium includes a gelatin or albumin protein to protect the

virus from inactivation and antibiotics to avoid the replication of bacteria and fungi. Because of the unstable state of the viruses, specimens collected for virus isolation must be placed in a refrigerator (4°C) until they reach their destination. Viral culture is the gold standard for viral isolation (Hsiung, 1984). Embryonated chicken eggs, laboratory animals, and cell cultures can be used for viral isolation. With the discovery of cell culture techniques, the use of laboratory animals in experiments has decreased drastically (Freshney, 2000). A primary cell culture can be obtained from human or animal tissues. Cells are extracted from tissues by mechanical scraping, mincing, or breaking tissue using trypsin or collagenase to obtain viable cells (Richter et al., 2021). A liquid culture medium in a Petri dish or tissue culture flask is required for the primary cell cultures to provide a solid surface for attachment and growth. When cells in primary culture undergo mitosis, they keep proliferating until they occupy the surface of a culture vessel. This is known as contact inhibition, which stops mitosis and prevents the density of cells from becoming too high (Levine et al., 1965). These cells can be transferred to another culture vessel with a fresh growth medium called secondary cell culture. Cell density in this culture must be reduced continuously by removing some cells and adding more medium to provide space and nutrients for cell growth (Freshney, 2016). These are called immortal cells as they are not affected by contact inhibition, allowing them to grow in piles regardless of cell density.

1.4.1. Viral Cytology

Cell cultures can be observed daily using an inverted microscope to identify cytopathic effects (CPEs) (Landry and Hsiung, 2000). CPE indicates structural changes in the host cell resulting from viral infection, such as rounding of the infected cell or fusion with adjacent cells to form syncytia (Baron, 1996). Viruses that produce characteristic CPE can be identified using viral cytopathology, which is the oldest form of rapid diagnostics (Al-Hajjar, 2012). This technique is performed by cutting a piece of skin vesicle with a sterile swab and smearing it onto a microscope slide. The skin cells on the slide are fixed using 95% ethanol, Zenker's or Bouin's solution. The slide is left to dry at room temperature and then stained by Giemsa, Wright or Papanicolaou stain to be observed under the inverted optical microscope (Al-Hajjar, 2012).

The main viruses identified by CPE in cytology include human papillomavirus (HPV), human polymovirus, herpes simplex virus/varicella-zoster (HSV/VZ), cytomegalovirus, RSV and AdV (Tille, 2017). For instance, the name RSV derives from the fact that it can form syncytia not only in the tissue culture but also in the lungs of infected patients (Morris et al., 1956; Papenburg and Boivin, 2010). On the other hand, AdVs make infected cells swell and clump together in grape-like clusters (Louten, 2016). Orthomyxoviruses (e.g. Influenza) and paramyxoviruses (e.g. parainfluenza) may not be able to produce an apparent CPE in infected cell cultures (Al-Hajjar, 2012). However, these viruses can still be detected based on the haemadsorption phenomenon. During haemadsorption, infected host cells express viral receptors on their surface. These viral receptors are able to bind to the red blood cells (RBCs) to make them attach to the infected cells, causing the formation of a lattice. This is known as haemagglutination, and it forms the basis of an assay to detect and quantify influenza virus from a sample.

1.4.2. Electron Microscopy

Viruses are intracellular organisms that cannot be identified using optical microscopes. Electron microscopy has been used for many years to rapidly detect viruses in clinical specimens. This technique is based on the identification of viruses according to their characteristic morphology. Electron microscopes have a greater detection capacity than optical microscopes; they exhibit a magnification of more than 10 million times, while optical microscopes exhibit less than 2000 times (Egerton, 2016). Transmission electron microscopy (TEM) can be exclusively used for detecting viruses due to its nanometer-scale resolution (Roingeard et al., 2018). TEM can be used to identify multiple infections caused by more than a single virus, which could be missed by molecular or antigen tests. However, the virus must be present in the range of 10^5-10^6 particles per ml to be detected by TEM (Roingeard et al., 2018). Specimens, including the ones with less known and difficult-to-detect viruses, from different sources like body fluids or biopsies can be analysed directly or after cell culture, which is the most significant advantage of this technique.

Negative staining is a method that detects viral particles by providing precise information about the morphology, enabling the classification of these viruses into their morphologically similar groups (Brenner and Horne, 1959). This method detects viruses from liquid samples deposited on small carbon-coated TEM grids. A droplet of liquid sample is applied to the surface of a carbon-coated TEM grid. Once the sample is attached to the surface, the grid is rinsed to eliminate unbound viruses. Heavy metal salts, like uranyl acetate or phosphotungstic acid, are used to stain the grid, creating a dark border to emphasise the shape of the virus. Excess liquid is washed away off the grid with filter paper strips. The grid can be stored in a grid box at room temperature until TEM imaging (Harris, 2007). In addition to viral detection, this method can also be used to identify different biological samples, including protein complexes and small nanoparticles (Harris, 2007; Bradley, 1967; Suzuki et al., 1987).

TEM explored many viruses from biological samples between the 1960s and 1990s. The use of TEM increased drastically between the 1970s and 1980s due to its significant participation in discovering AdVs, enteroviruses, reoviruses, and paramyxoviruses (Tyrrell and Almeida, 1967). In 1995, during an outbreak of fatal respiratory disease among horses and humans in Australia, TEM was used to identify a previously unknown virus, now called the Hendra virus, from *Paramyxoviridae* family (Murray et al., 1995). In 2003, the aetiology of the coronavirus causing the SARS pandemic was characterised by TEM in Hong Kong and South China. In 2020, TEM was combined with scanning electron microscopy (SEM) to produce early images of the novel SARS- CoV-2. The results confirmed a resemblance of SARS-CoV-2 with both 2012 MERS- CoV and 2013 SARS-CoV (Blancett et al., 2017). With the development of immunological and molecular detection methods, scientists have started to use TEM much less frequently for routine diagnosis.

1.4.3. Immunofluorescence

Immunofluorescence can be used to detect and localise antiviral antibodies within a cell or tissue using a fluorescence microscope. Antibodies are labelled with a fluorescent dye, also known as a fluorophore, such as FITC. In direct (primary)

immunofluorescence, a single antibody labelled with a fluorophore is used to recognise the target antigen and bind to a specific region on the antigen named epitope. Once the attachment occurs, fluorophore emits a specific wavelength of light, which can be detected by a fluorescence microscope (Ladner, 2007; Marks and Nolan, 2006). The direct attachment of the fluorophore to the antibody provides some advantages. It reduces the number of steps in the sample preparation process, so the procedure is fast, and there is less chance of having a non-specific background signal during analysis, eliminating the risk of antibody cross-reactivity (Piña et al., 2022). Only a limited number of antibodies can bind to the antigen during this method, which might affect the sensitivity of detection (Joshi and Yu, 2017).

For indirect (secondary) immunofluorescence, an unconjugated primary antibody and a fluorophore-conjugated secondary antibody are used (Odell and Cook, 2013). In this method, the primary antibody binds to the epitope of the target antigen, while the secondary antibody binds to the primary antibody to emit light. Target antigens must be immobilised using a fixative, such as formaldehyde or glutaraldehyde, to reduce the risk of autolysis (Im et al., 2019). Fixation allows immobilisation of the target antigen without interfering with the cellular structure, so the antibodies can successfully reach any targeted cellular component. Organic solvents, such as methanol and acetone, can be used in addition to fixatives to get rid of lipids and dehydrate cells, leading to the denaturation of cellular components to increase the permeability of the cell membranes (Ramos-Vara, 2005). Following fixation, tissues are inserted into paraffin to let the sample solidify for tissue sectioning. Thin slices are inserted into a hard matrix to allow dyes, probes, and antibodies reach their target sites successfully without being affected by multiple cell layers. The paraffin sections are sliced and placed on a glass slide. To ensure that only tissue sections stay on the glass slide for antigen retrieval, they must be deparaffinated by xylene and rehydrated by ethanol or distilled water (Harlow and Lane, 1999). Antigen retrieval is a technique used to reverse structural modifications that occur to the proteins during fixation. Fixation may change the protein structure in such a way that the epitope of interest is covered and can no longer bind to the primary antibody. When this happens, antigen retrieval can be used to break down the cross-links formed during fixation to unmask the target epitope, allowing the epitope to bind to the primary antibody (Im et al., 2019).

One of the limitations of immunofluorescence is that it can only be used on fixed or dead cells, as the antibodies cannot penetrate through the cellular membranes of the living cells due to being large proteins (Battifora, 1991). Recombinant proteins containing fluorescent protein domains, such as green fluorescent protein (GFP), can be used to observe living cells but these may change the genetic information of the cells (Ehrhardt, 2003). Another possible problem is photobleaching, where fluorophores lose their ability to emit light (Piña et al., 2022). This can be avoided by reducing the intensity or timespan of light exposure to retain the functionality of fluorophores. Autofluorescence, spectral overlap, and non-specific staining are other issues that can come across when using this technique (Joshi and Yu, 2017).

Autofluorescence happens when the tissue naturally emits fluorescence through a broad excitation and emission spectra (Schnell et al., 1999). This is not desirable in experiments as it can interfere with the fluorescent signal of a specific labelled protein, leading to a failure in tissue examination and analysis (Baschong et al., 2001; Romijn et al., 1999). Sudan Black B dye is commonly used to treat tissues to eliminate the risk of autofluorescence. This lipid-soluble dye binds to lipofuscin molecules to suppress autofluorescence. Lipofuscin is a granular iron that is found in lysosomes at older ages. It is present in most fixed mammalian tissues and is strongly fluorescent through multiple wavelengths (Erben et al., 2016; Sun et al., 2011). In addition to lipofuscin, some tissues naturally cause more autofluorescence than others. These include the liver, kidney, pancreas, and some areas of the brain (Clancy and Cauller, 1998; Erben et al., 2016; Sun et al., 2011; Viegas et al., 2007), which contain RBCs with fluorescent haemoglobin (Alpert et al., 1980; Hirsch et al., 1980). Unfortunately, Sudan Black B dye is likely to increase background staining and fluorescence at high red wavelengths, so using a different dye may be necessary (Romijn et al., 1999; Schnell et al., 1999). TrueBlack lipofuscin autofluorescence quencher (Biotium) can be used to replace Sudan Black B dye, as it does not mask the intensity of fluorescent antibody signal. It can also be reused, making it suitable for routine immunofluorescence staining (Whittington and Wray, 2017). Spectral overlap is a phenomenon when fluorochromes exhibit fluorescence that falls into a detector channel where it is not supposed to show up. This happens because most fluorochromes have a broad emission spectrum. Using fluorescent dyes that are far apart and excited by different lasers will eliminate this

problem. Non-specific staining results from a primary antibody binding to amino acids rather than those within the desired epitope of antigen, which might be caused by different factors. The most common cause is excessively high antibody concentrations, where antibodies will bind to lower affinity targets. Another reason is the binding of antibodies to Fc receptors, which are antibody-binding proteins on the immune cell surface. To avoid these problems, antibody concentration can be optimised, and Fc blocking reagent can be used.

1.4.4. Viral Serology

Viral serology is used to determine the presence of virus-specific IgM antibodies or a significant rise in the number of antiviral IgG antibodies between two consecutive samples taken 7-10 days apart. Upon infection, viruses start multiplying, then shedding after an incubation period. Antibodies against the virus appear within a few days or weeks after disease onset, known as the window period (Vainionpää and Leinikki, 2008). IgM antibodies are the first ones to appear when the antibodies against the virus reach a certain level of detection. The levels of IgM antibodies peak at 7-19 days after disease onset, followed by a decline. These antibodies completely disappear after some weeks or months in more severe cases. IgG antibodies appear a few days after the release of IgM antibodies, reducing the number of infectious viruses (Hou et al., 2020). If this is the first encounter with this virus, it is called the primary immune response, where IgG antibody levels are maintained to stay at a low level. In later contact with the same antigen, known as the secondary immune response, IgG levels rise drastically in a few days, whereas IgM response may not even be detectable (Vainionpää and Leinikki, 2008). Both IgG and IgM antibodies are capable of neutralisation, as they can reduce the infectious capacity of the virus. These are produced during an infection and often persist throughout the patient's life. In some situations, the number of antibodies cannot reach a certain level to induce a sufficient response against the virus. For instance, newborns do not have enough maternal antibodies, which may affect the way their body fights with an infection. On the other hand, immunocompromised patients typically fail to have a strong immune response to fight an infection, which is generally associated

with insufficient antibodies. In these cases, alternative diagnostic methods must be pursued.

The most common serological tests include neutralising antibody assays, haemagglutination inhibition tests, complement fixation tests, and immunoassays. The serum samples from humans contain non-specific inhibitors that may cause false positive results. Therefore, a receptor-destroying enzyme (RDE) is used to treat these samples before running the assays (Jordan and Oseasohn, 1954). A neutralising antibody assay is used to detect antibodies that can neutralise the infectivity of a virus. Serial dilutions of the serum to be tested are mixed with a reference strain of a viable virus (Bourgeois and Oaks, 2014). This mixture is incubated for a short period of time so the antibodies can bind and neutralise the virus. Neutralisation prevents viral attachment to the host cell and protects the host cell membrane from viral penetration. Regarding novel viruses, the attachment of a single antibody may not be sufficient to neutralise the virus. In this case, the virus can penetrate and start infecting the cells, resulting in specific CPEs which can be detected by an optical microscope. The titre is the highest dilution (i.e. the least amount of antibody) that neutralises infectivity. Even though this method is typically very sensitive and specific, it is difficult to maintain as it requires the use of living cell cultures, tittered virus stocks and trained personnel. The protocol is also time-consuming and very expensive to carry out.

Haemagglutination inhibition assay (HIA) is used to measure the concentration of antibodies that can neutralise the virus in a serum sample. It can also classify or subtype haemagglutinating viruses like influenza (Cohen and Biddle, 1963; Anderson et al., 2012). These viruses have the surface glycoprotein HA attached to them, which binds to the RBC receptors of the host. Interaction between the HA protein and the RBCs creates a lattice of aggregated RBCs. This prevents RBCs from clumping at the bottom of the well. In this assay, a serial dilution of the serum to be tested is mixed with the virus of interest. This mixture is incubated for a short period of time so the antibodies in the serum can bind to the viral HA protein. RBCs are added to the mixture to detect any haemagglutination caused by the virus. Occupied viruses cannot bind to the RBCs, so the RBCs do not form a lattice and fall to the bottom of the well, indicating a positive test result. If the serum sample does not have any viruses, RBCs can bind to the viral HA protein and form a web of linked RBCs, indicating a negative test result. The

highest serum dilution inhibiting haemagglutination is recorded as the HAI titre (Landolt et al., 2014). This measures the concentration of virus particles capable of agglutinating RBCs in a sample. This type of detection method has historically been described as the gold standard for influenza antibody subtyping. It is relatively affordable as it does not require expensive equipment and is quick as the results can be obtained in about 2 hours. The assay can detect antibodies or viruses depending on desire and allows using various sample types, including serum, plasma, allantoic fluid, and cell culture supernatant (Swayne et al., 2013).

A complement fixation test is a blood test that can identify the presence of any antibody against a particular antigen in the sample. This technique is based on the activation and fixation of complement in the presence of a specific antigen-antibody reaction. Complements are the proteins in the blood plasma that enhance host immunity during an infection. When antigen and antibody interact, they form an antigen-antibody complex that binds and fixes the complement protein. After fixing, the complement protein degrades to form two fragments of different sizes. The larger fragments are attached to the antigen of the complex, while the smaller fragments act as signalling molecules. The signalling molecules send signals to the immune cells, like macrophages, to destroy antigens. If the sample has antibodies against the target antigen, the antigen-antibody complex will be formed once the complementary reactant (i.e. antigen) is added along with the complement. The complement is fixed by the antigen-antibody complex formed. When sensitised RBCs, coated with a mix of antigens and antibodies, are added as an indicator system, they will not be able to react with the complement as all available complement is already fixed by the antigen-antibody complex. Sensitised RBCs remain intact and settle down in the sample, which is associated with a positive test result. If the sample has no antibodies against the target antigen, there will be no antigen-antibody complex formation upon the addition of the complementary reactant. The complement will not be fixed and will remain free. When sensitised RBCs are added to the sample, they form an antigen-antibody complex to fix the complement. This results in the haemolysis of the RBCs, changing the colour of the sample, which is associated with a negative test result. This type of detection method allows the screening of many different viral infections simultaneously. Unfortunately, it measures specific antibodies that occur only during the acute phase of infection, so it

cannot be used to investigate the immune status. The test is time-consuming and not as sensitive as other diagnostic methods, such as immunoassays (Vainionpää and Leinikki, 2008).

1.4.5. Immunoassays

There are two main types of enzyme immunoassays based on the separation criteria of immunocomplexes: homogenous and heterogenous assays (Darwish, 2006). Enzyme multiplied immunoassay technique (EMIT) is an example of a homogenous immunoassay, which can be used to detect the presence of an antigen of interest in a solution (Engvall, 1980). In this technique, a reporter enzyme, with the target antigen attached near the active site, binds to its substrate on the active site to promote a colour change in the solution. Once the antibodies against the target antigen are added to the solution with the antigens, they can bind some of the free antigens in the solution or some of the antigens attached to the reporter enzymes to block the active sites for the substrates. Substrates can bind the remaining active sites in this case, triggering a fluorescent colour change. The intensity of the colour change is associated with the antigen concentration in the solution. When there is no antigen in the solution, the antibodies can only bind to the antigens attached to the reporter enzyme, blocking all the active sites for the substrates. Therefore, there is no enzyme-substrate complex formation to generate a fluorescent colour change in the solution. This technique is often used to detect small molecules with low molecular weight, such as hormones and drugs (Ullman, 2013).

Enzyme-linked immunosorbent assay (ELISA) is a heterogeneous assay that is referred to as the gold standard of immunoassays (Aydin, 2015). It can be used to detect specific antigens in a serum sample. There are four different types of ELISA assays: direct, indirect, sandwich and competitive (Alhajj et al., 2023). ELISAs typically run in 96-well microplates that provide a solid surface for the immobilisation of a target antigen (Engvall, 2010). In a direct ELISA, the target antigen is immobilised directly on the wells of the plate by the capture antibodies. Wells are rinsed to remove any unbound

antigen. Detection antibody conjugated to an enzyme, such as horseradish peroxidase (HRP) or alkaline phosphatase (AP), is added to the well to bind to the antigen (Shah and Maghsoudlou, 2016). Wells are rinsed again to remove any unbound antibodies. A substrate specific to the enzyme is also added to the wells to bind to the enzyme on the antibody, promoting a colour change in the sample, which can be measured by a spectrophotometer or absorbance microplate reader.

Indirect ELISA can be used to detect specific antibodies in a serum sample. An unconjugated primary detection antibody is added to the wells to bind to the target antigen in the sample. An enzyme-conjugated secondary antibody is also added to the wells to bind to the primary antibody. A substrate specific to the enzyme on the antibody binds to the enzyme to promote a colour change. The indirect ELISA is more sensitive than the direct ELISA. It is also more affordable and flexible as it allows the use of many possible primary antibodies (Kohl and Ascoli, 2017). Unfortunately, there is a possibility of cross-reactivity between the secondary detection antibodies, which must be addressed when this type of ELISA is used. (Shah and Maghsoudlou, 2016).

Sandwich ELISA uses two different antibodies for the same target antigen. These antibodies bind to different epitopes of this target antigen. Once the sample with the antigen is added to the well, it binds to the capture antibodies immobilised in the well. Enzyme-conjugated secondary antibodies are then added to the sample to bind to the antigens attached to the capture antibodies. Substrate is added to bind to the enzyme on the antibody to promote a colour change. Although the sandwich ELISA is the most sensitive among all the ELISA types (Kohl and Ascoli, 2017), it is time-consuming and expensive to perform. It also requires the use of "matched pair" (divalent/multivalent antigen) and secondary antibodies (Shah and Maghsoudlou, 2016).

Competitive ELISA is used to measure the amount of a small protein when the protein of interest is too small to be efficiently sandwiched between two antibodies. An unlabelled primary antibody is incubated with the sample containing antigen. Depending on how much antigen is present in the sample, some of the primary antibodies will bind to the antigens, and some will remain unbound. Unbound antibodies are removed by washing the plate. Antigen-antibody complexes are added to

the well, which is already coated with the same target antigen. The more antigens present in the sample, the fewer antibodies can bind to the antigen in the well. An enzyme-conjugated secondary antibody specific to the primary antibody is added to the well, followed by the substrate to elicit a fluorescent signal. Unlike in other ELISA assays, the more colour change occurs, the less the target antigen is present in the sample (Shah and Maghsoudlou, 2016). This is because the more target antigens present in the sample, the more antibodies are bound by them. As a result, fewer free antibodies are left to bind to the antigens in the wells. Therefore, less enzyme-conjugated secondary antibodies can bind, producing a weaker signal. This type of ELISA can be used to measure a variety of antigens, including the smaller ones, from a given sample. It also requires less sample purification compared to the other ELISAs. However, competitive ELISA has low specificity, so it cannot be used for diluted samples (Kohl and Ascoli, 2017).

1.4.6. Hybridisation

Nucleic acid hybridisation is a process that can be used to identify specific viral DNA or RNA sequences. There are two types of widely used hybridisation techniques: northern blotting and southern blotting. Northern blotting is used to detect specific DNA sequences by labelled probes complementary to those sequences in the sample (He and Green, 2013). Meanwhile, southern blotting is used to detect specific RNA sequences in the sample by labelled DNA probes (Brown, 2001). The probe must be labelled with a radioisotope or a fluorescent molecule, while the target sequence must be bound to a nylon membrane (Sterchi, 2008). If a complementary base pairing occurs between the probe and the target sequence, a positive hybridisation signal is produced, which can be observed by an X-ray film in the case of radio-labelled probes or confocal microscopy in the case of fluorescent probes (Amann et al., 1995).

In situ hybridisation (ISH) is used for specific mRNA detection and localisation within a cell or tissue (Pardue and Gall, 1969). To measure the mRNA content at a particular time, the mRNA must be preserved using cross-linking fixatives, such as formaldehyde (Russell et al., 2013). Radioactive isotopes, such as ^{32}P, ^{35}S, and ^{3}H, were commonly used for labelling

probes in the first ISH experiments, as these can identify very low levels of transcripts. However, they have a very long development period and need a better histological resolution (Olivier and Walter, 1998). Using non-radioactive probes, such as digoxigenin (DIG) or fluorescently labelled ones, has significantly reduced the development time and improved the resolution (Singer and Ward, 1982; Farquharson et al., 1990; Morris et al., 1990). Once the probe is modified by labelling, double strands of the DNA are denatured using a hybridisation buffer, so the desired sequence is available for binding to the probe. The probe then becomes localised in the tissue using either autoradiography or fluorescence microscopy. Once the presence of a particular mRNA sequence is detected for a specific protein, the number of mRNAs coding for that protein can be identified at a given time. If the number of mRNAs is measured at different time intervals, a specific expression pattern will form, which can be used to build a microarray technology. The main advantage of this technique is that it allows maximum use of tissue that is hard to obtain. Unfortunately, low levels of DNA and RNA copies may be challenging to identify when using this technique. Additionally, background signals from the complexing of the probe may lead to false positive results (Nuovo, 1992).

1.4.7. Microarrays

A DNA microarray, which is commonly known as gene chips or DNA chips, is a group of microscopic DNA spots bound to a solid surface. Each DNA spot has thousands of copies of a specific DNA sequence called probes. Microarrays are very useful when multiple probes are required. These microarrays contain many oligonucleotides on a chip to allow the collection of a large dataset in one experiment. This technique allows the genetic analysis of a sample suspected of a viral infection, which has already been standardised at the genus and species level (Vira et al., 2016; Bilitewski, 2009). Whenever some genes are expressed or active, many copies of mRNA corresponding to the genes are produced by a process called transcription. These mRNAs then synthesise the corresponding protein by translation. mRNAs can be considered surrogate markers, so evaluating them will provide an understanding of the different processes behind modified gene expression and genetic information. As these markers degrade easily,

they must be converted into a more stable cDNA form, which can be labelled by fluorochrome dyes Cy3 (green) or Cy5 (red). The unknown DNA molecules are cut into fragments by an endonuclease restriction enzyme. Markers labelled with fluorochromes are attached to these DNA fragments, which are allowed to react with the probes. Target DNA fragments with complementary sequences bind to the DNA probes, so the target DNA emits fluorescence, which can be identified by passing a laser beam. The specific pattern of fluorescence produced is recorded, and the number of transcripts in the target sample is identified using a computer (Kaliyappan et al., 2012).

1.5. Current Molecular Diagnostics for Respiratory Viral Infections

1.5.1. RT-qPCR as a Diagnostic Gold Standard

RT is a significant first step in molecular diagnostics when working with RNA molecules. It allows the conversion of viral RNA to cDNA before the amplification. RT- qPCR uses primers, DNA polymerase, nucleotides, specific ions, and DNA template, with the standard main steps being DNA denaturation, primer annealing and extension. During denaturation, the double helix structure of the DNA is broken down by heating at 95°C. Once the temperature is reduced to 55°C, primers start annealing to both new single strands. The temperature is raised to 72°C to allow nucleotide addition to the annealed ends of the primer by *Taq* DNA polymerase to produce a new DNA strand. DNA amplification can be monitored in real-time by measuring fluorescence. The intensity of the fluorescence at different stages of amplification represents the number of DNA amplicons produced in the sample, which can be measured after each cycle (**Figure 1**). The fluorescence may not be detectable until the reaction reaches a specific number of cycles during amplification, which is known as the cycle threshold (Ct). It allows the estimation of the number of nucleic acid molecules in the sample by using a calibration curve based on serial dilutions of standard samples with known concentrations (Yang and Rothman, 2004; Kubista et al., 2006; Bustin et al., 2009)

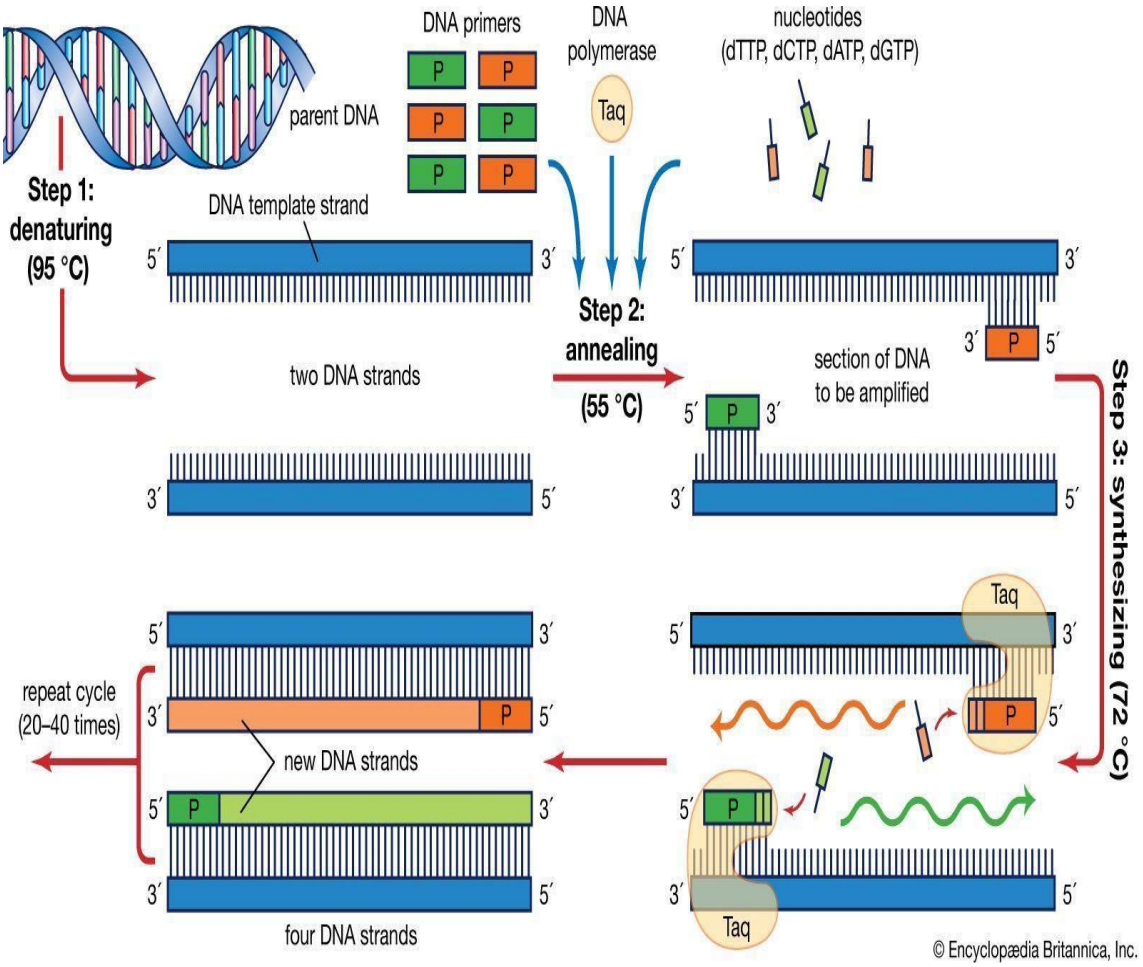

Figure 1. Overview of the standard RT-qPCR process.

Initially, RNA is isolated and reverse-transcribed into cDNA, which serves as a template for qPCR. This process consists of three main thermal cycling steps: denaturation (95°C), annealing (55°C), and extension (72°C). These steps are repeated for 20-40 cycles to amplify the target DNA, allowing for its quantitative detection (Image Source: Shaikh et al., 2024).

1.5.2. RT-LAMP as an Isothermal RT-qPCR Alternative

LAMP is an isothermal amplification method that uses a strand displacement reaction of DNA polymerase to amplify specific sequences of pathogens (Gosselin et al., 2017; Suwancharoen et al., 2016; Song et al., 2016). RT-LAMP can detect specific RNA viruses, including Ebola, Zika, West Nile, Yellow Fever, and SARS-CoV-2 (Lin et al., 2019; Cao et al., 2016; Ahn et al., 2019). RT-LAMP has a similar sensitivity to DNA

amplification to the standard LAMP method (Li et al., 2011); both methods can amplify up to 10^9-10^{10} copies of DNA within an hour. This does not require any thermal cycling,and it is not as time-consuming as qPCR, with lower chances of false positives due to non-specific amplification (Asaga et al., 2011). However, aerosol pollution can easily affect RT-LAMP because of its high sensitivity, leading to false positive results (Hu et al., 2015).

LAMP reactions are initiated by DNA polymerase with strand displacement activity, followed by two of the primers forming a loop structure to proceed with the amplification reaction. There are 4-6 different primers involved: 2 inner primers (FIP – forward inner primer and BIP – backward inner primer) and 2 outer primers (F3 – forward outer primer and B3 – backward outer primer) with optional loop primers (FL – forward loop primer and BL – backward loop primer) that are designed to detect 6-8 distinct regions on the target gene (**Figure 2**). Inner primers FIP and BIP are long (45-49 bp), and they have complementary sequences to both sense and antisense strands of the target DNA; one for priming in the first step and the other for self-priming in later steps. Outer primers F3 and B3 are shorter (21-24 bp), and they are added to the reaction mixture in smaller concentrations to allow slower template binding than the inner primers (Soroka et al., 2021).

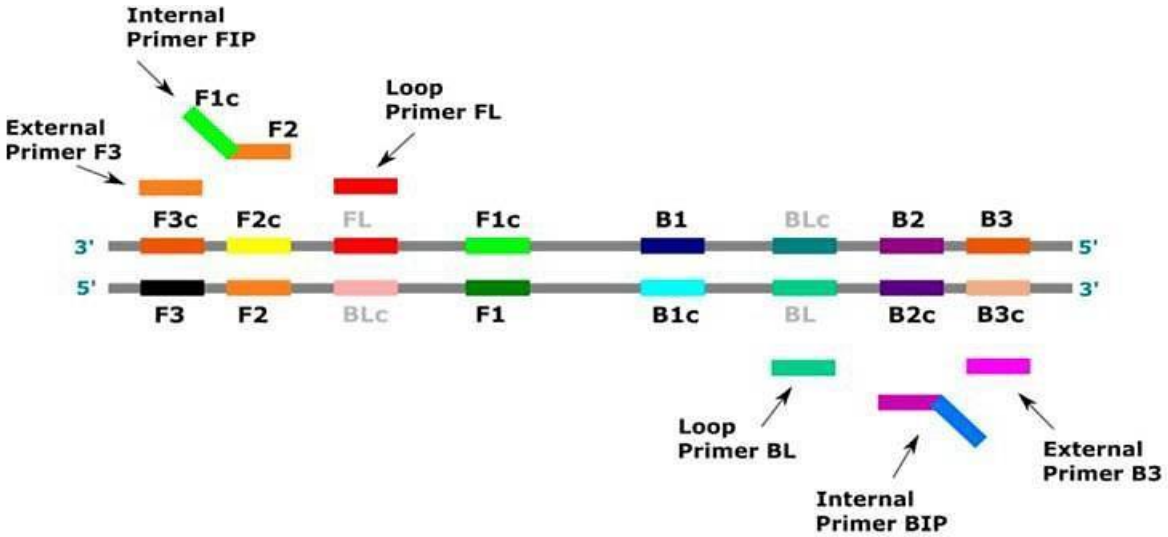

Figure 2. Arrangement of LAMP primers and their complementary DNA binding sites.

FIP consists of an F2 region with a complementary sequence with F2c of the matrix and a free F1c region complementary to F1 on the newly formed strand. On the other hand, BIP consists of a B2 region with a complementary sequence with B2c of the template and a free B1c region

that is complementary to B1 on the newly formed strand. F3 comprises the F3 region, which has a complementary sequence to the F3c region, and the B3 primer comprises the B3 region, [5] which has a complementary sequence to the B3c region of the template. Forward loop primer (FL) is complementary to the loop region between F1 and F2 regions, whereas backward loop primer (BL) is complementary to the loop region between B1 and B2 regions (Image Source: Tomlinson., 2021).

Amplification and detection of the target gene can be performed in a single step within a tube containing the sample, 4-6 different primers (BIP, FIP, F3 and B3 with optional loop primers), *Bst* DNA polymerase with strand displacement activity, and the substrates. This reaction occurs at a constant temperature (~65°C) in an hour (Dukes et al., 2006; Liu et al., 2014). The first stage of the reaction involves the formation of a dumbbell-like DNA acting as a template for the following amplification stages (Parida et al., 2008). Optional loop primers are complementary to dumbbell-like DNA, and they can increase the number of starting points by allowing the amplification of up to 8 DNA sequences in total once they are added to the reaction mixture (Nagamine et al., 2002). Therefore, using loop primers can increase the efficiency and sensitivity of the LAMP while reducing the time taken for amplification by half. Unlike the gold standard, LAMP does not have any DNA denaturation step due to the strand displacement activity of DNA polymerase, which allows the reaction to be carried out under isothermal conditions (Notomi et al., 2000).

To start complementary strand synthesis, FIP hybridises to F2c, and F3 gradually hybridises to F3c in the target DNA. DNA polymerase releases the FIP-linked complementary strand by strand displacement activity to generate a stem-loop structure at one end. Stem-loop formation is the first sign of BIP-initiated DNA synthesis and subsequent B3-primed strand displacement DNA synthesis, forming a dumbbell-shaped DNA. The dumbbell-shaped DNA is immediately differentiated into stem-loop DNA via self-primed DNA synthesis. New stem-loop DNA is the starting material for the LAMP cycling, which is the second stage of the reaction. The LAMP cycling begins when FIP hybridises to the stem-loop DNA, facilitating DNA synthesis once again via DNA polymerase strand displacement activity. This generates an intermediate structure named one-gapped stem-loop DNA with an inverted copy of the target sequence. One-gapped

stem-loop DNA later forms a mixture of multiple loops with cauliflower-like structures via self-primed strand displacement DNA synthesis to promote elongation and recycling, which are the final stages of the reaction (**Figure 3**).

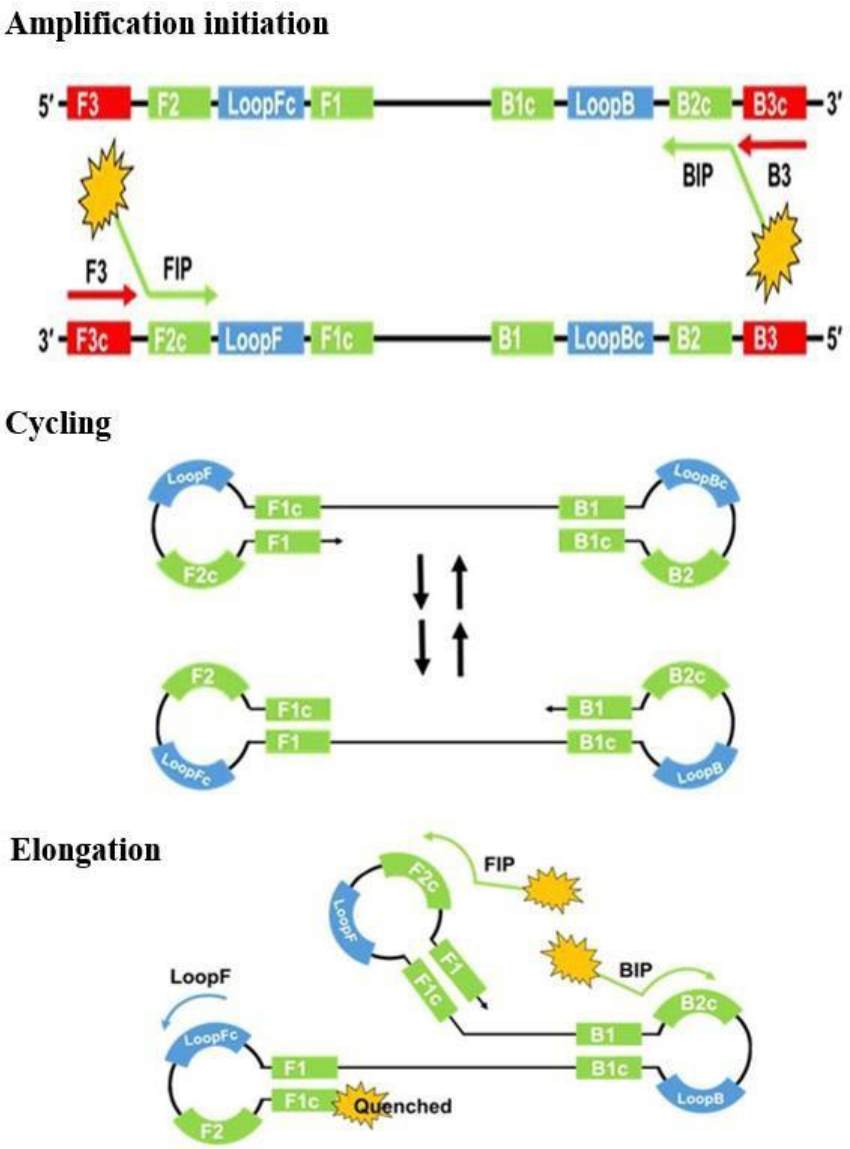

Figure 3. Three main stages of a standard LAMP assay.

Firstly, displacement primers F3 and B3 separate the DNA strands. Internal primers FIP and BIP then bind to their target regions to initiate the synthesis of complementary strands, forming a dumbbell-shaped DNA structure. This structure serves as a template for subsequent amplification cycles. Loop primers LoopF and LoopB promote the formation of intermediate structures, further amplifying the DNA. Continuous DNA synthesis produces multiple loops from the dumbbell-like DNA with a characteristic cauliflower-like structure. Primer recognition

sites are colour-coded for different primers used in LAMP assay. Red is for displacement primers, green is for internal primers, and blue is for loop primers (Image Source: Hardinge and Murray, 2019).

1.5.3. RT-RPA for POC Diagnostics

RT-RPA is considered one of the most promising candidates for point-of-care testing (POCT). This is because it uses very low incubation temperatures (37-42°C) and can detect single copies of DNA and smaller amounts of RNA from diverse species in a 10-minute reaction time with no prior nucleic acid purification (Piepenburg et al., 2006, Kalsi et al., 2015; James and Macdonald, 2015). It does not require any thermal or chemical melting, eliminating the use of sophisticated equipment like thermocyclers. The RPA products can be visualised through agarose gel electrophoresis (Piepenburg et al., 2006) or LFD detection (Jaroenram and Owens, 2014). Real-time detection of RPA products is possible by adding a specific probe, such as TwistAmp® exo probe, which is associated with real-time fluorescence detection using a real-time PCR machine (Euler et al., 2012).

Three core enzymes form the backbone of the RPA technology: recombinase, a single-stranded DNA-binding protein (SSB), and a DNA polymerase with strand displacement activity (Li et al., 2019). First, the recombinase and a loading factor bind an oligonucleotide primer while scanning the duplex DNA for complementary sequences. The recombinase complex then inserts these primers into the DNA via strand exchange, forming a D-loop structure in an ATP-dependent reaction and unwinding the DNA's helical structure. The SSB binds to the displaced strand, stabilising the primers, which initiates DNA synthesis by the strand-displacing DNA polymerase at the binding site. The parental strand is displaced, and elongation continues until two new duplexes are formed (**Figure 4**).

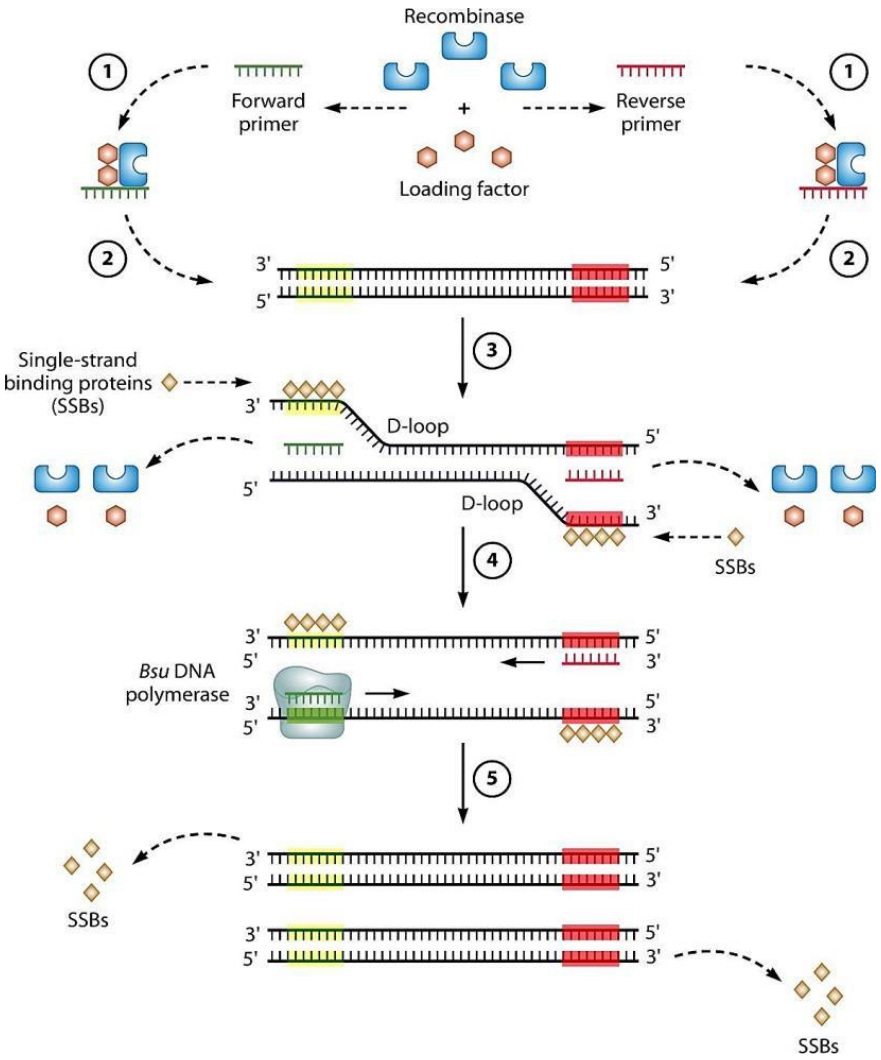

Figure 4. Schematic representation of RPA mechanism.

Firstly, recombinase proteins bind to forward and reverse primers with the assistance sequences of a loading factor to form recombinase-primer complexes. These complexes check the DNA for complementary target sequences, ensuring precise strand invasion. Secondly, the complexes promote strand invasion upon recognising complementary target sequences in the template DNA. The strand-displacement activity of the recombinase displaces the complementary DNA strand, forming a D-loop structure. Thirdly, SSBs bind and stabilise the displaced DNA strand, avoiding reannealing and retaining the D-loop structure. Lastly, *Bsu* DNA polymerase binds to the 3' end of the forward and reverse primers to initiate DNA synthesis. Finally, the continuous displacement and extension of the newly synthesised DNA produce amplified products. SSBs are released during the process to maintain repeated cycles of amplification (Image Source: Lobato and O`Sullivan, 2018).

In addition to its simplicity and speed, RT-RPA is increasingly considered a more efficient and environmentally friendly alternative to RT-qPCR for viral diagnostics, particularly in decentralised and low-resource settings. Unlike RT-qPCR, which requires thermocycling between 50–95°C for 1.5 to 2 hours and consumes approximately 0.4–0.8 kWh per run, RT-RPA operates isothermally at 37–42°C and typically completes amplification within 20–30 minutes, using less than 0.1 kWh under optimised conditions (Yu et al., 2021). Therefore, the reduced energy requirements, elimination of complex thermal cyclers, and compatibility with minimal laboratory infrastructure support its potential as a low-footprint diagnostic method. The environmental benefits are further reinforced by its reduced reliance on cold-chain storage, lower reagent volumes, and compatibility with portable detection formats such as lateral flow dipsticks, which minimises plastic waste associated with qPCR cartridge-based systems (Bellassai et al., 2025; Sritong et al., 2023; Edoardo Ongaro et al., 2022).

1.6. RPA Operating Parameters

1.6.1. Primer Design

Even though it was initially thought that specific RPA primers (30-35bp) were required for the reactions, PCR primers (18-23bp) were later confirmed to work just fine in many cases to achieve efficient amplification (Yamanaka et al., 2017). Longer primers can be used in RPA; however, they may cause the formation of secondary structures, leading to potential primer artefacts. Therefore, primers longer than 45bp are not recommended. Avoiding too many guanines at the 5’ end is suggested; however, using cytidines can be beneficial. Both guanines and cytidines at the 3’ end tend to improve the performance. A GC content is required to be <30% or >70% as they help with the stability of the primer due to having stronger hydrogen bonds than AT. Having too many repeating G or C bases can cause primer-dimer formation. RPA can amplify sequences up to 1kb; however, it works better with shorter amplicons in the range of 80-400bp (100-200bp optimal) (Piepenburg et al., 2006). There are no melting temperature requirements for

RPA primers and probes as the primer annealing and elongation are enzyme-mediated and not temperature-driven (Daher et al., 2016).

1.6.2. Temperature

RPA reactions can occur at temperatures from 22 to 45°C, and it does not need precise control of temperature (Kersting et al., 2014; Lillis et al., 2014; Chandu et al., 2016). According to the most published reports, temperatures from 37 to 42°C were optimal for RPA reactions. Incubators, heating blocks and chemical heaters can be used to adjust the reaction temperature (Lillis et al., 2014).

1.6.3. Effect of Crowding Agent and Mixing

Crowding agents, such as polyethylene glycol and ficoll, affect the way that a chemical process works in RPA reactions (Alfano et al., 2024). It stops the recombinase-primer complex from falling apart on its own when SSBs are present for the amplification. The crowding agent does not work well with RPA reactions and low target copy levels. This happens as it becomes thick and slows down the movement of the chemicals in the reaction, prolonging the amplification process. In order to eliminate this problem, a mixing step can be included 5 min after initiating the RPA reaction. On the other hand, mixing can be replaced by reducing the total volume of the reaction mixture to 5ul (Lillis et al., 2016). Alternatively, the reaction solution can be mixed continuously. This method uses a special setup called an active matrix for electrowetting-on-dielectric, which provides constant mixing of 270nL or 750nL of the RPA mixture. Therefore, the sensitivity of this assay can be improved by 100 times compared to the regular benchtop assay (Kalsi et al., 2015).

1.6.4. Incubation Time

Number of initial DNA copies determines the time required to amplify the DNA to

detectable levels. Amplification time is typically around 20 min, although <5 min has been observed (Xia et al., 2014). Long incubation times are not preferred as the recombinase enzyme consumes all the available ATP during solution phase RPA within 25 min.

1.6.5. Sample Types

RPA can be used to amplify various types of DNA, including double-stranded DNA, single-stranded DNA, methylated DNA (Wee et al., 2015), and the cDNA generated through RT of RNA or micro-RNA (miRNA) (Wee and Trau, 2016). RPA can target multiple different organisms, such as bacteria, viruses, protozoa, fungi, animals, and plants. Samples from these targets can be provided by cultured microorganisms, body fluids (e.g. urine, sputum, blood, plasma, saliva, nasal, vaginal, and anal swabs), surgical biopsy specimens, organ tissues (e.g. skin, lymphatic nodes, liver, lungs, stomach, kidney), as well as animal and plant products (e.g. eggs, shrimps, rice, milk, fruit). Alternatively, special microfluidic devices that use one-step digital plasma separation and autonomous parallel separation can be combined with RPA to amplify nucleic acids (Yeh and Lee, 2013). Scientists have also developed a valveless microfluidic chip and an isotachophoresis chip, which were respectively designed to pre-concentrate bacteria in urine by using anion exchange magnetic beads (Valiadi et al., 2016) and to extract DNA from the blood samples before using RPA (Eid and Santiago, 2017).

RPA can also detect non-nucleic acid targets by using aptamers as RPA templates. The first example was an aptamer-based bio-barcode assay (Loo et al., 2013). An aptamer is a short single-stranded nucleic acid sequence that can bind to a target molecule with high affinity and specificity. This assay uses magnetic beads labelled with capturing antibodies and aptamers in a solution that is selective for different epitopes of the same target. When a target is present in the solution, a large complex of magnetic beads, antibodies, target, and aptamer forms. This complex is captured by magnets, the solution is removed, and the bound aptamers are amplified using RPA and detected by

fluorescence. Another example involves the immobilisation of β-conglutin on magnetic beads, where the aptamers attached to the target on the magnetic beads are eluted after a competition assay. Then, the aptamers are amplified by RPA, followed by fluorescence (Jauset-Rubio et al., 2017) or LFD detection (Wee et al., 2015).

1.6.6. Solid Phase RPA

Amplification using RPA can be executed in two different ways; it can either happen in solution, with both primers in the liquid, or on a solid surface, when one primer is immobilised, and the other is in the liquid. A more challenging version of the latter is known as the bridge amplification, where both forward and reverse primers are immobilised on a surface. Fortunately, most studies on RPA focus on solution-phase amplification (Daher et al., 2016; James and Macdonald, 2015). In the solution-phase method, the amplification process is faster, and the limit of detection is better. This is because the primers and other reagents can move freely in the solution, increasing the reaction kinetics. Even though the solid-phase method is not as efficient as the liquid one, it allows multiplexed or combined amplification with various other techniques, such as ring resonators (Shin et al., 2013; Sabaté del Rio et al., 2015; Shin et al., 2015), electrochemical (De La Escosura-Muñiz et al., 2016; Lau et al., 2017; Koo et al., 2016), and colourimetric detection (Yamanaka et al., 2017; Santiago-Felipe et al., 2014; Liu et al., 2016). Scientists have tried to reduce the amplification time and improve the limit of detection in the solid-phase method by adjusting the surface chemistry of the immobilised primers by adding vertical and horizontal spacers to increase primer accessibility (Sabaté del Rio et al., 2017). Alternatively, they could transfer the immobilised primer into a liquid, which is a method known as hemi-nested asymmetric solid-phase amplification (Tortajada-Genaro et al., 2015; Santiago-Felipe et al., 2014; Kunze et al., 2016).

1.6.7. Presence of Inhibitors

RPA can work efficiently in serum and even in the presence of substances that typically interfere with the PCR, known as PCR inhibitors, such as haemoglobin, ethanol, and heparin (Kersting et al., 2014). However, RPA can become less effective when high genomic DNA concentrations (20-100ng/uL) exist in the blood samples. This problem can be eliminated by enriching the target DNA before the amplification process (Rohrman and Richards-Kortum, 2015) or heating the DNA extract from blood or swab samples with Trizol and VL buffer before centrifugation (Yang et al., 2016). RPA can also effectively work in urine (Krõlov et al., 2014), pleural fluids (Liljander et al., 2015), seed powders (Chandu et al., 2016), milk (Choi et al., 2016), and stool samples (Wu et al., 2016). This amplification process only requires heat lysis, direct lysis with nuclease-free water, or using a specific PCR buffer called EzWay Direct PCR buffer (Choi et al., 2016). Unfortunately, an issue was identified with the urine samples. If the urine concentration is higher than 10% and there is only a tiny amount of target DNA (100fg) in the sample, there is a possibility of no amplification. This inhibition does not occur when the target DNA concentration is increased (10pg) with 10% urine (Rosser et al., 2015). RPA can amplify DNA from crude extracts, while PCR cannot. Even though RPA pellets are more expensive than PCR reagents, less sample preparation before amplification makes the overall assay simpler and more cost-effective (Londoño et al., 2016).

1.6.8. Multiplexing

RPA can detect multiple DNA targets from the same solution, which is highly dependent on target sequences, amplicon size, and primer design (Kersting et al., 2014). Optimisation of primer sets, probe ratios and concentrations are essential for each multiplexing assay. Lack of optimisation can cause competition between primers for the recombinase, suppressing a reaction (Kim and Lee, 2016). Examples of successful multiplexing with RPA include detecting different Methicillin-resistant *Staphylococcus aureus* (MRSA) alleles (Piepenburg et al., 2006), a fluorescent duplex RPA assay for Staphylococcal Cassette Chromosome mec (Hill-Cawthorne et al., 2016), and a real-

time fluorescent duplex RPA assay in chicken products (Kim and Lee, 2016). Solid-phase amplification and fluorescence detection were also used for three bacterial pathogens (Kersting et al., 2014). A similar study used solid-phase amplification and chemiluminescence detection for human viruses and bacteria (Kunze et al., 2016). Other examples include duplex RPA for cancer genotyping with Surface Enhanced Raman Spectroscopy (SERS) detection (Wang et al., 2017) and triplex RPA for identifying plant pathogens with SERS nanotags and modified primers (Lau et al., 2016).

1.6.9. Storage

Reagents required for the RPA are available in the kits, including pellets, rehydration buffer, and magnesium acetate (MgOAc). MgOAc is the reaction initiator, so it is not found in the rehydration buffer and is provided separately. Pellets can stay intact for a year or more when they are stored in the freezer (< −15°C), fridge (2-8°C) or at room temperature for up to 6 months (22-28°C) (Chandu et al., 2016). It was reported that some scientists made their pellets, including primers, components in the rehydration buffer and the MgOAc. These pellets are the most effective when stored at −20°C for optimum sensitivity. Reconstituted solutions can be stored at 4°C; however, they have a 10-fold less limit of detection when compared with fresh solutions. It is not a good idea to store homemade pellets at 37°C as they can break down and inhibit amplification (Liljander et al., 2015).

1.6.10. Specificity

RPA is very specific in most cases, providing 100% specificity for detecting DNA sequences. This means it can detect those target sequences with 100% accuracy, strongly depending on careful assay design, including primer and probe selection (Lobato and O'Sullivan, 2018). RPA is also sensitive to mismatches in closely related DNA sequences. One or more mismatches in certain positions may not be differentiated but having more than one mismatch at the 3' end of primers or 3 mismatches at the 5'

and 3’ ends can inhibit or reduce amplification (Daher et al., 2015). Although this mismatch tolerance may limit the use of specific RPA primers, it can also help determine the presence of emerging pathogens without the need to distinguish them from the wild-type (Boyle et al., 2013). An example could be a method developed to detect different strains of HIV-1, with 9 mismatches across the primer and probe binding sites being tolerated by RPA. This mismatch tolerance may cause cross-reactivity, which was reported in a study where the RPA assay was developed to detect different genotypes of the Chikungunya virus. Due to having 4-7 mismatches in the primers, the cross-reactivity of the Chikungunya virus with another alphavirus named O’nyong’nyong was reported (Patel et al., 2016). An alternative approach would be using shorter primers (19-21mer) to reduce the binding stability between the primers and the target DNA. This increases the ability of the method to specifically detect single nucleotide polymorphisms (SNPs) when a mismatch at the 3’ end of the primer was included.

1.7. Detection of RPA Amplicons

1.7.1. End-point Detection

Several detection methods can be used post-amplification to identify the presence or absence of a target nucleic acid. End-point detection typically requires less equipment than real-time detection, reducing the cost of the experiment and making it more suitable for settings with limited resources. The most well-known end-point detection for RPA relies on LFD assays, where the results can be observed quickly. A primer set consisting of forward and reverse primers, a probe, and the TwistAmp® nfo kit are commonly used for assay designs to carry out LFD detection. The probe is recommended to be 46-52bp long and is modified at the 5’ end with an antigenic label at the 3’ end. Carboxyfluorescein group (FAM) is primarily used as an antigenic label, along with other labels like Alexa fluor488 or DIG (Crannell et al., 2016). Tetrahydrofuran (THF) is an abasic nucleotide that replaces a conventional nucleotide. This is also known as dSpacer, which is positioned at least 30 nucleotides away from

the 5’ end and 15 nucleotides away from the 3’ end of the probe. When the probe with dSpacer forms double-stranded DNA, dSpacer gets cleaved by nfo nuclease. This forms a new 3’ hydroxyl group in the probe, transforming it into a primer. Along with the probe, an opposing amplification primer labelled at the 5’ end with another label, such as biotin, is required. All reactions using RPA followed by LFD detection were performed in less than an hour, succeeding a limit of detection as low as 1-10 DNA copies. Alternatively, tailed primers can produce double-tailed amplicons for LFD assays. Tailed primers contain a carbon stopper to produce double-stranded DNA bound by single-stranded tails. Gold nanoparticles (AuNPs) were used as reporter probes. Meanwhile, oligonucleotides were used as capture probes in the test and control lines, replacing the traditional antigen label and antibody capture method to reduce the cost (Jauset-Rubio et al., 2016).

Bridge flocculation assay is an equipment-free assay that allows binary naked-eye visualisation, meaning the outcome is either a clear positive or negative. Because it does not require specialised laboratory equipment, it is appropriate for settings with limited resources. This assay is based on the reversible flocculation of carboxyl-functionalised magnetic beads, which is affected by salt concentration, pH, and the length of DNA. The DNA length is required to be 100bp at the least for the cross-linking process to occur. This allows the amplicons to be easily distinguished from the primers. To perform this assay, a solution containing magnetic beads is added to the amplification products. After an ethanol wash step, the beads are re-suspended in a low-pH buffer. If the beads remain flocculated, it indicates a positive outcome (Wee et al., 2015).

Colourimetric detection can also be combined with RPA, which allows the visualisation and quantification of the target based on a colour change. In this method, primers or dNTPs are modified with biotin, which results in the production of labelled amplicons during the RPA. Streptavidin-HRP is added post-amplification, which has a strong affinity for biotin, so it binds to the biotin-labelled amplicons. A colour change occurs once adding 3,3’, 5,5’-Tetramethylbenzidine (TMB) and hydrogen peroxide (H_2O_2). The intensity of the colour change corresponds to the concentration of the amplicons produced.

Fluorescence detection can also be implemented with RPA, which allows the

simultaneous detection of multiple DNA targets via multiplexing. This can be achieved by immobilising forward primers onto array spots and modifying the reverse primers by adding a fluorophore. Once the RPA process is completed, amplicons can be visualised using a laser scanner.

Sometimes, Quantum Dot (QD) barcodes may be used instead of traditional fluorophores to allow multiplexed fluorescence detection. In this process, polystyrene beads are loaded with different types of QDs, where the barcodes are specific for each target. The beads were placed on microfabricated slides, and a smartphone was used to detect the location of each barcode. Following RPA, a single-stranded DNA is produced and sandwiched between the barcode and an Alexa Fluor 647-labelled reporter probe. The fluorescent signal is then measured with the smartphone (Kim et al., 2016). Electrochemical transduction is another method that can be used to detect RPA products via capturing single-stranded DNA generated from the amplicon between a surface-immobilised complementary probe and an enzyme-labelled reporter probe. A different approach involves using forward primers labelled with magnetic beads and reverse primers labelled with AuNPs. Amplicon is captured by a magnet embedded in a working electrode, and the AuNPs are detected through electrocatalytic hydrogen evolution (De La Escosura-Muñiz et al., 2016).

1.7.2. Real-time Detection

Fluorescent probes and fluorimeters can be used for the real-time DNA quantification of RPA. The most common fluorimeters include the ESE Quant Tube scanner device (Qiagen), Genie III (OptiGene), and Twista (TwistDx), which are portable and rechargeable. These fluorimeters can be placed in lab-in-a-suitcase or diagnostics-in-a-suitcase (Mondal et al., 2016; Abd El Wahed et al., 2015), making them easily accessible to perform RPA in a field setting. Although non-specific intercalating fluorophores like SYBR Green (Piepenburg et al., 2006) or Eva Green (Loo et al., 2013) can be used for real-time detection, these are likely to cause false positives as they cannot distinguish between amplicons and primer-dimer artefacts. To eliminate this problem, specific probes like exo and fpg probes can be used. Probes used for the PCR,

like Taq-Man, are not suitable for RPA due to Taq-Man polymerases digesting the displaced strand during the strand displacing process, inhibiting DNA amplification.

The exo probe is an oligonucleotide complementary to the target amplicon and blocked at the 3′ end to prevent elongation. It contains a fluorophore and a quencher positioned on bases flanking a tetrahydrofuran (THF) residue, typically separated by 2–5 nucleotides. When the probe is unbound in solution, the quencher suppresses the fluorophore signal. Upon hybridisation to the complementary DNA target, the DNA repair enzyme E. coli endonuclease IV (nfo) recognises the THF site and cleaves the probe, generating two fragments. This cleavage separates the fluorophore from the quencher, releasing a detectable fluorescent signal (Lobato and O'Sullivan, 2018).

The fpg probe is an oligonucleotide with a part matching the target amplicon blocked at the 3' end. It contains a quencher and a fluorophore, which have 4-5 bases (7 at maximum) between them within the nucleotide sequence. The quencher is placed at the 5' end of the probe, while the fluorophore is bound to an abasic nucleotide, known as the dR group. When there is no target, the fluorophore signal will be quenched. When the fpg probe is annealed to the complementary DNA target, the fpg enzyme cuts the probe at the dR position to generate two fragments. This separates the fluorophore from the quencher to release fluorescence (Lobato and O'Sullivan, 2018).

Real-time assays are typically carried out in Eppendorf tubes. A different approach involves the use of the SlipChip platform for RPA. This chip is made up of clamped plates containing three separate lanes to load samples, RPA master mix, and MgOAc. Once each lane is loaded, the plates move to let the components mix, allowing amplification in real-time (Tsaloglou et al., 2015).

Another approach referred to as a digital microfluidic platform, has been studied for real-time detection, which is based on an active matrix electrowetting-on-dielectric. This platform includes 16,800 electrodes that can be controlled independently to manipulate several droplets of around 45nL. This causes the continuous movement and heating of the droplets to provide a better detection limit than the benchtop assays (Kalsi et al., 2015).

Additionally, ligation-based assays can be combined with RPA to detect mRNA. Right- hand and left-hand side ligation probes are designed to have universal reverse and forward-specific sequences included at either side of the ligation site. Probes are amplified once the ligation has occurred, and the signal is produced by the SYTOQ fluorescent dye. This technique allows simultaneous detection of three targets in an hour (Koo et al., 2017).

1.8. Combination with Other Isothermal Amplification Techniques

Combination of RPA with generic multiplex LFD detection (**Figure 5**) is useful due to being very rapid and easy solution for field-amenable low-resource nucleic acid testing (Piepenburg et al., 2006; Kersting et al., 2014; Mekuria et al., 2014; Crannel et al., 2015; Chao et al., 2015; Rosser et al., 2015; Yang et al., 2016; Yang et al., 2017). LFDs are easy to carry around and easy to interpret. This combination of technologies will provide more efficient infectious disease diagnosis against the increased number of biomarkers (Rusling et al., 2010) due to higher information density, reducing the false positive or negative reporting in cases. This will also reduce diagnostic time and costs as there will not be a need to perform multiple single tests. If this combination of technologies can be applied to low- and middle-income countries, it will reduce community transmission while increasing the testing capacity, particularly in resource-limited settings (Sheridan, 2020). Even though the benefits mostly outweigh the limitations, there is a significant drawback of the standard LFDs. They only allow a single target within a single reaction tube without using probes or primer sets. This type of detection is known as singleplex detection, which may cause insufficient disease diagnosis in the simultaneous detection of multiple viral targets. This type of detection is known as multiplex detection, which strictly uses specific primer sets and probes labelled with distinct fluorophores.

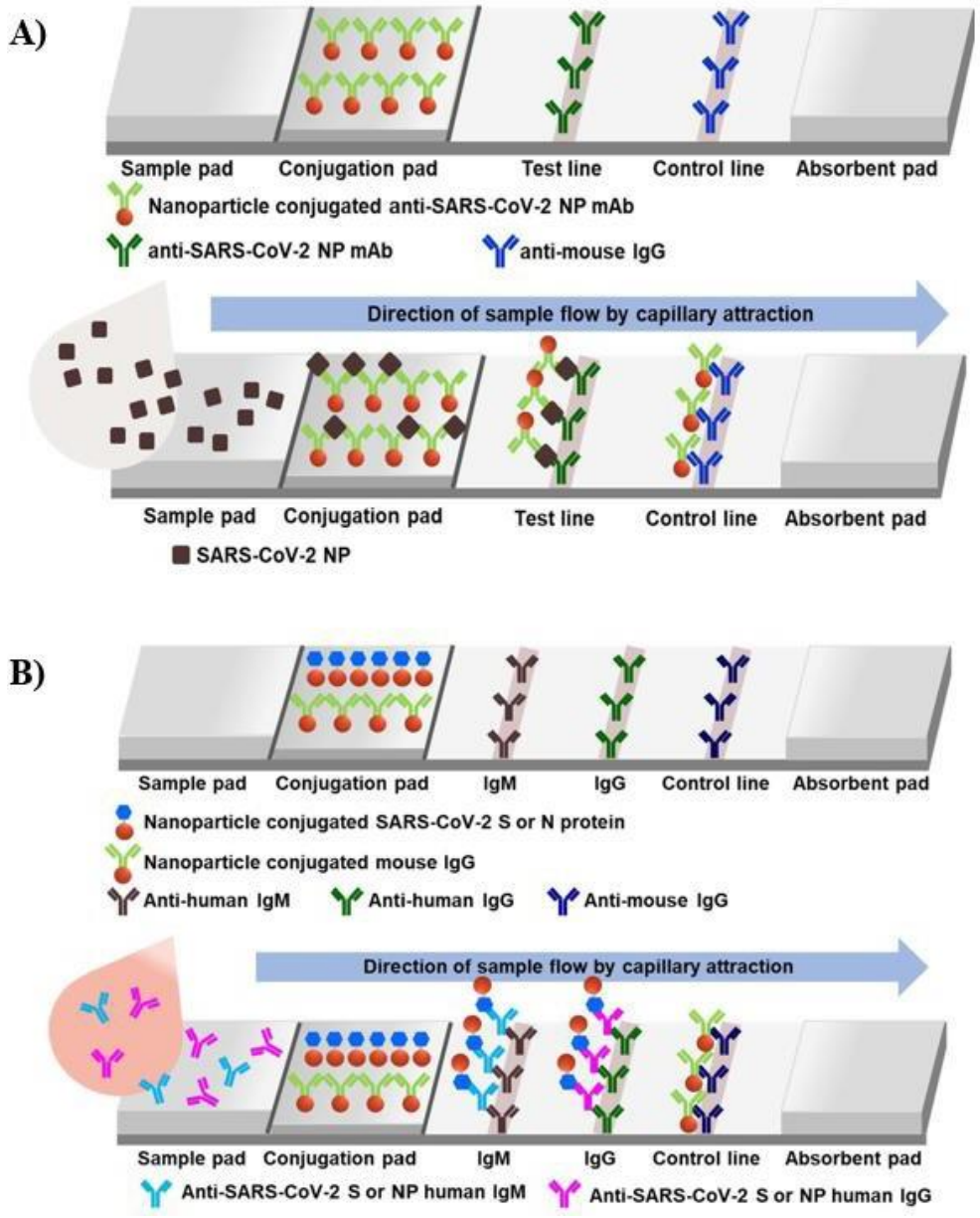

Figure 5. Mechanism of lateral flow assay for SARS-CoV-2 detection.

(A) Lateral flow assay of SARS-CoV-2 antigen detection: The conjugation pad is preloaded with anti-SARS-CoV-2 nucleoprotein (NP) monoclonal antibodies conjugated with AuNPs. When a sample containing SARS-CoV-2 NP is applied to the sample pad, the NP binds to the AuNP-conjugated antibodies to form complexes, which then travel via capillary flow until they reach the absorbent pad. At the test line, immobilised anti-SARS-CoV-2 NP monoclonal antibodies will capture the NP-antibody complexes to produce a visible signal. The control line has immobilised anti-mouse IgGs, which bind excess AuNP-conjugated antibodies to confirm the assay's validity. **(B)** Lateral flow assay of SARS-CoV-2 antibody detection: A sample

containing SARS-CoV-2 specific IgM or IgG antibodies is applied to the sample pad, which travels through the conjugation pad containing AuNP-conjugated SARS-CoV-2 spike (S) or NP proteins and AuNP-conjugated mouse IgG for control validation. The antibodies in the sample bind to the S or NP antigens to form antigen-antibody complexes. The IgM test line captures antigen-IgM complexes, while the IgG test line captures antigen-IgG complexes, generating visible signals that indicate a positive test result. A signal at the IgM test line indicates a recent or active infection, whereas a signal at the IgG test line indicates prior exposure or developed immune response. Signals at both test lines confirm the presence of both antibodies, suggesting a transition phase (Image Source: Hwang et al., 2021).

Multiplex LFDs perform through accumulation of lines and dots incorporated within one device, where a single line or dot represents the detection of a single analyte (Tian et al., 2014; Blažková et al., 2009; Noguera et al., 2011; Lattanzio et al., 2012; Kolosova et al., 2007; Shim et al., 2009; Huang et al., 2012; Xu et al., 2014). This technology was recently combined with RPA to increase the detection capacity of an assay (Crannell et al., 2016), which is still limited due to a decrease in distance from the conjugate pad based on reduced flow rate. This causes possible inaccurate interpretation due to the overaccumulation of lines and dots incorporated. There is a solution to eliminate this problem where the LFD technology is combined with another technology named binary and molecular encoding (**Figure 6**). Binary encoding involves the presence or absence of sensor output, like on/off or 1/0 (Poje et al., 2014); meanwhile, molecular encoding is about using various molecular labels. These two methods merge to produce a barcode- like identification (Li and Macdonald, 2016). This whole process enhances the multiplex detection capacity by providing a 7-segment display output that is very easy to interpret without requiring any expertise (Li and Macdonald, 2016).

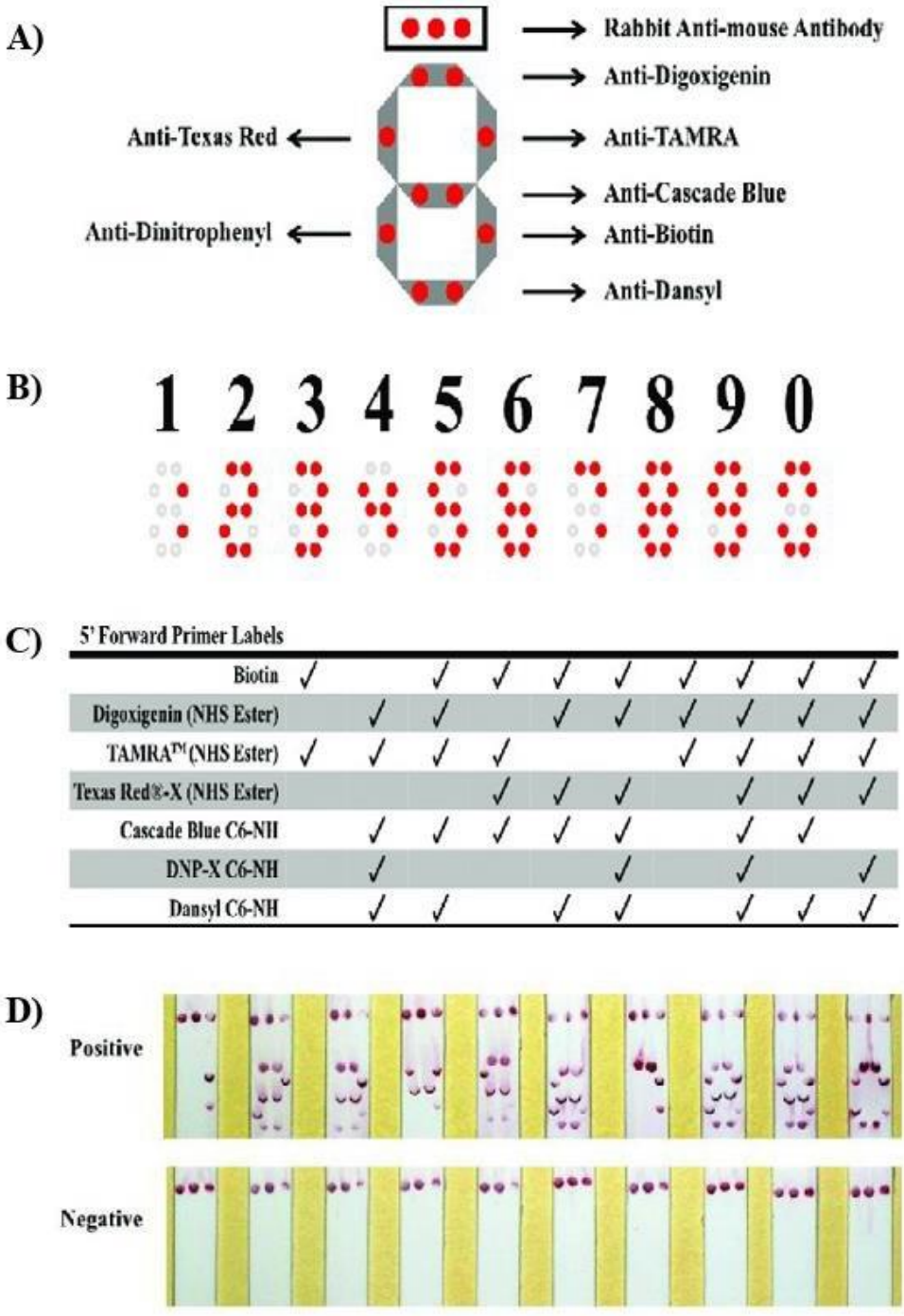

Figure 6. Molecular colourimetric 7-segment display for multiplex detection of primer labels.

(A) Detection antibodies are positioned to generate a 7-segment display to detect various 5' primer labels. Red dots on these segments represent captured targets, detected by their respective antibodies to generate a visible colourimetric signal. **(B)** Colourimetric signals are arranged in the 7 segments of the display, where each number corresponds to a specific combination of primer labels to allow multiplex detection. **(C)** A set of 5' forward primer labels

are listed on the table. Checkmarks indicate the successful detection of each label, confirming specificity and compatibility with the display format. **(D)** Photographic results of the 7-segment display show positive samples that produced visible signals and generated unique numerical patterns corresponding to the detected primer labels; meanwhile, negative results showed no colourimetric signal, validating the assay's specificity. (Image Source: Li and Macdonald, 2016).

1.8.1. RPA Combined with Ligase-based Technology

Ligase-based technologies have been used for many years for gene rearrangement and SNP detection (Albrecht et al., 2013; Ruiz et al., 2020), even though they have never been used for RNA detection. This is because the ligase-based technologies have low amplification efficiency associated with the slightly inefficient RNA templates, causing low sensitivity of detection (Nilsson et al., 2001; Bullard and Bowater, 2006; Lohman et al., 2014). However, this issue can be avoided using a high concentration of T4 DNA ligase, which will enhance the RPA sensitivity. On the other hand, a high-quality RNA template is essential for the RT procedure since the RNA is prone to degradation by environmental ribonucleases (RNases). Therefore, the RNA samples must be prepared with extra care to prevent RNase contamination. Otherwise, there will be a significant chance of having false negatives when conditions do not meet the requirements for preparing RT templates. In ligase-based RPA assay, selected probes have a complementary region to the RNA biomarker and an amplification arm to promote RPA (**Figure 7**). The probe set will bind to the biomarker to be ligated into a single-stranded DNA fragment via T4 DNA ligase when the viral RNA is present. The DNA fragment produced is ready to be amplified through RPA reactions, forming an amplification signal that can be observed in real-time using a fluorescent dye, such as SYBR Green I, in less than 30 min with no sophisticated thermocycling equipment.

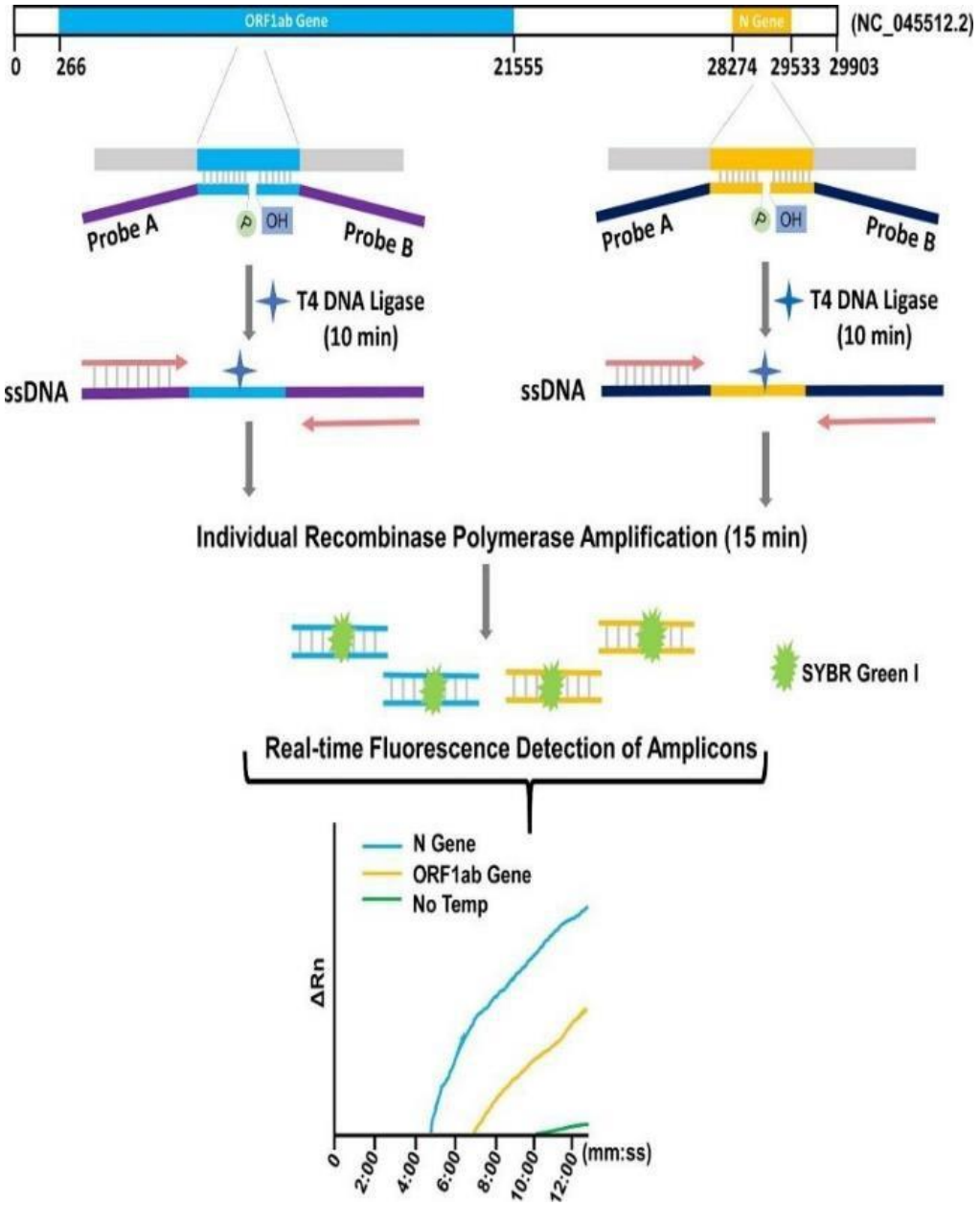

Figure 7. Workflow of ligase-based RPA assay with real-time fluorescence detection.

This assay is also known as probe-based RPA assay, which is used to detect SARS-CoV-2-specific open reading frame 1ab (ORF1ab) and N genes. For each target, two probes (Probe A and B) are designed with annealing portions (blue and yellow bars) complementary to the target biomarkers. These probes also include artificial amplification arms (purple and dark blue bars) that extend beyond the annealing portions to allow downstream amplification. The annealing portions of the probes make them bind adjacent regions of the single-stranded DNA. T4 DNA ligase seals the gap between Probe A and B to generate a continuous DNA template in a 10-min ligation reaction. The ligated DNA template, which contains both the target-specific annealing

portions and artificial amplification arms, is ready to be amplified by RPA in a 15-min reaction. During this reaction, the artificial amplification arms facilitate the rapid replication of the ligated templates. SYBR Green I is added to the double-stranded amplicons to allow real-time fluorescence detection. The fluorescence detection curve shows the real-time amplification of the target genes. Both genes produced distinct amplification curves. The negative control without the template, indicated by the green curve, did not show any amplification as expected (Image Source: Wang et al., 2021).

1.8.2. RPA Combined with CRISPR/Cas Technology

Bacteria and archaea use CRISPR/Cas as an adaptive immune system to eliminate their risk of infection by phages, viruses, and other foreign genetic elements (Deveau et al., 2010; Horvath and Barrangou, 2010). It consists of CRISPR repeat-spacer arrays transcribed into CRISPR RNA (crRNA) and trans-activating CRISPR RNA (tracrRNA), as well as CRISPR-associated (Cas) genes which encode Cas proteins with endonuclease activity (Koonin and Makarova, 2009). When these prokaryotes are faced with an infection, Cas proteins cut foreign DNA into short fragments, which are then integrated into the CRISPR array as new spacers (Makarova et al., 2011). Upon subsequent infection by the same invader, crRNA will recognise and pair with the foreign DNA, guiding the Cas protein to cut target sequences of the same DNA. CRISPR-Cas systems can be divided into 2 classes (Class 1 and Class 2), 6 types (I to VI) and several subtypes. Class 1 systems (Type I, III, and IV) consist of multi-Cas protein effector complexes, whereas Class 2 systems (Type II, V, and VI) consist of a single effector protein (Koonin et al., 2017; Jiang and Doudna, 2017). Type II CRISPR/Cas9 system is mainly acquired from *Streptococcus pyogenes* (SpCas9) (Jiang and Doudna, 2017; Mali et al., 2013). The main components of the CRISPR/Cas9 system include the RNA-guided Cas9 endonuclease and a single-guide RNA (sgRNA) (Ran et al., 2013). Cas9 has two main nuclease domains, HNH and RuvC, each cleaving one strand of the target double-stranded DNA (Chen et al., 2014). The Cas9 nuclease combines with sgRNA to produce Cas9 ribonucleoprotein (RNP), which can bind and cleave the DNA target (Jinek et al., 2012). The binding ability of Cas9 RNP to target

DNA is promoted by a protospacer adjacent motif (PAM) sequence (Ran et al., 2013). During genome editing, sgRNA recruits Cas9 endonuclease to a specific genome site, inducing a double-stranded break (DSB) that is repaired either by error-prone non-homologous end joining (NHEJ) pathway or homology-directed repair (HDR) pathway (Ceccaldi et al., 2016). NHEJ can cause random insertions or deletions within the cleavage sites, resulting in frameshift mutations or premature stop codons within the ORF of the target genes (Weterings and Chen, 2008; Lieber, 2010).

Gootenberg *et al.* developed the SHERLOCK (Specific High Sensitivity Enzymatic Reporter UnLOCKing) nucleic acid detection platform based on Cas13a, crRNA, and fluorescent RPA reporters (Gootenberg et al., 2017) (**Figure 8**). Upon recognition and cleavage of the target RNA, Cas13a cuts the reporter RNA to release a fluorescent signal, allowing detection. This method has been used previously to detect viruses, differentiate pathogenic bacteria, genotype human DNA, and identify tumour DNA mutations (Li et al., 2019). The SHERLOCK system was later improved and renamed SHERLOCKv2, which could detect four different viruses simultaneously (Gootenberg et al., 2018).

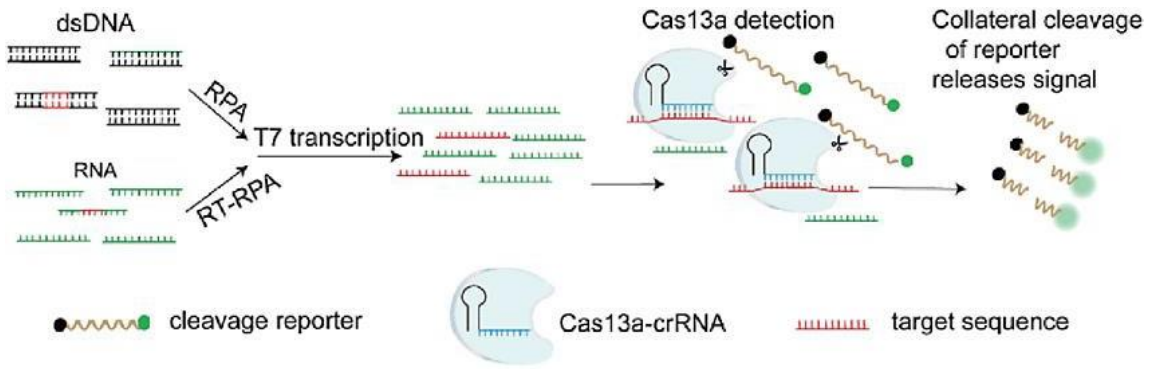

Figure 8. Schematic diagram of the SHERLOCK detection platform.

SHERLOCK detection platform uses RPA, T7 transcription, and CRISPR-Cas13a-mediated RNA cleavage for nucleic acid detection. Double-stranded DNA or RNA can be used as a template for RPA reactions. RPA can directly amplify the double-stranded DNA target, whereas RT is required for RNA targets to produce cDNA that is later amplified by RPA. The amplified DNA is subsequently transcribed into RNA via T7 RNA polymerase to generate multiple RNA copies of the target sequence. The transcribed RNA is ready to undergo CRISPR-Cas13a

detection. Cas13a is guided by a crRNA specifically designed to recognise the target RNA sequence. Once Cas13a is bound to its target, it becomes activated and begins collateral cleavage of nearby RNA molecules. The activated Cas13a cleaves single-stranded RNA reporters (synthetically designed RNA molecules) with a fluorophore and quencher. The quencher of the reporter suppresses the fluorophore when there is no Cas13a cleavage. Once the reporter cleavage occurs, the fluorophore and quencher separate to emit a detectable fluorescent signal. The intensity of the signal corresponds to the amount of the target nucleic acid present (Image Source: Yin et al., 2021).

In addition to Cas13 enzymes, Cas12 enzymes also exhibit collateral cleavage activity (Zetsche et al., 2015). Chen *et al*. introduced DETECTR (DNA endonuclease targeted CRISPR *trans* reporter) nucleic acid detection platform based on Cas12a, also known as Cpf1 (Chen et al., 2018) (**Figure 9**). This system has been previously used to detect cervical cancer-associated HPV subtypes (HPV16 and HPV18) in human cell lines or clinical patient samples. CRISPR-based molecular diagnostic methods provide higher sensitivity and single-base specificity, cost-effectiveness, simplicity, and suitability for field detection than traditional molecular diagnostic methods (Li et al., 2019; Chertow, 2018). Currently, several companies are working on developing CRISPR diagnostic kits for home use, targeting certain diseases like rabies, HIV and *Toxoplasma gondii*.

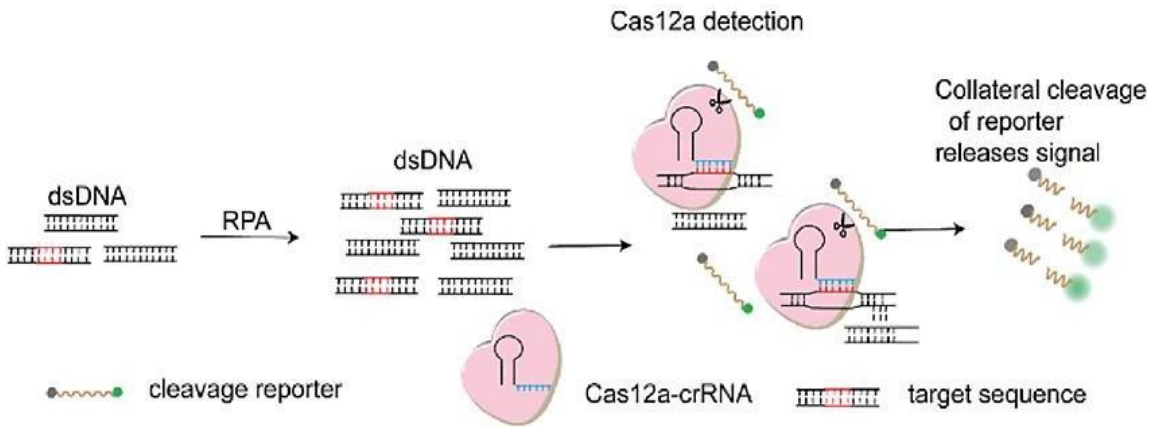

Figure 9. Schematic diagram of the DETECTR detection platform.

DETECTR detection platform uses RPA and CRISPR-Cas12a-based system to detect double-stranded DNA targets. RPA can directly amplify the DNA target to produce

multiple DNA copies of the target sequence. The amplified DNA is detected by Cas12a, which is guided by crRNA containing a spacer sequence complementary to the target DNA. Once Cas12a is bound to its target, it becomes activated and begins collateral cleavage activity of nearby DNA molecules. The activated Cas12a also cleaves double-stranded DNA reporters with a fluorophore and quencher linked together. Reporter cleavage separates the fluorophore from the quencher to emit a detectable fluorescence signal (Image Source: Yin et al., 2021).

1.9. Critical Evaluation of RT-RPA for Respiratory Virus Diagnostics

1.9.1. Research Gaps in Molecular Diagnostics for Respiratory Infections

Despite significant advancements in molecular diagnostics, substantial gaps remain in detecting respiratory viruses, particularly in decentralised and low-resource settings. The current gold standard, RT-qPCR, requires thermocycling instrumentation, trained personnel, and a stable power supply, making it impractical in many field and point-of-care (POC) contexts (Parida et al., 2008; Carter et al., 2020). Although multiple isothermal amplification methods exist, such as RT-LAMP, they often struggle with complex primer design requirements and reduced robustness in clinical applications. RPA has emerged as a promising alternative due to its low reaction temperature, tolerance to sample inhibitors, and minimal equipment requirements (Piepenburg et al., 2006). However, most existing RPA applications in respiratory virology have been limited to the detection of single viruses using synthetic or contrived samples. They also lacked rigorous comparative evaluation with established diagnostic platforms (Lillis et al., 2016; Wu et al., 2024). Respiratory infections are often caused by overlapping pathogens, resulting in co-infections that complicate clinical management (Almeida et al., 2022). In this case, a diagnostic approach with high sensitivity and applicability is required. Developing RT-RPA in this study specifically addresses these limitations by targeting multiple high-burden respiratory viruses and validating the assay using clinical and laboratory-generated RNA templates.

Doing so fills an important gap between laboratory assay development and the practical implementation of diagnostics for syndromic respiratory infections.

1.9.2. Innovations and Scope of the Present Study

Although RT-RPA has previously been used for pathogen detection, this study provides a distinct and comprehensive evaluation of its application for detecting respiratory viruses. It combines the design and validation of novel primer sets for multiple respiratory pathogens, including Influenza A and B, RSV-A and RSV-B, HPIVs, HRVs, hMPV, and hADV. It also uses TOPO TA cloning and in vitro transcription to produce synthetic RNA standards. This enabled standardised and controlled validation of the assay's performance. Unlike most published RT-RPA studies, which focus on single pathogens or rely on synthetic DNA templates (Lillis et al., 2016; Wang et al., 2020), this research evaluated a broad viral panel using both fluorescence-based and lateral flow formats. Using the same clinical sample set, a direct comparison was conducted with RT-qPCR, the clinical gold standard, and RT-LAMP, an established isothermal method.

Although this study could be partly classified as a comparative analysis, its range extends beyond simple benchmarking. It includes novel primer design for each virus, dual-modality detection systems, and assay validation against synthetic RNA and SARS-CoV-2-positive patient samples. The performance evaluation of RT-RPA comprised analytical sensitivity, specificity, time-to-result, and cross-reactivity, offering a robust and clinically relevant diagnostic characterisation. These features distinguish this research from conventional proof-of-concept or comparative studies, positioning it as a hybrid project that focuses on both the development of diagnostic methods and their practical implementation in decentralised healthcare settings (Parida et al., 2018; Lillis et al., 2016; Piepenburg et al., 2006).

1.9.3. Barriers to RT-RPA Clinical Adoption and Contribution to Present Study

RT-RPA offers significant advantages in pathogen detection, particularly in POC diagnostics, including rapid amplification at constant low temperatures, minimal equipment requirements, high sensitivity, and tolerance to sample inhibitors. Despite these benefits, RT-RPA has not yet been widely adopted in routine clinical practice. One of the significant limitations of this technique is the proprietary nature of the core enzymes and reagents, which are controlled by a limited number of manufacturers, such as TwistDx. This results in higher costs and restricted access to the supply chain, limiting large-scale implementation (Li et al., 2019). Additionally, regulatory approval processes have been slower for RPA-based assays compared to more established techniques, such as RT-qPCR, with only a few achieving CE marking or FDA authorisation. Moreover, multiplexing remains technically challenging due to the risk of primer cross-reactivity and non-specific amplification, particularly in lateral flow formats where visual interpretation can be subjective (Wu et al., 2024). There are further concerns about variability in reagent batches and a lack of standardised protocols for processing complex clinical samples, such as nasopharyngeal (NP) swabs, which undermines reproducibility (Daher et al., 2016). Despite these limitations, there is a growing desire to improve RPA technologies for decentralised diagnostics. This study contributes to that effort by addressing several key implementation barriers, such as assay optimisation for lateral flow readout, systematic clinical validation, and the development of synthetic RNA standards through TOPO TA cloning to ensure consistent performance evaluation.

1.9.4. Historical Evolution of Viral Diagnostic Methods

Viral diagnostics have undergone significant evolution over the past century, transitioning from morphology-based techniques to molecular diagnostics for the rapid and sensitive detection of viruses. Early diagnostic methods included electron microscopy and the observation of CPEs in viral cultures, enabling visual

confirmation of viral particles. However, these methods were labour-intensive, time-consuming, and lacked sensitivity (Madeley and Peiris, 2002). Immunoassays, such as ELISAs and immunofluorescence assays, were later developed, allowing for the detection of viral antigens or host antibodies. However, these were limited by low sensitivity and long seroconversion windows (Panning et al., 2007). The introduction of nucleic acid amplification techniques, particularly PCR, marked a turning point in viral diagnostics. By enabling the precise detection of RNA viruses, RT-PCR has established itself as the gold standard for diagnosing respiratory infections, such as influenza, RSV, and SARS-CoV-2 (Mahony et al., 2007). To simplify molecular diagnostics for broader accessibility, methods such as LAMP and RPA were developed to perform rapid amplification under isothermal conditions with reduced equipment dependency (Notomi et al., 2000; Piepenburg et al., 2006). Major respiratory disease outbreaks, such as the 2009 H1N1 influenza and 2019 COVID-19 pandemics, further catalysed the development of POC molecular diagnostics, highlighting the need for rapid, deployable tools outside conventional laboratory environments (Yüce et al., 2021). This has increased the demand for isothermal methods, particularly for low-resource settings where the limitations of PCR platforms remain a critical barrier.

1.9.5. Diagnostic Limitations in Low-Resource Settings

Diagnostic testing in low-resource settings continues to suffer from several persistent issues, including inadequate laboratory infrastructure, unreliable electricity supplies, limited access to cold-chain logistics, and a lack of trained personnel. These barriers are particularly prominent in rural or underserved regions where delays in pathogen detection can significantly halt prompt treatment and disease containment (Peeling et al., 2006; Land et al., 2019). Although conventional molecular diagnostics are highly sensitive, they require complex thermocycling instruments and precise temperature controls for reagent storage. These limitations make them less suited for field-based or decentralised settings

(Carter et al., 2020). Oppositely, isothermal amplification methods like RT-RPA offer several operational benefits. RPA is performed at a constant low temperature (37-42 °C), allowing for incubation with simple heating blocks or even body heat in emergencies (Crannell et al., 2014). RPA can also tolerate crude sample inputs and potential inhibitors that would typically disrupt PCR, reducing the need for extensive nucleic acid purification. In this study, the field applicability of the assay was improved by adapting it to a lateral flow format, which eliminates the need for specialised fluorescence readers or digital analysis tools. This allows results to be interpreted visually within 30 minutes. In vitro transcribed RNA templates were generated to maintain assay standardisation and performance benchmarking, thereby reducing dependency on clinical specimens, which can be challenging to access in low-resource settings. These features make RT-RPA well-suited for decentralised testing and promote rapid disease detection in outbreak scenarios where traditional testing infrastructure is unavailable.

1.9.6. Prior Applications of RT-RPA as an RT-PCR Alternative

Several studies have successfully used RT-RPA as an alternative to RT-PCR for viral diagnostics, highlighting its potential for POC and decentralised applications. For instance, Wang et al. (2020) developed an RT-RPA assay for detecting SARS-CoV-2, achieving sensitivity and specificity comparable to RT-PCR in under 30 minutes, without relying on thermal cycling. Lillis et al. (2016) applied RT-RPA to detect Zika virus RNA from field-collected mosquito and urine samples, showing high sensitivity and simplicity in a field setting. Lau et al. (2021) utilised RT-RPA to detect African swine fever virus, demonstrating reliable amplification in crude serum samples while significantly reducing the amplification time compared to RT-PCR. These studies consistently report that RT-RPA provides faster turnaround times and simplified workflows, particularly in settings with limited infrastructure and technical capacity. Furthermore, RPA's adaptability has allowed its successful integration into portable diagnostic platforms. For instance, Crannel et al. (2016) combined RT-RPA with lateral flow strips for detecting HIV,

thereby eliminating the reliance on traditional PCR systems. Together, these studies demonstrate that RT-RPA has been effectively applied across various pathogens and sample types, reinforcing its potential as a practical alternative to RT-PCR where diagnostic resources, time, or specialist training are limited.

1.9.7. Diagnostic Strengths and Technical Limitations of RT-RPA

RT-RPA offers multiple advantages over traditional nucleic acid amplification methods. It can operate at low, constant temperatures without the need for thermocyclers, thereby significantly reducing energy requirements. RT-RPA reactions can be completed within 15 to 30 minutes, and the assay is very tolerant to inhibitors present in crude biological samples, allowing simpler and less resource-intensive sample preparation (Daher et al., 2016). Additionally, RT-RPA is compatible with various detection methods, including real-time fluorescence, lateral flow strips, and microfluidic platforms, making it suitable for laboratory and field settings (Piepenburg et al., 2006). On the other hand, there are some limitations associated with RT-RPA. For instance, primer design is less standardised than in PCR, which increases the risk of non-specific amplification, particularly in multiplex detection. False positives can occur due to recombinase-driven strand invasion, which is more likely in poorly optimised reactions. The exclusive production of key enzymes and reagents by a few commercial suppliers restricts the cost-efficiency and worldwide distribution of RT-RPA (Li et al., 2019). There are reports of variability between reagent batches and reduced reagent stability outside of controlled storage conditions, which can be very challenging in low-resource settings. Fortunately, scientists are actively working to improve reagent chemistry and assay optimisation, increasing the practicality and reliability of RT-RPA.

1.9.8. Consideration of Multiplexing Strategies in RT-RPA

Multiplex RT-RPA has been discovered to simultaneously detect multiple pathogen targets in a single reaction, offering potential benefits in syndromic respiratory diagnostics. For instance, Aebischer et al. (2014) successfully developed a multiplex isothermal amplification assay to detect Schmallenberg and bovine viral diarrhoea viruses simultaneously. Meanwhile, Abd El Wahed et al. (2013) achieved robust sensitivity and specificity for detecting filovirus in field conditions. Despite promising results, the inherent assay complexity limits the reproducibility of multiplex RT-RPA. The simultaneous use of multiple primer sets increases the risk of primer-dimer formation, cross-reactivity, and non-specific amplification due to the recombinase-driven mechanism of strand invasion. In lateral flow-based formats, overlapping signals may interfere with visual interpretation, particularly when test lines are closely spaced or faint. For these reasons, this study focused on optimising and validating singleplex RT-RPA assays for each viral target. This ensured high specificity, consistent amplification efficiency, and compatibility with fluorescence-based and lateral flow detection systems. While multiplexing was considered, it was deliberately excluded from the study to prioritise assay reliability and clinical translatibility. Future studies can build upon this work to further explore RT-RPA, using carefully optimised primer sets and multiplex-compatible probe systems to overcome the limitations currently associated with multiplex RT-RPA.

Chapter 2: Methodology

2.1. Ethics Statement for Clinical Samples

The clinical samples used in this study were collected from Royal Lancaster Infirmary (RLI), NHS. They were approved by the Faculty of Health and Medicine Research Ethics Committee (FHMREC) under reference number FHMREC19112.

2.2. COVID-19 Clinical Sample Collection, RNA Extraction and Primer Design

A total of 150 NP swabs were individually collected from SARS-COV-2 suspected patients through routine NHS collection procedure for COVID-19 screening. The patients gave informed consent, and the samples were anonymised to avoid bias; therefore, patient demographic information such as age and sex was not available. These samples were stored and transported in virus transport media to the Biomedical and Life Sciences laboratories at Lancaster University, Lancaster, UK. These samples were stored at -80°C until processing for RNA extraction.

Viral RNA was extracted from suspected COVID-19 clinical samples using the QIAamp Viral RNA Mini kit (Qiagen, Valencia, CA, USA). All available complete genome sequences were retrieved from NCBI (National Center for Biotechnology Information) and downloaded in FASTA format. Multiple sequence alignment was done using MAFFT: Multiple Alignment using Fast Fourier Transform (https://mafft.cbrc.jp/alignment/server/). Aligned sequences were opened in Geneious Prime (https://www.geneious.com/features/sequence-alignment/) to identify the conserved regions of the sequences. In order to avoid non-specific amplification, the conserved regions with the lowest mutation frequencies within the genome were used as a template to design different sets of primers. They were selected with PrimerExplorer V5 (http://primerexplorer.jp/elamp4.0.0/index.html) for appropriate primer features

such as length, melting temperature and GC content. A sequence homology search was performed through all known template sequences to check for alternative priming sites using BLAST: Basic Local Alignment Search Tool (http://www.ncbi.nlm.gov/BLAST).

2.3. Synthetic RNA Preparation for Assay Optimisation

The coding sequence of the nucleocapsid (N) gene from SARS-CoV-2/Wuhan/China/2020 strain (accession number: NC_045512.2 199) was chemically synthesised and cloned into pVAX1 plasmid (Invitrogen, Carlsbad, CA, USA) between KpnI and NotI restriction sites. The plasmid DNA was later purified using MiniPrep Qiagen Kits (Qiagen, Valencia, CA, USA). The T7 RiboMAX™ Express Large-Scale RNA Production System (Promega, Madison, WI, USA) and recombinant plasmid were used for in vitro transcription of the RNA and RNeasy MinElute Cleanup Kit (Qiagen, Valencia, CA, USA) was used for purification. RNA concentration was measured using NanoDrop™ 2000c Spectrophotometers (ThermoFisher Scientific, Waltham, MA, USA), which was later used to determine the number of in vitro transcribed RNA copies.

2.4. Real-Time Fluorescence-based RT-RPA

Fluorescence-based RT-RPA reactions were performed according to the manufacturer`s instructions for the TwistAmp® exo kit (TwistDx Limited, Maidenhead, United Kingdom). A 50ul reaction contained 43.5ul of the reaction mixture, 4ul of 20ng/uL RNA template, and 2.5ul of 280mM MgOAc. The reaction mixture had 29.5ul of primer-free rehydration buffer, 2.5ul of 200U/uL RevertAid® reverse transcriptase (ThermoFisher Scientific, Waltham, MA, USA), 2.1ul of 10pmol/uL forward and reverse primers (detailed in Chapter 4), 0.6ul of 10pmol/uL TwistAmp® exo probe, and 6.7ul of nuclease-free water. Finally, a 2.5ul of 280mM MgOAc and 4ul of 20ng/uL RNA template were added to the lid of each tube to initiate the reactions simultaneously. These were briefly mixed, centrifuged, and remixed, followed by placing the tubes in the CFX96 Touch Real-Time PCR Detection System

(BioRad Laboratories, Watford, UK). The tubes were incubated at 42°C for 30 min. The results were interpreted and compared to the RT-qPCR and RT-LAMP results.

2.5. LFD-based RT-RPA

LFD-based RT-RPA reactions were performed according to the manufacturer's instructions for the TwistAmp® basic kit (TwistDx Limited, Maidenhead, United Kingdom). A 50ul reaction contained 42.5ul of the reaction mixture, 5ul of 20ng/uL RNA template, and 2.5ul of 280mM MgOAc. The reaction mixture had 29.5ul of primer-free rehydration buffer, 2.1ul of 10pmol/uL forward and reverse primers, 2.5ul of 200U/uL RevertAid® reverse transcriptase (ThermoFisher Scientific, Waltham, MA, USA), 0.5ul of 40U/uL RiboLock® RNase inhibitor (ThermoFisher Scientific, Waltham, MA, USA), 0.6ul of 10pmol/ul TwistAmp® basic probe, and 7.2ul of nuclease-free water. Then, a 2.5ul of 280mM MgOAc and 5ul of 20ng/uL RNA template were added to the lid of each tube to initiate the reactions simultaneously. These were briefly mixed, centrifuged, remixed, and then incubated at 42°C for 30 minutes. After incubation, the amplicons produced were prepared for LFD detection according to the manufacturer's instructions of HybriDetect® 2T (Milenia Biotec GmbH, Gieβen, Germany). A volume of 25ul of the amplicon products was diluted at a 1:25 ratio with HybriDetect® 2T assay buffer. This diluted solution was then combined with 75ul of the same buffer. Out of this 100ul buffer solution, 10ul was carefully dispensed onto the designated area of the HybriDetect® 2T test strip. Immediately afterwards, the test strips were inserted into their respective Eppendorf tubes containing 80ul of HybriDetect® 2T assay buffer. The visualisation of the strips for a positive or negative result was conducted within a time frame of 5-10 min.

2.6. Real-Time RT-qPCR

Superscript III Platinum One-Step RT-qPCR kit (Invitrogen Carlsbad, CA, USA) was used to carry out RT-qPCR according to the manufacturer`s instructions. A total of 25ul

of reaction mixture was made up of 12.5ul 2X Reaction Mix, 0.5ul of 0.2uM forward (5'-CCCTGTGGGTTTTACACTTAA-3') and reverse primers (5'-ACGATTGTGCATCAGCTGA-3'), 0.25ul of 0.1uM probe (5'-FAM-CCGTCTGCGGTATGTGGAAAGGTTATGG-BHQ1-3'), 0.5ul of SuperScript® III RT/Platinum® *Taq* Mix, 5ul of 20ng/uL RNA template and 5.75ul of nuclease-free water. RT-qPCR-based amplification was detected using CFX96 Touch Real-Time PCR (Applied Biosystems) or CFX96 Touch Real-Time PCR Detection System (BioRad). The PCR cycling conditions included an initial denaturation of 95°C for 2 min, followed by 40 cycles of 95°C for 15 sec (denaturation) and 60°C for 30 sec (annealing/extension).

2.7. Sensitivity of RT-RPA

In order to estimate how often RT-RPA assay can give true positive results, the sensitivity assay was carried out by using TwistAmp® exo kit (TwistDx Limited, Maidenhead, United Kingdom) according to the manufacturer`s instructions. Serial dilutions of the synthesised RNA standards (106-101 RNA copies per reaction) were screened using HybriDetect® 2T (Milenia Biotec GmbH, Gieβen, Germany). RT-RPA assay detection was calculated using a diagnostic sensitivity formula (Trevethan, 2017).

2.8. Specificity of RT-RPA

In order to estimate how often RT-RPA assay can give true negative results, the specificity assay was carried out on the Respiratory (21 Targets) Control Panel (Microbiologics, Inc., Minnesota, United States) that provides the genomes of different viruses and bacteria using TwistAmp® basic kit (TwistDx Limited, Maidenhead, United Kingdom) according to the manufacturer`s instructions and the assay was conducted. The assay specificity of the RT-RPA assay for SARS-CoV-2 detection was calculated using a diagnostic specificity formula (Trevethan, 2017).

2.9. Generating PCR Products for TOPO TA Cloning and Transformation

A 25ul PCR reaction was performed according to the manufacturer's instructions of TOPO™ TA Cloning™ Kit for Sequencing (ThermoFisher Scientific, Waltham, MA, USA). The reaction mixture involved 1ul of *Taq* polymerase (1 unit/uL), 5ul of 10X PCR buffer, 0.5ul of 50mM dNTPs, 1ul of 100ng DNA template, 1ul of 200ng forward and reverse primers from the RPA reactions, and 16.5ul of sterile water. *Taq* polymerase adds a single deoxyadenosine (A) to the 3' ends of PCR products. The linearised plasmid vector (pCR™ 4-TOPO®) provided by the kit has an overhanging 3' deoxythymidine (T) residues to allow efficient ligation of PCR inserts with the vector. The general PCR conditions for *Taq* polymerase used were 94°C for 5 min and one cycle for initial denaturation, 30 cycles of denaturation at 94°C for 30 sec, annealing at 55°C for 30 sec, and extension at 72°C for 10 min to ensure that all PCR products are full length and 3' adenylated.

2.10. TOPO TA Cloning

A 6ul of TOPO® cloning reaction was prepared by using 4ul of amplified DNA, 1ul of salt solution (1.2M NaCl; 0.06M MgCl2), and 1ul of TOPO vector both provided by the TOPO™ TA Cloning™ Kit for Sequencing. These were all mixed gently in a sterile microcentrifuge tube and incubated at room temperature for 5 min. After incubation, the reaction mixture was placed on ice to carry out One Shot® chemical transformation.

2.11. One Shot Chemical Transformation

One vial of One Shot® *E.coli* DH5α cells (50ul) was thawed on ice for each transformation. 2ul of TOPO® cloning reaction mixture was added into each vial of One Shot® cells to be transformed. The vials were then incubated on ice for 30 min, followed by a heat shock for 30 sec at 42°C. 250ul of room temperature SOC medium was added to the cells. The vials were closed and shaken (250rpm) at 37°C for an hour. 50ul of each transformation was spread on pre-warmed LB plates containing X-gal and 100ug/mL ampicillin. These plates were incubated overnight at 37°C.

2.12. Analysis of Positive Clones

A single colony was picked by using a loop from the LB plate. The colony was then placed into 5ml of LB medium containing ampicillin. This culture was incubated overnight at 37°C with shaking (200rpm) to promote bacterial growth. After incubation, 2 ml of bacterial culture was aliquoted into a sterile microcentrifuge tube. The bacterial culture was then centrifuged at 8,000 x g for 5 min at room temperature, forming a pellet at the bottom of the tube. The supernatant was removed by decanting, and the plasmid DNA pellet was left intact. The plasmid DNA was purified according to the manufacturer's instructions of PureLink™ Quick Plasmid Miniprep Kit (Thermofisher Scientific, Waltham, MA, USA). The plasmids were then analysed for inserts using PCR according to the manufacturer's instructions of Platinum™ PCR SuperMix High Fidelity (ThermoFisher Scientific, Waltham, MA, USA). Agarose gel electrophoresis was carried out to analyse the PCR products, and the SYBR™ Safe (ThermoFisher Scientific, Waltham, MA, USA) was used to stain the bands to allow visualisation.

2.13. In Vitro Transcription of RNA Using TOPO Cloned Genes

Pre-linearised plasmid was mixed with an in vitro transcription mixture according to the manufacturer's instructions of T7 RiboMAX™ Express Large-Scale RNA Production System (Promega, Madison, WI, USA). The transcription reaction was placed in a water bath and incubated at 37°C for an hour. Following transcription,

the RNA was purified using the isopropanol precipitation protocol. A small aliquot of RNA was run on the agarose gel and compared to the marker to ensure the transcript was of the expected size.

2.14. Use of Viral RNA as a Template for Primer Validation

When in vitro transcription was not conducted or successful, viral RNA extracted from the virus infected cells were used for primer optimisation. The RNA was extracted using TRIzol/Chloroform method and the NanoDrop™ 2000/2000c Spectrophotometer (ThermoFisher Scientific, Waltham, MA, USA) was used to measure the integrity and quantity of the viral RNA before using in the RPA reactions. Successful amplification and subsequent verification were performed before using the viral RNA in assay validation process.

Chapter 3: Direct and Comparative Performance of RPA with Gold Standard RT-qPCR and Isothermal RT-LAMP for Detecting SARS-CoV-2 in Clinical Samples

3.1. Introduction

3.1.1. Advancements in Diagnostic Methods for Respiratory Viruses

Respiratory viruses are the most common cause of infection in England (UK Health Security Agency, 2023). Certain types of respiratory viruses, such as influenza strains, have been linked to global pandemics throughout history, resulting in millions of deaths (Noor and Maniha, 2020). Due to the significance of these viruses, numerous diagnostic methods have been employed to ensure accurate treatment decisions. Nucleic acid detection and immunoassay techniques are currently widely used for identifying viral infections at their source (Cassedy et al., 2021). RT-qPCR is a leading example of nucleic acid detection, typically providing high sensitivity for both DNA and RNA targets. Although RT-qPCR is considered the gold standard for detecting viral infections, it is expensive as it relies on specialised laboratory equipment and trained personnel. Furthermore, its specificity can be influenced by assay design and sample quality. These limitations have led to growing interest in isothermal amplification methods such as LAMP and RPA, which are faster, more cost-effective, and do not require thermocyclers.

Clinical evaluations have demonstrated that optimised RT-LAMP and RT-RPA assays independently achieve high analytical specificity in SARS-CoV-2 diagnostics. RT-LAMP achieves this through the use of 4-6 primers targeting multiple distinct genomic regions, which significantly reduces non-specific amplification (Notomi et al., 2000). A large-scale clinical evaluation reported 100% specificity in NP swabs and 99% specificity in saliva samples when benchmarked against RT-qPCR (Hooman Hanifehpour et al., 2024). Another study reported 99.7% specificity with extracted RNA and 99.5% specificity using a direct

swab-to-assay protocol (Thi et al., 2020). RT-RPA achieves high specificity through recombinase-mediated strand invasion and strand displacement, which facilitates precise primer–template binding while minimising non-specific amplification (Piepenburg et al., 2006). The clinical validation of the SARS-CoV-2 RT-RPA assay demonstrated 100% specificity with no cross-reactivity to other respiratory pathogens (Lau et al., 2021). However, no published study to date has directly compared the specificity of RT-LAMP and RT-RPA in a head-to-head experimental format for SARS-CoV-2 detection, and their relative diagnostic performance is therefore inferred from separate evaluations rather than a direct comparison. Collectively, these findings confirm that, when properly optimised, both RT-LAMP and RT-RPA routinely provide specificity exceeding 99% and are comparable to RT-qPCR in minimising false-positive results.

LFD detection is a type of immunoassay that is less sensitive than nucleic acid-based detection but can still provide robustness and lower costs. Moreover, most respiratory infections involve co-infections or are caused by pathogens that present overlapping clinical symptoms (Zhang et al., 2020; Musuuza et al., 2021). Therefore, developing a diagnostic method that can simultaneously detect more than one infection in a single patient would provide significant benefits. This study investigated the performance of RT-RPA using fluorescence- and LFD-based detection methods across positive and negative clinical samples by comparing it with conventional RT-qPCR and RT-LAMP workflows.

3.1.2. Diagnostic Challenges of SARS-CoV-2 and Related Viruses

These combined technologies were used to detect COVID-19 caused by SARS-CoV-2, which can severely infect various animal species, including humans, causing severe respiratory symptoms in some patients (Hui and Zumla, 2019; Zumla et et., 2016). The most common symptoms of COVID-19 include high body temperature, continuous cough, shortness of breath, and flu-like symptoms, which can cause difficulty distinguishing between influenza viruses, RSVs, and SARS-CoV-2 based on symptoms alone. The clinical overlap significantly limits symptom-based screening and emphasises the dependence on molecular diagnostics for accurate identification. In

addition, researchers identified a similarity between SARS-CoV-2 and SARS-CoV sequences with 82% sequence identity (Wu et al., 2010), and a lesser similarity between SARS-CoV-2 and MERS-CoV (Chan et al., 2020), further complicating genomic differentiation. This emphasised the importance of a diagnostic test with high specificity and accuracy, particularly in regions where multiple coronaviruses may co-circulate.

Beyond clinical and genomic overlap, some technical limitations persist when detecting COVID-19 using conventional diagnostic techniques. Despite being widely used and considered the gold standard, RT-qPCR is time-consuming and costly, and it relies on thermocyclers and trained personnel, making it less suited for field or low-resource settings. Additionally, the possibility of co-infections with other respiratory pathogens can interfere with the detection of SARS-CoV-2, particularly in the absence of multiplex testing. These challenges highlight the need for diagnostic platforms that are rapid, cost-effective, and capable of achieving high analytical specificity. This study addresses these limitations by exploring RT-RPA as a viable diagnostic alternative with potential benefits in decentralised and time-sensitive testing environments.

3.2. Hypothesis and Objectives

Hypothesis:

Current molecular diagnostics for respiratory viruses are insufficiently adaptable for decentralised and low-resource settings. RT-RPA, when optimised and clinically validated, offers a feasible alternative that overcomes logistical, technical, and infrastructural barriers associated with RT-qPCR and other conventional methods.

Objectives:

1. To evaluate and compare the diagnostic performance of fluorescence and LFD-based RT-RPA with RT-qPCR and RT-LAMP for SARS-CoV-2 detection.

2. To assess the operational suitability of RT-RPA for POCT through lateral flow adaptation.

3. To determine whether fluorescence- or LFD-based RT-RPA provides a more reliable diagnostic output.

4. To investigate practical limitations of RT-LAMP relative to RT-RPA in the context of isothermal diagnostics for respiratory viruses.

3.3. Results

3.3.1. Designing Primers for RT-RPA

Genomic sequences for SARS-CoV-2 were aligned using the MAFFT algorithm, and conserved regions were identified using Geneious Software, which served as a template to design primers for RT-RPA (**Figure 10**). Rather than using predesigned PCR primers, new primers were specifically designed to meet the biochemical requirements of RPA, including efficient strand invasion at lower isothermal temperatures and reduced risk of non-specific amplification. Conventional PCR primers are typically optimised for thermocycling at high temperatures, so they may struggle to perform sufficiently under RPA conditions due to differences in enzyme behaviour, hybridisation dynamics, and reaction kinetics. New primers were designed to provide compatibility across RT-RPA and RT-PCR workflows. This dual-platform strategy enabled consistent evaluation while avoiding compromises in amplification efficiency or specificity. Primer sets were selected based on multiple criteria to ensure compatibility with both RT-RPA and RT-PCR. First, primers were positioned within conserved genomic regions to allow broad detection across viral strains. To reduce the risk of primer-dimer formation or hairpin structures, any primers with four or more continuous self-complementary bases, or eight in total, were excluded during selection. The primer length was kept within 18-32 nucleotides to support stable annealing and efficient amplification. Additionally, melting temperatures (Tm) were considered, even though Tm is not critical for RPA alone due to the recombinase-mediated binding

mechanism. However, since the same primers were used for RT-PCR, which requires precise annealing, a Tm range of 55–62°C was targeted. This temperature range ensures that the primers can function effectively under the thermal cycling conditions of PCR while still maintaining compatibility with the lower, constant temperatures required for RPA.

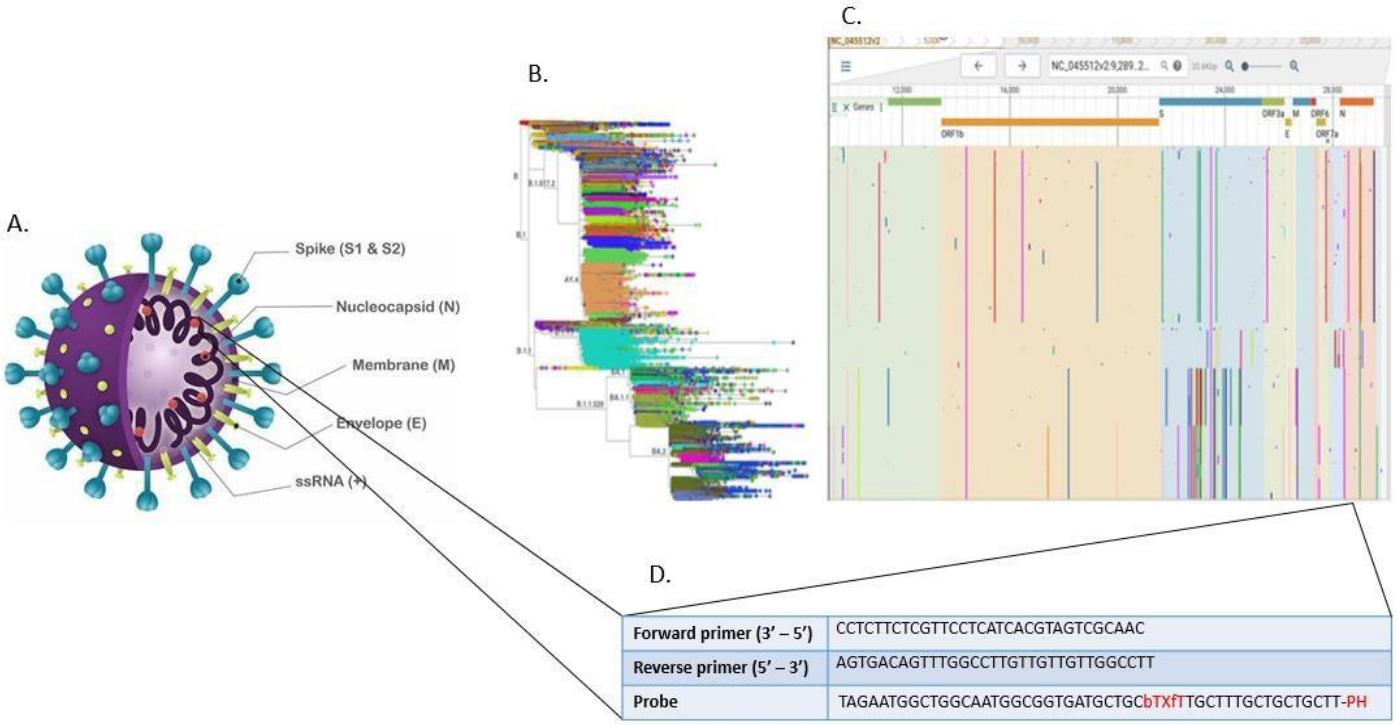

Figure 10. Primer design outline for SARS-CoV-2.

A. Schematic diagram of SARS-CoV-2 with the genes encoding the major structural glycoproteins – Spike (S), Membrane (M), and Envelope (E) – with the structural Nucleocapsid (N) protein. **B.** Phylogenetic tree of most recent Omicron variants, where each sub-variant is indicated by a branch line with different colours to show genetic diversity. **. C.** Alignment of SARS-CoV-2 genomes illustrating similarities and differences of nucleotides across variants. Coloured vertical lines indicate variable sites, while the most conserved regions are shown by the absence or scarcity of such lines; the N gene represents the most conserved region and was selected for primer design. **D.** The table shows the RT-RPA oligonucleotides and the probe specifically designed for the N gene of SARS-CoV-2 (Image Source: Santos et al., 2022).

3.3.2. Optimisation of Real-time Fluorescence-based RT-RPA

RNAs from the clinical samples were amplified through RT-RPA using primer sets designed and the TwistAmp® exo probe provided by the TwistAmp® exo kit, followed by real-time fluorescence detection using the CFX96 Touch Real-Time PCR Machine. For assay optimisation, SARS-CoV-2 synthetic RNA was used as a template (i.e. the positive control). Only one clinical sample from a positive patient was included during the optimisation phase, using the same primer sets and probe. The patient sample and the synthetic RNA control (i.e. kit-positive control) both showed positive amplification within 30 minutes, while the kit-negative control showed no amplification (**Figure 11**). These results suggested that fluorescence-based RT-RPA could successfully detect SARS-CoV-2 in clinical samples. While using a single clinical sample can provide preliminary validation, capturing the full variability encountered in real-world samples is not sufficient. Therefore, the assay was later evaluated on a broader panel of clinical samples during the validation phase to ensure robustness and reproducibility. Although fluorescence-based RT-RPA demonstrated superior diagnostic speed and comparable sensitivity to conventional methods, its implementation in low-resource settings may be constrained by the need for fluorescence readers. To overcome this, lateral flow-based formats were also developed in this study, offering a more portable and cost-effective alternative while retaining compatibility with the same primer sets.

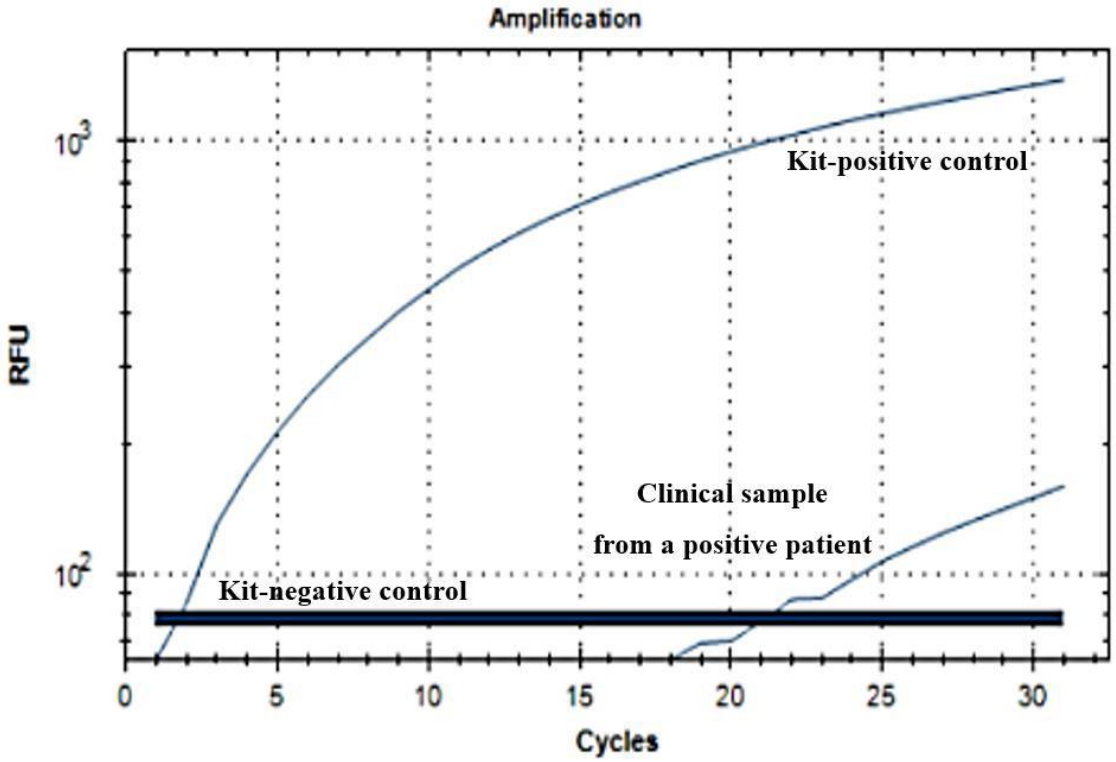

Figure 11. Real-time amplification curve of fluorescence-based RT-RPA detection of SARS-CoV-2 N gene RNA.

The amplification curve for the kit-positive control validates the functionality of the assay. The TwistAmp® exo kit was used for the RT-RPA reactions, and the synthetic SARS-CoV-2 RNA provided within the kit served as the positive control. This control template is highly purified and optimised, typically exhibiting fast and uniform amplification, as reflected in the amplification curve. The clinical sample from a SARS-CoV-2-positive patient showed a strong amplification signal, confirming the presence of SARS-CoV-2 N gene RNA in the sample. The kit-negative control showed no amplification, indicating the absence of contamination. Compared to the kit-positive control, variability in the amplification kinetics of the clinical sample can be attributed to differences in template concentration and RNA integrity.

3.3.3. Optimisation of LFD-based RT-RPA

For assay optimisation, synthetic SARS-CoV-2 RNA served as the kit-positive control, while a no-template RT-RPA reaction was used as the kit-negative control. Although

the use of a SARS-CoV-2-negative clinical sample would offer additional assurance of assay specificity, this was not feasible at the optimisation stage due to limited sample availability and prioritisation of preliminary assay setup. The no-template control was chosen in line with standard early-phase optimisation practices to detect contamination and evaluate assay baseline reactivity. The clinical sample, confirmed SARS-CoV-2-positive, was amplified using the same primer sets and probe to determine whether viral RNA could be detected via LFD-based RT-RPA. After a 5–10-minute incubation at room temperature, the test results were visualised: a control (C) line confirmed proper strip function, and the appearance of a test (T) line indicated a positive result. The kit-positive and clinical sample produced a T line, whereas the kit-negative control did not (**Figure 12**), suggesting the absence of non-specific amplification under these assay conditions. Although cross-reactivity with non-target respiratory viruses was not directly assessed, this was considered unnecessary due to the known specificity of the primer-probe design and the exclusive use of confirmed SARS-CoV-2-positive samples during this phase. Non-specific binding was monitored through the use of no-template controls and by ensuring that amplification was only observed in SARS-CoV-2-positive clinical and synthetic samples; any amplification in negative controls would have indicated potential non-specific activity.

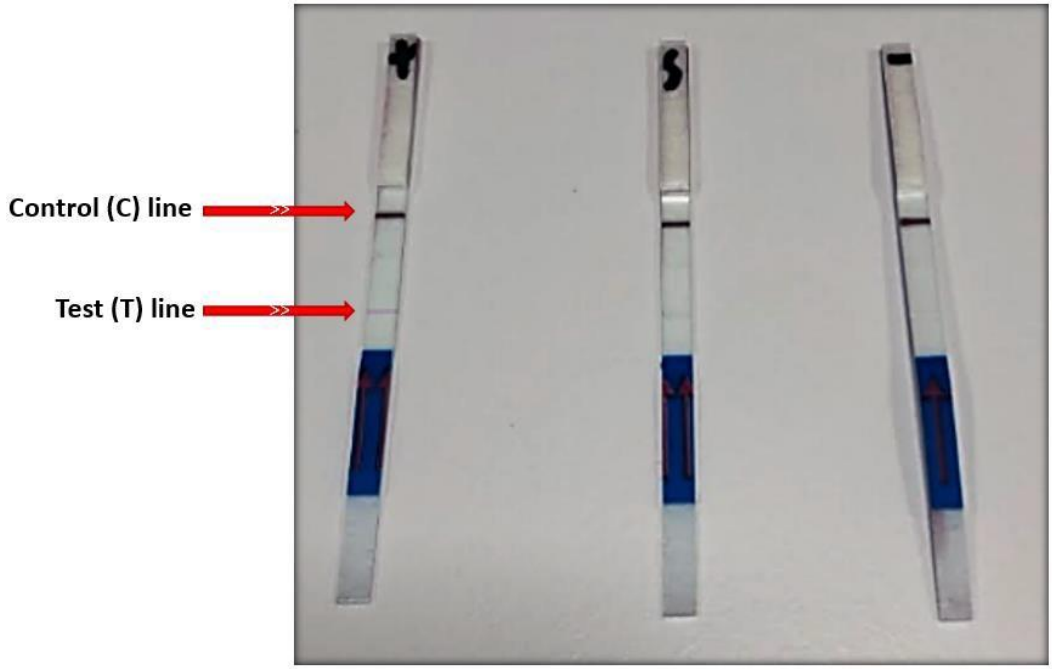

Figure 12. Detection of SARS-CoV-2 N gene RNA using HybriDetect 2T lateral flow test strips for RT-RPA.

The strip on the left is the kit-positive control (synthetic SARS-CoV-2 RNA), which produced both the C and T lines, confirming the functionality of the assay. The middle strip represents the SARS-CoV-2-positive clinical sample, which also produced distinct C and T lines, indicating the presence of SARS-CoV-2 N gene RNA. The strip on the right is the no-template RT-RPA reaction, used as the kit-negative control, which produced only the C line and no T line, confirming the absence of SARS-CoV-2 N gene RNA and the lack of non-specific amplification. The presence of a C line on all strips validates the proper functioning of the test.

3.3.4. Evaluation of the Assay Sensitivity

To determine the sensitivity of the RT-RPA assay, 10-fold serial dilutions of synthetic SARS-CoV-2 RNA (10^6 to 10^1 copies/µL) were used as starting templates. Following RT-RPA, the products were analysed using LFD detection. Test lines were observed on strips corresponding to RNA concentrations from 10^6 to 10^1 copies/µL, indicating successful detection at these concentrations. The strip labelled "0", which contained no RNA, served as the no-template negative control and did not produce a T line (**Figure 13**), confirming the absence of non-specific amplification.

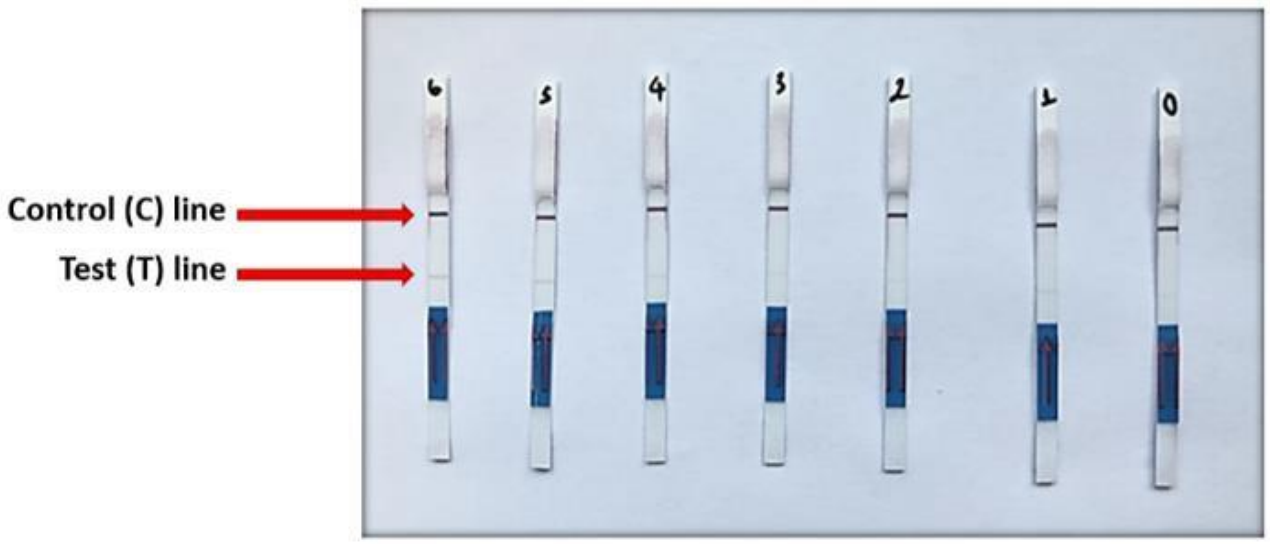

Figure 13. LFD test results for serial dilutions of SARS-CoV-2 RNA.

LFT test strips showing results from serial dilutions ranging from 10^6 copies/μL (strip labelled 6) to 10^0 copies/μL (strip labelled 0). T lines are observed on strips 6 through 1, indicating successful detection at these concentrations. Strip 0, the no-template control, did not produce a T line, confirming the absence of SARS-CoV-2 RNA and ruling out non-specific amplification.

Although the initial RNA concentrations were known, the number of RNA copies was not quantified after amplification, as the assay was evaluated qualitatively based on the presence or absence of a visible test line. Quantifying RNA yield, particularly near the lower detection limit, could have provided a more precise measure of the assay's analytical sensitivity. RNA from other respiratory viruses was not included in this assay, as the aim was to establish analytical sensitivity rather than cross-reactivity. Specificity was addressed separately through the use of sequence-specific primers and comparison with negative clinical samples.

As part of assay optimisation, several reaction conditions were considered and adjusted. Primer concentrations were tested in the 0.4-0.6 μM range to maximise sensitivity without promoting non-specific amplification. The MgOAc concentration was fixed at 14mM, as recommended for RPA reactions, which was found to support consistent amplification kinetics. The RT-RPA incubation time was optimised at 30 minutes at 42°C, balancing reaction speed and detectable signal strength. While these parameters yielded robust performance under the tested conditions, further validation across varied clinical matrices and viral loads would strengthen the assay's reproducibility and diagnostic applicability.

In this context, sensitivity refers to the proportion of SARS-CoV-2-positive samples correctly identified by the RT-RPA assay. To evaluate sensitivity, a total of 132 clinical samples were tested using both fluorescence- and LFD-based RT-RPA assays. Results were compared to two reference methods: RT-qPCR, which is the diagnostic gold standard, and RT-LAMP, which was included for benchmarking due to its increasing use as a rapid, isothermal alternative to RT-qPCR, particularly in resource-limited settings.

Sensitivity was calculated by dividing the number of true positive results (i.e. samples positive by both RT-qPCR and RT-RPA) by the total number of RT-qPCR-positive samples. Fluorescence-based RT-RPA achieved a sensitivity of 100% relative to RT-qPCR (**Table**

1A), correctly detecting all SARS-CoV-2-positive samples confirmed by the reference method. When compared to RT-LAMP, sensitivity was 71%, suggesting that 29% of the RT-LAMP-positive results were not detected by RT-RPA. These cases were considered probable false positives, as RT-qPCR did not confirm them.

The sensitivity of LFD-based RT-RPA was 84% relative to RT-qPCR (**Table 1B**), indicating that it failed to detect 16% of positive cases. Compared to RT-LAMP, the LFD-based RT-RPA yielded a sensitivity of 57%, again reflecting discrepancies primarily due to presumed false positives from RT-LAMP. Although visualising the raw data using graphs and incorporating statistical analysis would further strengthen the interpretation, the current comparison highlights the performance trends across detection methods.

Table 1. Percentage of sensitivity, specificity, PPV and NPV calculated using the raw data for **(A)** fluorescence-based and **(B)** LFD-based RT-RPA compared to RT-qPCR and RT-LAMP.

A)

	Values in % compared to fluorescence-based RT-RPA	
	RT-qPCR	**RT-LAMP**
Sensitivity	100%	71%
Specificity	92%	87%
Positive Predictive Value (PPV)	90%	89%
Negative Predictive Value (NPV)	100%	67%
Overall Accuracy	**95%**	**77%**

B)

	Values in % compared to LFD-based RT-RPA	
	RT-qPCR	**RT-LAMP**
Sensitivity	84%	57%
Specificity	97%	89%
Positive Predictive Value (PPV)	96%	88%
Negative Predictive Value (NPV)	89%	56%
Overall Accuracy	**92%**	**68%**

3.3.5. Validation of the Assay Specificity

In this context, specificity refers to the proportion of SARS-CoV-2-negative samples that are correctly identified as negative by RT-RPA. To determine the specificity of the RT-RPA assay, a panel of viral and bacterial targets was tested using the Respiratory (21 Targets) Control Panel (**Table 2**). RT-RPA products were electrophoresed on an agarose gel, and the presence of non-specific amplification and SARS-CoV-2-specific

detection was confirmed. For fluorescence-based RT-RPA, specificity was calculated by dividing the number of true negative results (i.e. samples negative by both RT-qPCR and RT-RPA) by the total number of RT-qPCR-negative samples. This yielded a specificity of 92% (**Table 1A**), indicating high concordance with the diagnostic reference method. LFD-based RT-RPA showed even higher specificity, at 97% compared to RT-qPCR (**Table 1B**), correctly identifying nearly all uninfected individuals. Compared to RT-LAMP, fluorescence-based RT-RPA achieved 89% specificity, indicating fewer false positives. These results support the conclusion that RT-RPA exhibits strong specificity, especially when benchmarked against RT-qPCR.

Table 2. List of respiratory viruses and bacteria that were tested against SARS-CoV-2 for the specificity assay along with the results obtained through agarose gel electrophoresis.

VIRUSES	Fluorescence-based RT-RPA	LFD-based RT-RPA	RT-PCR
Coronavirus 229E	-	-	-
Recombinant Coronavirus HKU1	-	-	-
Recombinant Coronavirus NL63	-	-	-
Recombinant Coronavirus OC43 Strain 1	-	-	-
Recombinant Coronavirus OC43 Strain 2	-	-	-
Adenovirus Type 6	-	-	-
Human Rhinovirus	-	-	-
Influenza A	-	-	-
Influenza A subtype H1	-	-	-
Infleunza A subtype H1-2009	-	-	-
Influenza B	-	-	-
Parainfluenza Virus 1	-	-	-
Parainfluenza Virus 2	-	-	-
Parainfluenza Virus 3	-	-	-
Recombinant Parainfluenza Virus 4a	-	-	-
Respiratory Syncytial Virus	-	-	-
Recombinant Human Metapneumovirus	-	-	-
Influenza A subtype H3	-	-	-
BACTERIA	-	-	-
Chlyamydia pneumoniae	-	-	-
Bordetella parapertussis	-	-	-
Bordetella pertussis	-	-	-
Mycoplasma pneumoniae	-	-	-
SARS-CoV-2	+	+	+

3.3.6. Determination of Predictive Values

In diagnostic testing, predictive values assess the likelihood that a test result accurately reflects the patient's true infection status. The positive predictive value (PPV) refers to

the probability that individuals with a positive RT-RPA result are indeed infected. For RT-RPA, PPV was calculated by dividing the number of true positive results (i.e. samples positive by both RT-qPCR and RT-RPA) by the total number of RT-RPA-positive samples. The negative predictive value (NPV) refers to the probability that individuals with a negative RT-RPA result are not infected. For RT-RPA, NPV was calculated by dividing the number of true negative results (i.e. samples negative by both RT-qPCR and RT-RPA) by the total number of RT-RPA-negative samples.

The results demonstrated that the PPV of fluorescence-based and LFD-based RT-RPA assays were 90% and 96%, respectively, when benchmarked against RT-qPCR (**Table 1).** This suggests that the vast majority of positive results from both RT-RPA methods correctly identified infected individuals. Compared to RT-LAMP, the PPVs for fluorescence and LFD-based RT-RPA were slightly lower, at 89% and 88%, respectively, reflecting higher discordance with RT-LAMP results, likely due to false positives.

The NPV of fluorescence-based RT-RPA was 100% compared to RT-qPCR (**Table 1A**), meaning all RT-qPCR-negative samples were also identified as negative by fluorescence-based RT-RPA. For LFD-based RT-RPA, the NPV was 89% compared to RT-qPCR (**Table 1B**), indicating slightly lower but still strong reliability. Against RT-LAMP, NPVs were lower: 67% for fluorescence-based and 56% for LFD-based RT-RPA, suggesting that some negative results from RT-RPA may not align with the more variable outcomes of RT-LAMP.

3.3.7. Validation of Diagnostic Accuracy

Diagnostic accuracy refers to a test's ability to correctly identify the presence (true positives) and absence (true negatives) of infection. However, diagnostic performance is not fixed and may vary depending on study design, sample characteristics, and population context. Several factors can contribute to misdiagnosis, including disease prevalence, spectrum bias, poor sample quality, variability in viral load, suboptimal primer design, operator error, and differences in the timing of sample collection relative

to disease onset. These variables can influence sensitivity and specificity, leading to false positives or false negatives. For RT-RPA, diagnostic accuracy was calculated by dividing the sum of true positive and true negative results (i.e. samples correctly identified by both RT-qPCR and RT-RPA) by the total number of samples tested.

The diagnostic accuracy of fluorescence-based RT-RPA was 96% compared to RT-qPCR (**Table 1A**), showing strong concordance with the gold standard. Compared to RT-LAMP, its accuracy dropped to 77%, likely due to false positives produced by RT-LAMP. LFD-based RT-RPA demonstrated 92% accuracy relative to RT-qPCR and 68% compared to RT-LAMP (**Table 1B**). These results confirm that both RT-RPA formats align closely with RT-qPCR, indicating reliable performance in identifying true positive and true negative cases.

The lower accuracy values reported in comparison to RT-LAMP may appear concerning; however, this should be interpreted in the context of the reference standard. Since RT-qPCR was used as the diagnostic gold standard in this study, the high concordance of RT-RPA assays with RT-qPCR supports their reliability in correctly identifying both positive and negative cases. The reduced accuracy relative to RT-LAMP is likely due to the increased rate of false positives observed in RT-LAMP results rather than a failure of RT-RPA to identify healthy individuals. Consequently, there is limited evidence to suggest that RT-RPA misclassifies uninfected individuals when compared against the more robust RT-qPCR benchmark.

Despite these promising results, further refinement would be required if the assay demonstrated inadequate accuracy during validation. This could include redesigning primers to enhance target specificity, optimising reaction conditions to minimise non-specific amplification, and expanding the validation cohort to incorporate a broader range of clinical samples and viral strains. Confirmatory testing with complementary molecular methods, alongside appropriate statistical evaluation in future studies, would further strengthen robustness prior to clinical application.

3.3.8. Selection of Clinical Samples for Assay Performance

Clinical samples were used to evaluate both fluorescence- and LFD-based RT-RPA assays. The same samples were also tested using RT-qPCR, and the results were compared to identify any discrepancies. RT-LAMP was conducted in parallel to support further comparison. 140 clinical samples were initially tested using both RT-RPA detection formats. However, 8 of these samples were excluded from the final analysis due to invalid RT-RPA results. Specifically, these samples produced either a positive or negative result by fluorescence-based RT-RPA. Still, they failed to show a C line on the LFD test strip, even after repeated testing. The absence of a C line indicated that the LFD device had malfunctioned, rendering the result invalid and unusable for comparative analysis. Possible causes for these may include degradation during storage, timing of collection relative to the infection stage, or manufacturing inconsistencies in the LFD components. Due to their unreliability, these samples were removed from the dataset. The remaining 132 samples were included in the final analysis, where results from both RT-RPA methods were compared against RT-qPCR and RT-LAMP.

3.3.9. Comparative Performance of Fluorescence-based RT-RPA with RT-qPCR and RT-LAMP

Clinical samples were tested using both fluorescence- and LFD-based RT-RPA assays. The same samples were also assessed by RT-qPCR to enable comparative analysis, and RT-LAMP was conducted in parallel to support additional benchmarking. A total of 140 samples were initially processed, and 8 of these were excluded due to invalid RT-RPA results, as described in Chapter 9.1. These exclusions primarily involved cases where fluorescence-based RT-RPA yielded a result, but the corresponding LFD strip lacked a visible C line, rendering the result invalid despite repeat testing. The likely causes included suboptimal collection timing, improper storage, or manufacturing inconsistencies in the LFD device. The remaining 132 samples were retained for comparative evaluation.

Following sample validation, diagnostic performance was assessed across all platforms. Technical replicates were routinely performed for RT-qPCR and RT-LAMP, consistent

with standard diagnostic validation protocols. In contrast, RT-RPA assays were not replicated systematically but were repeated selectively in cases of inconclusive outcomes or missing LFD control lines. This selective repetition reflected the preliminary nature of the RT-RPA optimisation study and the qualitative format of the LFD readout. All discordant results were cross-checked against RT-qPCR, which served as the diagnostic reference standard.

When fluorescence-based RT-RPA results were compared to RT-qPCR, 43% of the samples were identified as true positives and 52% as true negatives (**Table 3A**), reflecting a 95% agreement. Approximately 5% of samples were classified as false positives, and no false negatives were observed. Compared to RT-LAMP, 42% of samples were true positives and ~35% were true negatives (**Table 3B**), resulting in 77% agreement, with ~5% false positives and 17% false negatives. These figures reflect the diagnostic consistency of fluorescence-based RT-RPA across reference platforms. Taken together, the results indicate that fluorescence-based RT-RPA is diagnostically superior to RT-LAMP and exhibits strong concordance with the RT-qPCR gold standard.

Table 3. Comparative sample positivity between fluorescence-based **(A)** RT-RPA & RT-PCR and **(B)** RT-RPA & RT-LAMP.

Each section shows the number of positive and negative clinical samples detected by the fluorescence-based RT-RPA compared to RT-qPCR and RT-LAMP. The percentages for positive and negative clinical samples were also included.

A)

Fluorescence-based RT-RPA

RT-qPCR	Positive	Negative	Total
Positive	57 (43%)	0 (-)	57
Negative	6 (~5%)	69 (52%)	75
Total	63	69	132

B)

RT-LAMP	Positive	Negative	Total
Positive	56 (42%)	23 (17%)	79
Negative	7 (~5%)	46 (~35%)	53
Total	63	69	132

3.3.10. Comparative Performance of LFD-based RT-RPA with RT-qPCR and RT-LAMP

For the LFD-based RT-RPA, 34% of the samples were tested to be true positive and 55% were tested to be true negative (**Table 4A**), meaning 89% of the samples gave the same test results as RT-qPCR. Only ~2% of the samples were false positive, followed by 9% being false negative (**Table 4A**). When RT-RPA was compared to RT-LAMP, ~32% of the samples were found to be true positive, and 36% were found to be true negative (**Table 4B**), meaning ~68% gave the same test results as RT-LAMP. ~5% of the samples were found to be false positive, and the remaining 28% were identified to be false negative (**Table 4B**). Therefore, fluorescence-based RT-RPA gave better results than LFD-based RT-RPA, having the most comparable results to RT-qPCR.

Table 4. Comparative sample positivity between LFD-based **(A)** RT-RPA & RT-PCR and **(B)** RT-RPA & RT-LAMP.

Each section shows the number of positive and negative clinical samples detected by the LFD-based RT-RPA compared to RT-qPCR and RT-LAMP. The percentages for positive and negative clinical samples were also included.

A)

LFD-based RT-RPA

RT-qPCR	Positive	Negative	Total
Positive	48 (34%)	9 (9%)	57
Negative	2 (~2%)	73 (55%)	75
Total	47	85	132

B)

RT-LAMP	Positive	Negative	Total
Positive	45 (32%)	34 (28%)	79
Negative	6 (~5%)	48 (36%)	54
Total	48	85	132

3.4. Discussion

3.4.1. Comparative Analysis of RT-RPA, RT-qPCR, and RT-LAMP for SARS-CoV-2 Detection

This study used RT-RPA to detect SARS-CoV-2 in clinical samples, which is one of the most recent isothermal amplification methods. The test results were observed using fluorescence detection. They were compared to the current choice of diagnostic gold standard RT-qPCR and other isothermal alternative RT-LAMP. In order to determine if the SARS-CoV-2 RT-RPA assay can provide high diagnostic sensitivity and specificity, the N gene of the SARS-CoV-2 was targeted and amplified for evaluation. The N gene RT-RPA assay produced perfect sensitivity (100%) to RT-qPCR, meaning no false negatives were observed. The diagnostic specificity of the N gene RT-RPA was lower due to having some false positives - 28% of individuals with no infection were incorrectly identified as positives. The N gene RT-RPA produced sensitivity (68%) less similar to RT-LAMP, with slightly better specificity (~88%) than RT-qPCR. This means both false positives and false negatives were identified. However, there were more false negatives than false positives – around 32% of infected individuals incorrectly identified as negatives and around 12% of individuals with no infection incorrectly identified as positives. There might be several reasons for false positives and negatives, which will be further discussed.

3.4.2. Optimal Specimen Collection Methods for Viral Detection

A sufficient amount of specimen collection from the site of infection while the individual is still infected with the target pathogen is necessary (Lippi et al., 2020; De Virgilio et al., 2020). For SARS-CoV-2, the gold standard for specimen collection includes placing the samples in universal or viral transport media after collecting them from the upper respiratory tract. It is recommended to collect the samples using a flocked NP swab (Charlton et al., 2019; Schleihauf et al., 2015; LeBlanc et al., 2020). This type of swab is much better than standard cotton swabs on wooden sticks as those are covered with multi-length fibres that allow better collection due to multi-length fibres providing many contact points at the site of infection. This increases the number

of target cells, enhancing the sensitivity of the test. Universal and viral transport media provide a stable environment during the transportation of the samples to the laboratory (Druce et al., 2012). If the flocked NP swabs cannot be used, the next best alternative may include nasal mid-turbine swabs, sampling of the anterior nares, oropharyngeal (OP) swabs, or aspirates from the nasopharynx, nose, and throat (LeBlanc et al., 2020; Patriquin et al., 2020; Garnett et al., 2020; Tang et al., 2020; Guo et al., 2020).

Combining different specimen collection methods can also be useful. Viral infection begins in the upper respiratory tract, emphasising the significance of NP swabs in combination diagnostics. However, the NP swabs and universal transport media have been used continuously during the pandemic and for the samples collected for this study. Therefore, they are currently short in supply. In that case, collecting samples using an OP swab with a sample from the anterior nares was reported to be consistent with the results obtained from NP swab collection of SARS-CoV-2 detection (WHO, 2020; US Centers for Disease Control and Prevention, 2021; LeBlanc et al., 2020; Patriquin et al., 2020). Even though the gold standard is the sample collection from the upper respiratory tract using flocked NP swabs, some hospitalised patients carrying the infection for a while are likely to develop lower respiratory tract disease. Therefore, additional sample collection from the lower respiratory areas would be useful (Tang et al., 2020). In this case, bronchoalveolar lavage fluid, 43 endotracheal secretions, or sputum can be used as a specimen when lower tract infection is suspected (Kowalik et al., 2020; Joob and Wiwanitkit, 2020; Wang et al., 2020; Yang et al., 2020; Wong et al., 2020; Bwire et al., 2021; Mohammadi et al., 2020; Hanson et al., 2020; Norz et al., 2020).

Non-invasive collection methods like saliva and throat gargles are becoming more popular as these allow self-collection by the patient with no expertise (Zhu et al., 2020; Guest et al., 2020; Jamal et al., 2020; Wyllie et al., 2020; Bennett et al., 2017; Malecki et al., 2021). There is a controversy about the performance of this collection method; some studies have reported that the performance of the saliva sample is very comparable to NP or nasal swab collections for SARS-CoV-2 detection (Jamal et al., 2020; Wyllie et al., 2020; Khurshid et al., 2020; Iwasaki et al., 2020; Zheng et al., 2020; Rutgers Clinical Genomics Laboratory, 2020), while the others thought the opposite

(Becker et al., 2020) due to some patient-associated inconsistencies. For instance, patients from different populations may require further analysis (Becker et al., 2020; Xu et al., 2020). Interestingly, detecting SARS-CoV-2 infection from the stool is still possible even when the GI symptoms do not exist (van Doorn et al., 2020). However, this may not be a good idea for low-prevalence settings due to the high risk of faecal-oral transmission from using wastewater (van Doorn et al., 2020; Mathavarajah et al., 2021). One of the main aspects of this project is developing a highly sensitive and specific diagnostic assay that is accessible to everyone, so using a stool as a specimen for SARS-CoV-2 detection would not be ideal due to certain restrictions.

3.4.3. Alternative Transport Media for Specimen Collection

If there is no chance of using universal or transport media due to limited supplies, Amies transport medium, sterile normal saline, phosphate-buffered saline (PBS), M4 medium, and minimal essential medium (MEM) can be used as an alternative since they also provide suitable transport and storage conditions (Patriquin et al., 2020; Garnett et al., 2020; Rogers et al., 2020). In a recent study, specimens collected by the NP swabs were placed in three different transport media: sterile saline, PBS without calcium and magnesium, and then MEM and M4 medium, respectively. 12 different samples were used for each transport medium, and none of them showed any reduction in RNA stability before SARS-CoV-2 detection (Rodino et al., 2020). There has been another research about using a sexually transmitted infection (STI) testing kit in specimen transport media for SARS-CoV-2 detection. In this study, Aptima swabs were used to collect specimens from the posterior oropharynx and bilateral anterior nares, which were stored in specimen transport media (Avaniss-Aghajani et al., 2020). It was later identified that the results obtained from this sample/media combination were equivalent to those obtained from the gold standard combined with NP swabs and universal transport media. Therefore, using various transport media is not critical in SARS-CoV-2 diagnosis. Collectively, these findings indicate that alternative transport media can preserve RNA integrity for 48–72 hours under refrigerated conditions and up to 24–48 hours at room temperature, while prolonged exposure to elevated temperatures

significantly compromises RNA stability.

3.4.4. Impact of Specimen Collection Timing on Test Accuracy

The timing of specimen collection is critical, as it may lead to false negatives. For instance, testing too early (during the presymptomatic stage) or too late (during recovery) is likely to give false negative results (Dinnes et al., 2020). It would be best to test the patient 2–3 days after showing the symptoms using RT-qPCR, with the average disease onset being 5 days post-exposure (Danis et al., 2020; Kim et al., 2020). This corresponds to days 5-7 post-exposure, which is considered the optimal window for optimal detection when the viral load in the upper respiratory tract peaks (He et al., 2020; Singanayagam et al., 2020). In some suspected cases where the patient exhibits multiple respiratory symptoms despite testing negative for SARS-CoV-2, it is necessary to repeat the test after a few days. The average minimum time required for detecting SARS-CoV-2 RNA in the upper respiratory tract with mild illness is 7.9 to 20 days. Meanwhile, it is 6 to 30.8 days for patients with moderate to severe disease (Weiss et al., 2020). According to a study, symptomatic patients are more likely to have a high viral load, while asymptomatic patients have a much lower viral load (Golemba et al., 2023). However, in some other studies, no difference was observed in the viral load between the two groups (Walsh et al., 2020; Li et al., 2020; Zhou et al., 2020).

Viral shedding occurs when the virus particles bind to specific viral receptors lining the respiratory tract during the COVID-19 infection. The majority of patients with mild illness can clear the virus within 10 to 20 days, but in more severe cases, this period tends to be longer (Widders et al., 2020). For example, the longest time taken for viral shedding was recorded as 83 days and 111 days after symptom onset (Zhou et al., 2020; Li et al., 2020). Despite prolonged RNA detectability, studies show that RT-PCR positivity beyond day 9 after symptom onset does not correlate well with culturable virus, indicating reduced infectiousness (Bullard et al., 2020). Therefore, while RT-PCR can detect residual viral RNA for weeks, its diagnostic utility is highest during the first week of symptoms. The presence of SARS-CoV-2 in the sample does not always indicate high viral load or infectivity. In such cases, RNA detection may be

compromised by poor sample collection quality, prolonged transportation periods, or laboratory processing issues, resulting in samples that are likely to yield false negative results upon waiting (Kinloch et al., 2020). The chances of identifying SARS-CoV-2-positive patients decline after the second week of symptom onset. Therefore, suitable treatment should be provided to alleviate COVID-19 symptoms rather than exclusively focusing on test results.

Faecal shedding in patients without respiratory symptoms is very rare; for instance, in one UK household study, none of the respiratory-negative individuals had detectable SARS-CoV-2 RNA in their stool (Vaselli et al., 2021). On the other hand, SARS-CoV-2 RNA can be detected in stool samples even in the absence of GI symptoms. A meta-analysis by van Doorn et al. (2020) reported that ~27% of patients without GI symptoms had detectable stool RNA. Viral RNA may also persist in stool after respiratory clearance (Cheung et al., 2020). This might be due to viral shedding taking longer in stool specimens than the respiratory ones, which must be considered when the test results of the patient from the respiratory specimens are negative, but they are still suspected of having the disease (Kipkorir et al., 2020; Kim et al., 2020; van Doorn et al., 2020). Individuals infected with SARS-CoV-2 who tested positive for the virus in GI specimens but tested negative in respiratory specimens showed an average period of viral shedding of 12.5 days (Wu et al., 2020; van Doorn et al., 2020). This confirms that viral shedding in stool lasts significantly longer, with a duration of up to 70 days after symptom onset (Kim et al., 2020).

Besides molecular detection, serological testing is commonly used to detect SARS-CoV-2 from specimens like NP swabs and saliva. Lateral flow assays can be used to detect suspected antigens or antibodies from the samples, which are typically less sensitive than molecular methods (Dinnes et al., 2020; WHO, 2020). Lateral flow assays can be used for detection in later stages of infection where the viral load is high. For instance, the optimal time for testing is between day 1 and day 3 before symptom onset or between day 5 and day 7 after symptom onset. However, antigen testing after these days may give false negative results due to a decrease in viral load in the second week after symptom onset (WHO, 2020).

3.4.5. Preprocessing Techniques for Viral Detection in Various Specimens

SARS-CoV-2 can be successfully identified from respiratory specimens using molecular or serological testing. These methods may require some preprocessing, such as heat lysis or inactivation using guanidium salts, depending on the type of specimen used (WHO, 2020; US Centers for Disease Control and Prevention, 2021; Norz et al., 2020). For instance, mucolytic agents like dithiothreitol (DTT), N acetyl-L-cysteine (NALC), or proteinase K (PK) may be used for mucus specimens to make them less thick before testing (Peng et al., 2020). Other examples include centrifugation for stool specimens (Kim et al., 2020) and PK for tissue specimens. Placing the specimens into compatible tubes for testing is significant. In this study, it is unclear what preprocessing steps were applied to the clinical samples or if any modification was applied to the usual steps, which might affect the stability of the test of choice.

3.5. Conclusion

Overall, selecting the right specimen and timing the collection is crucial for accurately detecting SARS-CoV-2. Knowing the specimen type and precise collection time helps minimise false positive and false negative results. Since early in the pandemic, RT-qPCR has yielded robust detection across multiple specimen types: NP and OP swabs remain the standard, but saliva has demonstrated comparable sensitivity (Bastos et al., 2021; Teo et al., 2021), and low-level RNA detection has also been observed in blood and urine, though much less commonly (Wang et al., 2020). In this study, fluorescence-based RT-RPA achieved perfect sensitivity (100%) with a specificity of 92%, resulting in an overall diagnostic accuracy of 95% when compared to RT-qPCR. In contrast, LFD-based RT-RPA demonstrated slightly lower sensitivity (84%) but higher specificity (97%), with a total accuracy of 92%. These findings confirm that fluorescence-based detection performs marginally better than LFD-based detection on average.

For RT-LAMP, sensitivity was limited to 71% and 89% when compared to fluorescence- and LFD-based RT-RPA, respectively. This reduced sensitivity may be attributed to the higher amplification temperature (65°C) and longer reaction time (approximately one hour), which increases the likelihood of non-specific amplification. Although RT-LAMP showed reasonable specificity (87%–89%), it did not outperform RT-RPA in either detection format. These results establish RT-RPA as a more effective isothermal diagnostic tool, with fluorescence-based detection offering the best performance overall. Nevertheless, following further optimisation, LFD-based RT-RPA remains a strong candidate for POCT due to its portability, ease of use, and high specificity.

RT-RPA also offers clear environmental advantages over RT-qPCR. It requires a constant low temperature (37–42°C) and can be performed without the need for thermocyclers or a continuous power supply. This substantially reduces energy consumption and the associated carbon footprint. In addition, the simplified workflow and reduced need for consumables contribute to lower plastic waste, making RT-RPA more sustainable and better suited to decentralised or low-resource settings.

Compared to earlier developments of RPA assays, this study introduced several technical improvements. These included the design of highly specific primers for fluorescence and lateral flow detections, optimisation of reaction conditions to minimise non-specific amplification and validation on a large panel of clinical samples using RT-qPCR as the gold standard. In contrast, many previous RPA studies either lacked clinical validation or relied on synthetic or contrived templates. The resulting RT-RPA assay in this study not only achieved higher sensitivity than prior versions but also showed excellent concordance with RT-qPCR, supporting its applicability as a reliable, scalable, and field-deployable diagnostic method.

Chapter 4: Design of RPA-based Respiratory Panel and Generating In Vitro Transcribed Templates for Assay Performance

4.1. Introduction

4.1.1. Role of Molecular Cloning in Viral Detection

One of the most important uses of molecular cloning involves detecting specific DNA sequences associated with infectious agents like respiratory viruses. Molecular cloning allows the replication of specific DNA sequences to produce large amounts of identical DNA fragments for further analysis. This process is significant for developing highly sensitive and specific diagnostic tests, including PCR-based ones (Tombuloglu et al., 2022). In a traditional cloning experiment, the DNA to be cloned is isolated from the cell of interest and treated with a specific restriction enzyme to be broken, producing shorter DNA sequences with overhangs, known as sticky ends. The same restriction enzyme cuts the vector DNA so that the sticky ends of the shorter DNA sequences join the vector DNA via complementary base pairing, forming weak hydrogen bonds between the base pairs to produce recombinant DNA molecules. DNA ligase enzyme facilitates the formation of two covalent phosphodiester bonds between the adjacent DNA fragments in an ATP-dependent reaction. The recombinant DNA is transferred into an easy-to-grow host organism, such as the laboratory strain of *E. coli*, so that the recombinant DNA molecules are replicated along with the host DNA. PCR is used to amplify the ligated DNA fragments to confirm the presence of an insert by using the primers hybridised at the ends of the assembled construct (Li and Elledge, 2007). PCR amplification can also be used at the beginning to prepare the insert from the template DNA rather than using restriction enzymes.

4.1.2. Types of Molecular Cloning

There are two major types of molecular cloning: ligase-dependent and ligase-independent. A few ligase-independent cloning methods, such as Gateway (Hartley et al., 2000), LIC (Bonsor et al., 2006), USER (Geu-Flores et al., 2007), SLIC (Li and Elledge, 2007), PIPE (Klock and Lesley, 2009), CPEC (Quan and Tian, 2009), OEC (Bryskin and Matsumara, 2010), FastCloning (Li et al., 2011), SLiCE (Zhang et al., 2012), and In-Fusion (Sleight and Sauro, 2013) have been developed in recent years. These methods are based on DNA pairing and homologous recombination. Therefore, designing compatible regions between vectors and DNA inserts may complicate experiments. Several ligase-dependent cloning methods can be used for the covalent ligation of a DNA insert to a plasmid vector: blunt-end ligation, sticky-end ligation, and TA cloning (Yao et al., 2016). Blunt-end ligation involves joining blunt-ended DNA fragments by the DNA ligase. These fragments do not need to match or complement each other for the ligation process. Restriction enzymes (e.g. EcoRV, SmaI) produce a straight cut in the vector and the insert, creating non-overhanging or blunt ends. The main advantage of this cloning strategy is that the desired insert does not need any restriction sites in its sequence. This is because the blunt-ended DNA fragments are already generated during PCR and may be ligated into a blunt-ended vector generated from restriction digest. As blunt ends do not have protruding ends, the ligation reaction only depends on the random collisions between them, making it 100 times less efficient than sticky-end ligation.

Sticky-end ligation, also known as cohesive-end ligation, is one of the most used strategies for molecular cloning. Restriction enzymes (e.g. EcoRI, HindIII) produce a staggered cut in the vector and the insert, creating sticky and overhanging ends. This type of ligation is based on joining two sticky ends with matching or complementary bases. Unfortunately, selecting appropriate sites for restriction digestion can be challenging in some cases due to the presence of internal sites. Additionally, cloning libraries of different inserts must include the prior addition of adapters. Adapters are chemically synthesised oligonucleotide sequences with one blunt and one sticky end, which can be used to correct restriction site mismatches. Sticky-end ligation is generally considered a better option than blunt-end ligation in molecular cloning, as it ensures that the DNA fragment of interest is inserted into the vector in the correct direction (Nguyen et al., 2018).

4.1.3. TOPO TA Cloning Technology

TA cloning is one of the most efficient strategies for cloning PCR products. Any desirable fragment with an extra A overhang can be cloned into any linearised vector with a complementary T overhang. Traditional TA cloning must have a ligation step to seal the joints of the vector with an insert. TOPO TA cloning is the restriction digestion-free and ligation-free version of TA cloning. This technique uses thermophilic *Taq* DNA polymerase to leave a single A overhang on the 3' end of PCR products. The complementary T overhang comes from a pre-cut, linear, cloning-ready TOPO vector, such as pCR™ 4-TOPO®, with a DNA topoisomerase I attached to its 3' end. DNA topoisomerase I, derived from the vaccinia virus, functions as both a restriction enzyme and a ligase. Restriction domain of DNA topoisomerase I detects and cleaves a single DNA strand at the pentapyrimidine sequence 5'-C/TCCTT-3' (Shuman et al., 1991, 1992), forming a covalent bond with the phosphate at the 3' T, followed by joining complementary A and T ends without using additional enzymes.

Since this enzyme works simultaneously as a restriction enzyme and a DNA ligase, TOPO TA cloning does not require additional restriction enzymes or a ligase, so it provides a quick and easy way to clone a fresh PCR product into a plasmid. In this study, TOPO® TA Cloning® Kits for Sequencing, along with the linearised plasmid vector pCR™ 4-TOPO®, were used to clone the desired DNA fragment. To ensure sufficient DNA was cloned into the vector, the sequence of interest was first amplified using PCR with primers specifically designed for conserved regions of the viral genome, identified through multiple sequence alignment. *Taq* polymerase was used for amplification due to its ability to add A overhangs to the 3' ends of PCR products, making them compatible with TOPO TA cloning. The amplified DNA and pCR™ 4-TOPO® vector were then mixed and joined by DNA topoisomerase I before being transformed into competent *E. coli* DH5α cells.

Following transformation, the plasmid DNA was extracted and validated through PCR and agarose gel electrophoresis to confirm the successful cloning of the target gene. The

linearised plasmid was subsequently used as a template for in vitro transcription, enabling the production of RNA corresponding to the cloned DNA. RNA transcripts were further analysed via agarose gel electrophoresis to assess their integrity and quality. Although, TOPO TA cloning, there are some limitations associated with this method which must be considered. Unfortunately, only a few plasmid backbones are TOPO-ready, and producing a TOPO vector alone is not convenient. The reaction efficiency may also fluctuate depending on the polymerase used, and additionally, the single A overhangs degrade over time, which may further affect ligation efficiency.

4.1.4. Factors Affecting PCR Efficiency and Strategies for Gene Amplification

Since oligonucleotides cannot efficiently anneal to the mismatched sequences, they may or may not produce a signal, which can cause the underestimation of copy numbers or the inability to detect them. In addition to sequence matching, primer-dimer formation, GC content, DNA template quality, PCR master mix, and inhibitors in the sample can influence the mismatch-induced effects and diagnostic efficiency (Stadhouders et al., 2010; Kralik and Ricchi, 2017; Ruijter et al., 2009). If the organism of interest is closely related to a species with existing sequence data, the gene can be amplified through PCR and sequenced using primers based on the known sequence information. Protein sequences of interest from several related species are aligned to identify conserved regions. Degenerate oligonucleotides, a mix of similar but not identical primers, are produced to allow the amplification of a portion of the gene of interest in related species using PCR. The template used for this amplification can be either genomic DNA or cDNA produced from the RNA. The resulting PCR fragments are then inserted into PCR cloning vectors and sequenced.

Designing degenerate primers creates a dilemma of increased sequence ambiguities and sufficient sequence specificity (Lang and Orgogozo, 2011). The higher the number of degenerate primers, the more annealing to the sites of interest. However, an increase in degeneracy will also increase the possibility of annealing to non-specific sites, which may lead to unwanted background amplification. Using genomic DNA as a template

offers the advantage of containing all members of a gene family in equal amounts. However, the introns may interfere with primer binding sites or produce a long PCR product that cannot be amplified as efficiently as shorter, non-specific PCR products (Lang and Orgogozo, 2011). Even though cDNA templates require additional steps to obtain, they can be used to overcome this issue as they produce PCR products of a known size. Genomic DNA can be extracted manually or using commercial kits, while cDNA requires RNA extraction followed by RT. Degenerate primers are not typically suitable for direct sequencing of the PCR fragments, as they can produce multiple overlapping peaks in the chromatogram. This means PCR products must be cloned into a plasmid vector, and the primers used for sequencing must be annealed to the insert-flanking vector sequence.

4.2. Hypothesis and Objectives

Hypothesis:

Accurate primer design targeting conserved viral genomic regions, combined with efficient cloning strategies such as TOPO TA cloning, enhances the specificity and reliability of molecular assays for detecting respiratory viruses. Optimising these parameters is essential for the development of robust diagnostic platforms, particularly those based on PCR and isothermal amplification.

Objectives:

1. To design and validate primers targeting highly conserved regions of essential respiratory virus genes to ensure specific amplification across diverse viral strains.

2. To evaluate the impact of degenerate bases in primer sequences on amplification efficiency and specificity, including risks of primer-dimer formation and non-specific products.

3. To assess the suitability of TOPO TA cloning for capturing and preserving viral gene targets, particularly in the context of assay development for RT-RPA.

4. To identify and address technical limitations associated with PCR-based amplification and TOPO TA cloning, particularly when working with variable sequence regions or larger amplicons.

4.3. Results

4.3.1. Primer Design for Influenza Virus Detection

After confirming SARS-CoV-2 detection using RT-RPA, additional viral targets were incorporated into the assay to evaluate its detection capacity and broaden its applicability across multiple pathogens. The gene target for each virus was determined based on the genetic conservation observed from their sequence alignment (**Table 5**). The gene targets were used to design specific PCR primers for the viruses as in Chapter 2.2., so that these target-specific primers would flank and bind to a part of the viral genome that encodes for the gene of interest.

Table 5. Name of the family, genus, and gene target of the selected viruses to be amplified by RT-RPA prior detection.

Accession Number	Virus	Family	Genera	Gene Target
PP878633.1	Human Influenza A	Orthomyxoviridae	Alphainfluenzavirus	M gene
OQ845404.1	Human Influenza B	Orthomyxoviridae	Betainfluenzavirus	M gene
KY296734.1	Human Respiratory Syncytial Virus A	Paramyxoviridae	Orthopneumovirus	F gene
OR466401.1	Human Respiratory Syncytial Virus B	Paramyxoviridae	Orthopneumovirus	N gene
OZ075302.1	Human Metapneumovirus	Paramyxoviridae	Metapneumovirus	N gene
MT232426.1	Human Parainfluenza Virus 1	Paramyxoviridae	Respirovirus	HN gene
LC486598.1	Human Parainfluenza Virus 2	Paramyxoviridae	Rubulavirus	HN gene
OR416987.1	Human Parainfluenza Virus 3	Paramyxoviridae	Respirovirus	HN gene
MN369047.1	Human Parainfluenza Virus 4	Paramyxoviridae	Rubulavirus	HN gene
LC817388.1	Human Rhinovirus A	Picornaviridae	Enterovirus	UTR
PP194099.1	Human Rhinovirus B	Picornaviridae	Enterovirus	UTR
OZ075367.1	Human Rhinovirus C	Picornaviridae	Enterovirus	UTR
MF085394.1	Human Adenovirus	Adenoviridae	Mastadenoviruses	L3 gene

Influenza viruses, particularly Influenza A, have one of the most diverse and evolutionary distinct genomes due to the presence of multiple subtypes (e.g. H1N1, H3N2) and strains. Influenza A and B viruses consist of 8 RNA segments, each encoding different proteins. These viruses often undergo antigenic drift and antigenic shift, causing significant genetic variability (Schotsaert and García-Sastre, 2016). Therefore, it is challenging to use only a single set of primers for specific influenza detection (**Figure 14A** and **Figure 15A**). To determine the most conserved region within the influenza genome, the matrix (M) gene was targeted as it shows the highest genetic conservation among all 8 genome segments of Influenza A and B viruses. A set of primers was designed for each virus to target the conserved regions, covering the most recent and available isolates (**Figure 14B** and **Figure 15B**). To further enhance primer coverage, degenerates were introduced, spanning the highly conserved and sequence- verified mismatches (**Figure 14C** and **Figure 15C**).

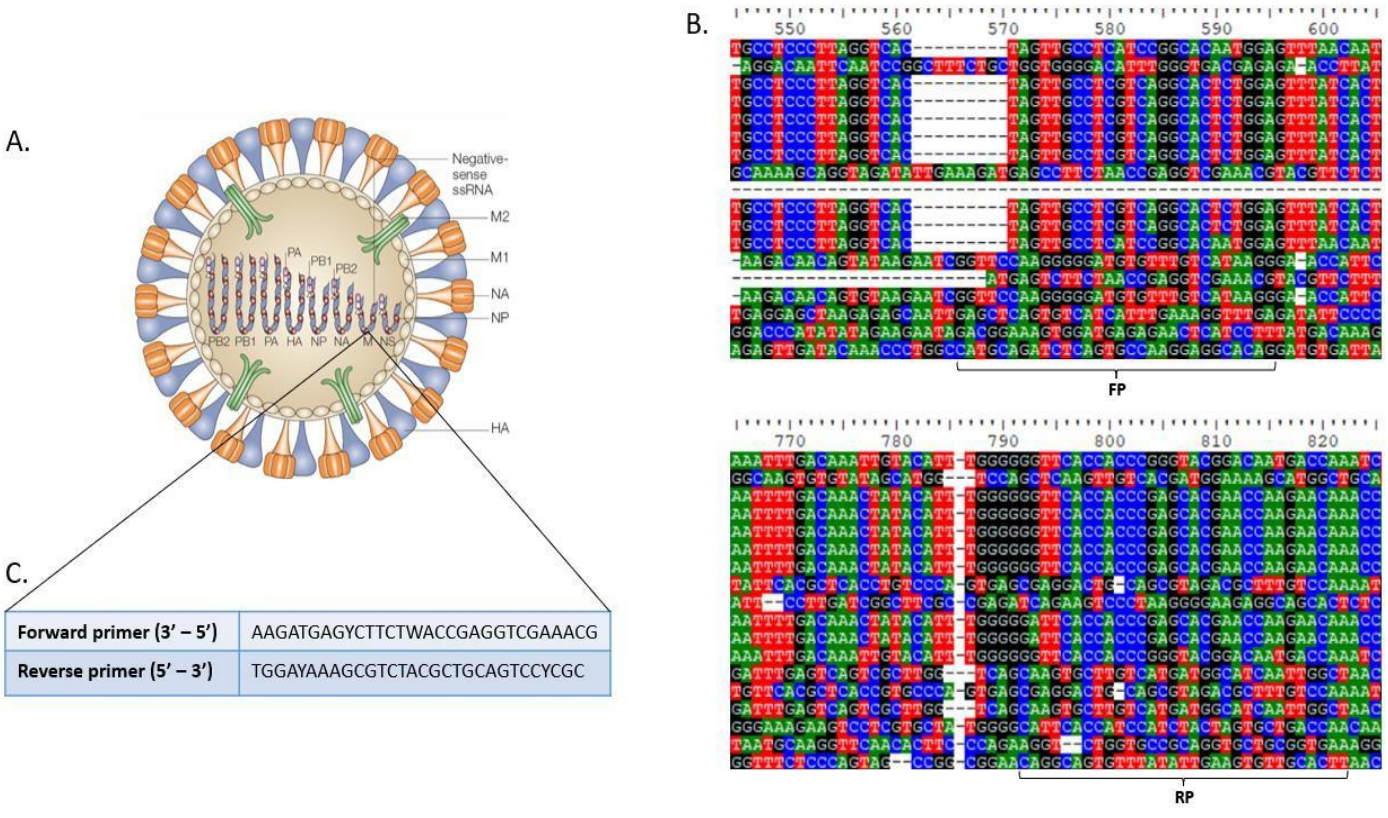

Figure 14. Primer design outline for Influenza A.

A. Schematic diagram of Influenza A virion with all the essential proteins involved in its life cycle and infectivity, pointing to the M gene as the main target for viral detection. **B.** Multiple sequence alignment of the M gene from various Influenza A strains, showing the most conserved regions within the genome selected for primer binding sites. Forward primer (FP) and reverse primer (RP) regions are indicated by brackets, highlighting minimal sequence variability across isolates. **C.** Specifically designed forward and reverse primer sequences to amplify a conserved fragment of the M gene by RT-RPA, allowing broad compatibility across Influenza A variants. Degenerate bases, W (represents A or T) and Y (represents C or T), were incorporated into forward and reverse primer sequences to account for minor sequence variability and improve primer inclusivity (Image Source: Warnatsch, 2013).

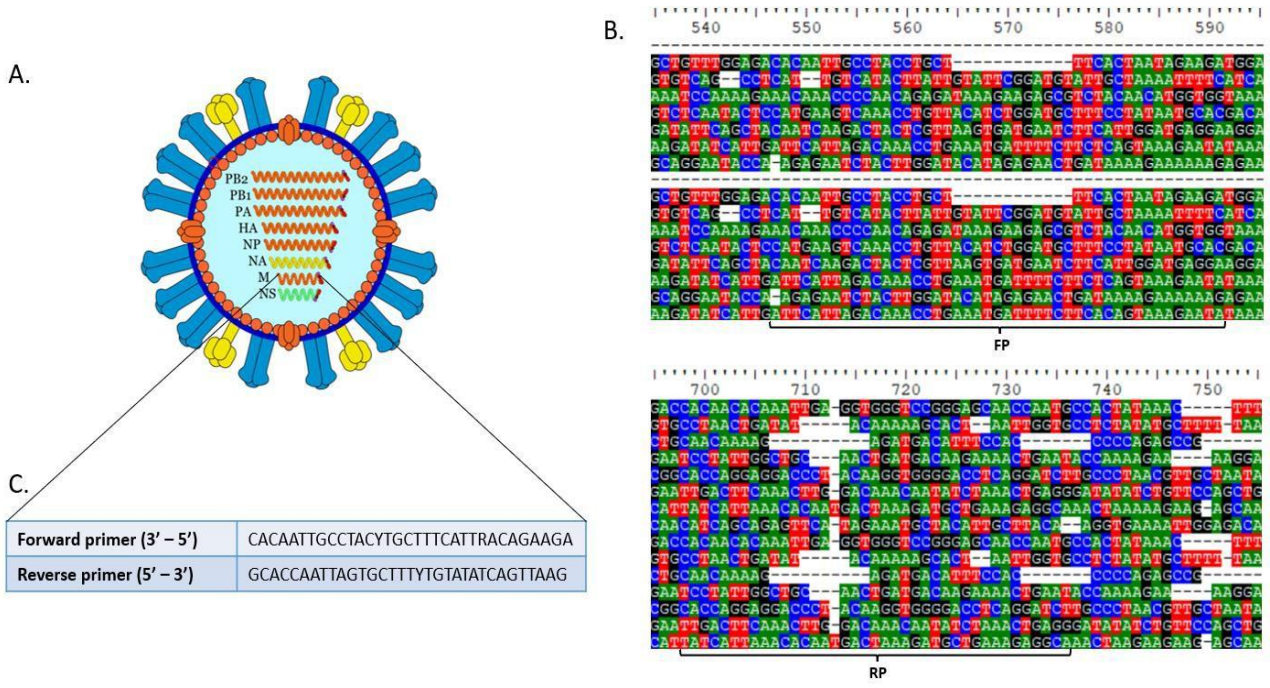

Figure 15. Primer design outline for Influenza B.

A. Schematic diagram of the Influenza B virion with all the essential proteins involved in its life cycle and infectivity, pointing to the M gene as the main target for viral detection. **B.** Multiple sequence alignment of the M gene from various Influenza B strains, showing the most conserved regions within the genome selected for primer binding sites. Forward primer (FP) and reverse primer (RP) regions are indicated by the brackets, highlighting minimal sequence variability across isolates. **C.** Specifically designed forward and reverse primer sequences to

amplify a conserved fragment of the M gene by RT-RPA, allowing broad compatibility across Influenza B variants. Degenerate bases, Y (represents C or T) and R (represents A or G), were incorporated into forward and reverse primer sequences to account for minor sequence variability and improve primer inclusivity (Image Source: Ruangrong Cheepsattayakorn, 2013).

4.3.2. Primer Design for RSV-A and RSV-B Detection

RSV has 2 major subtypes, RSV-A and RSV-B, which show significant genetic variability, particularly in the glycoprotein (G) gene. Like many other RNA viruses, they also have a high mutation rate driven by the error-prone RdRP, which can cause sequence variability within specific regions of the viral genome. Having a high mutation rate complicates the primer design, making it a challenge to use a single set of primers (**Figure 16A and Figure 17A**). The most conserved regions within the RSV genome were identified to be fusion (F) and nucleocapsid (N) genes for RSV-A and RSV-B, respectively (**Figure 16B and Figure 17B**). This is because they showed the highest genetic conservation among 10 different genes encoded by the RSV genome. A set of primers was designed for each virus to target the conserved regions, covering the most recent and available isolates **(Figure 16C and Figure 17C**).

A.

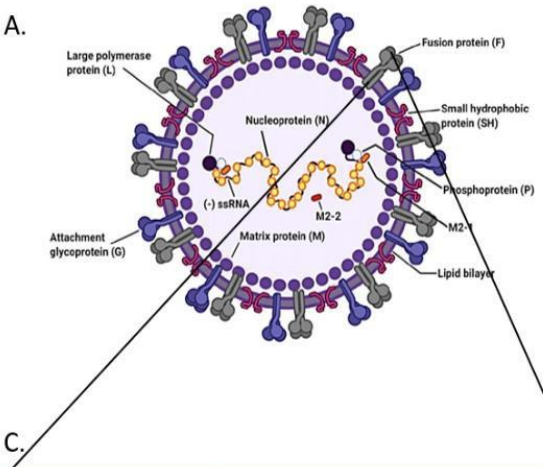

B.

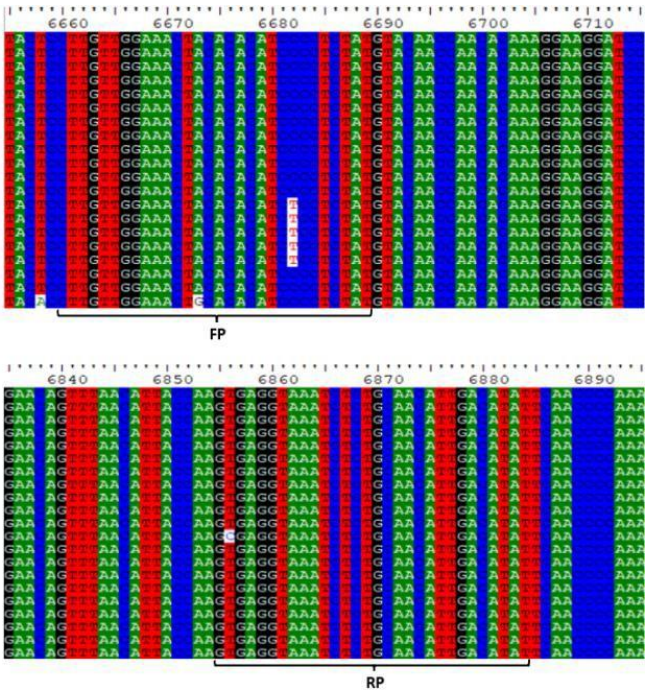

C.

Forward primer (3′ – 5′)	CTTGTTGGAAACTACACACATCCCCTCTAT
Reverse primer (5′ – 3′)	TGAATATGTCAATGTTGCAGAGATTTACCTCAC

Figure 16. Primer design outline for RSV-A.

A. Schematic diagram of RSV-A virion with all the essential proteins involved in its life cycle and infectivity, pointing to the F gene as the main target for viral detection. **B.** Multiple sequence alignment of the F gene from various RSV-A strains, showing the most conserved regions within the genome selected for primer binding sites. Forward primer (FP) and reverse primer (RP) regions are indicated by the brackets, highlighting minimal sequence variability across isolates. **C.** Sequences of the forward and reverse primers specifically designed to amplify a conserved fragment of the F gene by RT-RPA, allowing broad compatibility across RSV-A variants (Image Source: Alrashedi et al., 2021).

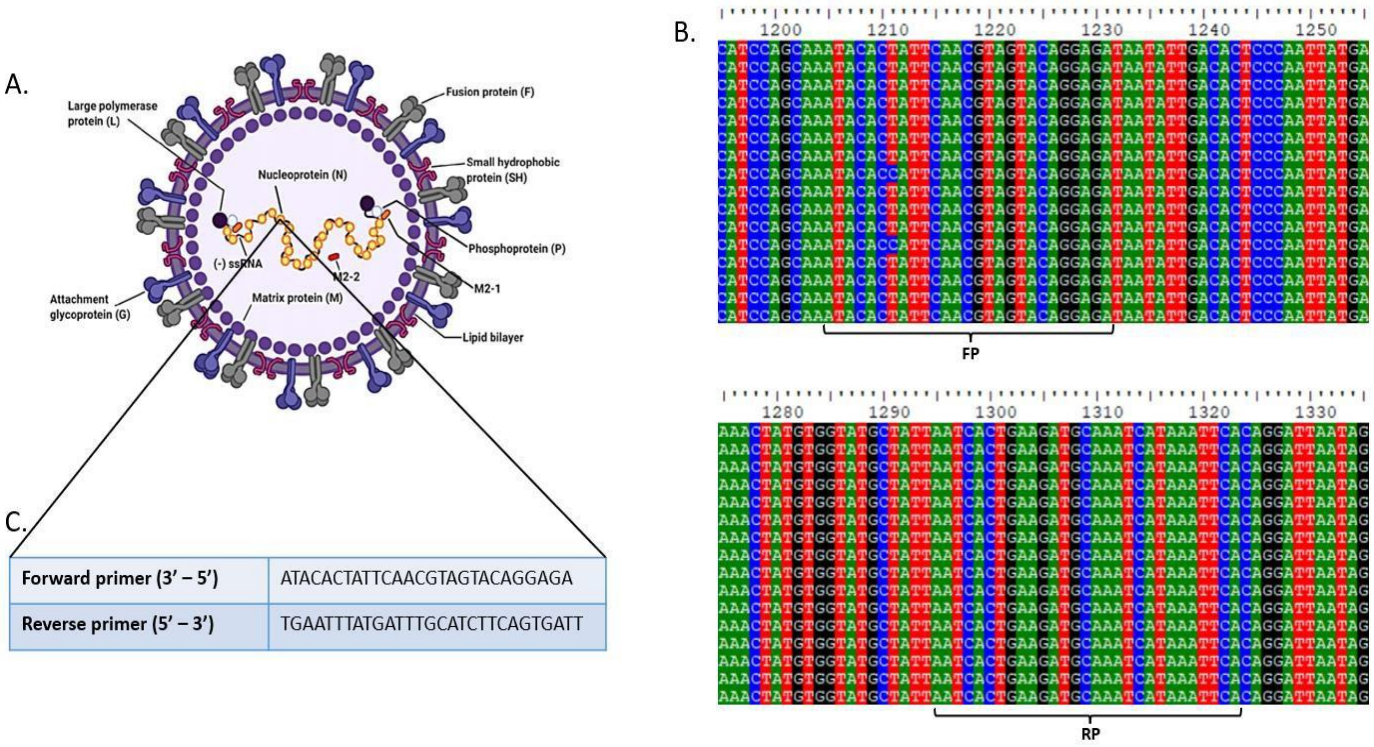

Figure 17. Primer design outline for RSV-B.

A. Schematic diagram of RSV-B virion, with all the essential proteins involved in its life cycle and infectivity, pointing to the N gene as the main target for viral detection**. B.** Multiple sequence alignment of the N gene from various RSV-B strains, showing the most conserved regions within the genome selected for primer binding sites. Forward primer (FP) and reverse primer (RP) regions are indicated by the brackets, highlighting minimal sequence variability across isolates. **C.** Sequences of the forward and reverse primers specifically designed to amplify a conserved fragment of the N gene by RT-RPA, allowing broad compatibility across

RSV-B variants.

4.3.3. Primer Design for hMPV Detection

hMPV has 2 major genetic lineages, A and B, each further divided into A1, A2, B1, and B2 sublineages. Even with 2 primary lineages, there is variability in the nucleotide sequences, particularly in the glycoprotein (G) and fusion (F) genes, which often undergo mutations due to immune pressure. This makes it difficult for a single set of primers to effectively bind to all variants, possibly leading to incomplete or biased detection (**Figure 18A).** The most conserved region within the hMPV genome was identified to be nucleocapsid (N) gene as it shows the highest genetic conservation among 8 different genes encoded by the hMPV genome. This is due to its significant role in viral replication and transcription, causing functional constraints on its variability. A set of primers was designed to target the conserved regions, covering the most recent and available isolates (**Figure 18B**). Degenerates were then introduced to span the highly conserved and sequence-verified mismatches (**Figure 18C**).

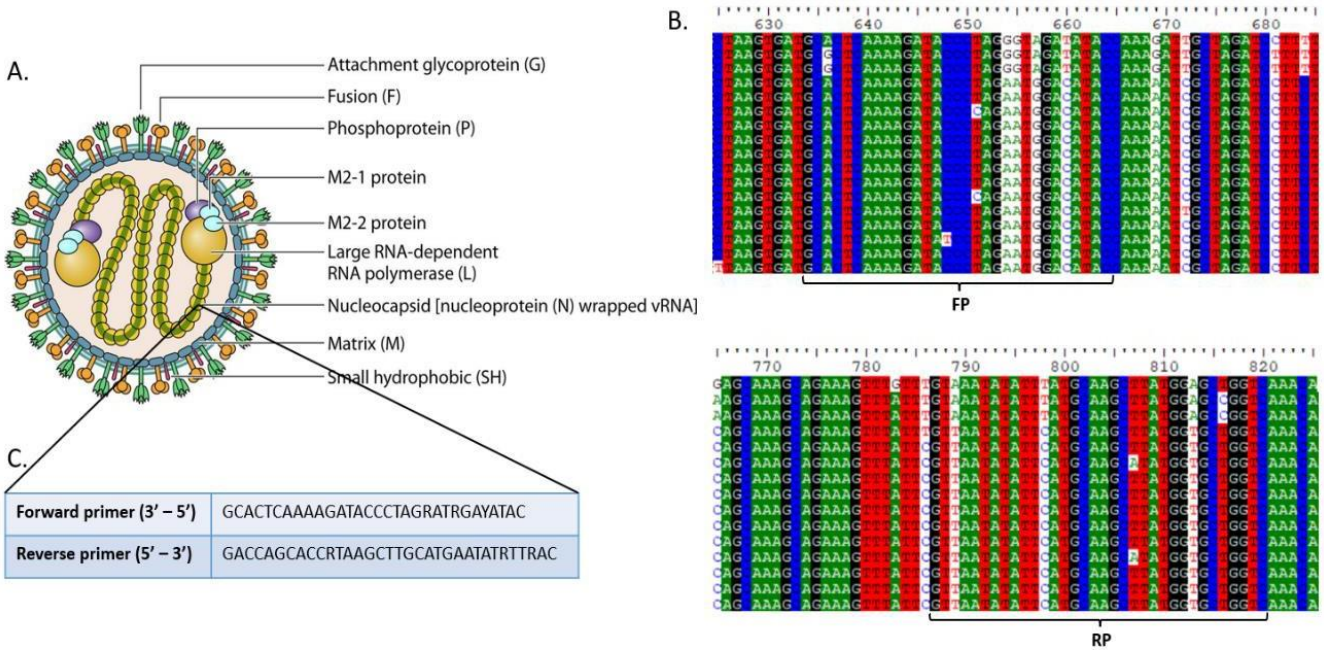

Figure 18. Primer design outline for hMPV.

A. Schematic diagram of the hMPV virion with all the essential proteins involved in its life cycle and infectivity, pointing to the N gene as the main target for viral detection. **B.** Multiple sequence alignment of the N gene from various hMPV strains, showing the most conserved regions within the genome selected for primer binding sites. Forward primer (FP) and reverse primer (RP) regions are indicated by the brackets, highlighting minimal sequence variability across isolates. **C.** Sequences of the forward and reverse primers specifically designed to amplify a conserved fragment of the N gene by RT-RPA, allowing broad compatibility across hMPV variants. Degenerate bases, R (represents A or G) and Y (represents C or T), were incorporated into forward and reverse primer sequences to account for minor sequence variability and improve primer inclusivity (Image Source: Céspedes et al., 2016).

4.3.4. Primer Design for HPIV Detection

There are 4 main types of HPIV, which are HPIV-1, HPIV-2, HPIV-3, and HPIV-4. Each of these viruses is genetically distinct, with differences in their genomic organisation and sequence variability. Therefore, using a single set of primers that can effectively amplify sequences from all 4 types is challenging, reducing amplification efficiency and specificity (**Figure 19A, Figure 20A, Figure 21A, and Figure 22A**). The most conserved region within the HPIV genome was determined to be the haemagglutinin-neuraminidase (HN) gene across all 4 types, as it shows the highest genetic conservation among 6 major genes encoded by the HPIV genome. The HN gene encodes a surface glycoprotein, which is highly exposed and subject to immune system recognition, making it a suitable candidate as a gene target. A set of primers was designed for each virus to target the conserved regions, covering the most recent and available isolates (**Figure 19B, Figure 20B, Figure 21B, and Figure 22B**). Degenerates were then introduced to span the highly conserved and sequence-verified mismatches (**Figure 19C, Figure 20C, Figure 21C, and Figure 22C**).

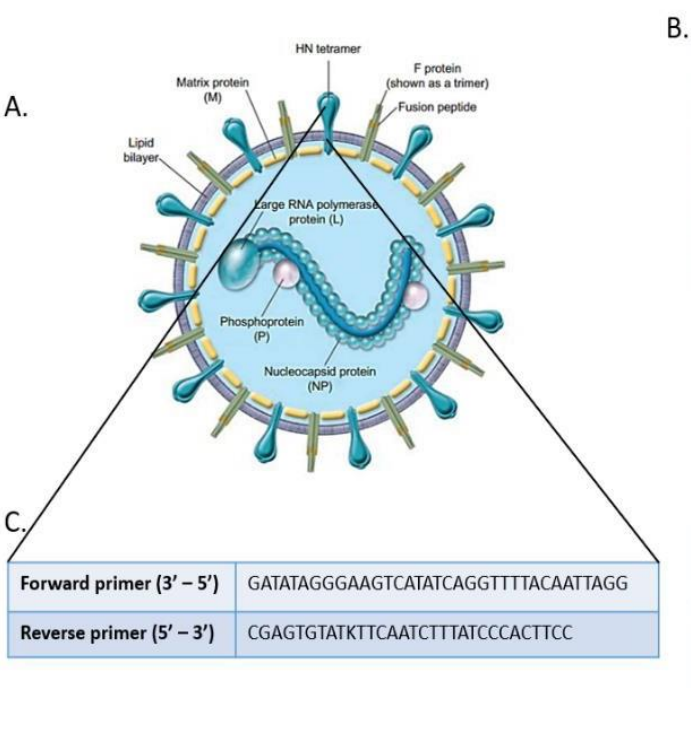

C.

Forward primer (3′ – 5′)	GATATAGGGAAGTCATATCAGGTTTTACAATTAGG
Reverse primer (5′ – 3′)	CGAGTGTATKTTCAATCTTTATCCCACTTCC

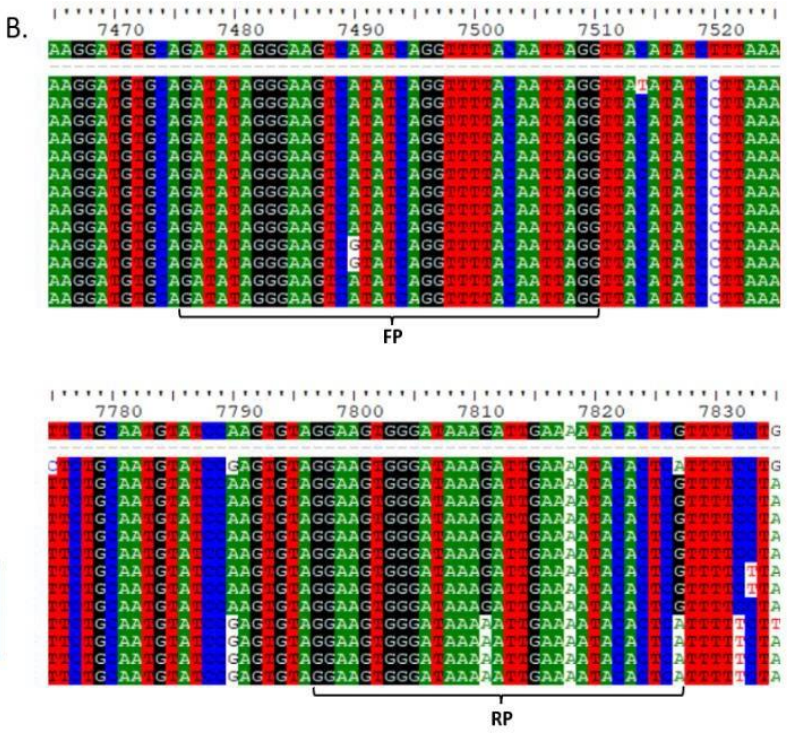

Figure 19. Primer design outline for HPIV-1.

A. Schematic diagram of the HPIV-1 virion with all the essential proteins involved in its life cycle and infectivity, pointing to the HN gene as the main target for viral detection. **B.** Multiple sequence alignment of the HN gene from various HPIV-1 strains, showing the most conserved regions within the genome selected for primer binding sites. Forward primer (FP) and reverse primer (RP) regions are indicated by the brackets, highlighting minimal sequence variability across isolates. **C.** Sequences of the forward and reverse primers specifically designed to amplify a conserved fragment of the HN gene by RT-RPA, allowing broad compatibility across HPIV-1 variants. Degenerate bases, K (represents G or T) and Y (represents C or T), were incorporated into reverse primer sequence to account for minor sequence variability and improve primer inclusivity (Image Source: Falsey, 2012).

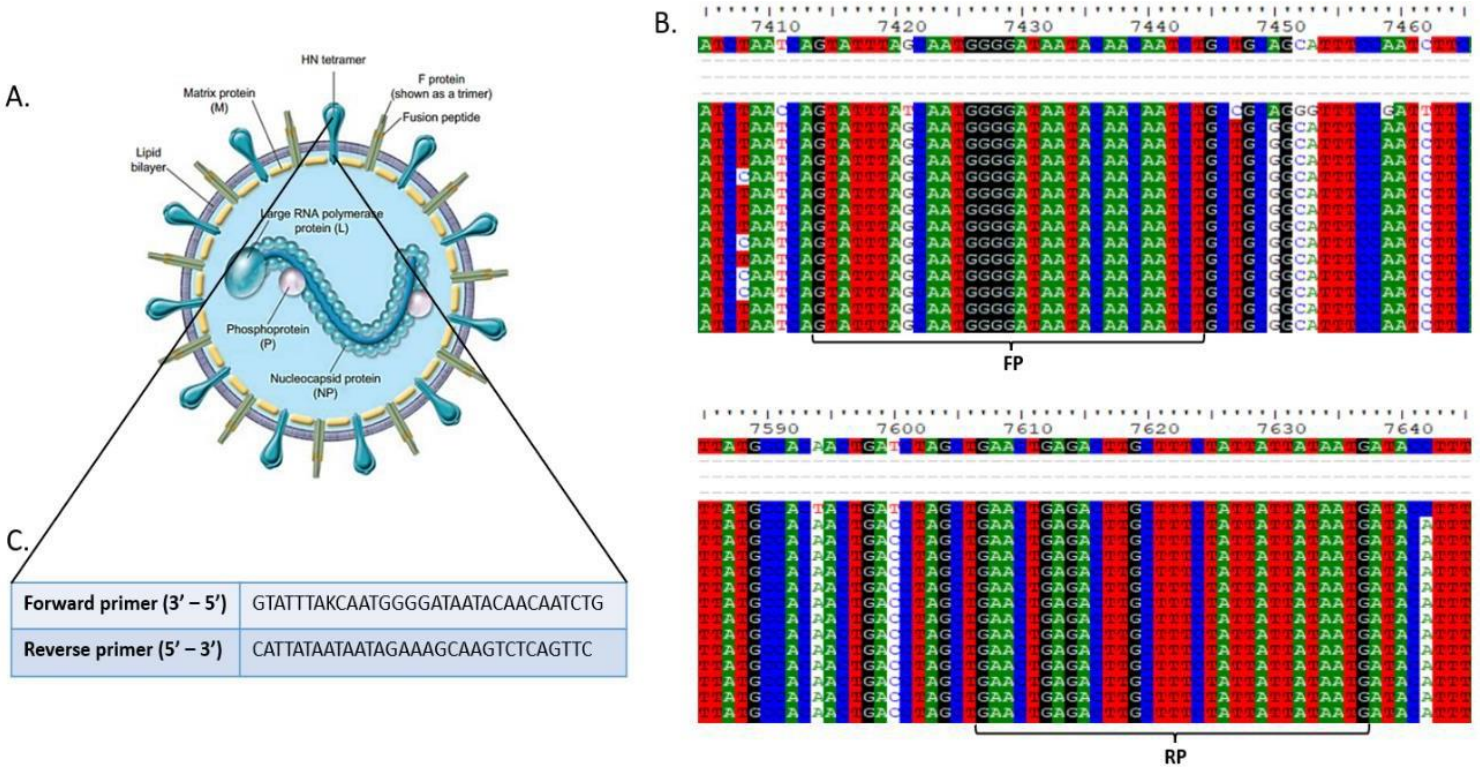

Figure 20. Primer design outline for HPIV-2.

A. Schematic diagram of the HPIV-2 virion with all the essential proteins involved in its life cycle and infectivity, pointing to the HN gene as the main target for viral detection. **B.** Multiple sequence alignment of the HN gene from various HPIV-2 strains, showing the most conserved regions within the genome selected for primer binding sites. Forward primer (FP) and reverse primer (RP) regions are indicated by the brackets, highlighting minimal sequence variability across isolates. **C.** Sequences of the forward and reverse primers specifically designed to amplify a conserved fragment of the HN gene by RT-RPA, allowing broad compatibility across HPIV-2 variants. Degenerate bases, K (represents G or T), were incorporated into forward primer sequence to account for minor sequence variability and improve primer inclusivity.

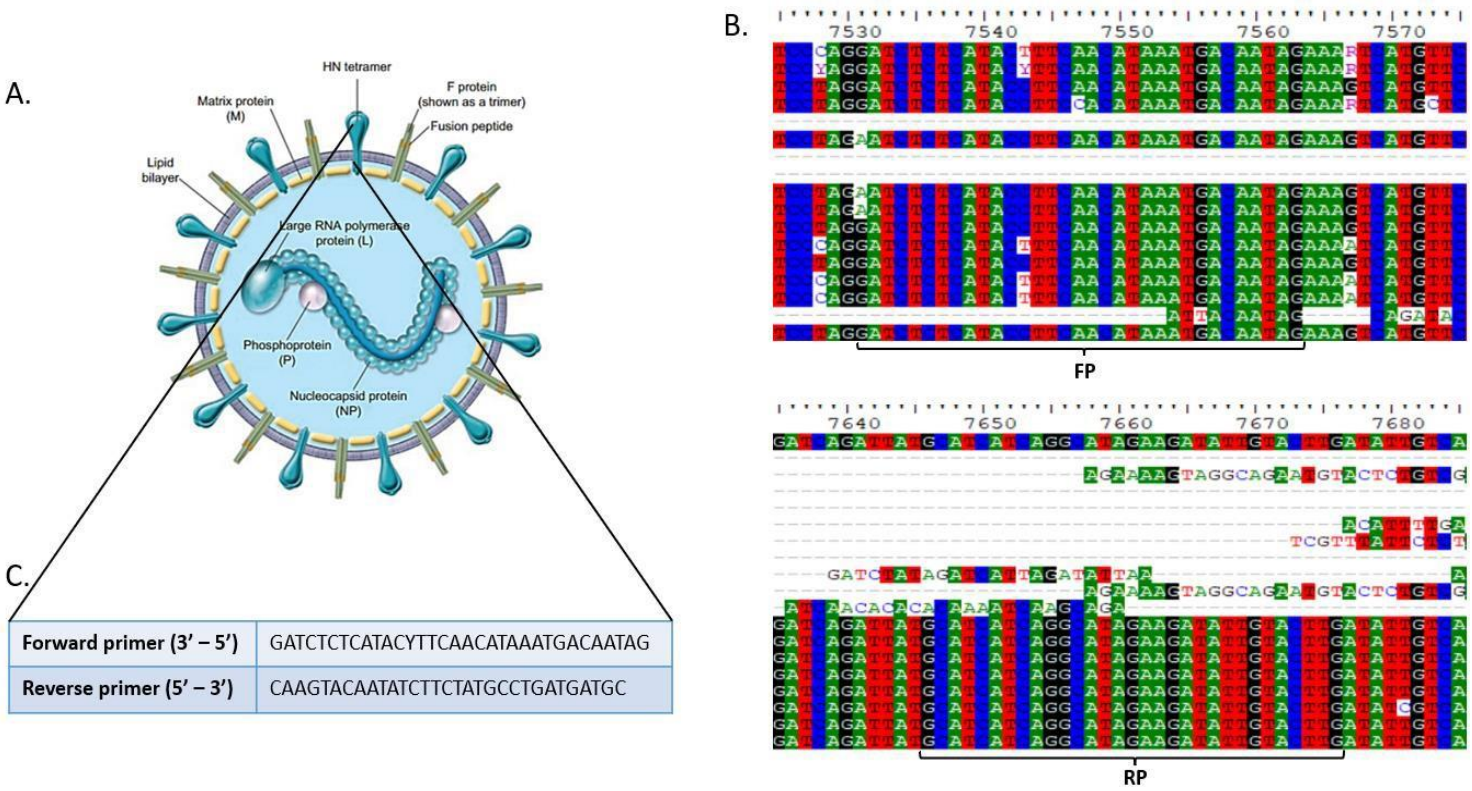

Figure 21. Primer design outline for HPIV-3.

A. Schematic diagram of the HPIV-3 virion with all the essential proteins involved in its life cycle and infectivity, pointing to the HN gene as the main target for viral detection. **B**. Multiple sequence alignment of the HN gene from various HPIV-3 strains, showing the most conserved regions within the genome selected for primer binding sites. Forward primer (FP) and reverse primer (RP) regions are indicated by the brackets, highlighting minimal sequence variability across isolates. **C**. Sequences of the forward and reverse primers specifically designed to amplify a conserved fragment of the HN gene by RT-RPA, allowing broad compatibility across HPIV-3 variants. Degenerate bases, Y (represents C or T), were incorporated into forward primer sequence to account for minor sequence variability and improve primer inclusivity.

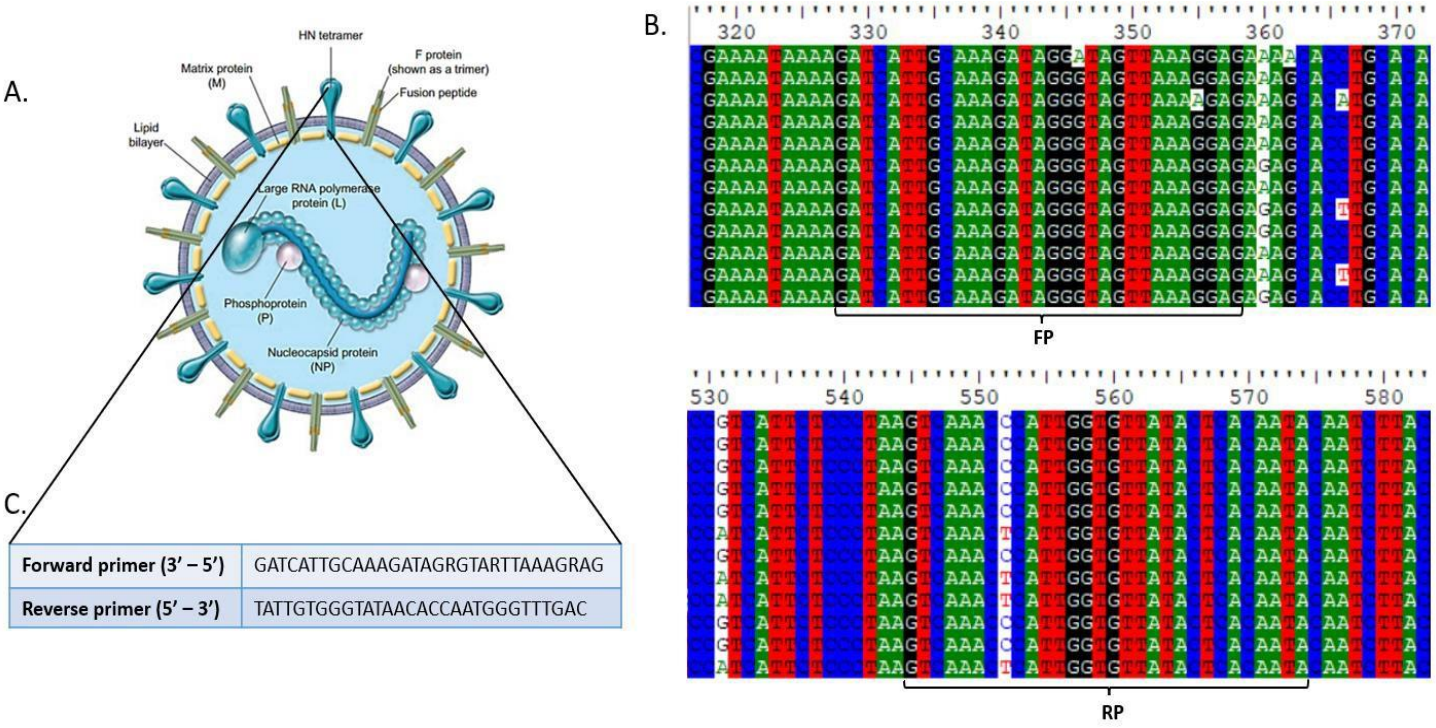

Figure 22. Primer design outline for HPIV-4.

A. Schematic diagram of the HPIV-4 virion with all the essential proteins involved in its life cycle and infectivity, pointing to the HN gene as the main target for viral detection. **B**. Multiple sequence alignment of the HN gene from various HPIV-4 strains, showing the most conserved regions within the genome selected for primer binding sites. Forward primer (FP) and reverse primer (RP) regions are indicated by the brackets, highlighting minimal sequence variability across isolates. **C**. Sequences of the forward and reverse primers specifically designed to amplify a conserved fragment of the HN gene by RT-RPA, allowing broad compatibility across HPIV-4 variants. Degenerate bases, R (represents A or G), were incorporated into forward primer sequence to account for minor sequence variability and improve primer inclusivity.

4.3.5. Primer Design for HRV Detection

HRV is one of the most genetically diverse viruses with over 150 serotypes, divided into three species: HRV-A, HRV-B, and HRV-C. HRV has highly variable regions, particularly in its capsid and non-structural proteins. These regions are significantly variable among different serotypes, causing a challenge to design primers

complementary to all HRV variants (**Figure 23A, Figure 24A, and Figure 25A**). The most conserved region within the HRV genome was determined to be the 5' untranslated region (UTR) as it shows the highest conservation among 11 genes (4 structural and 7 non-structural) encoded by the HRV genome. Even though 5' UTR does not code for any proteins, it is critical in promoting viral translation through the internal ribosome entry site. A set of primers was designed for each virus to target the conserved regions, covering the most recent and available isolates (**Figure 23B, Figure 24B, and Figure 25B**). Degenerates were then introduced to span the highly conserved and sequence-verified mismatches (**Figure 23C, Figure 24C, and Figure 25C**).

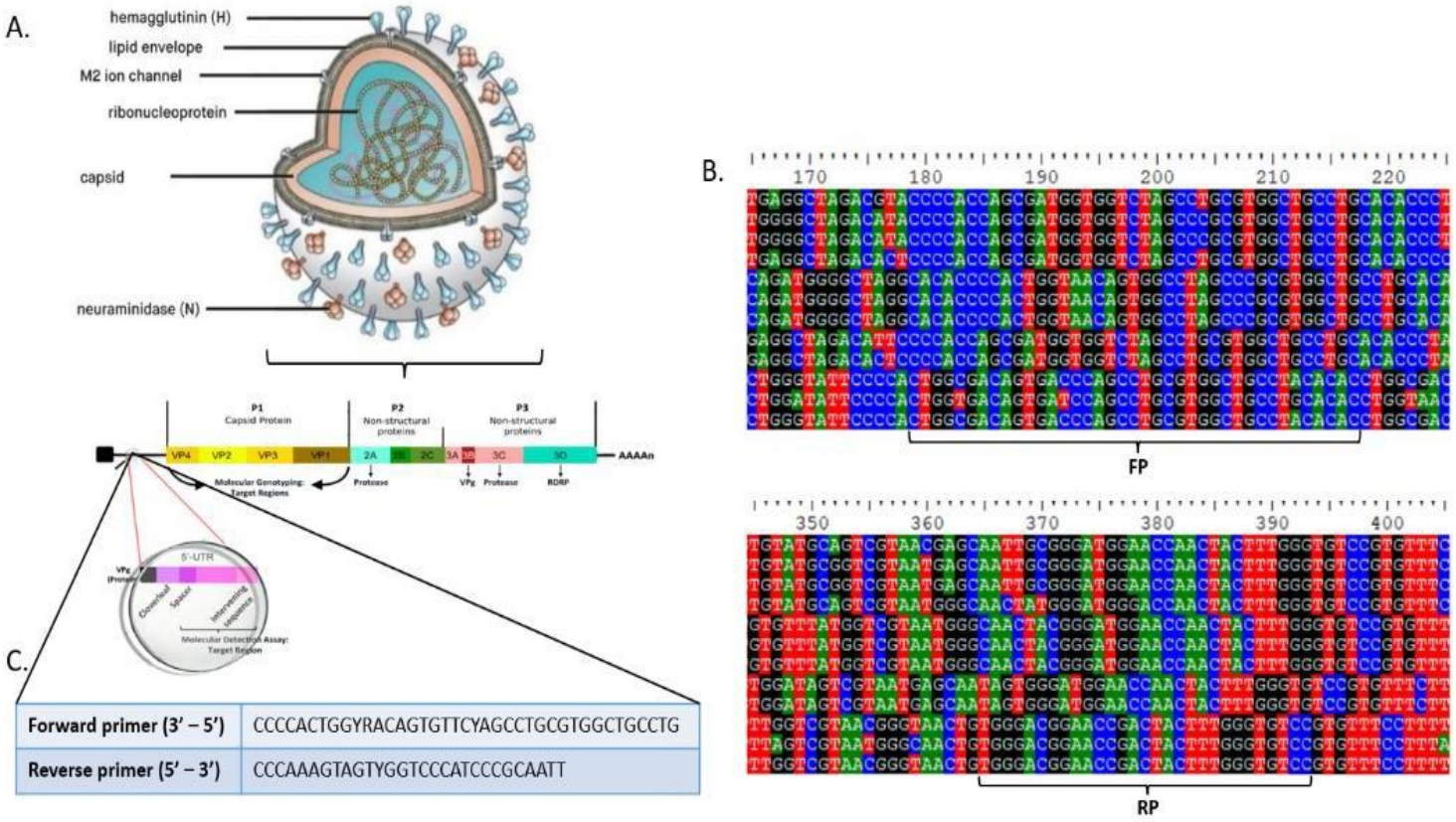

Figure 23. Primer design outline for HRV-A.

A. Schematic diagram of the HRV-A virion with all the essential proteins involved in its life cycle and infectivity, pointing to the 5' UTR as the main target for viral detection. **B.** Multiple sequence alignment of the 5' UTR from various HRV-A strains, showing the most conserved regions within the genome selected for primer binding sites. Forward primer (FP) and reverse primer (RP) regions are indicated by the brackets, highlighting minimal sequence variability

across isolates. **C.** Sequences of the forward and reverse primers specifically designed to amplify a conserved fragment of the 5' UTR by RT-RPA, allowing broad compatibility across HRV-A variants. Degenerate bases, Y (represents C or T) and R (represents A or G), were incorporated into forward and reverse primer sequences to account for minor sequence variability and improve primer inclusivity (Image Source: Khan et al., 2021).

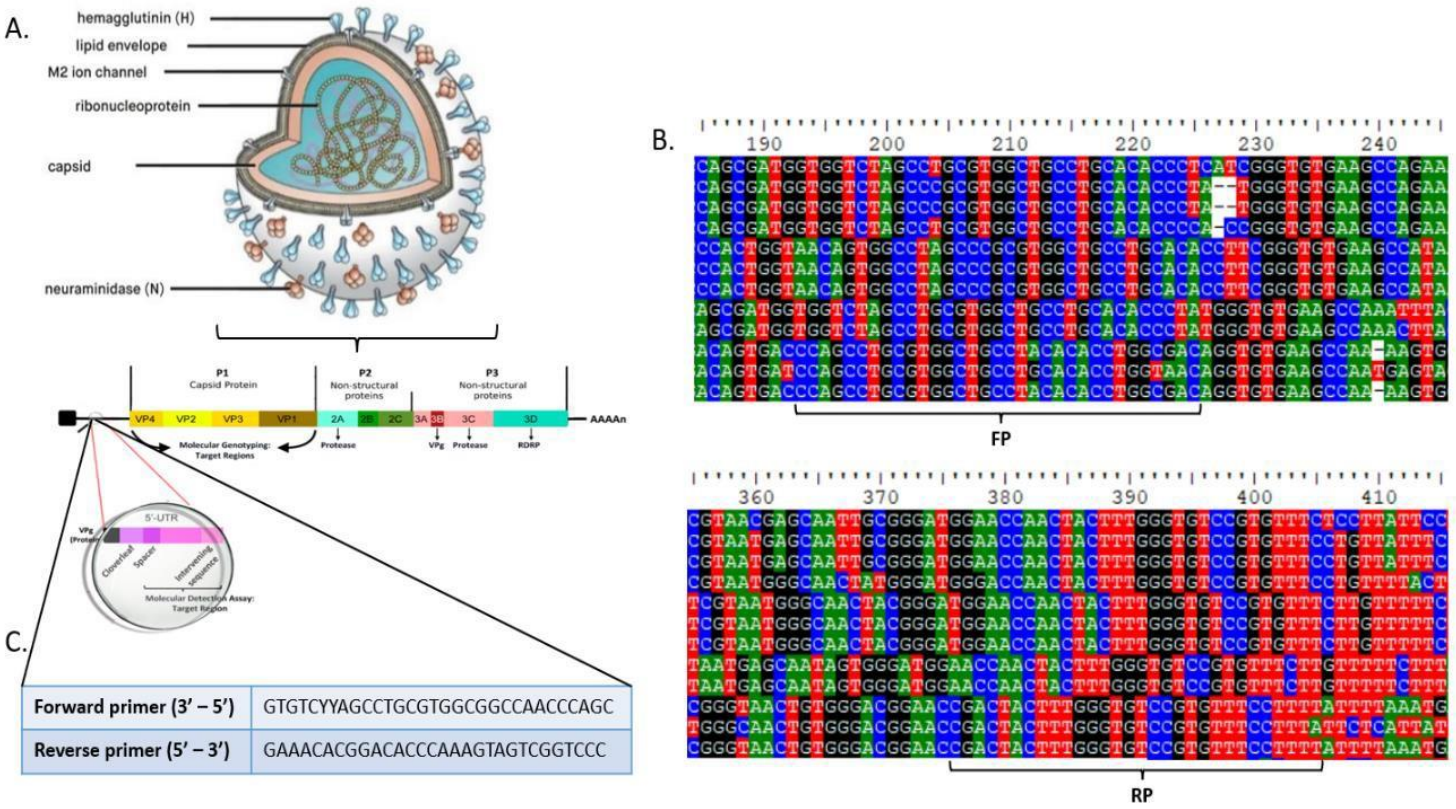

Figure 24. Primer design outline for HRV-B.

A. Schematic diagram of the HRV-B virion with all the essential proteins involved in its life cycle and infectivity, pointing to the 5' UTR as the main target for viral detection**. B.** Multiple sequence alignment of the 5' UTR from various HRV-B strains, showing the most conserved regions within the genome selected for primer binding sites. Forward primer (FP) and reverse primer (RP) regions are indicated by the brackets, highlighting minimal sequence variability across isolates**. C.** Sequences of the forward and reverse primers specifically designed to amplify a conserved fragment of the 5' UTR by RT-RPA, allowing broad compatibility across HRV-B variants. Degenerate bases, Y (represents C or T), were incorporated into forward primer sequence to account for minor sequence variability and improve primer inclusivity.

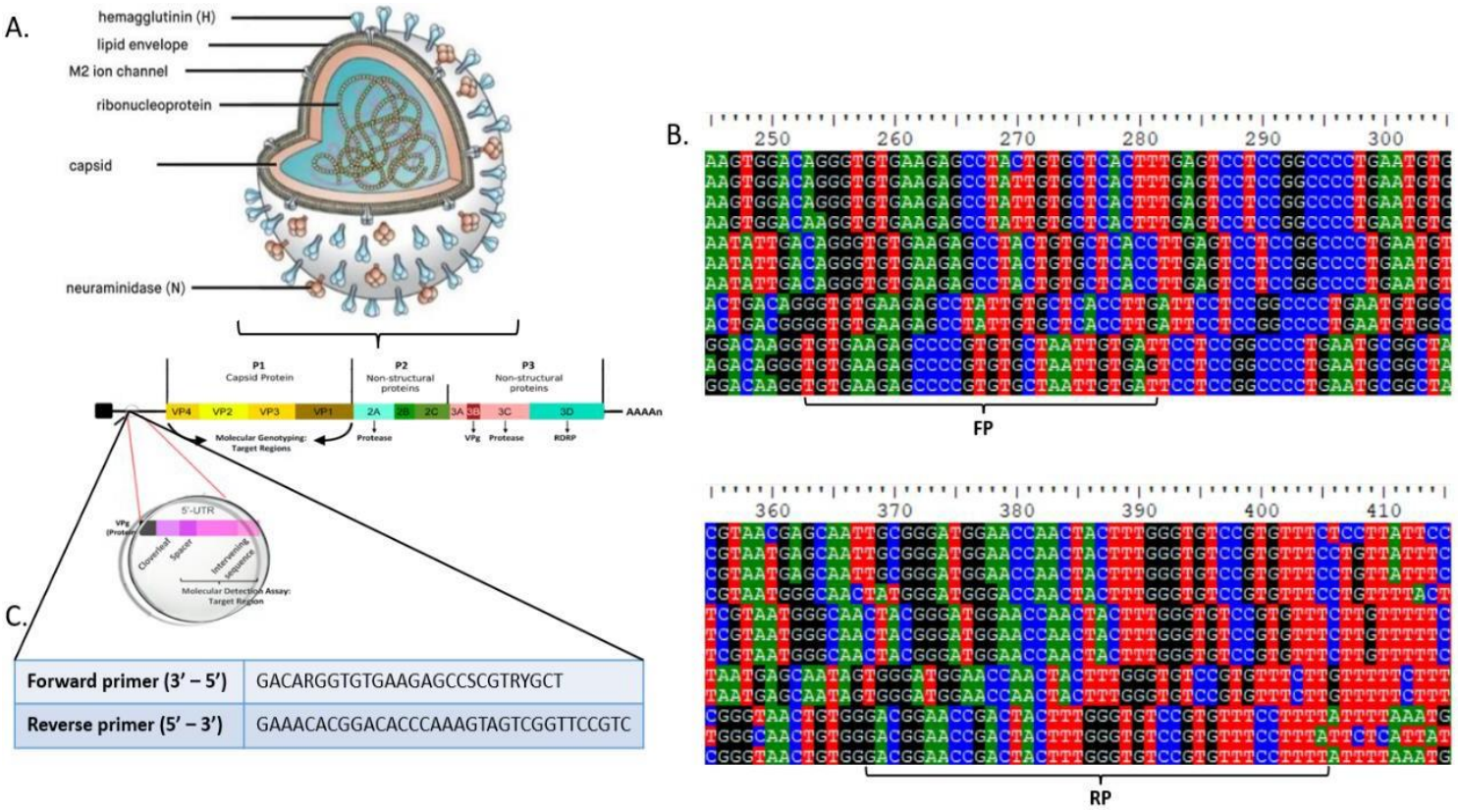

Figure 25. Primer design outline for HRV-C.

A. Schematic diagram of the HRV-C virion with all the essential proteins involved in its life cycle and infectivity, pointing to the 5' UTR as the main target for viral detection. **B.** Multiple sequence alignment of the 5' UTR from various HRV-C strains, showing the most conserved regions within the genome selected for primer binding sites. Forward primer (FP) and reverse primer (RP) regions are indicated by the brackets, highlighting minimal sequence variability across isolates. **C.** Sequences of the forward and reverse primers specifically designed to amplify a conserved fragment of the 5' UTR by RT-RPA, allowing broad compatibility across HRV-C variants. Degenerate bases, R (represents A or G), S (represents C or G), and Y (represents C or T), were incorporated into forward primer sequence to account for minor sequence variability and improve primer inclusivity.

4.3.6. Primer Design for hAdV Detection

More than 100 serotypes of hAdV are classified into seven species, from A to G. These serotypes have significant genetic variability, particularly in regions encoding structural proteins like the hexon, penton base, and fibre proteins, which play a significant role in host receptor binding and immune evasion. This variability complicates the design of a single set of primers that can efficiently target all serotypes (**Figure 26A**). The most conserved region within the hAdV genome was determined to be the L3 gene, specifically encoding the major late protein, hexon, as it shows the highest conservation among the 5 early (E1 to E4) and 5 late genes (L1 to L5) encoded by the hAdV genome. A set of primers was designed to target the conserved regions, covering the most recent and available isolates (**Figure 26B**). Degenerates were then introduced to span the highly conserved and sequence-verified mismatches (**Figure 26C**).

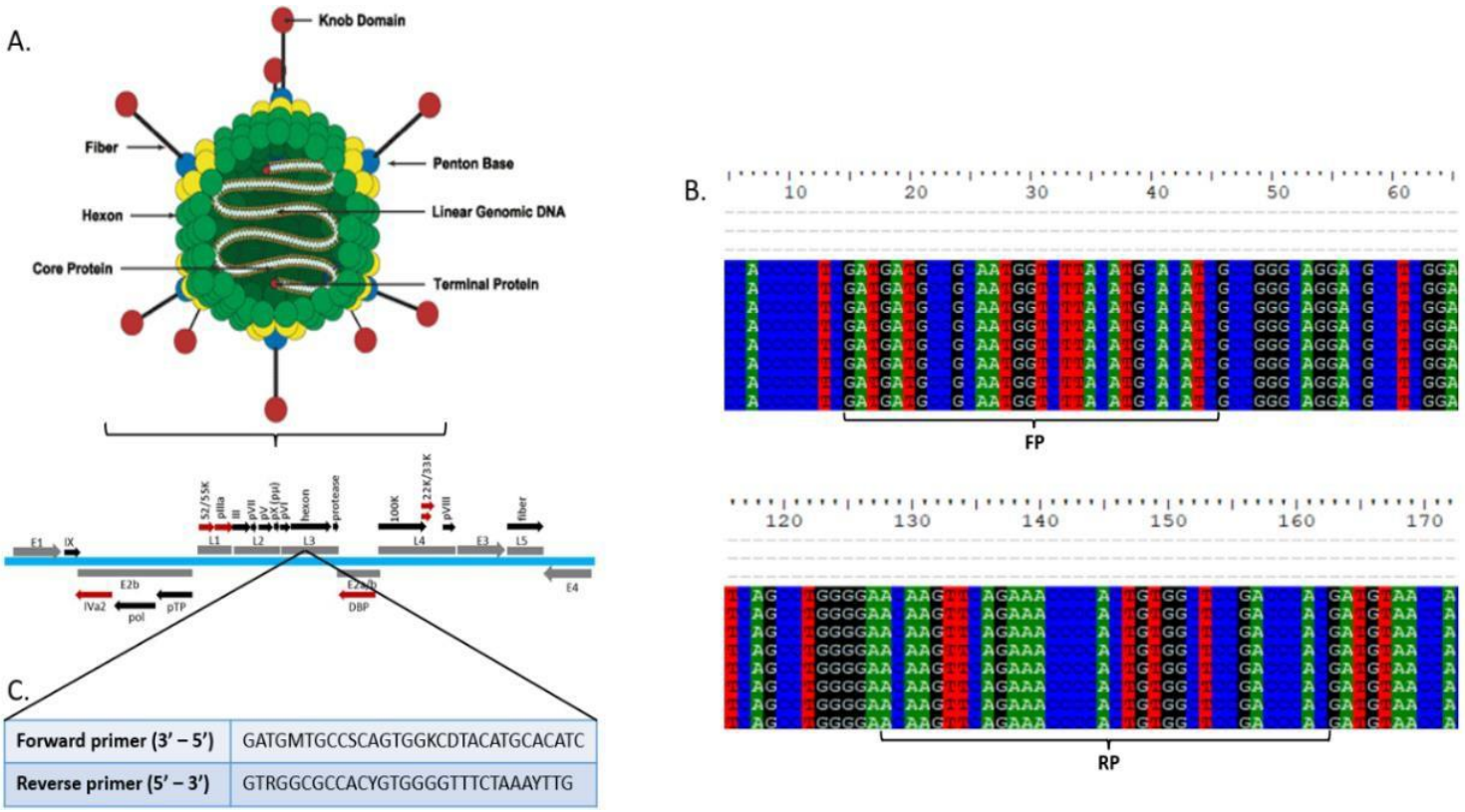

Figure 26. Primer design outline for hAdV.

A. Schematic diagram of the hAdV virion with all the essential proteins involved in its life cycle and infectivity, pointing to the L3 gene as the main target for viral detection. **B.** Multiple

sequence alignment of the L3 gene from various hAdV strains, showing the most conserved regions within the genome selected for primer binding sites. Forward primer (FP) and reverse primer (RP) regions are indicated by the brackets, highlighting minimal sequence variability across isolates**. C.** Sequences of the forward and reverse primers specifically designed to amplify a conserved fragment of the L3 gene by RT-RPA, allowing broad compatibility across hAdV variants. Degenerate bases, M (represents A or C), S (represents C or G), K (represents G or T), D (represents A, G, or T), R (represents A or G), and Y (represents C or T), were incorporated into forward and reverse primer sequences to account for minor sequence variability and improve primer inclusivity (Image Source: Kamel et al., 2009).

4.3.7. Extraction and Amplification of Viral Genetic Materials

DNA and RNA extraction was performed to isolate the genetic material of interest from the cultured DNA and RNA viruses. RT process was used to produce cDNA from the isolated viral RNA using RT enzyme. The gene targets were used to design specific PCR primers for the viruses as in Chapter 2.2., so that these target-specific primers would flank and bind to a part of the viral genome that encodes for the gene of interest. Then, the flanked regions of each viral genome were amplified by PCR using their calculated annealing temperatures (Thermofisher.com, 2024) (**Table 6**).

Table 6. Name of the viruses, their forward and reverse primers, and specific annealing temperatures used in PCR prior TOPO TA cloning.

Virus	Forward Primer	Reverse Primer	Annealing Temperature (°C)
Human Influenza A	AAGATGAGYCTTCTWACCGAGGTCGAAACG	TGGAYAAAGCGTCTACGCTGCAGTCCYCGC	49
Human Influenza B	CACAATTGCCTACYTGCTTTCATTRACAGAAGA	GCACCAATTAGTGCTTTYTGTATATCAGTTAAG	49
Human Respiratory Syncytial Virus A	CTTGTTGGAAACTACACACATCCCCTCTAT	TGAATATGTCAATGTTGCAGAGATTTACCTCAC	54
Human Respiratory Syncytial Virus B	ATACACTATTCAACGTAGTACAGGAGA	TGAATTTATGATTTGCATCTTCAGTGATT	49
Human Metapneumovirus	GCACTCAAAAGATACCCTAGRATRGAYATAC	GACCAGCACCRTAAGCTTGCATGAATATRTTRAC	49
Human Parainfluenza Virus 1	GATATAGGGAAGTCATATCAGGTTTTACAATTAGG	CGAGTGTATKTTCAATCTTTATCCCACTTCC	49
Human Parainfluenza Virus 2	GTATTTAKCAATGGGGATAATACAACAATCTG	CATTATAATAATAGAAAGCAAGTCTCAGTTC	49
Human Parainfluenza Virus 3	GATCTCTCATACYTTCAACATAAATGACAATAG	CAAGTACAATATCTTCTATGCCTGATGATGC	49
Human Parainfluenza Virus 4	GATCATTGCAAAGATAGRGTARTTAAAGRAG	GTCAAACCCATTGGTGTTATACCCACAATA	49
Human Rhinovirus A	CCCCACTGGYRACAGTGTTCYAGCCTGCGTGGCTGCCTG	CCCAAAGTAGTYGGTCCCATCCCGCAATT	49
Human Rhinovirus B	GTGTCYYAGCCTGCGTGGCGGCCAACCCAGC	GAAACACGGACACCCAAAGTAGTCGGTCCC	49
Human Rhinovirus C	GACARGGTGTGAAGAGCCSCGTRYGCT	GAAACACGGACACCCAAAGTAGTCGGTTCCGTC	49
Human Adenovirus	GATGMTGCCSCAGTGGKCDTACATGCACATC	GTRGGCGCCACYGTGGGGTTTCTAAAYTTG	60

4.3.8. PCR Amplification and TOPO TA Cloning for Assay Development

To generate a working template and evaluate assay performance, each gene corresponding to the intended viruses (**Table 5**) was amplified using standard PCR conditions. The amplified PCR products were then used to clone into the pCR®4-TOPO® TA vector (**Figure 27**) using the Invitrogen TOPO® TA Cloning Kit according to the manufacturer's instructions. TOPO TA cloning is based on the principle that a single A overhang left by the Taq polymerase on the 3' end of the PCR product interacts with the pre-cut, linear, cloning-ready TOPO vector, which already has a complementary T overhang. DNA topoisomerase I is covalently attached to the TOPO vector on the 3' end, which acts as both a restriction enzyme and a ligase. It cleaves and joins DNA strands at the 3' phosphate group, allowing efficient ligation of PCR inserts with the vector. The TOPO vector containing the gene of interest was transformed into competent *E. coli* DH5α cells using heat shock (42°C for 45 sec) to facilitate DNA uptake. Transformed cells were then plated onto selective agar plates with ampicillin to allow the growth of colonies with recombinant plasmids. Isolated colonies were then grown in liquid culture, and plasmid DNA was extracted using a PureLink™ Quick Plasmid Miniprep Kit according to the manufacturer’s instructions. Successful cloning of the insert was verified by PCR using specific RPA primers.

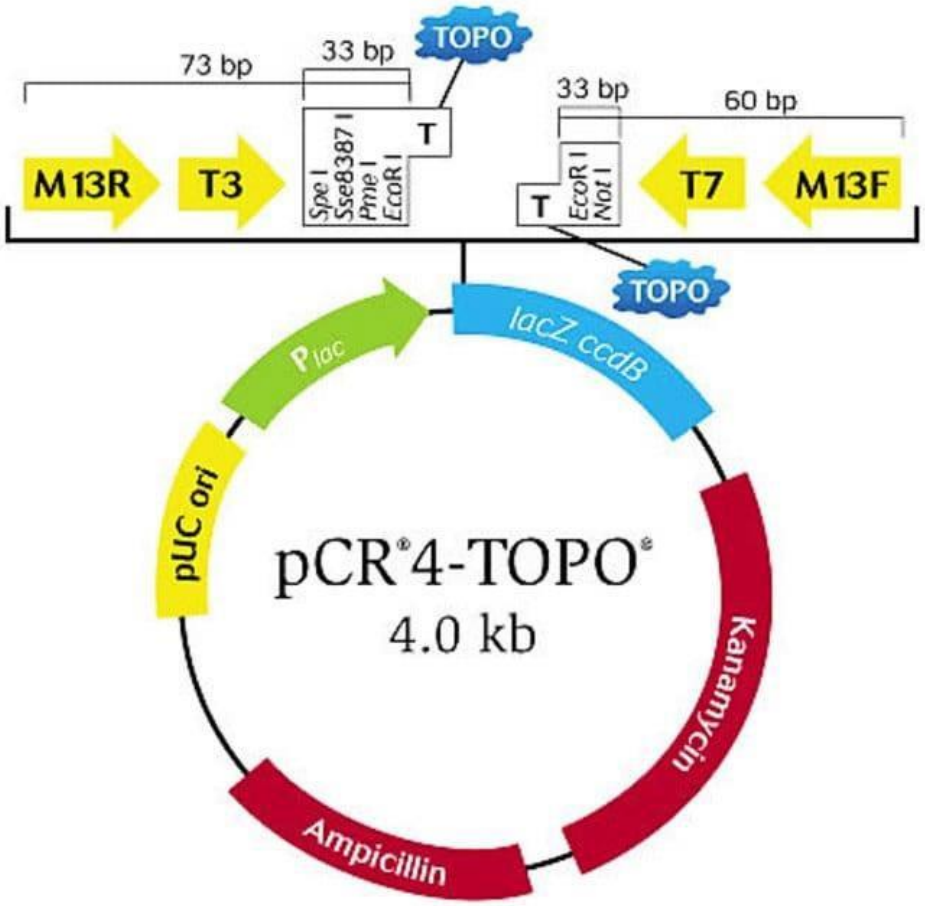

Figure 27. Schematic diagram of pCR®4-TOPO® TA vector.

This vector comes with 3´T overhangs for efficient ligation of *Taq*-amplified PCR products containing 3´A overhangs. The vector contains both ampicillin and kanamycin resistance markers, as well as a LacZα-ccdB gene fusion for positive selection and blue/white colony screening. Multiple cloning sites have been removed from the vector to shorten the distance between sequencing primer sites and the insert site to as little as 33bp. The remaining cloning sites still include flanking EcoRI sites for simplified excision of cloned PCR products and a unique Sse8387I site for generating nested deletions before sequencing. The vector also comes with four common sequencing primers: M13 forward, M13 reverse, T7, and T7 (Image Source: Thermofisher.com, 2024).

4.3.9. Screening and Verification of TOPO TA Clones

The TOPO TA cloning method involves ligating a specific PCR product with a known size into a TOPO vector. In an ideal situation, the vector will only contain that one

desired insert with a specific length. Since only a single DNA sequence is targeted, there will be only one distinct band corresponding to the length of the insert. Following TOPO TA cloning, agarose gel electrophoresis was used to screen for positive clones and verify the presence of the desired insert. Colonies were selected, and plasmid DNA was isolated and analysed to confirm successful cloning.

Visible bands at ~197bp correspond to the M gene insert of Influenza A (**Figure 28, left panel**). The size of the bands was consistent with the expected size of the amplified M gene, indicating successful cloning of the PCR product into the pCR®4-TOPO® TA vector. The presence of a single, distinct band at the expected size for the M gene confirms that the plasmid contains the desired insert without any contaminating products (**Figure 28, right panel**).

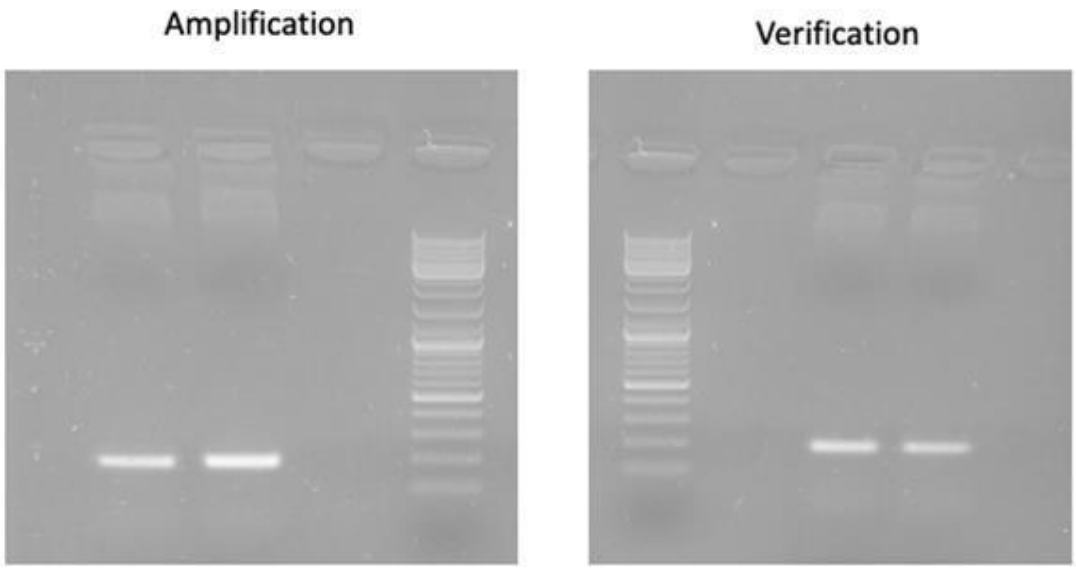

Figure 28. Screening for recombinant plasmids containing the M gene of Influenza A using agarose gel electrophoresis.

A 2% agarose gel was used to analyse plasmid DNA from transformed colonies, following TOPO TA cloning of the M gene of Influenza A into the pCR®4-TOPO® TA vector. The GeneRuler 1kb Plus DNA Ladder was included with fragment sizes ranging from 75bp to 20,000bp. The left panel shows a visible band at approximately 197bp, whereas the right panel shows the verification of the band size after plasmid purification, both corresponding to the

expected size of the M gene insert. A single, distinct band in each lane indicates successful cloning of the M gene into the vector without additional products.

Visible bands at ~107bp correspond to the M gene insert of Influenza B (**Figure 29, left panel**). The size of the bands was consistent with the expected size of the amplified M gene, indicating successful cloning of the PCR product into the pCR®4-TOPO® TA vector. The presence of a single, distinct band at the expected size for the M gene confirms that the plasmid contains the desired insert without any contaminating products (**Figure 29, right panel**).

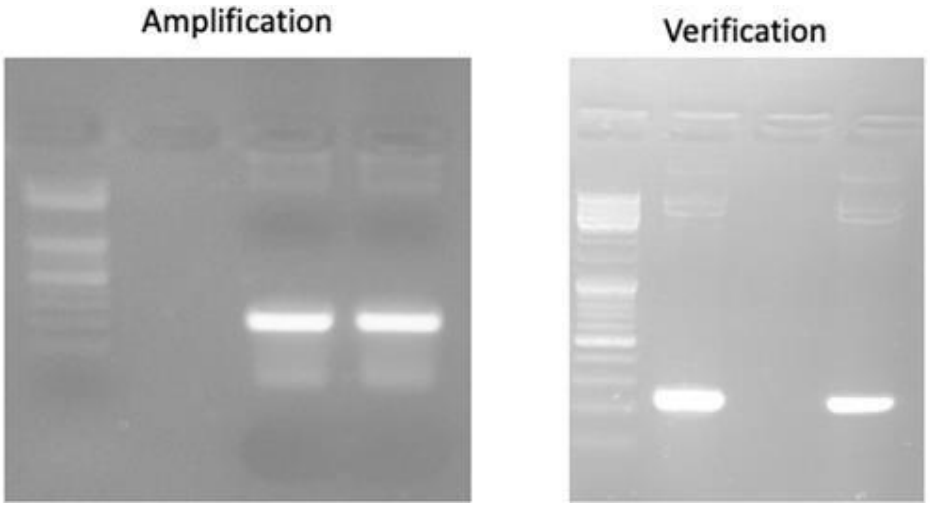

Figure 29. Screening for recombinant plasmids containing the M gene of Influenza B using agarose gel electrophoresis.

A 2% agarose gel was used to analyse plasmid DNA from transformed colonies, following TOPO TA cloning of the M gene of Influenza B into the pCR®4-TOPO® TA vector. The GeneRuler 1kb Plus DNA Ladder was included with fragment sizes ranging from 75bp to 20,000bp. The left panel shows visible bands at approximately 107bp, whereas the right panel shows the verification of the band size after plasmid purification, both corresponding to the expected size of the M gene insert. A single, distinct band in each lane indicates successful cloning of the M gene into the vector without additional products.

Visible bands at ~166bp correspond to the F gene insert of RSV-A (**Figure 30, left panel**). The size of the band was consistent with the expected size of the amplified F gene, indicating successful cloning of the PCR product into the pCR®4-TOPO® TA vector. The presence of a single, distinct band at the expected size for the F gene confirms that the plasmid contains the desired insert without any contaminating products (**Figure 30, right panel**).

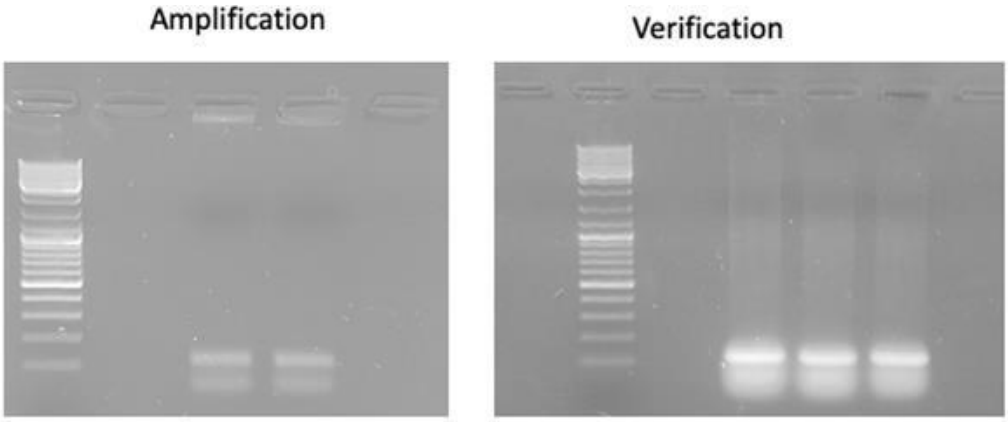

Figure 30. Screening for recombinant plasmids containing the F gene of RSV-A using agarose gel electrophoresis.

A 2% agarose gel was used to analyse plasmid DNA from transformed colonies, following TOPO TA cloning of the F gene of RSV-A into the pCR®4-TOPO® TA vector. The GeneRuler 1kb Plus DNA Ladder was included with fragment sizes ranging from 75bp to 20,000bp. The left panel shows visible bands at approximately 166bp, whereas the right panel shows the verification of the band size after plasmid purification, both corresponding to the expected size of the F gene insert. A single, distinct band in each lane indicates successful cloning of the F gene into the vector without additional products.

Visible bands at ~64bp correspond to the N gene insert of RSV-B (**Figure 31, left panel**). The size of the bands was consistent with the expected size of the amplified N gene, indicating successful cloning of the PCR product into the pCR®4-TOPO® TA vector. The presence of a single, distinct band at the expected size for the N gene confirms that the plasmid contains the desired insert without any non-specific

amplification or contaminating products (**Figure 31, right panel**).

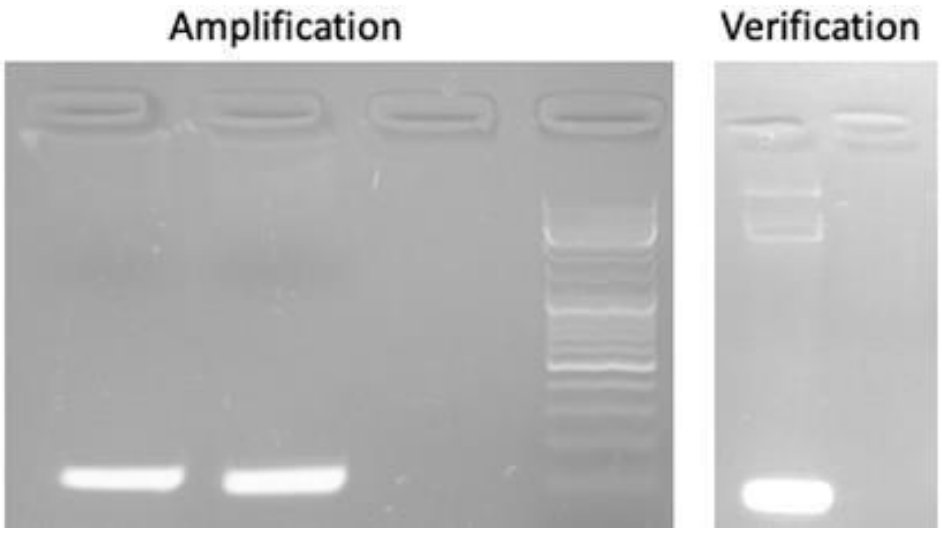

Figure 31. Screening for recombinant plasmids containing the N gene of RSV-B using agarose gel electrophoresis.

A 2% agarose gel was used to analyse plasmid DNA from transformed colonies, following TOPO TA cloning of the N gene of RSV-B into the pCR®4-TOPO® TA vector. The GeneRuler 1kb Plus DNA Ladder was included with fragment sizes ranging from 75bp to 20,000bp. The panel shows visible bands at approximately 64bp, whereas the right panel shows the verification of the band size after plasmid purification, both corresponding to the expected size of the N gene insert. A single, distinct band in each lane indicates successful cloning of the N gene into the vector without additional products.

Visible bands at ~123bp correspond to the N gene insert of hMPV (**Figure 32, left panel**). The size of the bands was consistent with the expected size of the amplified N gene, indicating successful cloning of the PCR product into the pCR®4-TOPO® TA vector. The presence of a single, distinct band at the expected size for the N gene confirms that the plasmid contains the desired insert without any contaminating products (**Figure 32, right panel**).

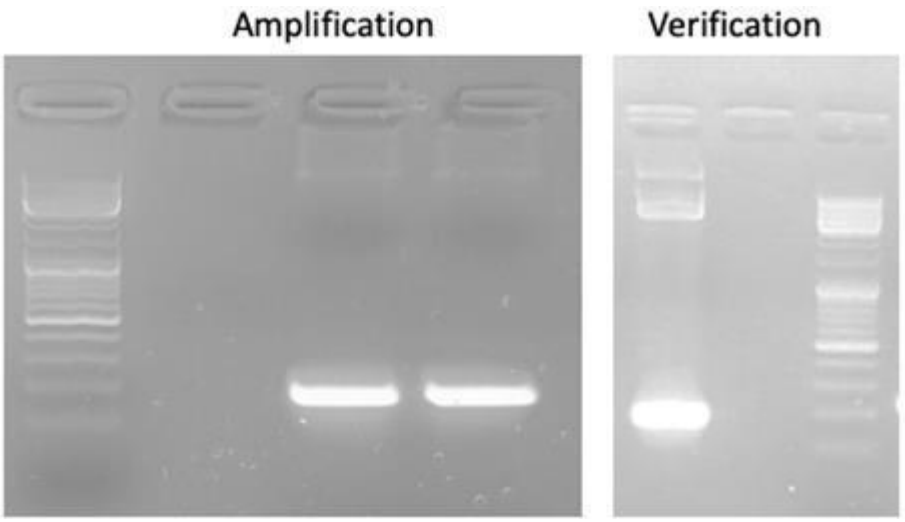

Figure 32. Screening for recombinant plasmids containing the N gene of hMPV using agarose gel electrophoresis.

A 2% agarose gel was used to analyse plasmid DNA from transformed colonies, following TOPO TA cloning of the N gene of hMPV into the pCR®4-TOPO® TA vector. The GeneRuler 1kb Plus DNA Ladder was included with fragment sizes ranging from 75bp to 20,000bp. The left panel shows visible bands at approximately 123bp, whereas the right panel shows the verification of the band size after plasmid purification, both corresponding to the expected size of the N gene insert. A single, distinct band in each lane indicates successful cloning of the N gene into the vector without additional products.

The first set of visible bands at ~287bp correspond to the HN gene of HPIV-1, with a size consistent with the expected PCR product. The second set of visible bands at ~163bp correspond to the HN gene of HPIV-2, also matching the expected size. The third set of visible bands at ~83bp correspond to the HN gene of HPIV-3, which is also the same size as the PCR product. Similarly, the last visible bands at ~187 correspond to the HN gene of HPIV-4 (**Figure 33, upper panel**). These results indicate successful cloning of the HN genes for HPIV-1, HPIV-2, HPIV-3, and HPIV-4 into the pCR®4-TOPO® TA vector. The presence of a single, distinct band at the expected sizes for the HN gene confirms that the plasmids contain the desired inserts without any contaminating products (**Figure 33, lower panel**).

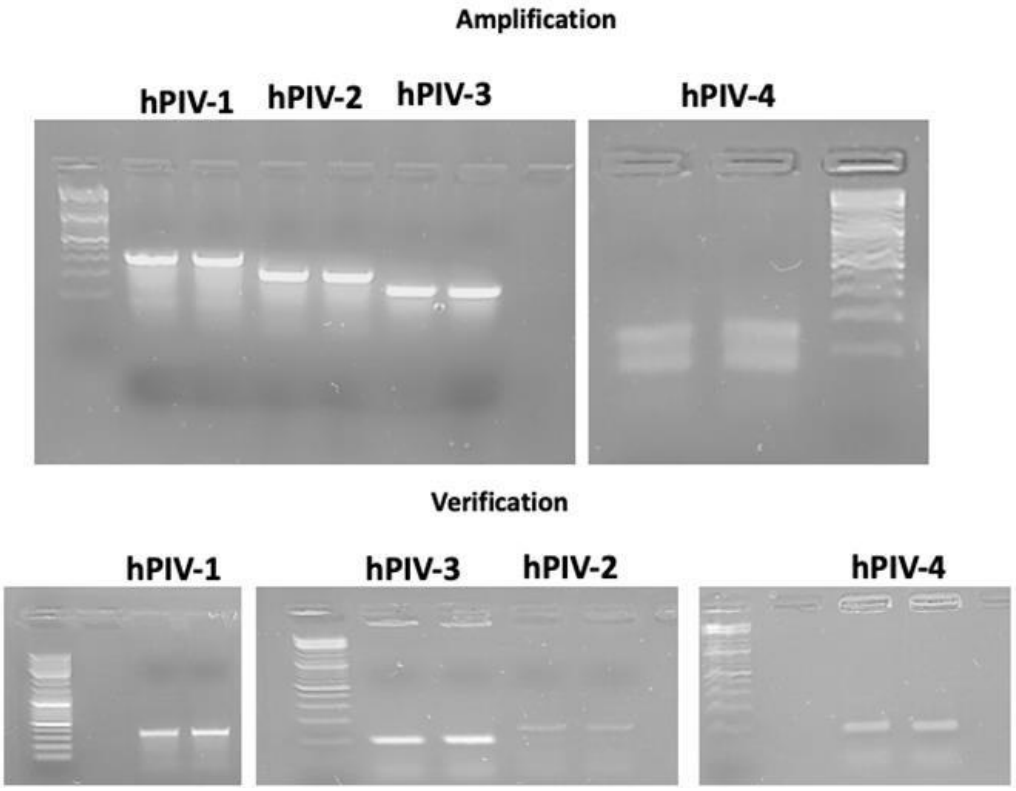

Figure 33. Screening for recombinant plasmids containing the HN gene of HPIV-1, HPIV-2, HPIV-3, and HPIV-4 using agarose gel electrophoresis.

A 2% agarose gel was used to analyse plasmid DNA from transformed colonies, following TOPO TA cloning of the HN gene of HPIV-1, HPIV-2, HPIV-3, and HPIV-4 into the pCR®4-TOPO® TA vector. The GeneRuler 1kb Plus DNA Ladder was included with fragment sizes ranging from 75bp to 20,000bp. The upper panel shows visible bands at approximately 287bp for HPIV-1, 163bp for HPIV-2, 82bp for HPIV-3, and 187bp for HPIV-4. The lower panel shows the verification of the band sizes after plasmid purification, all corresponding to the expected size of the HN gene insert. A single, distinct band in each lane indicates successful cloning of the HN gene insert into the vector without additional products.

Visible bands at ~148bp correspond to the 5' UTR insert of HRV-A (**Figure 34, left panel**). The size of the bands was consistent with the expected size of the amplified 5' UTR, indicating successful cloning of the PCR product into the pCR®4-TOPO® TA vector. The presence of a single, distinct band at the expected size for the 5' UTR confirms that the plasmid contains the desired insert without any contaminating

products (**Figure 34, right panel**).

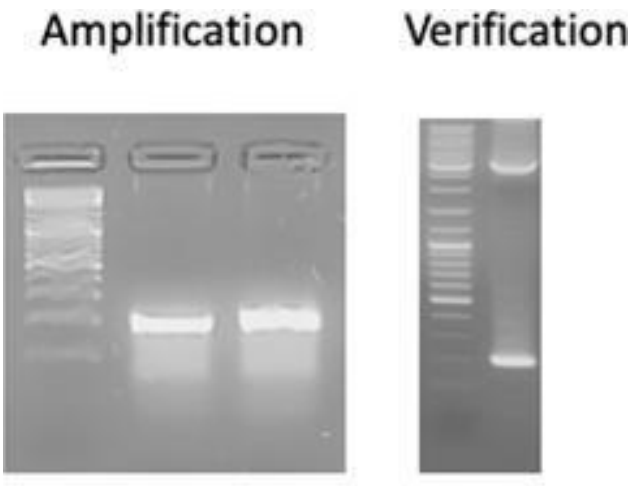

Figure 34. Screening for recombinant plasmids containing the 5' UTR of HRV-A using agarose gel electrophoresis.

A 2% agarose gel was used to analyse plasmid DNA from transformed colonies, following TOPO TA cloning of the 5' UTR of HRV-A into the pCR®4-TOPO® TA vector. The GeneRuler 1kb Plus DNA Ladder was included with fragment sizes ranging from 75bp to 20,000bp. The left panel shows visible bands at approximately 148bp, whereas the right panel shows the verification of the band size after plasmid purification, both corresponding to the expected size of the 5' UTR insert. A single, distinct band in each lane indicates successful cloning of the 5' UTR into the vector without additional products.

Visible bands at ~83 correspond to the L3 gene insert of hAdV (**Figure 35, left panel**). The size of the bands was consistent with the expected size of the amplified L3 gene, indicating successful cloning of the PCR product into the pCR®4-TOPO® TA vector. The presence of a single, distinct band at the expected size for the L3 gene confirms that the plasmid contains the desired insert without any contaminating products (**Figure 35, right panel**).

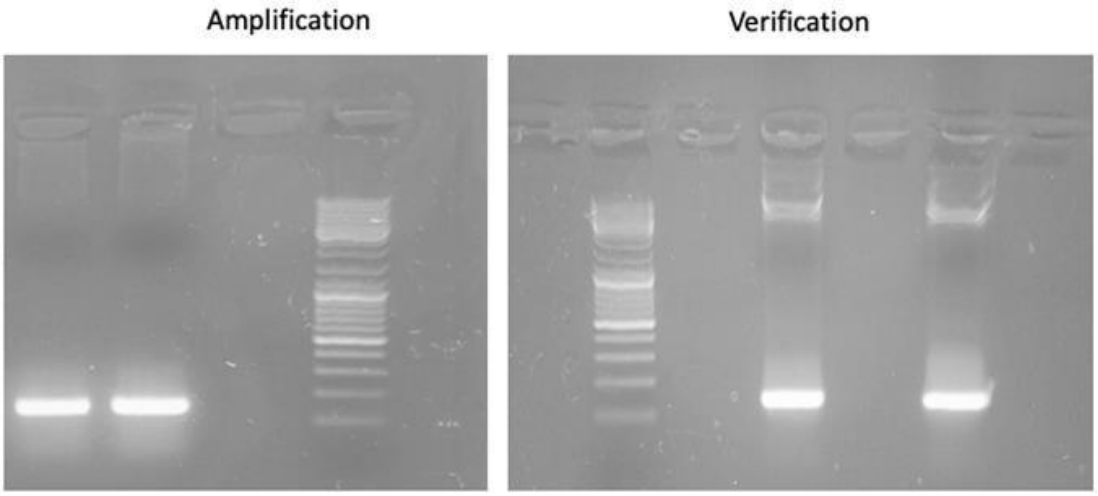

Figure 35. Screening for recombinant plasmids containing the L3 gene of hAdV using agarose gel electrophoresis.

A 2% agarose gel was used to analyse plasmid DNA from transformed colonies, following TOPO TA cloning of the L3 gene of hAdV into the pCR®4-TOPO® TA vector. The GeneRuler 1kb Plus DNA Ladder was included with fragment sizes ranging from 75bp to 20,000bp. The left panel shows visible bands at approximately 83bp, whereas the right panel shows the verification of the band size after plasmid purification, both corresponding to the expected size of the L3 gene insert. A single, distinct band in each lane indicates successful cloning of the L3 gene into the vector without additional products.

4.3.10. In Vitro Transcription and RNA Integrity Verification

Once the positive clones were confirmed, the linearised plasmid DNA containing the target gene was used as a template for in vitro transcription to produce RNA corresponding to the cloned target gene. Using a linearised plasmid as a template ensures that the RNA polymerase generates full-length transcripts corresponding to the target gene with a clear transcription stop point. This step is significant in maintaining RNA integrity so the RNAs produced remain intact and full-length. Agarose gel electrophoresis was used to confirm the size, quality, and integrity of the RNA transcripts.

The first distinct band at ~197bp corresponds to the expected size of the full-length RNA transcript of the M gene of Influenza A. The second distinct band at ~107bp corresponds to the expected size of the full-length RNA transcript of the M gene of Influenza B. The third distinct band at ~166bp corresponds to the expected size of the full-length RNA transcript of the F gene of RSV-A. The last distinct band at ~123bp corresponds to the expected size of the full-length RNA transcript of the N gene of hMPV, confirming that the transcriptions were successful. The presence of a single, distinct band for each target suggests that the RNA transcripts are intact and unaffected by any degradation or contamination. These results indicate that the genes were successfully cloned and efficiently transcribed from the pCR®4-TOPO® TA vector (**Figure 36**).

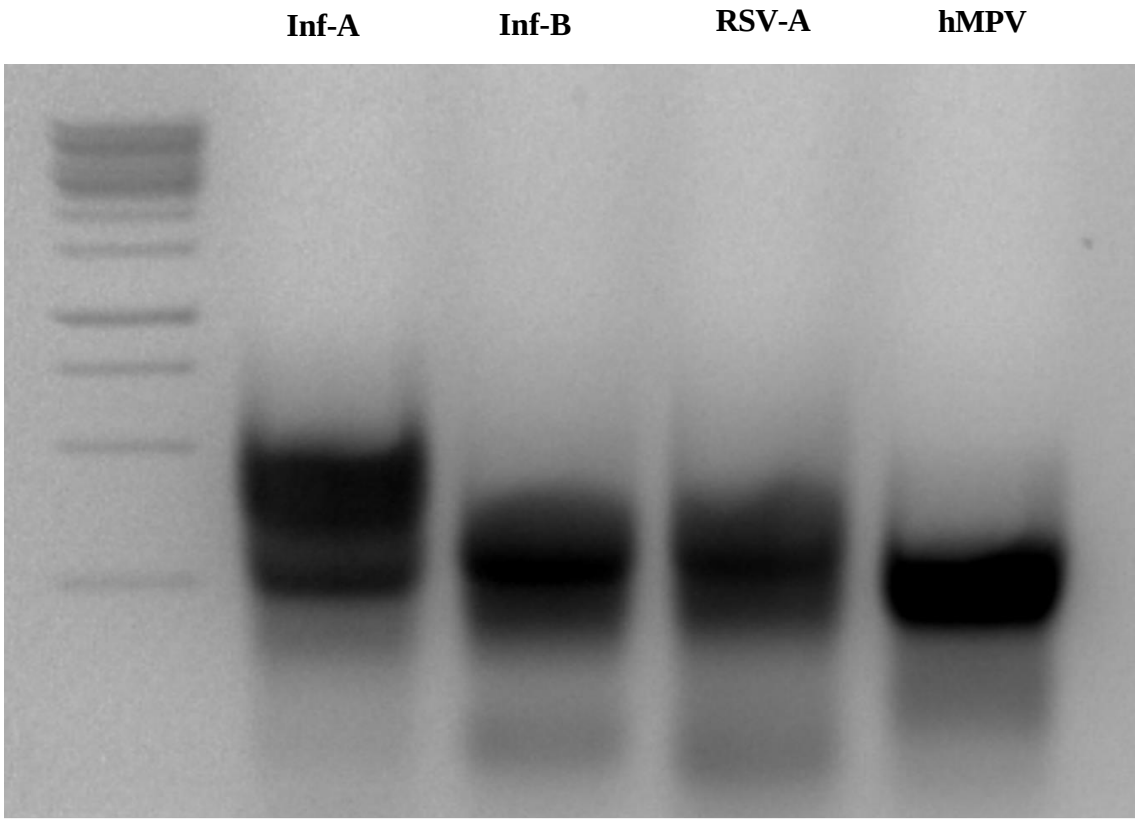

Figure 36. Analysis of RNA transcripts of the M genes of Influenza A and B, the F gene of RSV-A, and the N gene of hMPV produced via in vitro transcription.

A 2% agarose gel was used to analyse RNA transcripts produced via in vitro transcription of the M genes of Influenza A and B, the F gene of RSV-A, and the N gene of hMPV from linearised plasmid DNA templates. The GeneRuler 1kb Plus DNA Ladder was included with fragment sizes ranging from 75bp to 20,000bp. Lane 2 shows a visible band at approximately 197bp for Influenza A, lane 3 shows a visible band at approximately 107bp for Influenza B, lane 4 shows a visible band at approximately 64bp for RSV-A, and the last lane shows a visible band at approximately 123bp for hMPV, all corresponding to the expected sizes of the full-length RNA transcripts cloned into the pCR®4-TOPO® TA vector. The absence of additional bands confirms the specificity, integrity, and full-length transcription of the target gene products.

4.4. Discussion

4.4.1. Role and Design of Primers in PCR

Primers are short, single-stranded nucleotide sequences designed to complement a specific viral DNA or RNA region so they can bind and flank the region to be amplified. During annealing in PCR, primers can initiate DNA replication by providing a starting point for DNA polymerase once they hybridise to the target region on the template. DNA polymerase cannot initiate DNA synthesis independently, requiring a free 3' hydroxyl group to extend the DNA strand. This is because DNA polymerase can only synthesise DNA in the 5' to 3' direction by sequentially adding nucleotides to the 3' hydroxyl group on the existing DNA strand (Cooper, 2016). Since the new strand only grows in the 5' to 3' direction, the template strand must be read in the 3' to 5' direction to ensure complementary base pairing. Primers bind to the 3' ends of each template strand to stop self-hybridisation (Ghannam and Varacallo, 2018).

In DNA replication, an enzyme called primase synthesises short segments of RNA primers, which are complementary to the DNA template strand, providing a starting point for DNA polymerase. The RNA primer provides the free 3' hydroxyl group for DNA polymerase to start adding DNA nucleotides in the 5' to 3' direction using the 3' to

5' DNA template strand. In PCR, synthetic DNA primers replace the natural RNA primers and are designed specifically for the target region of interest. Two primers are required to amplify both DNA strands during PCR. One primer (the forward primer) binds the antisense (-) DNA strand that serves as a template during transcription and runs in a 3' to 5' direction. The other primer (the reverse primer) binds the sense (+) DNA strand that carries the translatable code and runs in a 5' to 3' direction. This dual-primer system ensures that both DNA strands are simultaneously amplified in the PCR reaction. Both primers must be highly specific to the target region of interest, ensuring that the PCR only amplifies the target of interest rather than any other DNA or RNA in the sample. Highly specific primers reduce the risk of false positives and non-specific amplification while improving assay sensitivity by allowing the detection of minimal amounts of viral genetic material. This is particularly significant during the early stages of infection when the viral load is much lower.

4.4.2. Impact of Primer-Template Mismatches on PCR Efficiency and Specificity

Full complementarity between primer and template sequences is significant to allow specific nucleic acid sequence amplification. This is often difficult to achieve with the presence of mismatches, which can severely reduce priming efficiency. Regardless of their position within the primer sequence, every mismatch will cause reduced thermal stability of the primer-template duplex and efficiency of DNA polymerase extending the primer (Cha and Thilly, 1992; Arnheim and Erlich, 1992; Kwok et al., 1990; Huang et al., 1992; Bru et al., 2008; Smith et al., 2002; Christopherson et al., 1997), potentially affecting PCR specificity (Klein et al., 2001). Mismatches located in the 3’ end region of the primer are known to have significantly larger effects on priming efficiency than the mismatches that are located closer to the 5’ end region (Kwok et al., 1990; Klein et al., 2001; Whiley and Sloots, 2005). This is because the 3’ end mismatches can disrupt the nearby DNA polymerase active site (Johnson and Beese, 2004). PCR amplification is most affected by 3’ end mismatches, resulting in effects ranging from a 2-fold underestimation of the initial copy number to a complete

extermination of amplification (Stadhouders et al., 2010). Although these effects are significantly diminished for the mismatches at the penultimate, third and fifth bases due to increased/decreased duplex stability or steric hindrance, some impact can still be occasionally observed (Johnson and Beese, 2004). Klungthong *et al.* determined that a single mismatch at the third base of the primer significantly lowered the sensitivity of detection for Influenza A/H1N1/2009 (Klungthong et al., 2010). Purine-purine (A-A, A-G, G-A, and G-G) and C-C mismatches have the most detrimental effect. Stadhouders *et al.* identified that one G-A mismatch at the 3' end of primer could lead to an increase of <8 Ct values depending on the position of the mismatch (Stadhouders et al., 2010). Pyrimidine- pyrimidine mismatches (T-T, C-T, and T-C) are the second most detrimental, followed by purine-pyrimidine mismatches (A-C, C-A, G-T, and T-G) with relatively minor effects. Bru *et al.* confirmed that a single internal mismatch within the second half of the primer can also be detrimental, causing up to a 1000-fold underestimation of the gene copy number (Bru et al., 2008).

4.4.3. Importance of Primer Design in PCR

One of the most significant factors for a successful PCR reaction is the primer quality and design. There may be a mismatch between a primer and a target in poorly designed primers, affecting amplification efficiency. An increase in the number of mismatches makes the target less likely to be amplified by PCR. Selecting conserved regions of the viral genome is necessary to reduce the possibility of mismatches between the primers and the target, as these regions are less likely to be affected by mutations. Coding regions of genes are known to be more conserved than intronic and intergenic regions (Housley et al., 2006), as they encode proteins critical for the survival and replication of the viruses. These proteins are crucial for the life cycle of these viruses, so their functionality makes them less likely to accumulate mutations (Hussein et al., 2024). If the target DNA sequence is known, specific primers complementary to both DNA strands can be designed. However, the DNA target sequence may sometimes be unknown or variable. In this case, the sequence can be estimated using related protein sequences (i.e. orthologs) from other organisms, which is known as reverse translation

(Chothia and Lesk, 1986). Orthologs are genes in different species that have evolved from a common ancestral gene, which typically retain similar functions. Since the amino acid sequence of proteins is associated with their function and structure, similar proteins across different organisms will have similar amino acid sequences. The genetic code is redundant, meaning multiple codons can encode the same amino acid. Unfortunately, the genetic code redundancy provides some uncertainty when predicting the exact DNA sequence from an amino acid, as several possible DNA sequences can encode the same protein. This issue can be avoided by using degenerate primers, which provide a mixture of similar primer sequences that include all the possible codon variants for a given amino acid sequence (Iserte et al., 2013). Therefore, degenerates increase the chances of successful amplification of the target gene. However, degenerate primers may cause non-specific amplification, generating artefactual bands (Rose et al., 2003). Great care must be taken to identify the target product among multiple bands, especially when building a genetic map, which is the opposite of the unique-sequence primers that typically produce only a single band (Housley et al., 2006).

Targeting conserved genes to design PCR primers helps to identify the presence of a specific virus rather than a specific strain, which is useful for general diagnosis when the strain is unknown or irrelevant. For instance, the M1 and NP genes of Influenza A and B are the most conserved across their respective lineages (ElHefnawi et al., 2011). The most conserved gene in RSV-A and RSV-B is the N gene, followed by the L gene, which is the pattern observed in hMPVs and HPIVs (Tan et al., 2012; Ogawa et al., 1992). Even though the degree of conservation varies for the HN gene across HPIV types, it was used to differentiate between different types of HPIV in this study. The HN gene exhibits significant variability across HPIV types, which is beneficial when differentiating between HPIV-1, HPIV-2, HPIV-3, and HPIV-4. Similarly, the 3Dpol gene is the most conserved in HRVs, which can be used for broad detection of these viruses. Although the hexon gene of hAdV contains hypervariable regions that can distinguish different adenovirus serotypes (Wohlfart, 1988; Crawford-Miksza and Schnurr, 1996), it has the most conserved regions that are stable across all AdV species (Wang et al., 2021). The L3 gene used in this study is conserved enough to be a gene target for hAdV while designing primers to avoid the hypervariable regions. The NP1

gene of HBoV is the most conserved region of the virus, according to the limited available data (Allander et al., 2005). On the other hand, choosing a genetically diverse gene as a target allows the detection of a wide range of viral variants. For instance, targeting the HA gene of influenza viruses will help to identify different subtypes of the virus as it has the highest genetic diversity due to undergoing the fastest mutation out of all the other genes, followed by the NA gene (Tewawong et al., 2015; Liu et al., 2023). The most extensive genetic variation among all the other proteins and major antigenic groups is associated with the G protein in RSV-A and RSV-B, as well as hMPV and HPIV (Bastien et al., 2004). In hAdV, the fibre gene shows the highest variability, particularly in its knob domain (Baker et al., 2024). Similarly, the VP1 gene of HRVs has the most sequence variability in their genomes, making these genes ideal candidates for distinguishing between different virus strains or subtypes (Waman et al., 2014).

4.4.4. Limitations and Challenges of PCR in Detecting Respiratory Viruses

Although PCR is the current gold standard for detecting viruses from clinical samples, it has a significant drawback associated with contamination. Even a tiny amount of RNA and DNA contamination in the sample can produce highly misleading false positive results. Another disadvantage is that the primers specifically designed for PCR must have sequence data, so they can only be used to determine the presence or absence of a known pathogen or gene. In some cases, primers may anneal to the sequences that are not targeted but are similar to the target gene (Smith and Osborn, 2009). The possibility of primer-dimer formation may be another issue while using PCR. The primer-dimer is made from primer molecules that have hybridised with each other due to the strings of complementary bases in the primers. When primer-dimers exist, DNA polymerase can amplify them, leading to a competition for PCR reagents that could be used to amplify the target sequences (Brownie et al., 1997).

4.4.5. Efficiency and Challenges of TOPO TA Cloning

TOPO vectors containing the LacZ-ccdB cassette allow direct selection of recombinants by interfering with the lethal *E. coli* gene, ccdB. The ligation of a PCR product interferes with the expression of the LacZ-ccdB gene fusion, allowing the growth of positive recombinants only upon transformation. Cells that contain non-recombinant vectors are killed upon plating, eliminating the need for blue/white screening. TOPO TA cloning does not require the use of DNA ligase to join the insert with the vector. Instead, it uses DNA topoisomerase I already attached to the vector to mediate the ligation (Shuman, 1991). The vector is already linearised and prepared with 3' T overhangs, allowing PCR products with 3' A overhangs to ligate straightforwardly. This means the entire cloning process can be completed in a single step, which speeds up the process significantly. Since the DNA topoisomerase I is covalently attached to the vector, only PCR products with A overhangs can be ligated, which significantly reduces the number of background colonies (Shuman, 1991). This type of cloning also does not need any specific restriction sites in the PCR product or the vector, meaning that even if the PCR product does not have any restriction sites, cloning can still occur. The PCR products can be directly used for TOPO TA cloning without any purification step, which reduces the possibility of sample loss. On the other hand, the kit used for the TOPO TA cloning is more expensive than the cloning methods that use restriction enzymes and ligases. TOPO TA cloning has limited cloning capacity, as it is more efficient when cloning smaller DNA fragments. Cloning larger DNA fragments (over 5kb) can be very challenging and much less efficient (Baotai and Bi, 2002). If the PCR product has more than one A overhang, there is a possibility of non-specific cloning or the insertion of multiple inserts, which may lead to incorrect or multiple inserts being cloned into the vector. Additionally, highly competent cells must be used in TOPO TA cloning to ensure efficient transformation. If suboptimal competent cells are used, transformation efficiency will likely be reduced significantly.

4.4.6. Enhancing Cloning Efficiency in PCR

Cloning efficiency can be improved by making certain adjustments to the pH, PCR extension time, and primer design. If the pH of the PCR amplification reaction is over 9,

it must be lowered back to 8 by adding 1M Tris-HCl. There is a likelihood of incomplete extension during PCR when longer PCR products are involved. The duration of the extension step can be increased up to 30 min (with a minimum of 7 min) during PCR, as the longer PCR products will need a longer extension time. Increasing extension time will also ensure that all 3' ends are adenylated, which can be useful if PCR products do not contain sufficient 3' A overhangs, despite using *Taq* polymerase in the reaction mixture. This is because *Taq* polymerase is less efficient at adding a non-template 3' A next to another A, and it is the most efficient at adding a non-template 3' A next to a C. Therefore, in some cases, redesigning primers may be necessary so that they contain a 5' G instead of a 5' T. On the other hand, transformation efficiency with the competent cells can also be improved. Competent cells must be thawed at room temperature, and the DNA must be added once the cells are thawed. It is important to make sure that the incubation times are followed as outlined in the competent cell protocol for the strain of interest, as the changes in length of time can decrease transformation efficiency. All the salt and other contaminants must be removed from the DNA sample before transformation, known as DNA purification, which can be done by using a spin column or phenol/chloroform extraction and ethanol precipitation.

4.5. Conclusion

In summary, the successful design and use of primers are significant factors for efficient PCR, specifically in amplifying viral genetic material. The primers must complement the viral target sequence to ensure specific amplification. Using highly conserved regions within the viral genome, particularly those within essential genes, increases the likelihood of specific and accurate amplification. However, the genetic variability within viral genomes may necessitate the use of degenerate primers to compensate for sequence diversity, even though this may lead to the formation of primer dimers and non-specific amplification. To improve design efficiency across different virus strains and subtypes, future researchers could leverage in silico comparative genomic analyses to align multiple viral genomes, enabling rapid identification of conserved primer-binding sites. Databases such as GISAID and NCBI

Virus can facilitate this process by providing access to up-to-date strain-level sequences, allowing automated tools to generate primer sets optimised for inclusivity and specificity.

TOPO TA cloning is a molecular biology technique offering a ligation- and restriction-free method for cloning PCR products. This type of cloning utilises the unique properties of DNA topoisomerase I, which acts as both a restriction enzyme and DNA ligase, eliminating the need for an additional restriction enzyme or ligase. This provides a quick and easy way to clone a fresh PCR product into a plasmid. However, there are still some challenges with TOPO TA cloning when handling larger DNA fragments, and highly competent cells are required for optimal transformation efficiency. While PCR is the current gold standard for viral detection, its success largely depends on the accuracy of primer design, the nature of the target sequence, and the cloning method employed. As an alternative to targeting broadly conserved regions, researchers could also consider designing primers against structurally constrained protein-coding regions that are functionally conserved but less prone to mutation, such as the HA stalk region in influenza viruses. This strategy could enable the development of standardised primer sets that do not require frequent adjustment for new strains or subtypes, thereby increasing long-term assay stability. Despite requiring careful optimisation to ensure the highest efficiency and accuracy, advanced cloning methods like TOPO TA cloning remain a valuable option for researchers working on viral detection. It is essential to address and work with the challenges of PCR and TOPO TA cloning to improve molecular research and diagnostics.

Chapter 5: Clinical Validation of RT-RPA for Common Respiratory Viruses

5.1. Introduction

5.1.1. Multiplex PCR-based Diagnostic Assays for Respiratory Pathogens

Multiplex PCR-based diagnostic assays, such as RPPs, are novel approaches to rapidly and accurately diagnosing common infectious diseases. Multiplex PCR tests combine several pathogens and resistance genes into a single assay to simultaneously detect multiple infections from a single patient sample (Buchan and Ledeboer, 2014; Graf and Pancholi, 2020). These tests are able to detect serious infections affecting the bloodstream, GI tract, and CNS, as well as infections that affect both the upper and lower respiratory tract. NP swabs, secretion samples, and sputum are specimens suitable for this type of detection (Subramony et al., 2016). Identifying the aetiological agent of upper and lower respiratory tract infections is challenging since different respiratory pathogens cause very similar respiratory symptoms (Thomas and Bomar, 2023), which can be eliminated using multiplex diagnostic tests. Using traditional diagnostic methods in these cases would be time-consuming, requiring separate tests for detecting each viral infection. Multiplex diagnostic tests also reduce the cases of administering broad-spectrum antibiotics only based on the clinical severity and seasonability of infection, avoiding the misuse of antibiotics in co-infection with bacteria and viral resistance (Stafylaki et al., 2022). These assays are particularly beneficial during peak seasons for respiratory infections, such as flu season or outbreaks of emerging pathogens.

5.1.2. Challenges and Considerations for Multiplex Diagnostic Tests

While multiplex diagnostic tests offer significant benefits, they have been mainly used per patient in tertiary care facilities rather than as a general screening tool (Dien Bard

and McElvania, 2020; Pinsky and Hayden, 2019; Poritz et al., 2011). Infections caused by influenza viruses and RSVs have been a concern for years in healthcare systems as they tend to cause severe cases and major recurrent epidemics. On the other hand, infections caused by other respiratory pathogens like enteroviruses, HRVs, hMPVs, hADVs, hPIVs, and classic endemic human coronaviruses are generally considered less severe in healthy individuals. However, for severely immunocompromised individuals such as cancer patients and those with chronic illnesses, there is a higher risk of developing severe complications from these milder pathogens, including respiratory failure or death. Therefore, rigorous testing of these individuals is critical, and general screening for these pathogens using multiplex diagnostic tests must be considered to allow early detection and intervention (Sharma et al., 2021; Zhao et al., 2020; Maziarz et al., 2009). These tests were confirmed to promote faster turnaround time compared to traditional diagnostic tests, leading to reduced hospital admissions, optimised antibiotic treatments, and decreased morbidity and mortality (Dumkow et al., 2021; Rappo et al., 2016; Brendish et al., 2017). However, the frequent use of these tests can increase the cost of detection, as they require multiple primer sets, probes, and high-throughput equipment that can simultaneously detect multiple different pathogens from a single reaction (Dien Bard and McElvania, 2020; Pinksy and Hayden, 2019).

5.1.3. Impact of COVID-19 on Molecular Diagnostics for Respiratory Pathogens

Seasonal influenza and RSV are the primary respiratory pathogens associated with a significant socioeconomic impact (Cassini et al., 2018; Simões, 2022). During the first waves of the COVID-19 pandemic, non-pharmaceutical interventions such as mask-wearing, social distancing, and lockdowns significantly reduced the spread of SARS-CoV-2, as well as other respiratory viruses like influenza and RSV (Adlhoch et al., 2021; Summeren et al., 2021), which re-emerged during the later pandemic phases (Ferrero et al., 2022). These viruses share similar clinical symptoms, making it difficult to distinguish from one another, particularly in cases of co-infections. Therefore, the COVID-19 pandemic acted as a catalyst for the expansion, modernisation, and

automation of molecular diagnostics, highlighting the need for quick and reliable molecular diagnostic approaches (Pritzker, 2021; Van Vooren et al., 2022).

Even though RPPs were already in use before the pandemic, their available platforms, such as Biofire (Poritz et al., 2011), GenMark (Jarrett et al., 2021), and QIAstat (Cassidy et al., 2022), gained more recognition during this period due to being PCR-based technologies. These platforms are commonly used as rapid POC tests for individual samples from a single assay. However, they cannot be easily improved to cover high-volume testing due to limitations in scalability and cost. RT-PCR remains the gold standard for detecting SARS-CoV-2, Influenza, and RSV, providing high sensitivity and specificity (Tang et al., 2020; Zuurbier et al., 2022). Even though the gold standard typically provides excellent diagnostic accuracy, it has significant drawbacks, including suboptimal turnaround times and the requirement for expensive equipment and trained laboratory staff (Domnich et al., 2022). Therefore, using PCR for on-site detection in low-resource settings is challenging, meaning reliable alternatives must be pursued (Yan et al., 2014).

5.1.4. Advantages and Optimisation of RPA for Nucleic Acid Detection

RPA is an isothermal alternative to the gold standard that optimally runs at 37-42°C without complex temperature control equipment, which makes it suitable for on-site detection in low-resource settings. Unlike PCR, RPA does not produce Ct values due to being an isothermal amplification method that does not depend on cycles for target amplification. Instead, it has Tt values that represent the time (in min or sec) at which the fluorescent signal exceeds the detection threshold. Ct and Tt values can be compared semi-quantitatively to assess the relative diagnostic performance of the assays. The results can be obtained in about 20 min by RPA, making it ideal for large-scale screening in a short period of time (Li et al., 2018). Regarding its sensitivity, RPA can detect trace-level nucleic acids in the sample. In some studies, it could even detect low concentrations of DNA that PCR could not detect (Daher et al., 2016). Regarding its specificity, RPA can amplify the target genes from the genomic DNA of different

species and specimen types. After the first hit of the COVID-19 pandemic, the scale of testing became bigger and bigger, promoting the application of RPA in nucleic acid detection (Bai et al., 2022). Since RPA can be performed under mild reaction conditions without requiring expensive equipment, uses low reaction temperatures, and provides high amplification efficiency, it can be beneficial for rapid clinical diagnosis, epidemic prevention and control, and on-site real-time detection. To further enhance the efficiency and convenience of RPA, several optimisation and improvement measures were applied regarding the amplification and reading system of RPA. Adding glycerol can help to stabilise the main enzymes involved in RPA reactions (Simpson and Richardson, 1985). Glycerol also enhances the solubility of reaction components so that nucleic acids do not aggregate, allowing enzymes and primers to interact freely during the amplification (Arakawa and Timasheff, 1982). Slightly changing the optimal temperature can help improve the interaction between enzymes and primers, increasing the amplification rate and yield (Piepenburg et al., 2006; Daher et al., 2016). Using MgOAc in RPA reactions is critical as the magnesium ions facilitate DNA polymerase activity. The amount of magnesium can affect the amplification performance. For instance, higher magnesium concentrations can increase the binding of primers to the template but can also increase the risk of non-specific amplification (Daher et al., 2016). Fine-tuning the pH of the reaction buffer, the template concentration, and the extension time allowed for DNA synthesis can also help to optimise the conditions required for an efficient amplification. Furthermore, no specialised software has been developed to design RPA primers. Therefore, only PCR software can be used to design and screen these primers. Typically, RPA primers (30-35 nucleotides) are longer than PCR primers (18-25 nucleotides), meaning that PCR software may not account for the longer primer length needed in RPA, so it may not achieve the optimal amplification efficiency. Moreover, only one company sells expensive RPA kits, which is TwistDx, causing a challenge in large-scale settings. Although these limitations show that RPA technology still needs further optimisation and improvement, it is expected to become the mainstream technology of nucleic acid amplification in the near future.

5.2. Hypothesis and Objectives

Hypothesis:

RT-RPA, when optimised, can serve as a rapid, accurate, and resource-efficient alternative to RT-PCR for the detection of multiple respiratory viruses in clinical samples, offering comparable sensitivity and specificity while addressing the limitations of RT-PCR in decentralised and POC settings.

Objectives:

1. To compare the diagnostic performance of RT-RPA and RT-PCR for multiple respiratory viruses across clinical samples.
2. To evaluate the correlation between RT-RPA Tt values and RT-PCR Ct values in quantifying viral load.
3. To identify any assay-specific discrepancies, such as false positives, and assess their diagnostic implications.
4. To determine the feasibility of using RT-RPA as a diagnostic tool in POC or low-resource environments.

5.3. Results

5.3.1. Comparative Performance of RT-RPA and RT-PCR in Detecting Influenza A Virus

A total of 14 clinical samples suspected of Influenza A virus were subjected to RT-PCR and RT-RPA simultaneously. Based on curated Tt/Ct values, both assays showed a similar variability, indicating comparable sensitivity in detecting a wide range of nucleic acid concentrations. RT-RPA consistently produced lower Tt values on average (10.8),

while RT-PCR gave higher Ct values on average (30.8), meaning the RT-PCR takes more time to detect the same target concentration (**Figure 37A**). This comparison suggests that RT-RPA can efficiently detect samples with higher concentrations (i.e. higher viral load), while RT- PCR is better suited for detecting samples with lower concentrations (i.e. lower viral load).

As shown in **Figure 37B**, none of the samples were detected by RT-RPA alone without RT-PCR, and all the samples labelled as "ND" (not detected) were not detected by either assay. This means that both assays showed a similar pattern of detection. A total of 14 clinical samples were used to determine the performance of RT-RPA compared to RT-PCR for detecting the Influenza A virus. Since all 10 clinical samples were correctly identified as positive by RT-RPA, the sensitivity of this assay is 100%. Since all 4 clinical samples were correctly identified as negative by RT-RPA, the specificity of this assay is also 100% (**Figure 37C**). This shows that RT-RPA performs equally well as RT-PCR based on this dataset, suggesting that RT-RPA could be a reliable alternative to RT-PCR in detecting Influenza A.

The line of best fit, calculated using simple linear regression, is described by the equation $Tt = 0.3851 \times Ct - 0.8936$, indicating a linear relationship between RT-PCR and RT-RPA detection values. Here, Tt (RT-RPA) is the dependent variable and Ct (RT-PCR) is the independent variable. The slope (0.3851) suggests that for each unit increase in Ct, the Tt increases by approximately 0.3851 units. The coefficient of determination ($R^2 = 0.828$) indicates that approximately 82.8% of the variability in Tt values is explained by the Ct values (**Figure 37D**). Although some individual data points appear skewed, no outliers were excluded, and the strength of correlation remains statistically robust. This confirms that RT-RPA provides comparable results to RT-PCR, while offering faster processing, affordability, and simplified instrumentation requirements.

A.

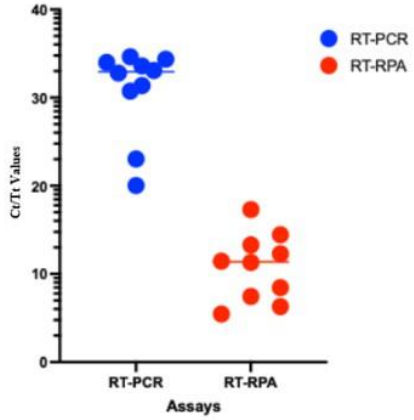

B.

Serial Number	Sample ID	RT-PCR		RT-RPA	
		Ct values	Pos/Neg/IC	Tt values	Pos/Neg/IC
1	C11	33.0788771	+	11.45	+
2	D05	33.59	+	12.3	+
3	D06	20.04	+	5.45	+
4	D07	33.99	+	13.3	+
5	D08	31.38	+	8.45	+
6	D09	32.79	+	11.3	+
7	D11	23.04	+	6.3	+
8	E01	30.7321856	+	7.45	+
9	E10	34.3530796	+	14.45	+
10	F09	ND	-	ND	-
11	G03	ND	-	ND	-
12	G04	34.628625	+	17.3	+
13	G07	ND	-	ND	-
14	H08	ND	-	ND	-

C.

Influenza A		RT-PCR	
		Positive	Negative
RT-RPA	Positive	10	0
	Negative	0	4
	Total	10	4
Sensitivity		100%	
Specificity		100%	

D.

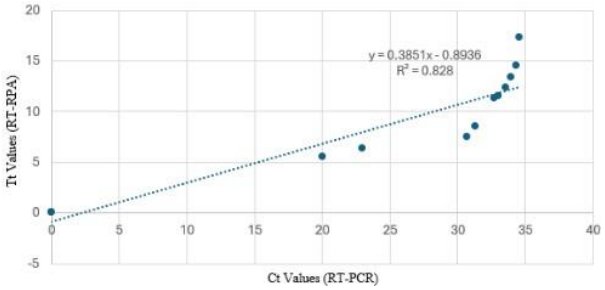

Figure 37. Comparing sensitivity, specificity, and Tt/Ct values of RT-RPA with RT-PCR to determine the overall performance of RT-RPA in detecting Influenza A virus.

A. Difference between the Tt values of RT-RPA and Ct values of RT-PCR assays for Influenza A virus. Both red and blue data points seem to have a similar range of values, indicating a comparable sensitivity between RT-RPA and RT-PCR. The average Ct value (30.8) for the blue dots (RT-PCR) is higher than the average Tt value (10.8) for the red dots (RT-RPA), indicating that RT-PCR generally yields higher values on average, reflecting the longer detection time. **B.** Comparison of RT-PCR and RT-RPA results for detecting Influenza A virus in different samples. The positive (+) or negative (-) results from both assays indicate whether Influenza A RNA was detected. "ND" indicates that the target was not detected in the sample, meaning no amplification occurred above the threshold. **C**. Diagnostic performance comparison of RT-RPA and RT-PCR for detecting Influenza A virus, where the RT-PCR was treated as the gold standard. RT-RPA exhibited comparable sensitivity (100%) and specificity (100%) to RT-PCR for this dataset. **D**. The relationship between the Tt values of RT-RPA and Ct values of RT-PCR. The equation ($y = 0.3851x – 0.8936$) indicates a linear relationship, where an increase in Ct values of RT-PCR corresponds to an increase in Tt values of RT-RPA. The coefficient of determination ($R^2 = 0.828$) suggests a high degree of correlation between the two assays, demonstrating that RT- RPA can reliably approximate the performance of RT-PCR.

5.3.2. Comparative Performance of RT-RPA and RT-PCR in Detecting Influenza B Virus

A total of 21 clinical samples suspected of Influenza B virus were subjected to RT-PCR and RT-RPA simultaneously. Based on curated Tt/Ct values, the Ct values of RT-PCR exhibited greater variability, possibly due to its sensitivity for detecting a broader range of nucleic acid concentrations. RT-RPA consistently produced lower Tt values on average (9.12), while RT-PCR assay yielded higher Ct values on average (14.2), indicating that the RT-PCR takes longer to detect the same target concentration (**Figure 38A**). Therefore, RT-RPA seems more efficient in detecting samples with higher concentrations (i.e. higher viral load), while RT-PCR seems better suited for detecting samples with lower concentrations (i.e. lower viral load).

As shown in **Figure 38B**, none of the samples were detected by RT-RPA alone without corresponding detection by RT-PCR. Additionally, all samples labelled as "ND" were negative in both assays, indicating a similar pattern of detection between the two methods. A total of 21 clinical samples were used to determine the performance of RT-RPA compared to RT-PCR for detecting Influenza B virus. Since all 8 clinical samples were correctly identified positive by RT-RPA, the sensitivity of this assay is 100%. Since all 13 clinical samples were correctly identified as negative by RT-RPA, the specificity of this assay is also 100% (**Figure 38C**). This shows that RT-RPA performs equally well as RT-PCR based on this dataset, suggesting its potential as a reliable alternative to RT-PCR in detecting Influenza B.

The line of best fit, calculated using simple linear regression, is described by the equation $Tt = 0.4795 \times Ct + 2.9292$, indicating a linear relationship between RT-PCR and RT-RPA detection values. Here, Tt (RT-RPA) is the dependent variable and Ct (RT-PCR) is the independent variable. The slope (0.4795) suggests that for each unit increase in Ct, the Tt increases by approximately 0.48 units. The coefficient of determination ($R^2 = 0.9658$) indicates that approximately 96.6% of the variability in Tt values is explained by the Ct values (**Figure 38D**). Although some individual data points appear skewed, no outliers were excluded, and the strength of correlation

remains statistically robust. This confirms that RT-RPA provides comparable results to RT-PCR, while offering faster processing, affordability, and simplified instrumentation requirements.

A.

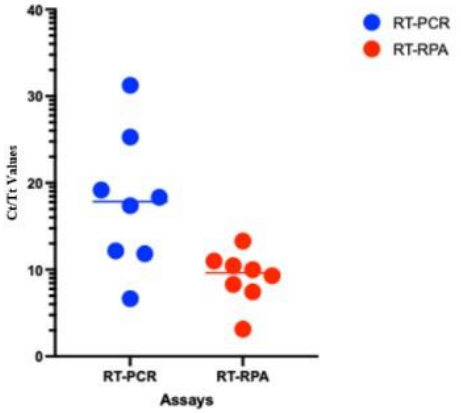

B.

Serial Number	Sample ID	RT-PCR		RT-RPA	
		Ct values	Pos/Neg/IC	Tt values	Pos/Neg/IC
1	A01	ND	-	ND	-
2	A03	19,1737403	+	10,45	+
3	A06	ND	-	ND	-
4	A07	ND	-	ND	-
5	A08	ND	-	ND	-
6	A10	25,2888703	+	11	+
7	B01	ND	-	ND	-
8	B02	17,3725114	+	9,3	+
9	B03	ND	-	ND	-
10	B04	ND	-	ND	-
11	B05	ND	-	ND	-
12	B06	ND	-	ND	-
13	B07	31,2511382	+	13,3	+
14	B08	ND	-	ND	-
15	B09	ND	-	ND	-
16	B10	11,8311995	+	7,45	+
17	C01	ND	-	ND	-
18	C02	12,168859	+	8,3	+
19	C03	6,66672326	+	3,15	+
20	C04	18,3394408	+	10	+
21	C05	ND	-	ND	-

C.

Influenza B		RT-PCR	
		Positive	Negative
RT-RPA	Positive	8	0
	Negative	0	13
	Total	8	13
Sensitivity		100%	
Specificity		100%	

D.

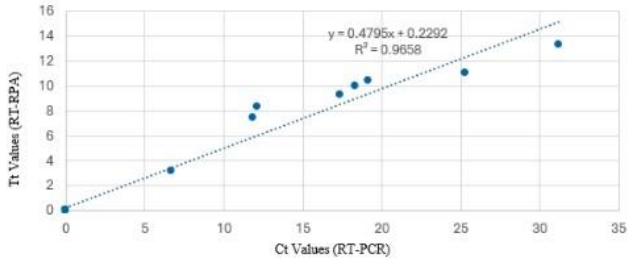

Figure 38. Comparing sensitivity, specificity, and Tt/Ct values of RT-RPA with RT-PCR to determine the overall performance of RT-RPA in detecting Influenza B virus.

A. Difference between the Ct values of RT-PCR and the Tt values of RT-RPA assays for Influenza B virus. Blue dots have a wider range of Ct values, indicating more variability in the RT-PCR results. Red dots are more tightly clustered, indicating that RT-RPA consistently produced lower Tt values. Observation of lower Tt values is associated with a higher concentration of the target RNA. The average Ct value (14.2) for the blue dots (RT-PCR) is higher than the average Tt value (9.12) for the red dots (RT-RPA), indicating that RT-PCR yielded higher Ct values on average. Higher Ct values are associated with a lower concentration of the target RNA. **B**. Comparison of RT-PCR and RT-RPA results for detecting Influenza B virus in different samples. The positive (+) or negative (-) results from both assays indicate whether Influenza B RNA was detected. "ND" indicates that the target was not detected in the sample, meaning no amplification occurred above the threshold. **C**. Diagnostic performance

comparison of RT-RPA and RT-PCR for detecting Influenza B virus, where the RT-PCR was treated as the gold standard. RT-RPA exhibited comparable sensitivity (100%) and specificity (100%) to RT-PCR for this dataset. **D**. The relationship between the Tt values of RT-RPA and the Ct values of RT- PCR. The equation ($y = 0.479x + 2.9292$) suggests a linear relationship, where an increase in Ct values of RT-PCR corresponds to an increase in Tt values of RT-RPA. The coefficient of determination ($R^2 = 0.9658$) indicates a high degree of correlation, demonstrating that RT-RPA can reliably approximate the performance of RT-PCR.

5.3.3. Comparative Performance of RT-RPA and RT-PCR in Detecting RSV-A

A total of 20 clinical samples suspected of RSV-A were subjected to RT-PCR and RT-RPA simultaneously. Based on curated Tt/Ct values, both assays exhibited similar variability in detecting a range of nucleic acid concentrations. RT-RPA consistently produced lower Tt values on average (10.1), while RT-PCR yielded higher Ct values on average (29.1), meaning the RT-PCR takes longer to detect the same target concentration (**Figure 39A**). Therefore, RT-RPA seems more efficient in detecting samples with higher concentrations (i.e. higher viral load), while RT-PCR seems better suited for detecting samples with lower concentrations (i.e. lower viral load).

As shown in **Figure 39B**, none of the samples were detected by RT-RPA alone without corresponding detection by RT-PCR. Additionally, all samples labelled as "ND" were negative in both assays, indicating a similar pattern of detection between the two methods. A total of 20 clinical samples were used to determine the performance of RT-RPA compared to RT-PCR for detecting RSV-A. Since all 6 clinical samples were correctly identified positive by RT-RPA, the sensitivity of this assay is 100%. Since all 14 clinical samples were correctly identified as negative by RT-RPA, the specificity of this assay is also 100% (**Figure 39C**). This shows that RT-RPA performs equally well as RT-PCR based on this dataset, suggesting its potential as a reliable alternative to RT-PCR in detecting RSV-A.

The line of best fit, calculated using simple linear regression, is described by the equation $Tt = 0.3594 \times Ct - 0.1441$, indicating a linear relationship between RT-PCR and RT-RPA

detection values. Here, Tt (RT-RPA) is the dependent variable and Ct (RT-PCR) is the independent variable. The slope (0.3594) suggests that for each unit increase in Ct, the Tt increases by approximately 0.36 units. The coefficient of determination ($R^2 = 0.8955$) indicates that approximately 89.6% of the variability in Tt values is explained by the Ct values (**Figure 39D**). Although some individual data points appear skewed, no outliers were excluded, and the strength of correlation remains statistically robust. This confirms that RT-RPA provides comparable results to RT-PCR, while offering faster processing, affordability, and simplified instrumentation requirements.

A.

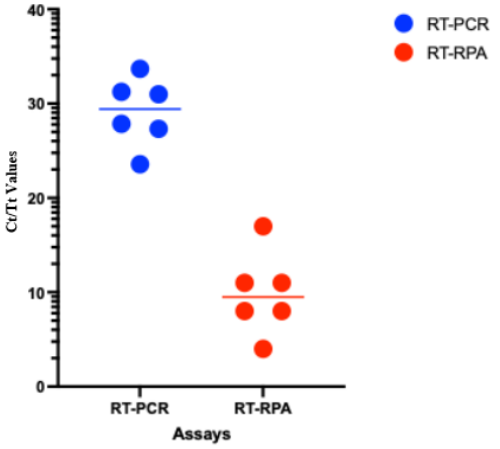

B.

Serial Number	Sample ID	RT-PCR		RT-RPA	
		Ct values	Pos/Neg/IC	Tt values	Pos/Neg/IC
1	A02	30,9921306	+	11,3	+
2	A03	ND	-	ND	-
3	A04	ND	-	ND	-
4	A05	23,5744868	+	4	+
5	A07	27,3328805	+	8	+
6	A09	31,252291	+	11,3	+
7	A10	ND	-	ND	-
8	A11	ND	-	ND	-
9	B01	ND	-	ND	-
10	B02	ND	-	ND	-
11	B03	ND	-	ND	-
12	B04	ND	-	ND	-
13	B05	27,8597445	+	8,15	+
14	B06	ND	-	ND	-
15	B07	33,6838443	+	17,3	+
16	B08	ND	-	ND	-
17	B10	ND	-	ND	-
18	C01	ND	-	ND	-
19	C06	ND	-	ND	-
20	C07	ND	-	ND	-

C.

RSV-A		RT-PCR	
		Positive	Negative
RT-RPA	Positive	6	0
	Negative	0	14
	Total	6	14
Sensitivity		100%	
Specificity		100%	

D.

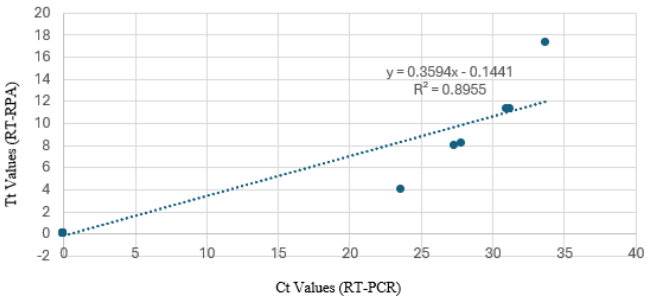

Figure 39. Comparing sensitivity, specificity, and Tt/Ct values of RT-RPA to RT-PCR to determine the overall performance of RT-RPA for detecting RSV-A.

A. Difference between the Ct values of RT-PCR and Tt values of RT-RPA assays for RSV-A. Both red and blue data points seem to have a similar range of values, indicating a comparable sensitivity between RT-RPA and RT-PCR. The average Ct value (29.1) for the blue dots (RT-PCR) is higher than the average Tt value (10.1) for the red dots (RT-RPA), indicating that RT-PCR generally yields higher values on average, reflecting the longer detection time. **B**. Comparison of RT-PCR and RT-RPA results for detecting RSV-A in different samples. The positive (+) or negative (-) results from

both assays indicate whether RSV-A RNA was detected. "ND" represents the target that was not detected in the sample, meaning no amplification occurred above the threshold. **C**. Diagnostic performance comparison of RT-RPA and RT-PCR for detecting RSV-A, where the RT-PCR was treated as the gold standard. RT-RPA exhibited comparable sensitivity (100%) and specificity (100%) to RT-PCR for this dataset. **D**. The relationship between the Tt values of RT- RPA and Ct values of RT-PCR. The equation ($y = 0.3594x – 0.1441$) suggests a linear relationship, where an increase in Ct values of RT-PCR corresponds to an increase in Tt values of RT-RPA. The coefficient of determination ($R^2 = 0.8955$) indicates a high degree of correlation, demonstrating that RT-RPA can reliably approximate the performance of RT-PCR.

5.3.4. Comparative Performance of RT-RPA and RT-PCR in Detecting RSV-B

A total of 16 clinical samples suspected of RSV-B were subjected to RT-PCR and RT-RPA simultaneously. Based on curated Tt/Ct values, both assays exhibited similar variability in detecting a range of nucleic acid concentrations. RT-RPA assay consistently produced lower Tt values on average (2.46), while RT-PCR assay yielded higher Ct values on average (34.0), indicating that the RT-PCR takes longer to detect the same target concentration (**Figure 40A**). Therefore, RT-RPA seems more efficient in detecting samples with higher concentrations (i.e. higher viral load), while RT-PCR seems better suited for detecting samples with lower concentrations (i.e. lower viral load).

As shown in **Figure 40B**, only sample A07 was detected by RT-RPA in the absence of RT-PCR. Most of the samples labelled as "ND" were not detected by both assays, apart from sample A07, which was only detected by RT-RPA. This means that both assays showed a similar pattern of detection, with only a few discrepancies. A total of 16 clinical samples were used to determine the performance of RT-RPA compared to RT-PCR for detecting RSV-B. Since all 7 clinical samples were correctly identified positive by RT-RPA, the sensitivity of this assay is 100%. 8 out of 9 clinical samples were correctly identified positive by RT-RPA, assuming that the RT-PCR is 100% accurate, making the specificity of this assay 89% (**Figure 40C**). Despite the false positive result, RT-RPA performed equally well as RT-PCR based on this dataset, suggesting that RT-

RPA could be a reliable alternative to RT-PCR in detecting RSV-B, as long as the basis of the false positive result can be identified.

The line of best fit, calculated using simple linear regression, is described by the equation Tt = 0.0771 × Ct + 0.0806, indicating a linear relationship between RT-PCR and RT-RPA detection values. Here, Tt (RT-RPA) is the dependent variable and Ct (RT-PCR) is the independent variable. The slope (0.0771) suggests that for each unit increase in Ct, the Tt increases by approximately 0.08 units. The coefficient of determination ($R^2 = 0.8298$) indicates that approximately 83.0% of the variability in Tt values is explained by the Ct values (**Figure 40D**). Although some data points deviate slightly from the line of best fit, no outliers were excluded, and the correlation remains statistically robust. This confirms that RT-RPA provides comparable results to RT-PCR, while offering faster processing, affordability, and simplified instrumentation requirements.

A.

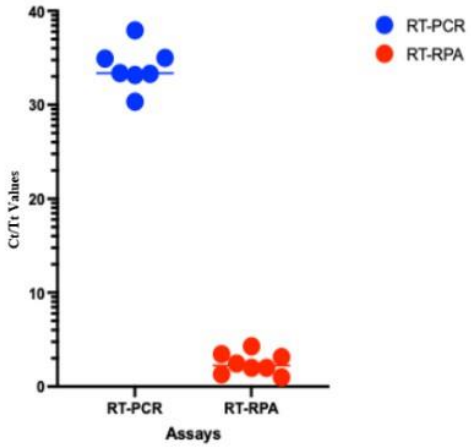

B.

Serial Number	Sample ID	RT-PCR		RT-RPA	
		Ct values	Pos/Neg/IC	Tt values	Pos/Neg/IC
1	A02	34,93	+	3,15	+
2	A03	33,37	+	2,45	+
3	A04	33,18	+	1,3	+
4	A05	33,3	+	2	+
5	A07	ND	-	1	+
6	A08	ND	-	ND	-
7	A09	ND	-	ND	-
8	A11	ND	-	ND	-
9	B01	34,99	+	3,45	+
10	B02	37,94	+	4,3	+
11	B03	30,34	+	2	+
12	B04	ND	-	ND	-
13	B05	ND	-	ND	-
14	B06	ND	-	ND	-
15	B07	ND	-	ND	-
16	B08	ND	-	ND	-

C.

RSV-B		RT-PCR	
		Positive	Negative
RT-RPA	Positive	7	1
	Negative	0	8
	Total	7	9
Sensitivity		100%	
Specificity		89%	

D.

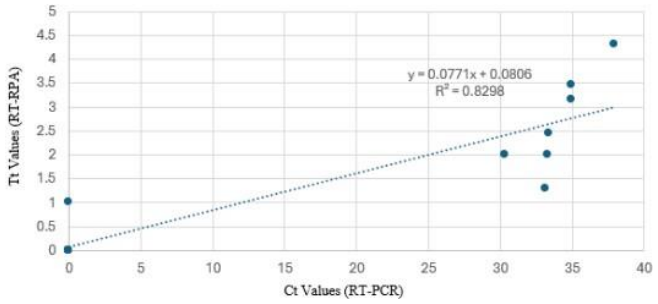

Figure 40. Comparing sensitivity, specificity, and Tt/Ct values of RT-RPA to RT-PCR to determine the overall performance of RT-RPA for detecting RSV-B.

A. Difference between the Tt/Ct values of RT-RPA and RT-PCR assays for RSV-B. Both red and blue data points seem to have a similar range of values, indicating a comparable sensitivity between RT-RPA and RT-PCR. The average Ct value (34.0) for the blue dots (RT-PCR) is higher than the average Tt value (2.46) for the red dots (RT-RPA), indicating that RT-PCR generally yields higher Ct values on average, reflecting the longer detection time. **B**. Comparison of RT-PCR and RT- RPA results for detecting RSV-B in different samples. The positive (+) or negative (-) results from both assays indicate whether RSV-B RNA was detected. "ND" indicates that the target was not detected in the sample, meaning no amplification occurred above the threshold. One sample was detected as positive by RT-RPA but not by RT-PCR (a false positive), showing a slight discrepancy between the two assays. **C**. Diagnostic performance comparison of RT-RPA to RT-PCR for detecting RSV-B, where the RT-PCR was treated as the gold standard. Despite having a discrepancy, RT-RPA exhibited comparable sensitivity (100%) and specificity (89%) to RT-PCR for this dataset. **D**. The relationship between the Tt values of RT-RPA and the Ct values of RT-PCR. The equation ($y = 0.0771x + 0.0806$) suggests a linear relationship, where an increase in Ct values of RT-PCR corresponds to an increase in Tt values of RT-RPA. The coefficient of determination ($R^2 = 0.8298$) indicates a high degree of correlation, demonstrating that RT-RPA can reliably approximate the performance of RT-PCR.

5.3.5. Comparative Performance of RT-RPA and RT-PCR in Detecting HPIV-1

A total of 18 clinical samples suspected of HPIV-1 were subjected to RT-PCR and RT-RPA simultaneously. Based on curated Tt/Ct values, the Ct values of the RT-PCR exhibited greater variability, possibly due to its sensitivity in detecting a wider range of nucleic acid concentrations. RT-RPA consistently produced lower Tt values on average (5.50) , while RT- PCR assay yielded higher Ct values on average (14.3), indicating that the RT-PCR takes longer for detecting the same target concentration (**Figure 41A**). Therefore, RT-RPA seems more efficient in detecting samples with higher concentrations (i.e. higher viral load), while RT-PCR seems better suited for detecting samples with lower concentrations (i.e. lower viral load).

As shown in **Figure 41B**, none of the samples were detected by RT-RPA alone without

corresponding detection by RT-PCR. Additionally, all samples labelled as "ND" were negative in both assays, indicating a similar pattern of detection between the two methods. A total of 18 clinical samples were used to determine the performance of RT-RPA compared to RT-PCR for detecting HPIV-1. Since all 7 clinical samples were correctly identified positive by RT-RPA, the sensitivity of this assay is 100%. Since all 11 clinical samples were correctly identified negative by RT-RPA, the specificity of this assay is also 100% (**Figure 41C**). This shows that RT-RPA performs equally well as RT-PCR based on this dataset, suggesting its potential as a reliable alternative to RT-PCR in detecting HPIV-1.

The line of best fit, calculated using simple linear regression, is described by the equation $Tt = 0.3398 \times Ct + 0.2455$, indicating a linear relationship between RT-PCR and RT-RPA detection values. Here, Tt (RT-RPA) is the dependent variable and Ct (RT-PCR) is the independent variable. The slope (0.3398) suggests that for each unit increase in Ct, the Tt increases by approximately 0.34 units. The coefficient of determination ($R^2 = 0.9466$) indicates that approximately 94.7% of the variability in Tt values is explained by the Ct values (**Figure 41D**). Although minor deviations from the line of best fit may exist, no outliers were excluded, and the correlation remains statistically robust. This confirms that RT-RPA provides comparable results to RT-PCR, while offering faster processing, affordability, and simplified instrumentation requirements.

A.

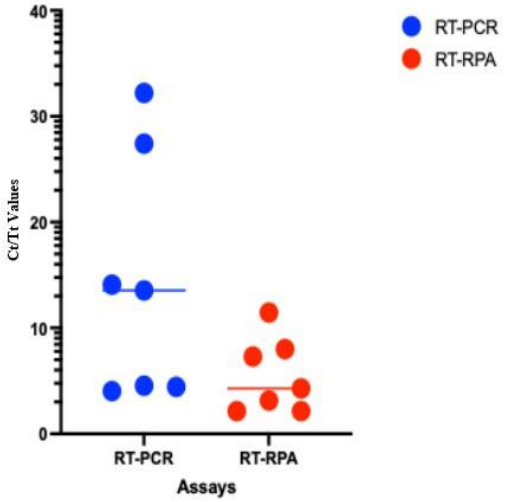

B.

Serial Number	Sample ID	RT-PCR		RT-RPA	
		Ct values	Pos/Neg/IC	Tt values	Pos/Neg/IC
1	E01	ND	-	ND	-
2	E02	4,55059232	+	3,15	+
3	E05	27,4237753	+	8	+
4	E06	13,5400073	+	4,3	+
5	E07	ND	-	ND	-
6	E10	ND	-	ND	-
7	E11	ND	-	ND	-
8	E12	ND	-	ND	-
9	F01	4,03411275	+	2,15	+
10	F02	ND	-	ND	-
11	F04	ND	-	ND	-
12	F05	4,42926222	+	2,15	+
13	F06	ND	-	ND	-
14	F07	ND	-	ND	-
15	F08	14,1005978	+	7,3	+
16	F10	ND	-	ND	-
17	F11	32,2181867	+	11,45	+
18	F12	ND	-	ND	-

C.

hPIV-1		RT-PCR	
		Positive	Negative
RT-RPA	Positive	7	0
	Negative	0	11
	Total	7	11
Sensitivity		100%	
Specificity		100%	

D.

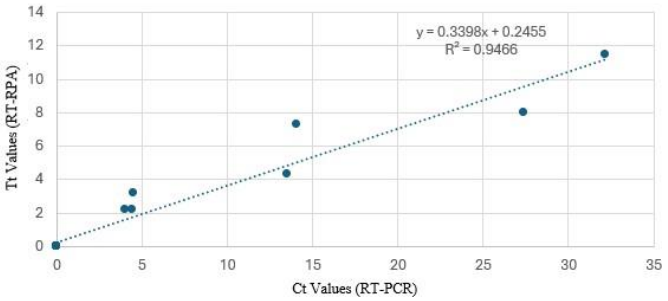

Figure 41. Comparing sensitivity, specificity, and Tt/Ct values of RT-RPA to RT-PCR to determine the overall performance of RT-RPA for detecting HPIV-1.

A. Difference between the Tt/Ct values of RT-PCR and RT-RPA assays for HPIV-1. Blue dots have a wider range of Ct values, indicating more variability in the RT-PCR results. Red dots are more tightly clustered, indicating that RT-RPA consistently produced lower Tt values. Observation of lower Tt values is associated with a higher concentration of the target RNA. The average Ct value (14.3) for the blue dots (RT-PCR) is higher than the average Tt value (5.50) for the red dots (RT-RPA), indicating that RT-PCR yielded higher Ct values on average. Higher Ct values are associated with a lower concentration of the target RNA. **B**. Comparison of RT-PCR and RT- RPA results for detecting HPIV-1 in different samples. The positive (+) or negative (-) results from both assays indicate whether HPIV-1 RNA was detected. "ND" indicates that the target was not detected in the sample, meaning no amplification occurred above the threshold. **C**. Diagnostic performance comparison of RT-RPA and RT-PCR for detecting HPIV-1, where the RT-PCR was treated as the gold standard. RT-RPA exhibited comparable sensitivity (100%) and specificity (100%) to RT-PCR for this dataset. **D**. The relationship between the Tt values of RT- RPA and Ct values of RT-PCR. The equation (y =

0.3398x + 0.2455) suggests a linear relationship, where an increase in Ct values of RT-PCR corresponds to an increase in Tt values of RT-RPA. The coefficient of determination (R^2 = 0.9466) indicates a high degree of correlation, demonstrating that RT-RPA can reliably approximate the performance of RT-PCR.

5.3.6. Comparative Performance of RT-RPA and RT-PCR in Detecting HPIV-2

A total of 18 clinical samples suspected of HPIV-2 were subjected to RT-PCR and RT-RPA simultaneously. Based on curated Tt/Ct values, the Ct values of the RT-PCR assay exhibited greater variability, possibly due to its sensitivity in detecting a wider range of nucleic acid concentrations. RT-RPA consistently produced lower Tt values on average (8.42), while RT- PCR assay provided higher Ct values on average (14.2), meaning that the RT-PCR takes longer to detect the same target concentration (**Figure 42A**). Therefore, RT-RPA seems more efficient in detecting samples with higher concentrations (i.e. higher viral load), while RT-PCR seems better suited for detecting samples with lower concentrations (i.e. lower viral load).

As shown in **Figure 42B**, none of the samples were detected by RT-RPA alone without corresponding detection by RT-PCR. Additionally, all samples labelled as “ND” were negative in both assays, indicating a similar pattern of detection between the two methods. A total of 18 clinical samples were used to determine the performance of RT-RPA compared to RT-PCR for detecting HPIV-2. Since all 7 clinical samples were correctly identified positive by RT-RPA, the sensitivity of this assay is 100%. Since all 11 clinical samples were correctly identified negative by RT-RPA, the specificity of this assay is also 100% (**Figure 42C**). This shows that RT-RPA performs equally well as RT-PCR based on this dataset, suggesting its potential as a reliable alternative to RT-PCR in detecting HPIV-2.

The line of best fit, calculated using simple linear regression, is described by the equation $Tt = 0.4135 \times Ct + 0.9956$, indicating a linear relationship between RT-PCR and RT-RPA detection values. Here, Tt (RT-RPA) is the dependent variable and Ct (RT-PCR) is the independent variable. The slope (0.4135) suggests that for each unit

increase in Ct, the Tt increases by approximately 0.41 units. The coefficient of determination ($R^2 = 0.7517$) indicates that approximately 75.2% of the variability in Tt values is explained by the Ct values (**Figure 42D**). Although some variability is unaccounted for, no outliers were excluded, and the correlation remains statistically robust. This confirms that RT-RPA provides comparable results to RT-PCR, while offering faster processing, affordability, and simplified instrumentation requirements.

A.

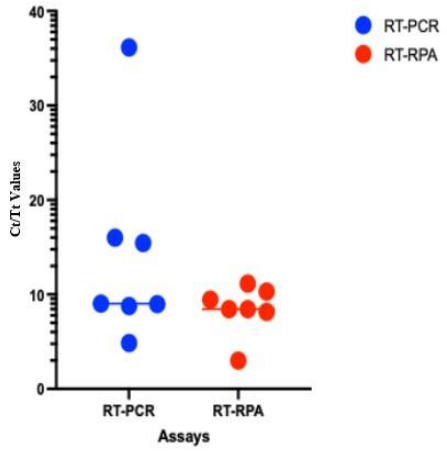

B.

Serial Number	Sample ID	RT-PCR		RT-RPA	
		Ct values	Pos/Neg/IC	Tt values	Pos/Neg/IC
1	G01	ND	-	ND	-
2	G02	4,86283504	+	3	+
3	G03	15,4440842	+	9,45	+
4	G04	ND	-	ND	-
5	G06	ND	-	ND	-
6	G07	8,97358277	+	8,45	+
7	G08	ND	-	ND	-
8	G09	ND	-	ND	-
9	G10	36,1389136	+	11,15	+
10	H01	ND	-	ND	-
11	H02	ND	-	ND	-
12	H04	ND	-	ND	-
13	H05	ND	-	ND	-
14	H06	ND	-	ND	-
15	H07	ND	-	ND	-
16	H10	16,0152323	+	10,3	+
17	H11	9,02563968	+	8,45	+
18	H12	8,77139482	+	8,15	+

C.

hPIV-2		RT-PCR	
		Positive	Negative
RT-RPA	Positive	7	0
	Negative	0	11
	Total	7	11
Sensitivity		100%	
Specificity		100%	

D.

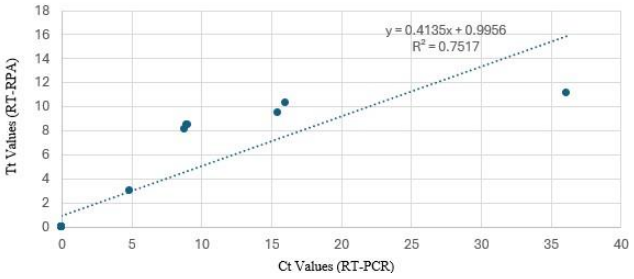

Figure 42. Comparing sensitivity, specificity, and Tt/Ct values of RT-RPA to RT-PCR to determine the overall performance of RT-RPA for detecting HPIV-2.

A. Difference between the Tt/Ct values of RT-PCR and RT-RPA assays for HPIV-2. Blue dots have a wider range of Ct values, indicating more variability in the RT-PCR results. Red dots are more tightly clustered, showing that RT-RPA produced more consistent results with lower Tt values. The average Ct value for the blue dots (RT-PCR) is around the same level as the average Tt value for the red dots (RT-RPA), indicating that both assays detected similar concentrations of viral RNA in the sample. **B**. Comparison of RT-PCR and RT-RPA results for detecting HPIV-2 in different samples. The positive (+) or negative (-) results from both assays indicate whether

HPIV-2 RNA was detected. "ND" indicates that the target was not detected in the sample, meaning no amplification occurred above the threshold. **C**. Diagnostic performance comparison of RT-RPA and RT-PCR for detecting HPIV-2, where the RT-PCR was treated as the gold standard. RT-RPA exhibited comparable sensitivity and specificity to RT-PCR for this dataset. **D**. The relationship between the Tt values of RT-RPA and the Ct values of RT-PCR. The equation ($y = 0.4135x + 0.9956$) suggests a linear relationship, where an increase in Ct values of RT-PCR corresponds to an increase in Tt values of RT-RPA. The coefficient of determination ($R^2 = 0.7517$) indicates a moderate degree of correlation, demonstrating that RT-RPA can reliably approximate the performance of RT-PCR.

5.3.7. Comparative Performance of RT-RPA and RT-PCR in Detecting HPIV-4

A total of 19 clinical samples suspected of HPIV-4 were subjected to RT-PCR and RT-RPA simultaneously. Based on curated Tt/Ct values, the Ct values of the RT-PCR exhibited greater variability, possibly due to its sensitivity in detecting a wider range of nucleic acid concentrations. RT-RPA consistently produced lower Tt values on average (6.83), while RT- PCR provided higher Ct values on average (14.0), meaning that the RT-PCR takes longer to detect the same target concentration (**Figure 43A**). Therefore, RT-RPA seems more efficient in detecting samples with higher concentrations (i.e. higher viral load), while RT-PCR seems better suited for detecting samples with lower concentrations (i.e. lower viral load).

As shown in **Figure 43B**, none of the samples were detected by RT-RPA alone without corresponding detection by RT-PCR. Additionally, all samples labelled as "ND" were negative in both assays, indicating a similar pattern of detection between the two methods. A total of 19 clinical samples were used to determine the performance of RT-RPA compared to RT-PCR for detecting HPIV-4. Since all 8 clinical samples were correctly identified positive by RT-RPA, the sensitivity of this assay is 100%. Since all 11 clinical samples were correctly identified negative by RT-RPA, the specificity of this assay is also 100% (**Figure 43C**). This shows that RT-RPA performs equally well as RT-PCR based on this dataset, suggesting its potential as a reliable alternative to RT-PCR in

detecting HPIV-4.

The line of best fit, calculated using simple linear regression, is described by the equation Tt = 0.3889 × Ct + 0.2284, indicating a linear relationship between RT-PCR and RT-RPA detection values. Here, Tt (RT-RPA) is the dependent variable and Ct (RT-PCR) is the independent variable. The slope (0.3889) suggests that for each unit increase in Ct, the Tt increases by approximately 0.39 units. The coefficient of determination ($R^2 = 0.724$) indicates that approximately 72.4% of the variability in Tt values is explained by the Ct values (**Figure 43D**). Although some variability remains unexplained, no outliers were excluded, and the correlation remains statistically robust. This confirms that RT-RPA provides comparable results to RT-PCR, while offering faster processing, affordability, and simplified instrumentation requirements.

A.

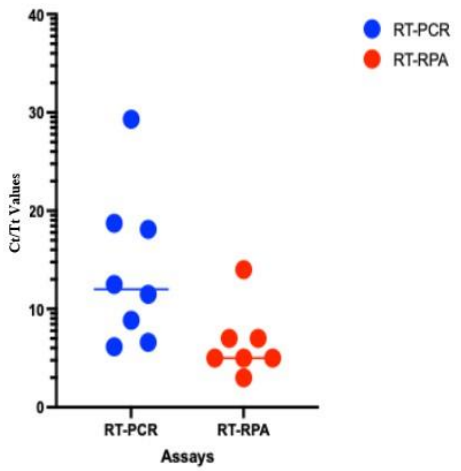

B.

Serial Number	Sample ID	RT-PCR		RT-RPA	
		Ct values	Pos/Neg/IC	Tt values	Pos/Neg/IC
1	F01	ND	-	ND	-
2	F03	8,8383883	+	5,45	+
3	F04	18,1055546	+	7,45	+
4	F06	ND	-	ND	-
5	F07	ND	-	ND	-
6	F08	11,497033	+	5,45	+
7	F10	ND	-	ND	-
8	F11	ND	-	ND	-
9	G01	ND	-	ND	-
10	G03	18,733269	+	ND	+
11	G04	ND	-	ND	-
12	G05	ND	-	ND	-
13	G06	ND	-	ND	-
14	G08	12,4945976	+	7	+
15	G09	ND	-	ND	-
16	G10	6,14748921	+	3,15	+
17	G12	29,3169647	+	14	+
18	H01	6,60666741	+	5,3	+
19	H03	ND	-	ND	-

C.

hPIV-4		RT-PCR	
		Positive	Negative
RT-RPA	Positive	8	0
	Negative	0	11
	Total	8	11
Sensitivity		100%	
Specificity		100%	

D.

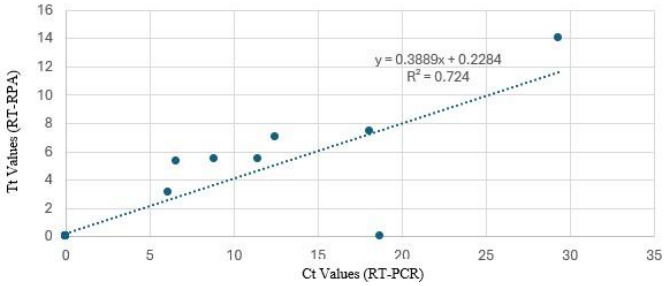

Figure 43. Comparing sensitivity, specificity, and Tt/Ct values of RT-RPA to RT-PCR to determine the overall performance of RT-RPA for detecting HPIV-4.

A. Difference between the Tt/Ct values of RT-PCR and RT-RPA assays for HPIV-4. Blue dots have a wider range of Ct values, indicating more variability in the RT-PCR results. Red dots are

more tightly clustered, indicating that RT-RPA consistently produced lower Tt values. Observation of lower Tt values is associated with a higher concentration of the target RNA. The average Ct value (14.0) for the blue dots (RT-PCR) is higher than the average Tt value (6.83) for the red dots (RT-RPA), indicating that RT-PCR generally yields higher Ct values on average. Higher Ct values are associated with a lower concentration of the target RNA. **B**. Comparison of RT-PCR and RT-RPA results for detecting HPIV-4 in different samples. The positive (+) or negative (-) results from both assays indicate whether HPIV-4 RNA was detected. "ND" indicates that the target was not detected in the sample, meaning no amplification occurred above the threshold. **C**. Diagnostic performance comparison of RT-RPA and RT-PCR for detecting HPIV-4, where the RT-PCR was treated as the gold standard. RT-RPA exhibited comparable sensitivity (100%) and specificity (100%) to RT-PCR for this dataset. **D**. The relationship between the Tt values of RT-RPA and Ct values of RT-PCR. The equation ($y = 0.3889x + 0.2284$) suggests a linear relationship, where an increase in Ct values of RT-PCR corresponds to an increase in Tt values of RT-RPA. The coefficient of determination ($R^2 = 0.724$) indicates a moderate degree of correlation, meaning that the two assays produced similar results, demonstrating that RT-RPA can reliably approximate the performance of RT-PCR.

5.3.8. Comparative Performance of RT-RPA and RT-PCR in Detecting HRV-A

A total of 20 clinical samples suspected of HRV-A were subjected to RT-PCR and RT-RPA simultaneously. Based on curated Tt/Ct values, it can be concluded that the Ct values of the RT-PCR assay exhibited greater variability, possibly due to its sensitivity in detecting a wider range of nucleic acid concentrations. RT-RPA consistently produced lower Tt values on average (3.93), while RT-PCR showed higher Ct values on average (21.3), meaning that the RT-PCR takes longer to detect the same target concentration (**Figure 44A**). Therefore, RT-RPA seems more efficient in detecting samples with higher concentrations (i.e. higher viral load), while RT-PCR seems better suited for detecting samples with lower concentrations (i.e. lower viral load).

As shown in **Figure 44B**, none of the samples were detected by RT-RPA alone without corresponding detection by RT-PCR. Additionally, all samples labelled as "ND" were

negative in both assays, indicating a similar pattern of detection between the two methods. A total of 20 clinical samples were used to determine the performance of RT-RPA compared to RT-PCR for detecting HRV-A. Since all 13 clinical samples were correctly identified as positive by RT-RPA, the sensitivity of this assay is 100%. Since all 7 clinical samples were correctly identified as negative by RT-RPA, the specificity of this assay is also 100% (**Figure 44C**). This shows that RT-RPA performs equally well as RT-PCR based on this dataset, suggesting its potential as a reliable alternative to RT-PCR in detecting HRV-A.

The line of best fit, calculated using simple linear regression, is described by the equation $Tt = 0.1428 \times Ct + 0.5736$, indicating a linear relationship between RT-PCR and RT-RPA detection values. Here, Tt (RT-RPA) is the dependent variable and Ct (RT-PCR) is the independent variable. The slope (0.1428) suggests that for each unit increase in Ct, the Tt increases by approximately 0.14 units. The coefficient of determination ($R^2 = 0.8905$) indicates that approximately 89.1% of the variability in Tt values is explained by the Ct values (**Figure 44D**). Although minor deviations from the line of best fit may exist, no outliers were excluded, and the correlation remains statistically robust. This confirms that RT-RPA provides comparable results to RT-PCR, while offering faster processing, affordability, and simplified instrumentation requirements.

A.

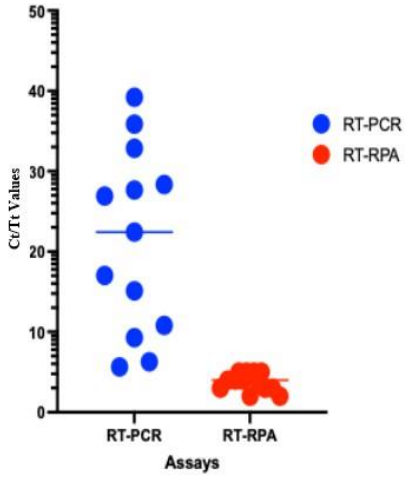

B.

Serial Number	Sample ID	RT-PCR		RT-RPA	
		Ct values	Pos/Neg/IC	Tt values	Pos/Neg/IC
1	A01	ND	-	ND	-
2	A02	ND	-	ND	-
3	A04	ND	-	ND	-
4	A05	27,666436	+	4,45	+
5	A06	6,28027187	+	2,30	+
6	A07	17,0196028	+	4	+
7	A08	35,8617134	+	5,15	+
8	A09	10,8055156	+	3,15	+
9	A10	26,9156735	+	4,15	+
10	A11	ND	-	ND	-
11	B02	9,28854971	+	3	+
12	B03	28,3381948	+	5	+
13	B05	32,850441	+	5	+
14	B06	22,4339421	+	4,15	+
15	B07	5,64752256	+	2,15	+
16	B08	ND	-	ND	-
17	B09	39,211872	+	5,15	+
18	B10	15,1176505	+	3,45	+
19	B11	ND	-	ND	-
20	B12	ND	-	ND	-

C.

hRVA		RT-PCR	
		Positive	Negative
RT-RPA	Positive	13	0
	Negative	0	7
	Total	13	7
Sensitivity		100%	
Specificity		100%	

D.

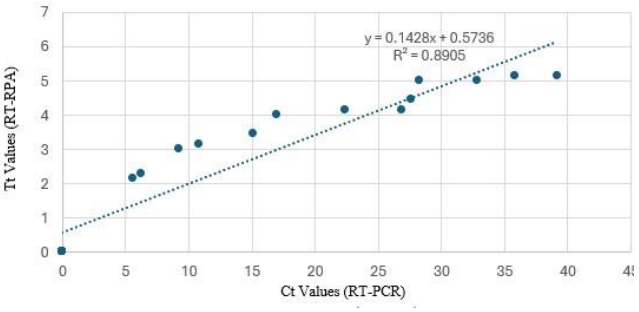

Figure 44. Comparing sensitivity, specificity, and Tt/Ct values of RT-RPA to RT-PCR to determine the overall performance of RT-RPA for detecting HRV-A.

A. Difference between the Tt/Ct values of RT-PCR and RT-RPA assays for HRV-A. Blue dots have a wider range of Ct values, indicating more variability in the RT-PCR results. Red dots are more tightly clustered, indicating that RT-RPA consistently produced lower Tt values. Observation of lower Tt values is associated with a higher concentration of the target RNA. The average Ct value (21.3) for the blue dots (RT-PCR) is higher than the average Tt value (3.93) for the red dots (RT-RPA), indicating that RT-PCR generally yields higher Ct values on average. Higher Ct values are associated with a lower concentration of the target RNA. **B**. Comparison of RT-PCR and RT-RPA results for detecting HRV-A in different samples. The positive (+) or negative (-) results from both assays indicate whether HRV-A RNA was detected. "ND" indicates that the target was not detected in the sample, meaning no amplification occurred above the threshold. **C**. Diagnostic performance comparison of RT-RPA and RT-PCR for detecting HRV-A, where the RT-PCR was treated as the gold standard. RT-RPA exhibited comparable sensitivity (100%) and specificity (100%) to RT-PCR for this

dataset. **D**. The relationship between the Tt values of RT-RPA and the Ct values of RT-PCR. The equation ($y = 0.1428x + 0.5736$) suggests a linear relationship, where an increase in Ct values of RT-PCR corresponds to an increase in Tt values of RT-RPA. The coefficient of determination ($R^2 = 0.8905$) indicates a high degree of correlation, demonstrating that RT-RPA can reliably approximate the performance of RT-PCR.

5.3.9. Comparative Performance of RT-RPA and RT-PCR in Detecting hMPV

A total of 12 clinical samples suspected of hMPV were subjected to RT-PCR and RT-RPA simultaneously. Based on curated Tt/Ct values, the Ct values of the RT-PCR assay exhibited greater variability, possibly due to its sensitivity in detecting a wider range of nucleic acid concentrations. RT-RPA assay consistently produced lower Tt values on average (5.31), while RT-PCR assay showed higher Ct values on average (19.0),meaning that the RT-PCR takes longer to detect the same target concentration (**Figure 45A**). Therefore, RT-RPA seems more efficient in detecting samples with higher concentrations (i.e. higher viral load), while RT-PCR seems better suited for detecting samples with lower concentrations (i.e. lower viral load).

As shown in **Figure 45B**, none of the samples were detected by RT-RPA alone without corresponding detection by RT-PCR. Additionally, all samples labelled as “ND” were negative in both assays, indicating a similar pattern of detection between the two methods. A total of 12 clinical samples were used to determine the performance of RT-RPA compared to RT-PCR for detecting hMPV. Since all 9 clinical samples were correctly identified positive by RT-RPA, the sensitivity of this assay is 100%. Since all 3 clinical samples were correctly identified negative by RT-RPA, the specificity of this assay is also 100% (**Figure 45C**). This shows that RT-RPA performs equally well as RT-PCR based on this dataset, suggesting its potential as a reliable alternative to RT-PCR in detecting hMPV.

The line of best fit, calculated using simple linear regression, is described by the equation $Tt = 0.3018 \times Ct + 0.3213$, indicating a linear relationship between RT-PCR and RT-RPA detection values. Here, Tt (RT-RPA) is the dependent variable and Ct

(RT-PCR) is the independent variable. The slope (0.3018) suggests that for each unit increase in Ct, the Tt increases by approximately 0.30 units. The coefficient of determination ($R^2 = 0.9704$) indicates that approximately 97.0% of the variability in Tt values is explained by the Ct values (**Figure 45D**). Although minor deviations from the line of best fit may occur, no outliers were excluded, and the correlation remains statistically robust. This confirms that RT-RPA provides comparable results to RT-PCR, while offering faster processing, affordability, and simplified instrumentation requirements.

A.

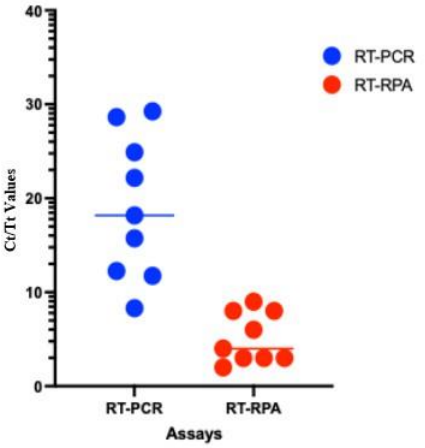

B.

Serial Number	Sample ID	RT-PCR		RT-RPA	
		Ct values	Pos/Neg/IC	Tt values	Pos/Neg/IC
1	C02	29,2623857	+	9,3	+
2	C05	15,7365437	+	3,3	+
3	C06	22,1707024	+	6,45	+
4	C09	12,2476249	+	3,15	+
5	C12	ND	-	ND	-
6	D02	ND	-	ND	-
7	D03	8,30370402	+	2	+
8	D05	24,9049955	+	8	+
9	D06	28,6351557	+	8	+
10	D08	18,169597	+	4,45	+
11	D09	11,737401	+	3,15	+
12	D12	ND	-	ND	-

C.

hMPV		RT-PCR	
		Positive	Negative
RT-RPA	Positive	9	0
	Negative	0	3
	Total	9	3
Sensitivity		100%	
Specificity		100%	

D.

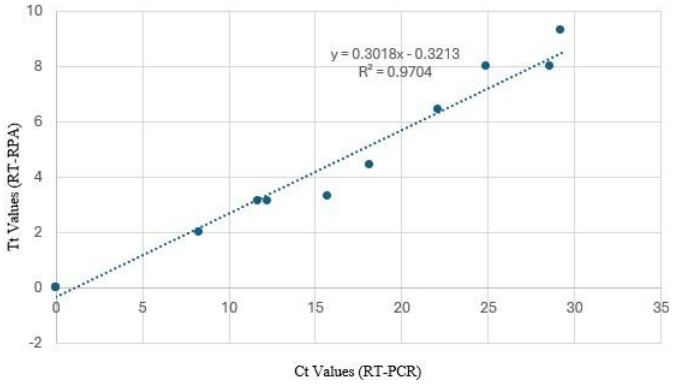

Figure 45. Comparing sensitivity, specificity, and Tt/Ct values of RT-RPA to RT-PCR to determine the overall performance of RT-RPA for detecting hMPV.

A. Difference between the Tt/Ct values of RT-PCR and RT-RPA assays for hMPV. Blue dots have a wider range of Ct values, indicating more variability in the RT-PCR results. Red dots are more tightly clustered, indicating that RT-RPA produced more consistent results with lower Tt values. Observation of lower Tt values is associated with a higher concentration of the target RNA. The average Ct value (19.0) for the blue dots (RT-PCR) is higher than the average Tt value (5.31) for the red dots (RT-RPA), indicating that RT-PCR generally yields higher Ct

values on average. Higher Ct values are associated with a lower concentration of the target RNA. **B**. Comparison of RT-PCR and RT-RPA results for detecting hMPV in different samples. The positive (+) or negative (-) results from both assays indicate whether hMPV RNA was detected. "ND" indicates that the target was not detected in the sample, meaning no amplification occurred above the threshold. **C**. Diagnostic performance comparison of RT-RPA and RT-PCR for detecting hMPV, where the RT-PCR was treated as the gold standard. RT-RPA exhibited comparable sensitivity (100%) and specificity (100%) to RT-PCR for this dataset. **D**. The relationship between the Tt values of RT-RPA and the Ct values of RT-PCR. The equation ($y = 0.3018x – 0.3213$) suggests a linear relationship, where an increase in Ct values of RT-PCR corresponds to an increase in Tt values of RT-RPA. The coefficient of determination ($R^2 = 0.9704$) indicates a high degree of correlation, demonstrating that RT-RPA can reliably approximate the performance of RT-PCR.

5.4. Discussion

5.4.1. Comparative Diagnostic Performance of RT-RPA and RT-PCR

This study compared the diagnostic performance of RT-RPA and RT-PCR in detecting multiple respiratory viruses from clinical samples. RT-PCR is the current gold standard for detecting viruses due to its high sensitivity and specificity. However, RT-RPA was identified to perform very similarly to RT-PCR for detecting a wide range of respiratory viruses. In this study, RT-RPA consistently produced lower Tt values, which showed its ability to detect high viral loads faster than RT-PCR. This was consistent with the previous studies where the RT-RPA has a rapid amplification speed that allows the detection of the amplification products in about 20 min (Li et al., 2018). RT-RPA is capable of detecting trace-level nucleic acids in samples at the lowest level, which was confirmed by 100% sensitivity in detecting all viruses tested in this study. In some studies, RT-RPA could even detect low concentrations of DNA that PCR could not detect, possibly due to differences in primer/probe designs, assay chemistry, or reaction conditions. This might explain why RSV-B was detected by RT-RPA, while it was not detected by RT-PCR. RT-RPA also provided 100% specificity with the exception of 89% for RSV-B, which might be caused by non-specific amplification or cross-reactivity

with other nucleic acids.

Additionally, the strong correlation between the Tt and Ct values of RT-RPA and RT-PCR was confirmed by the R^2 values as high as 0.9704 (97.04%), meaning that RT-RPA works just as well as RT-PCR in detecting viral nucleic acids. This is consistent with previous studies that reported a similarity between RPA and PCR results for pathogen detection, highlighting the robustness of RPA as a molecular diagnostic tool (Li et al., 2019; Lobato and O'Sullivan, 2018). In regression analysis, R^2 values over 0.7 are suggested to demonstrate a strong relationship between the two assays, implying that scores from one assay tend to align well with scores from the other. An R^2 value of 1 represents the data that perfectly fit the linear model. Any R^2 value less than 1 indicates at least some variability in the data that cannot be accounted for by the model (Poitras et al., 2015; Hamilton, 2015; Srinivasan, 2010). This indicates a strong but not perfect linear relationship, which may be due to the differences in assay sensitivity and amplification efficiency. In this study, there is an obvious correlation between the Tt and Ct values of RT-RPA and RT-PCR in detecting all the suspected viruses, meaning that two assays responded similarly across a range of nucleic acid concentrations despite having different amplification mechanisms. This shows that RT-RPA can serve as a reliable alternative, especially when quick detection is required. Unfortunately, the sample size used for this part of the study was relatively small, so the reliability of the R^2 value is limited. Using more clinical samples to cover more variability across a wider range of RNA concentrations is necessary to eliminate any sampling bias.

Moreover, Ct and Tt values were deliberately presented without error bars or conventional statistical testing. This is because these values represent diagnostic thresholds rather than experimental replicates drawn from normally distributed populations. Using statistical tests such as t-tests would not be meaningful in this context since diagnostic thresholds are intended for classification rather than for comparing mean differences. Instead, the diagnostic assay performance of RPA was more appropriately evaluated through sensitivity, specificity, and diagnostic accuracy relative to the gold standard, which were reported in this study. This approach aligns with accepted practice in assay validation and ensures that interpretation of the data reflects diagnostic utility rather than inferential statistical comparison.

5.4.2. Advantages of RT-RPA for POCT

The shorter processing time of RT-RPA confirmed the quick detection capacity of the assay, meaning that it can be performed in 20 min under isothermal conditions without the need for sophisticated thermocyclers (Piepenburg et al., 2006). This indicates the suitability of RT-RPA as an ideal candidate for POCT, where quick results and low-cost operations are necessary (Crannell et al., 2016). In POCs, it is essential to control the spread of respiratory viruses quickly and effectively, particularly in cases like disease outbreaks caused by Influenza, RSV, or SARS-CoV-2 (Wozniak et al., 2020). RT-RPA offers a rapid turnaround time, facilitating early diagnosis, timely decision-making, and efficient disease management.

5.4.3. Limitations and Challenges of RT-RPA

Although RT-RPA showed a very similar diagnostic performance to RT-PCR, it has identified a false positive in the case of RSV-B, which needs to be addressed before widespread clinical implementation. False positives can lead to misdiagnosis and inappropriate patient management, which may have significant implications for disease control and treatment decisions (Kokkinos et al., 2019). The reason behind this outcome has yet to be discovered. However, the possible causes include non-specific binding or cross-reactivity due to poor primer design or reaction conditions, as noted in other isothermal amplification methods (Guan et al., 2019). In this case, further optimisation of the primer design and reaction conditions may improve the specificity of RT-RPA and reduce the incidence of such errors.

Since RPA is still an emerging diagnostic method with a short development time, there are several other limitations that must be addressed while using RT-RPA. The multiplexing capacity of RT-RPA is more limited than that of RT-PCR, as the latter has well-established and more advanced protocols for multiplexing through the use of distinct fluorophores or primers for different targets. RT-RPA has an interference issue among primers with a risk of occasional non-specific amplification when multiple

targets are included in the reaction (Daher et al., 2016). Primers and probes used in RT-RPA require advanced optimisation as even small changes in primer and probe sequences can significantly affect amplification efficiency (Li et al., 2019). Lack of successful optimisation will likely cause non-specific amplification and primer-dimer formation, complicating the assay development. If precise temperature control is not possible in low-resource settings, this may affect the amplification efficiency of RT-RPA as it is very susceptible to temperature fluctuations (Crannell et al., 2016). Refrigeration options may also be limited in low-resource settings, affecting the stability of the stored reagents needed for RT-RPA (Daher et al., 2016). Since RPA is an isothermal process that can produce amplicons in about 20 min, there is a higher risk of contamination between reactions, particularly in settings where multiple reactions are being conducted in close proximity. If contamination precautions are not followed, amplicons from the previous reactions can contaminate the new reactions, causing false positive results (James et al., 2015). Serious contamination control measures, like dedicated work areas and physical barriers, must be taken to reduce the risk of contamination to a minimum.

5.4.4. Strategies for Improving RT-RPA Diagnostic Performance

Researchers should focus on minimising the limitations of RT-RPA by optimising the assay to avoid any false positives without compromising their sensitivity. Incorporating a wider range of viruses and more clinical samples can provide a more comprehensive outcome for the diagnostic performance of RT-RPA. Advanced bioinformatics tools, such as Primer3 or OligoAnalyser, can be used to optimise primer design, reducing the risk of dimerisation and secondary structures. False positives can arise from non-specific amplification, which generally occurs due to poor primer or probe design. Thermodynamic models, such as the nearest-neighbour model, can be used to predict primer-dimer formation, secondary structures, or non-specific amplification (Turner and Mathews, 2010). High-fidelity enzymes can be used in RPA reactions to reduce errors like mismatched bases during DNA synthesis. These enzymes exhibit a proofreading exonuclease activity that acts as a quality control mechanism to detect and remove incorrectly incorporated nucleotides before elongation continues (Bebenek and Ziuzia-

Gracyzk, 2018). They are also less prone to forming primer-dimers, which can cause non-specific amplification products. Unfortunately, RPA-specific high-fidelity enzymes are not commercially available, so enzymes like Phi29 DNA polymerase from rolling-circle amplification (RCA) or *Bst* polymerase from LAMP can be used as an inspiration for the development of more accurate polymerases for RPA (Vrtis et al., 2023). On the other hand, modifications can also be applied to the existing RPA enzymes, such as adding proofreading activity or suppressing errors (Tolar et al., 2019). RPA enzymes are typically highly active at room temperature, which increases the likelihood of non-specific amplification before reaching optimal reaction temperature. Therefore, hot-start versions of RPA enzymes can be developed by modifying them using chemicals, antibodies, or aptamers. Hence, they remain inactive at lower temperatures and become active only when they reach a certain temperature threshold. This process ensures that amplification begins when all reaction components are aligned so that non-specific amplification can be avoided.

Additionally, DNA-intercalating dyes like SYBR Green can be used with RPA for real- time fluorescence detection. The dye binds between the base pairs of double-stranded DNA without disrupting its structure and releases fluorescence. The dye becomes non- fluorescent (or much less fluorescent) when it detaches from the DNA. As the DNA product accumulates during the amplification, the dye binds to the newly synthesised DNA and releases fluorescence. There is a direct correlation between the amount of fluorescence released and the amount of amplification product being generated so that it can be monitored in real time (Hellyer et al., 2009). Multiplex reactions typically amplify multiple targets from a single reaction tube using specific primer sets and probes for each target. While this is the traditional way of running multiplex reactions, the physical separation of reactions into different tubes or compartments, such as microfluidic chips, minimises the risk of cross-contamination (Schoepp et al., 2017).

5.4.5. Post-Amplification Methods for Confirmation and Contamination Control

Several post-amplification methods can be used to confirm the identity of the amplified products and eliminate the risk of getting false positives. RPA can be combined with LFD detection to ensure that only target-specific products are amplified to give a true positive result (Jauset-Rubio et al., 2016). This approach is beneficial in field diagnostics as it offers quick detection of clinical samples, making it suitable for use in low-resource settings (Kolm et al., 2019; Wang et al., 2019; Wu et al., 2017). LFD works by attaching antibodies to the test strip that bind specifically to probes complementary to the target nucleic acid sequence, forming an antibody-probe complex. When the amplification product is added to the test strip, it binds to the complex, which is captured by a biotin-labelled ligand on the test line, producing a positive test result (Wang et al., 2019). Next-generation sequencing can also be used to eliminate false positives by confirming that the amplified product corresponds to the intended target sequence (Jeong et al., 2021). This approach requires nucleic acid purification before sequencing to remove excess primers, enzymes, and small by-products of the amplification reaction. Magnetic beads, spin columns, crude extraction, and chelex resin are the methods that can be used for the purification of nucleic acids in low-resource settings.

Magnetic beads are covered with antibodies that are specific to the target. When the beads are mixed with a clinical sample, the target molecules bind to the surface of the beads. A magnet is used to attract the beads, which are later washed to remove any unwanted materials (Rohland and Reich, 2012). A spin column has a filter that can trap nucleic acids while letting other molecules pass through. The filter catches the target molecules after adding the RT-RPA reaction mixture into the column. These molecules are washed and eluded with buffer to obtain the purified product (Hindson et al., 2011). Crude extraction involves breaking down the cells to release their contents and separating the target molecule from the remaining materials using physical (e.g. grinding) or chemical (e.g. detergents) methods. The lysate is mixed with an extraction buffer to stabilise the target molecules and then centrifuged to separate the heavier debris from the lighter target molecules, which can be further purified if required (LaBarre et al., 2011; Liu and Lee, 2014). All these techniques are rapid, cost-effective, and require minimal effort and equipment, making them well-suited for POCT, field

diagnostics, and research in remote areas.

5.5. Conclusion

The results of this study indicate that RT-RPA and RT-PCR are strongly comparable in detecting multiple respiratory viruses across several clinical samples. RT-RPA generally provided lower Tt values which is associated with more rapid detection of high viral loads. Meanwhile, RT-PCR provided a range of generally higher Ct values, representing its detection capacity for low and high viral loads. The sensitivity and specificity of RT-RPA were 100% in most cases, except for the false positive in detecting RSV-B. The high R^2 values (ranging from 72.4% to 97.04%) confirmed the linear relationship between both assays, indicating that RT-RPA results closely mirror those of RT-PCR. Considering the benefits of RT-RPA, such as faster processing times, lower equipment requirements, and cost-effectiveness, it has a potential to be used as a reliable alternative to RT-PCR, particularly in low-resource settings like POCs. However, any false positive cases, such as the one in RSV-B, require further investigation to refine the assay for broader diagnostic applications.

Chapter 6: General Discussion

This study compared the diagnostic performance of isothermal RT-RPA to traditional RT-PCR in detecting various respiratory viruses. RT-PCR is the current gold standard for viral diagnostics, offering high sensitivity and specificity. However, it uses expensive thermocyclers for the high reaction temperatures needed for amplification, has a slower amplification rate, and requires trained personnel to perform and analyse the assay. The isothermal nature of RT-RPA offers a rapid amplification rate at lower reaction temperatures with great sensitivity and specificity, making it a promising candidate for POCT in low-resource settings. However, there are some limitations associated with RT-RPA, including false positives caused by non-specific amplification, primer-dimer formation, or carryover contamination due to its rapid amplification kinetics. Additionally, it has a limited multiplexing capacity compared to RT-PCR, which has well-established protocols for the simultaneous detection of multiple targets using distinct fluorophores. RT-RPA is also likely to be affected by temperature fluctuations, possibly affecting its amplification efficiency, which must be addressed before solely depending on this method. TOPO TA cloning was used in this study to confirm the specificity of primers and verify the identity of the amplification products, followed by in vitro transcription to generate RNA templates for assay validation. Optimising primer design, using high-fidelity enzymes, or developing hot-start versions of RT-RPA enzymes can improve the assay reliability. With further refinement, RT-RPA remains a strong candidate as a rapid and cost-effective molecular diagnostic method in various settings.

6.1. Co-infections and Diagnostic Challenges

This study highlights the importance of rapid molecular detection tools for the early detection and management of respiratory viruses. Individuals with respiratory infections are often co-infected with multiple respiratory viruses, including SARS-CoV-2, influenza viruses, RSVs, and AdVs (Coyle and Kelly, 2020). Severe cases of influenza

and AdV co-infections are known to cause higher disease severity and mortality risks in immunocompromised individuals (Li and Zhang, 2021). However, the precise effect of these co-infections on clinical patients is yet to be fully understood. Therefore, developing advanced diagnostic tools is important to eliminate this uncertainty, as it can complicate the disease prognosis and treatment, particularly in low-resource settings.

RPP is a multiplex diagnostic test that allows the simultaneous detection of multiple pathogens from a single patient sample, which is beneficial in managing co-infections. Unfortunately, these tests were limited in some POCs during the COVID-19 pandemic due to global shortages of reagents, equipment, and personnel. Therefore, there was an increasing concern about delayed diagnosis and treatment of co-infections. As a result, healthcare personnel prioritised testing for influenza and RSV first to save resources, further delaying the detection of pathogens causing the infection (Ruis, 2020). It is crucial to use molecular diagnostic methods, such as RT-RPA, to eliminate these challenges. They are suitable for use in low-resource settings, allow early detection of viral RNA in both asymptomatic and pre-symptomatic cases, and reduce the risk of disease spread.

6.2. RT-RPA as a Diagnostic Alternative

Based on the findings of this study, RT-RPA and RT-PCR showed very similar diagnostic performance in detecting a wide range of respiratory viruses. Rapid amplification rate of RT-RPA enabled faster detection of high viral loads, which can be as low as 20 min. This observation was consistent with previous studies regarding the rapid amplification capabilities of RT-RPA (Li et al., 2018; Zhang et al., 2021). Due to its rapid amplification rate, RT-RPA can provide early diagnosis, disease management, and timely decision-making, which is significant in emergencies.

While RT-PCR remains the gold standard for detecting viral RNA due to its excellent sensitivity and specificity, its limitations cannot be avoided. These include dependencies on sophisticated equipment, trained personnel, and high costs during widespread diagnostic demands. When there is high demand, RT-PCR faces shortages of diagnostic

resources, as in the COVID-19 pandemic (Kearney and Stoecker, 2020). On the other hand, RT-RPA offers several advantages over the gold standard, including low costs, shorter turnaround times, minimal equipment usage, and adaptability to low- and middle-income countries with limited diagnostic resources. Additionally, RT-RPA can distinguish between SARS-CoV-2 and other human coronaviruses (e.g. HCoV-NL63, HCoV-OC43, and HCoV-229E) that cause similar respiratory symptoms (Lassaunière et al., 2020). Even though RT-RPA exhibited comparable sensitivity and specificity to RT-PCR, it still requires further refinement to reduce the risk of false positives and expand its multiplexing capacity. Hence, it can be used as a reliable diagnostic tool in diverse clinical settings.

6.3. Diagnostic Accuracy and Efficiency of RT-RPA

In this study, fluorescence-based RT-RPA demonstrated high sensitivity (100%) and specificity (92%). Meanwhile, LFD-based RT-RPA showed a reduced sensitivity (84%) with slightly higher specificity (97%). These findings indicate that both detection methods are diagnostically accurate; therefore, choosing between these methods may depend on the availability of diagnostic resources within the area of testing. Even though LFD-based detection is a simpler and more affordable option, fluorescence-based detection seems a better choice particularly when real-time disease monitoring is required.

RT-RPA provided 100% sensitivity in detecting all the viruses tested, even outperforming RT-PCR in detecting RSV-B. This confirms that RT-RPA can detect trace-level nucleic acids, which is consistent with the previous studies (Boyle et al., 2014; Daher et al., 2016; Euler et al., 2012). However, RT-RPA provided slightly reduced specificity for RSV-B (89%), emphasising the need for further optimisation for widespread clinical use to eliminate the risk of false positives. Regardless, RT-RPA is a reliable diagnostic method, confirmed by the strong correlation between RT-RPA and RT-PCR results, with R^2 values as high as 0.97 (97%). Even though both assays are highly sensitive and specific, RT-RPA has several advantages over the gold standard for

POCT, such as operating under isothermal reaction conditions and reduced reliance on sophisticated equipment, emphasising its suitability for low-resource settings (Piepenburg et al., 2006). Considering the limited availability of advanced resources in POCs during the COVID-19 pandemic, relying solely on RT-PCR is unsustainable.

Similar to RT-RPA, traditional RT-PCR has a limited multiplexing capacity as it cannot detect more than 3-4 target genes at a time due to challenges in primer/probe design and signal overlap. This is not feasible in cases where a co-infection is caused by over 3-4 different viruses (Corman et al., 2020). However, some advanced PCR-based multiplex platforms can detect more from a single reaction. In contrast, RT-RPA, while offering speed and simplicity, is usually less suitable for high-level multiplexing. Fortunately, RPA can still be customised to detect multiple targets, making it useful for monitoring specific co-infections (Corman et al., 2020).

6.4. Comparison with Other Isothermal Methods

RT-LAMP is another isothermal amplification method that can be used for detecting RNA viruses. Like RT-RPA, it provides a rapid amplification rate of viral RNA at lower temperatures (65°C) than RT-PCT. RT-LAMP is highly sensitive and capable of producing a good amplification yield – about 10^9-10^{10} copies within an hour (Notomi et al., 2000). However, its high sensitivity makes it very likely to be affected by contamination, leading to false positives (Nagamine et al., 2002). Aerosol contamination is one of the key limitations of RT-LAMP, which can be avoided by several control measures, such as using biosafety cabinets, HEPA filters, and closed-tube reaction systems (Tomita et al., 2008).

In this study, the diagnostic performance of RT-RPA was also compared to that of RT- LAMP as a well-established isothermal amplification method in detecting a range of viruses. Although RT-LAMP typically does not outperform RT-PCR regarding sensitivity and specificity, it is still valuable for field diagnostics or emergency outbreaks due to its speed and simplicity. Based on the findings of this study, fluorescence-based RT-RPA showed 100% sensitivity and 92% specificity

compared to RT-PCR. Meanwhile, RT-LAMP demonstrated a lower sensitivity of 71% and specificity of 87%, indicating that RT-RPA performs better than RT-LAMP as an isothermal diagnostic method. Therefore, RT-RPA can provide higher diagnostic accuracy for detecting viral infections at POCs. The lower sensitivity of RT-LAMP is likely to cause false negatives, where the assay fails to identify positive samples accurately. While the specificity of RT-LAMP is decent and may suffice for some applications, its vulnerability to false negatives and contamination challenges makes RT-LAMP less feasible for precise diagnostic testing in low-resource settings.

6.5. Primer Design and Gene Targeting for Viral Detection

Primer design is a critical step in molecular diagnostic methods, which provides target-specific amplification to allow accurate and reliable pathogen detection. In RT-RPA, even slight variations in primer sequences or concentrations can significantly affect the amplification efficiency, possibly causing false positives or primer-dimers (Daher et al., 2016). When designing primers, it is crucial to target conserved genes within the viral genome, such as those encoding structural or enzymatic proteins, to promote target-specific amplification of the pathogen, increasing the sensitivity of detection (Ali et al., 2020). In contrast, targeting genetically diverse genes within the viral genome can be used to distinguish between viral subtypes, which is useful for epidemiological disease monitoring and outbreak control but with reduced sensitivity of detection (Zhang et al., 2020).

Mismatches are better tolerated by RT-RPA, especially outside the 3' end of the primer, due to the strand-displacing polymerase of RPA, which is not dependent on temperature-driven primer annealing. Therefore, RT-RPA can be used to efficiently amplify polymorphic or variable target regions (Lobato and O'Sullivan, 2018). Both RT- PCR and RT-LAMP are more sensitive to mismatches; RT-PCR uses *Taq* polymerase, which has a lower mismatch tolerance, and RT-LAMP relies on multiple primers and loop structures. The loop structures play a significant role in the

exponential amplification mechanism; even minor mismatches can disrupt the strand displacement process to stop DNA polymerase from extending the primer (Tomita et al., 2008; Mori and Notomi, 2009). Mismatches at the 3' end are detrimental for all; however, RT-PCR and RT-LAMP are more affected by these mismatches than RT-RPA. Therefore, RT-RPA is better suited for variable regions but may exhibit lower specificity due to non-specific amplification. In contrast, RT-PCR and RT-LAMP work better with conserved targets to maintain high specificity even though they struggle with genetic variability (Daher et al., 2016). Using degenerate primers can be useful as they can detect viral strains with an unknown sequence by incorporating variations at specific positions to account for codon variability (Malhotra et al., 2017). Unfortunately, these primers may cause non- specific amplification, producing false positive results. Therefore, optimisation of primer design, reaction conditions such as primer concentration, and using advanced design software (e.g. Primer3, OligoAnalyser, NUPACK) are critical to eliminate these challenges (Arvidsson et al., 2008; Guo et al., 2020). Using large genomic databases (e.g. GISAID and GenBank) allows access to real-time sequence information so the primers can be designed to account for emerging viral mutations (Reich, 2023).

6.6. Advantages of RT-RPA for POCT

Choosing isothermal diagnostic assays like RT-RPA over traditional RT-PCR for POCT is essential to improve global testing capacity for detecting a wide range of respiratory viruses like SARS-CoV-2, Influenza, and RSV, particularly in low- and middle-income countries. The isothermal nature of this assay allows the amplification to occur at a constant temperature of 37-42°C, eliminating the use of expensive thermocyclers (Crannell et al., 2016). Since it does not require thermal cycling like RT-PCR, RT-RPA has a lower risk of contamination through aerosolised samples, which may cause false positives in PCR-based systems (Wu et al., 2024). While this does not entirely eliminate the risk of contamination, fewer processing steps in RT-RPA automatically reduce the chances of cross-contamination (Crannell et al., 2016). Additionally, RT-RPA offers rapid turnaround time, meaning the whole amplification process can be completed in as

little as 20 min, providing a significant advantage during pandemic outbreaks where early diagnosis and treatment are critical to reduce morbidity (Chow et al., 2020).

Combining RT-RPA with lateral flow devices can also facilitate accessibility and ease of use, so there is no need to rely on expensive fluorescence-based detection to produce reliable results. LFD test strips can provide results only within minutes after the amplification. Therefore, they can promote simplicity, accessibility, and quick decision-making in low-resource settings (Lau et al., 2020). Both RT-RPA and lateral flow assays are portable, adaptable, and cost-effective, so they are excellent candidates for POCT, particularly during disease outbreaks where early clinical management and disease control are required (Wozniak et al., 2020).

6.7. Limitations of RT-RPA and Potential for Improvement

Even though RT-RPA is a solid alternative to RT-PCR for POCT in low-resource settings, there are some limitations associated with this assay. One of the main concerns includes the risk of false positives and non-specific amplification, which can cause inaccurate clinical management and disease control (Kokkinos et al., 2019). A false positive result for RSV-B was recorded in this study, emphasising the need for optimisation in primer design and recombinase fidelity to improve specificity before broader clinical adoption. Another issue of RT-RPA is the limited multiplexing capacity due to primer interference and the lack of existing protocols for RPA multiplexing (Li et al., 2019). Primer interference occurs when multiple primer sets from a reaction compete for binding to each other or the target sequence, possibly leading to reduced amplification efficiency, cross-reactivity, and non-specific amplification (Joung et al., 2020). The temperature sensitivity of RT-RPA is another potential issue. Temperature control is limited in low-resource settings, affecting reagent stability and reaction conditions like enzyme activities and primer annealing (Crannell et al., 2016; Lau et al., 2021). Although RT-RPA provides a rapid amplification rate, there is an increased risk of contamination, particularly when the laboratories process multiple samples simultaneously (James et al., 2015). Pre- and post-amplification workspaces can be used to avoid contamination and cross-reactivity.

Finally, scalability and reagent stability are still ongoing concerns for RT-RPA. The enzymes and primers used in RT-RPA reactions are prone to degradation, particularly at high temperatures. Reagents also require storage at -20°C or 4°C to retain stability, which may not be feasible in low-resource settings due to unreliable electricity (Piepenburg et al., 2006). Lyophilisation is a process that involves freeze-drying reagents into a stable powder form so they can be rehydrated with water or buffer before use. There are lyophilised RT-RPA kits that are easier to transport and store, making them well-suited for POCT (Piepenburg et al., 2006). Chemical stabilisers, such as trehalose or glycerol, can be incorporated during the production of RT-RPA reagents to enhance their stability by protecting enzymes, primers, and probes from degradation caused by suboptimal conditions. Systems like the Cepheid GeneXpert or BioFire FilmArray are self-contained cartridges that include all reagents within a closed system to reduce the risk of contamination (Sanchez et al., 2021). These single-use and disposable cartridges contain all necessary reagents for sample preparation, nucleic acid extraction, amplification, and detection. They also provide high sensitivity and specificity, similar to the gold standard (Sanchez et al., 2021). Therefore, they are excellent candidates for quick, accurate, and reliable POCT in low-resource settings.

6.8. Conclusion

In conclusion, RT-RPA is a promising alternative for POCT as it provides rapid, cost-effective, and highly sensitive disease diagnosis. Additionally, RT-RPA offers faster turnaround times and reduced equipment requirements, making it well-suited for low-resource settings. Overall, RT-RPA showed a similar diagnostic performance to RT-PCR, the current gold standard, for detecting a range of respiratory viruses, including SARS-CoV-2, influenza, and RSV. Fluorescence and LFD-based detection methods were combined with RT-RPA. They were both compared to the gold standard regarding sensitivity and specificity. Fluorescence-based RT-RPA exhibited 100% sensitivity and 92% specificity, with a similar diagnostic accuracy to RT-PCR. Meanwhile, LFD-based RT-RPA showed reduced sensitivity at 84% and slightly higher specificity at 97%, making it a viable alternative in settings without access to real-time fluorescence

detection. On the other hand, the diagnostic performance of RT-RPA was also compared to that of RT-LAMP, which is another isothermal amplification method that can be performed at a constant temperature of 65°C. Comparing RT-RPA to both RT-PCR and RT-LAMP provides a more comprehensive analysis of its benefits and limitations regarding sensitivity, specificity, and suitability for different settings. RT-LAMP demonstrated lower sensitivity at 71% and specificity at 87% compared to both RT-RPA and RT-PCR, meaning it does not perform to the level of the gold standard.

Additionally, TOPO TA cloning was used in this study to confirm the presence and correct size of the amplified product, ensuring accuracy and reliability. In vitro transcription was also utilised to produce synthetic RNA templates, validating the sensitivity and specificity of RT-RPA across a range of respiratory viruses. These procedures emphasised the robustness and effectiveness of RT-RPA in detecting conserved regions of the viral genomes for precise pathogen detection.

While RT-RPA offers many advantages for POCT, it has several limitations that must be addressed, particularly associated with limited multiplexing capacity, specificity, and sensitivity against temperature fluctuations. Optimising primer design, taking contamination control measures, and using high-fidelity enzymes are some approaches that can significantly improve the diagnostic performance of RT-RPA. Conserved regions of the viral genome are used as gene targets for the specific detection of the desired pathogen. Targeting genetically variable regions within the genome prone to mutations can help differentiate between viral subtypes. Integration of RT-RPA with lateral flow assays, which can be used for immediate diagnosis, can improve the practicality of RT-RPA in POCs. With continued refinements, RT-RPA remains a significant alternative to the gold standard, which is a rapid, accessible, and cost-effective molecular diagnostic tool providing precise detection for respiratory viruses and beyond.

Chapter 7: Future Directions

The diagnostic performance of RT-RPA can be improved by specific strategies, particularly focusing on major limitations like specificity and the risk of false positives. Primer design optimisation is one of the critical elements of developing a diagnostic assay. Advanced computational tools like artificial intelligence (AI) can be used to predict primer performance (e.g. primer-dimers, secondary structures, amplification efficiency) based on thermodynamic models (Allawi and Pabbaraju, 2021; Jaroslaw Krzywanski et al., 2024). These tools can cover massive genomic datasets, such as GISAID and GenBank, to design primers adaptable to emerging mutations in viral genomes (Lenharo, 2023). Using high-fidelity enzymes in RPA reactions can also help to reduce primer-dimer formation via their proofreading exonuclease activity to remove mismatched nucleotides (Tolar et al., 2019). However, high-fidelity enzymes specific to RPA are not commercially available yet. Therefore, high-fidelity enzymes from different methods, such as Phi29 polymerase from RCA and *Bst* polymerase from LAMP, can be used as an inspiration to develop more accurate enzymes for RT-RPA (Kunkel, 2018). On the other hand, existing RPA enzymes can be modified to include proofreading activity. Another alternative is using hot-start versions of RPA enzymes, which can improve assay specificity and reduce the risk of getting false positives. These enzymes remain inactive at lower temperatures and only become active at optimal reaction temperatures, reducing the likelihood of non-specific amplification (Huang and Liu, 2021). This approach is particularly beneficial in low-resource settings to improve the precision of RT-RPA, where temperature control is difficult. Degenerate primers were used in this study, which can be further refined to expand their utility for detecting genetically diverse viral subtypes while eliminating concerns of non-specific amplification. This can be achieved by incorporating computational models to refine the degeneracy while maintaining sensitivity and specificity (Chukwuemeka et al., 2020). Using locked nucleic acids and peptide nucleic acids can improve primer binding specificity. These synthetic analogues of DNA and RNA are designed to enhance thermal stability and specific primer binding, significantly increasing the sensitivity and specificity of the assay (Levin et al., 2006; Briones and Moreno, 2012).

The limited multiplexing capacity of RT-RPA must be addressed as it is significant for the simultaneous detection of multiple pathogens from a single patient sample. Orthogonal primer sets allow simultaneous detection of multiple targets. These primer sets do not interact with each other to ensure that each primer pair amplifies only its specific target (Limberis and Metcalfe, 2023). They are also designed to avoid primer-dimers and secondary structures to prevent non-specific amplification. These can be coupled with corresponding sequence-specific probes, which can be labelled with fluorescent dyes for the real-time detection of the target sequence (Limberis and Metcalfe, 2023). Additionally, due to lack of clinical samples, RT-RPA for HRV-B, HRV-C, AdV, and HBoV were not validated, which warrant future consideration.

In addition to taking all these measures to avoid risk factors, specific post-amplification approaches can be applied to analyse the amplification product further. Combining RT-RPA with a lateral flow assay can visually confirm the amplification product on a test strip. This approach is simple, quick, and portable, so it is well-suited for field detection (Kolm et al., 2019). High-throughput sequencing technologies, such as next-generation sequencing, can also be used to confirm the identity of the amplification product. However, this method requires nucleic acid purification before sequencing to eliminate excess primers, enzymes, and by-products of the RT-RPA (Jeong et al., 2021). Magnetic bead-based extraction, spin columns, crude extraction, and Chelex resin are purification methods that can be easily integrated into diagnostic workflows (Mardiana, 2022).

TOPO TA cloning is a quick molecular process that can be completed in around 5 min at room temperature, confirming the identity of the amplified product (Wang et al., 2023). It works by facilitating the insertion of RPA-amplified products into a plasmid vector without using any restriction enzymes or ligases. The viral gene sequence can be further characterised once the product is cloned into a vector. TOPO TA cloning can be very useful in viral diagnostics, as it allows the study of viral variants and emerging strains by isolating and cloning the viral gene fragments from clinical samples. This is particularly important when studying mutations in viral genomes that may affect diagnostic accuracy. Integrating CRISPR/Cas technology with RT-RPA is an innovative way of optimising sensitivity, specificity, and amplification efficiency (Zeng et al., 2024). gRNAs specific to the target sequence are designed and combined

with RPA primers in a reaction containing the Cas enzyme. The gRNAs direct the Cas enzyme to the target sequence for precise cutting (Zeng et al., 2024). All these efforts will improve the diagnostic performance of RT-RPA even further regarding sensitivity, specificity, and overall accuracy. These will solidify the robustness and adaptability of RPA-based assays, making them more viable for POCT and global surveillance of viral pathogens.

Chapter 8: Bibliography

Abd El Wahed, A., Patel, P., Faye, O., Thaloengsok, S., Heidenreich, D., Matangkasombut, P., ... & Weidmann, M. (2013). Recombinase polymerase amplification assay for rapid diagnostics of Ebola virus infection. *PLoS Currents*, 5.

Abd El Wahed, A., Weidmann, M., Hufert, F.T. Diagnostics-in-a-Suitcase: development of a portable and rapid assay for the detection of the emerging avian Influenza A (H7N9) virus. *J. Clin. Virol.* 2015; 69:16–21.

Adams, P.F., Hendershot, G.E., Marano, M.A. Centers for Disease Control and Prevention/National Center for Health Statistics. Current estimates from the National Health Interview Survey, 1996. Vital Health Stat 10. 1999 Oct;(200):1-203.

Adlhoch, C., Mook, P., Lamb, F., Ferland, L., Melidou, A., Amato-Gauci, A.J., Pebody, R. (2021). Very little Influenza in the WHO European Region during the 2020/21 season, weeks 40 2020 to 8 2021. *Eurosurveillance*, 26(11).

Aebischer, A., Wernike, K., Hoffmann, B., & Beer, M. (2014). Rapid genome detection of Schmallenberg virus and bovine viral diarrhea virus by use of isothermal amplification methods and high-speed real-time reverse transcriptase PCR. *Journal of Clinical Microbiology*, 52(6), 1883–1892.

Aghapour, M., Raee, P., Moghaddam, S.J., Hiemstra, P.S., Heijink, I.H. (2018). Airway Epithelial Barrier Dysfunction in Chronic Obstructive Pulmonary Disease: Role of Cigarette Smoke Exposure. *American Journal of Respiratory Cell and Molecular Biology*, 58(2), pp.157–169.

Ahn, S. J., et al. Rapid and simple colorimetric detection of multiple Influenza viruses infecting humans using a reverse transcriptional loop-mediated isothermal amplification (RT-LAMP) diagnostic platform. *BMC Infect. Dis.* 19, 1–12 (2019).

Albrecht, J.C., Kotani, A., Lin, J.S., Soper, S.A., Barron, A.E. (2013). Simultaneous Detection of 19 K-ras Mutations by Free-Solution Conjugate Electrophoresis of Ligase Detection Reaction Products on Glass Microchips. *Electrophoresis* 34, 590–597.

Alfano, C., Fichou, Y., Huber, K., Weiss, M., Spruijt, E., Ebbinghaus, S., De Luca, G., Morando, M.A., Vetri, V., Temussi, P.A., Pastore, A. (2024). Molecular Crowding: The History and Development of a Scientific Paradigm. *Chemical Reviews*, [online] 124(6), pp.3186–3219.

Alhajj, M., Farhana, A., Zubair, M. (2023). *Enzyme Linked Immunosorbent Assay (ELISA)*. [online] PubMed.

Al-Hajjar, S. (2012). Laboratory Diagnosis of Viral Disease. *Textbook of Clinical Pediatrics*, [online] pp.923–928.

Ali, Z., Aman, R., Mahas, A., Rao, G.S., Tehseen, M., Marsic, T., ... & Mahfouz, M.M. (2020). iSCAN: An RT-LAMP-coupled CRISPR-Cas12 module for rapid, sensitive detection of SARS-CoV-2. *Virus Research*, 288, 198129.

Allander, T., Tammi, M.T., Eriksson, M., Bjerkner, A., Tiveljung-Lindell, A., Andersson, B. (2005). Cloning of a human parvovirus by molecular screening of respiratory tract samples. *Proceedings of the National Academy of Sciences of the United States of America*, [online] 102(36), pp.12891–12896.

Allawi, H.T. and Pabbaraju, K. (2021). *Evaluation of DNA primer design using the nearest-neighbour thermodynamic model and molecular dynamics simulations. BMC Bioinformatics*, 22(1), 1-14.

Allie, S. Rameeza and Randall, Troy D. (2017). Pulmonary immunity to viruses. *Clinical Science*, 131(14), pp.1737–1762.

Almeida, S. M., et al. (2022). Co-infection with respiratory viruses: a common feature in COVID-19 patients. *Frontiers in Public Health*, 10, 899492.

Alpert, B., Jameson, D.M., Weber, G. Tryptophan Emission From Human Hemoglobin and Its Isolated Subunits. *Photochem Photobiol.* 1980; 31:1–4.

Alrashedi, H., Al-Ataie, S., Banoon, S., Fayed, M. (2021). Potential Role of Medicinal Plants for the Treatment of Respiratory Viruses: A Review. *Egyptian Journal of Chemistry*.

Amann, R.I., Ludwig, W., Schleifer, K.H. (1995). Phylogenetic identification and in situ detection of individual microbial cells without cultivation. *Microbiological Reviews*, 59(1), pp.143–169.

Anderson, T.C., Crawford, P.C., Katz, J.M., Dubovi, E.J., Landolt, G., Gibbs, E.P. (2012) Diagnostic performance of the canine Influenza A virus subtype H3N8 hemagglutination inhibition assay. *J Vet Diagn Investig* 24(3):499–508.

Aninagyei, E., Ayivor-Djanie, R., Gyamfi, J., Owuani, T., Selassie Louis Ameke, Kpeli, G.S., Agbogli, H.K., Essandoh, P. and Kwabena Obeng Duedu (2024). Faecal shedding of SARS-CoV-2 from patients with asymptomatic and mild COVID-19 without gastrointestinal symptoms in Ghana. *BMC Research Notes*, 17(1).

Arabi, Y.M., Arifi, A.A., Balkhy, H.H., Najm, H., Aldawood, A.S., Ghabashi, A., Hawa, H., Alothman, A., Khaldi, A., Al Raiy, B. (2014). Clinical Course and Outcomes of Critically Ill Patients With Middle East Respiratory Syndrome Coronavirus Infection. *Annals of Internal Medicine*, 160(6), pp.389–397.

Arakawa, T. and Timasheff, S.N. (1982). Preferential interactions of proteins with salts in concentrated solutions. *Biochemistry*, 21(25), pp.6545–6552.

Arevalo-Rodriguez, I., Steingart, K.R., Tricco, A.C., Nussbaumer-Streit, B., Kaunelis, D., Alonso-Coello, P., Baxter, S., Bossuyt, P.M., Emparanza, J.I. and Zamora, J. (2020). Current methods for development of rapid reviews about diagnostic tests: an international survey. *BMC Medical Research Methodology*, 20(1).

Arnheim, N. and Erlich, H. Polymerase chain reaction strategy. *Annu Rev Biochem.* 1992; 61:131–156.

Arruda, E., Pitkäranta, A., Witek, T.J., Doyle, C.A., Hayden, F.G. (1997). Frequency and natural history of rhinovirus infections in adults during autumn. *Journal of Clinical Microbiology*, 35(11), pp.2864–2868.

Arvidsson, S., Kwasniewski, M., Riaño-Pachón, D.M., Mueller-Roeber, B. (2008). QuantPrime – a flexible tool for reliable high-throughput primer design for quantitative PCR. *BMC Bioinformatics*, 9(1).

Asaga, S., Kuo, C., Nguyen, T., Terpenning, M., Giuliano, A.E., Hoon, D.S.B. Direct serum assay for microRNA-21 concentrations in early and advanced breast cancer. *Clin. Chem.,* 57 (2011), pp. 84 91.

Aydin, S. A short history, principles, and types of ELISA, and our laboratory experience with peptide/protein analyses using ELISA. Peptides. 2015 Oct; 72:4-15.

Bai, Y., Ji, J., Ji, F., Wu, S., Tian, Y., Jin, B., Li, Z. (2022). Recombinase polymerase amplification integrated with microfluidics for nucleic acid testing at point of care. *Talanta*, 240, pp.123209–123209.

Bain, W., Yang, H., Shah, F.A., Suber, T., Drohan, C., Al-Yousif, N., et al. COVID- 19 versus non–COVID-19 acute respiratory distress syndrome: comparison of demographics, physiologic parameters, inflammatory biomarkers, and clinical outcomes. *Ann Am Thoracic Soc.* 2021;18(7):1202.

Baker, A.T., Greenshields-Watson, A., Coughlan, L., Davies, J.A., Uusi-Kerttula, H., Cole, D.K., Rizkallah, P.J., Parker, A.L. (2019) 'Diversity within the adenovirus fiber knob hypervariable loops influences primary receptor interactions', *Nature Communications*, 10, 741.

Baotai, G. and Bi, Y. (2002). Cloning PCR Products: An Overview. *Humana Press eBooks*, pp.111–119.

Bardi, T., Pintado, V., Gomez-Rojo, M., Escudero-Sanchez, R., Azzam Lopez, A., Diez-Remesal, Y., Martinez Castro, N., Ruiz-Garbajosa, P., Pestaña, D. (2021). Nosocomial infections associated to COVID-19 in the intensive care unit: clinical characteristics and outcome. *European Journal of Clinical Microbiology & Infectious Diseases.*

Barnes, P.J. (2007). Chronic Obstructive Pulmonary Disease: A Growing but Neglected Global Epidemic. *PLoS Medicine*, [online] 4(5), p.e112.

Baron, S. (1996). *Medical Microbiology*. 4th ed. [online] *PubMed*. Galveston (TX): University of Texas Medical Branch at Galveston.

Baschong, W., Suetterlin, R., Laeng, R.H. Control of Autofluorescence of Archival Formaldehyde— fixed, Paraffin— embedded Tissue in Confocal Laser Scanning Microscopy (CLSM) *Jounal Histochem Cytochem.* 2001; 49:1565–1572.

Bastien, N., Brandt, K., Dust, K., Ward, D., Li, Y. (2006). Human Bocavirus Infection, Canada. *Emerging Infectious Diseases*, 12(5), pp.848–850.

Bastien, N., Liu, L., Ward, D., Taylor, T., Li, Y. (2004). Genetic Variability of the G Glycoprotein Gene of Human Metapneumovirus. *Journal of Clinical Microbiology*, [online] 42(8), pp.3532–3537.

Bastos, M.L., Perlman-Arrow, S., Menzies, D. and Campbell, J.R. (2021). The Sensitivity and Costs of Testing for SARS-CoV-2 Infection With Saliva Versus Nasopharyngeal Swabs. *Annals of Internal Medicine*.

Battifora, H. (1991). Specificity of immunohistochemical expression of P- glycoprotein. *Human Pathology*, 22(5), p.506.

Battisti, A.S., Modi, P., Pangia, J. (2024). *Sinusitis*. [online] PubMed.

Bebenek, A. and Ziuzia-Graczyk, I. (2018) 'Fidelity of DNA replication—a matter of proofreading', *Current Genetics*, 64(5), pp. 985-996.

Bell, D.M. and World Health Organization Working Group on Prevention of International and Community Transmission of SARS. (2004). Public health interventions and SARS spread, 2003. *Emerging Infectious Diseases*, 10(11), pp.1900- 1906.

Bellassai, N., D'Agata, R. and Spoto, G. (2025). Advancements in the integration of isothermal nucleic acid amplification methods for point-of-care testing in resource-limited settings. *Sensors and Actuators Reports*, [online] 9, p.100285.

Bernal, A., Gomes da Silva, M.M., Musungaie, D.B., et al. Molnupiravir for Oral Treatment of Covid-19 in Nonhospitalized Patients. *N Engl J Med*. 2022;386(6):509- 520.

Bilitewski, U. DNA microarrays: an introduction to the technology. *Methods Mol Biol*. 2009; 509:1–14.

Bill, R.M. Recombinant protein subunit vaccine synthesis in microbes: a role for yeast? *J. Pharm. Pharmacol.* 2015; 67:319–328.

Bizzintino, J., Lee, W.M., Laing, I.A., Vang, F., Pappas, T., Zhang, G., Martin, A.C., Khoo, S.K., Cox, D.W., Geelhoed, G.C., McMinn, P.C., Goldblatt, J., Gern, J.E., Le

Souef, P.N. (2010). Association between human rhinovirus C and severity of acute asthma in children. *European Respiratory Journal*, [online] 37(5), pp.1037–1042.

Björnson, C.L. and Johnson, D.W. Croup. *Lancet.* 2008; 371:329–339.

Blancett, C.D., Fetterer, D.P., Koistinen, K.A., Morazzani, E.M., Monninger, M.K., Piper, A.E., Kuehl, K.A., Kearney, B.J., Norris, S.L., Rossi, C.A., Glass, P.J., Sun, M.G. (2017). Accurate virus quantitation using a Scanning Transmission Electron Microscopy (STEM) detector in a scanning electron microscope. *Journal of Virological Methods*, 248, pp.136–144.

Blažková, M., Koets, M., Rauch, P., Amerongen, A. Development of a nucleic acid lateral flow immunoassay for simultaneous detection of Listeria spp. and Listeria monocytogenes in food. *Eur. Food Res. Technol*. 2009, 229, 867–874.

Bodewes, R., Morick, D., de Mutsert, G., Osinga, N., Bestebroer, T., van der Vliet, S., Smits, S.L., Kuiken, T., Rimmelzwaan, G.F., Fouchier, R.A.M., Osterhaus, A.D.M.E. (2013). Recurring Influenza B Virus Infections in Seals. *Emerging Infectious Diseases*, 19(3), pp.511–512.

Bonsor, D.A., Butz, S.F., Solomons, J., Grant, S., Fairlamb, I.J.S., Fogg, M.J. (2006). Ligation independent cloning (LIC) as a rapid route to families of recombinant biocatalysts from sequenced prokaryotic genomes. *Organic & Biomolecular Chemistry*, 4(7), 1258-1260.

Bourgeois, M.A. and Oaks, J.L. (2014). *Chapter 12 - Laboratory Diagnosis of Viral Infections*. [online] ScienceDirect.

Boyle, D.S., Lehman, D.A., Lillis, L. Rapid detection of HIV-1 proviral DNA for early infant diagnosis using recombinase Polym.polymerase amplification. 2013; 4:1–8.

Boyle, D.S., McNerney, R., Teng Low, H., Leader, B.T., Pérez-Osorio, A.C., Meyer, J.C., O'Sullivan, D.M., Brooks, D.G., Pai, N.P., Gerlach, J. (2014). Rapid detection of Mycobacterium tuberculosis by recombinase polymerase amplification. *PLoS ONE*, 9(8), e103091.

Bradley, D.E. (1967). Ultrastructure of bacteriophage and bacteriocins. *Bacteriological Reviews*, 31(4), pp.230–314.

Brendish, N.J., Malachira, A.K., Armstrong, L., Houghton, R., Aitken, S., Nyimbili, E., Ewings, S., Lillie, P.J., Clark, T.W. (2017). Routine molecular point-of-care testing for respiratory viruses in adults presenting to hospital with acute respiratory illness (ResPOC): a pragmatic, open-label, randomised controlled trial. *The Lancet Respiratory Medicine*, [online] 5(5), pp.401–411.

Brenner, S. and Horne, R.W. (1959). A negative staining method for high resolution electron microscopy of viruses. *Biochimica et Biophysica Acta*, 34, pp.103–110.

Briones, C. and Moreno, M. (2012). Applications of peptide nucleic acids (PNAs) and locked nucleic acids (LNAs) in biosensor development. *Analytical and Bioanalytical Chemistry*, 402(10), pp. 3071–3089.

Brown, T. (2001). Southern Blotting. Current Protocols in Immunology, 6(1).

Brownie, J., Shawcross, S., Theaker, J., Whitcombe, D., Ferrie, R., Newton, C., Little, S. The elimination of primer-dimer accumulation in PCR. Nucleic Acids Res. 1997 Aug 15;25(16):3235-41.

Bru, D., Martin-Laurent, F., Philippot, L. Quantification of the detrimental effect of a single primer-template mismatch by real-time PCR using the 16S rRNA gene as an example. *Appl Environ Microbiol.* 2008; 74:1660–1663.

Brümmer, L.E., Katzenschlager, S., McGrath, S., Schmitz, S., Gaeddert, M., Erdmann, C., Bota, M., Grilli, M., Larmann, J., Weigand, M.A., Pollock, N.R., Macé, A., Erkosar, B., Carmona, S., Sacks, J.A., Ongarello, S. and Denkinger, C.M. (2022). Accuracy of rapid point-of-care antigen-based diagnostics for SARS-CoV-2: An updated systematic review and meta-analysis with meta-regression analyzing influencing factors. *PLOS Medicine*, 19(5), p.e1004011.

Bryksin, A.V. and Matsumura, I. (2010). Overlap extension PCR cloning: A simple and reliable way to create recombinant plasmids. *BioTechniques*, 48(6), 463-465.

Buchan, B.W. and Ledeboer, N.A. Emerging technologies for the clinical microbiology laboratory. *Clin Microbiol Rev* 2014; 27: 783–822.

Bukrinskaya, A.G., Vorkunova, N.K., Kornilayeva, G.V., Narmanbetova, R.A., Vorkunova, G.K. Influenza virus uncoating in infected cells and effect of rimantadine. *J Gen Virol* 1982; 60:49-59.

Bullard, D.R. and Bowater, R.P. (2006). Direct Comparison of Nick-Joining Activity of the Nucleic Acid Ligases From Bacteriophage T4. *Biochem. J.* 398, 135–144.

Bullard, J., Dust, K., Funk, D., Strong, J.E., Alexander, D., Garnett, L., Boodman, C., Bello, A., Hedley, A., Schiffman, Z., Doan, K., Bastien, N., Li, Y., Van Caeseele, P.G. and Poliquin, G. (2020). Predicting infectious SARS-CoV-2 from diagnostic samples. *Clinical Infectious Diseases*.

Burke, C.W., Bridges, O., Brown, S., Rahija, R., Russell, C.J. (2013). Mode of Parainfluenza Virus Transmission Determines the Dynamics of Primary Infection and Protection from Reinfection. PLoS Pathogens, [online] 9(11), p.e1003786.

Bush, R.M. Influenza as a model system for studying the cross-species transfer and evolution of the SARS coronavirus. In: McLean AR, May RM, Pattison J, Weiss RA, editors. *SARS: A case study in emerging infections.* Oxford: Oxford University Press; 2005. pp. 24–30.

Bustin, S.A., Benes, V., Garson, J.A., Hellemans, J., Huggett, J., Kubista, M., et al. (2009). The MIQE guidelines: minimum information for publication of quantitative real-time PCR experiments. *Clin. Chem*. 55, 611–622.

Campe, H., Hartberger, C., Sing, A. (2008). Role of Human Bocavirus infections in outbreaks of gastroenteritis. *Journal of Clinical Virology*, 43(3), pp.340–342.

Canetti, M., Barda, N., Gilboa, M., Indenbaum, V., Asraf, K., Gonen, T., Weiss-Ottolenghi, Y., Amit, S., Doolman, R., Mendelson, E., et al. Six-Month Follow-up after a Fourth BNT162b2 Vaccine Dose. *N. Engl. J. Med.* 2022, *387*, 2092–2094.

Cao, Z., et al. Visual detection of West Nile virus using reverse transcription loop- mediated isothermal amplification combined with a vertical flow visualization strip. *Front. Microbiol*. 7, 1 9 (2016).

Carter, L. J. et al. (2020). Assay techniques and test development for COVID-19 diagnosis. *ACS Central Science*, 6(5), 591–605.

Cassedy, A., Parle-McDermott, A., O'Kennedy, R. Virus Detection: A Review of the Current and Emerging Molecular and Immunological Methods. *Front Mol Biosci.* 2021; 8:637559.

Cassidy, H., van Genne, M.K., Lizarazo, E., Hubert and Gard, L. (2022). Evaluation of the QIAstat-Dx RP2.0 and the BioFire FilmArray RP2.1 for the Rapid Detection of Respiratory Pathogens Including SARS-CoV-2. 13.

Cassini, A., Colzani, E., Pini, A., Mangen, M.J.J., Plass, D., McDonald, S.A., Maringhini, G., van Lier, A., Haagsma, J.A., Havelaar, A.H., Kramarz, P., Kretzschmar, M.E. (2018). Impact of infectious diseases on population health using incidence-based disability-adjusted life years (DALYs): results from the Burden of Communicable Diseases in Europe study, European Union and European Economic Area countries, 2009 to 2013. *Eurosurveillance*, [online] 23(16).

Ceccaldi, R., Rondinelli, B., D'Andrea, A.D. Repair pathway choices and consequences at the double-strand break. *Trends Cell Biol.* 2016; 26:52–64.

Centers for Disease Control and Prevention (CDC). (2024). Overview of Influenza Testing Methods. Available at: https://www.cdc.gov/flu/hcp/testing-methods/index.html.

Cevik, M., Tate, M., Lloyd, O., Maraolo, A.E., Schafers, J. and Ho, A. (2020). SARS-CoV-2, SARS-CoV, and MERS-CoV viral load dynamics, duration of viral shedding, and infectiousness: a systematic review and meta-analysis. *The Lancet Microbe*, 2(1).

Cha, R.S. and Thilly, W.G. Specificity, efficiency, and fidelity of PCR. *PCR Methods Appl.* 1992; 3:18–29.

Chalkias, S., Harper, C., Vrbicky, K., Walsh, S.R., Essink, B., Brosz, A., McGhee, N., Tomassini, J.E., Chen, X., Chang, Y., et al. A Bivalent Omicron-Containing Booster Vaccine against COVID-19. *N. Engl. J. Med.* 2022, *387*, 1279–1291.

Chan, J.F.-W., Yip, C.C.-Y., To, K.K.-W., Tang, T.H.-C., Wong, S.C.-Y., Leung, K.-H., Fung, A.Y.-F., Ng, A.C.-K., Zou, Z., Tsoi, H.-W., Choi, G.K.-Y., Tam, A.R., Cheng, V.C.-C., Chan, K.-H., Tsang, O.T.-Y. and Yuen, K.-Y. (2020). Improved Molecular Diagnosis of COVID-19 by the Novel, Highly Sensitive and Specific COVID-19-RdRp/Hel Real-Time

Reverse Transcription-PCR Assay Validated In Vitro and with Clinical Specimens. *Journal of Clinical Microbiology*, 58(5).

Chandu, D., Paul, S., Parker, M., Dudin, Y., King-Sitzes, J., Perez, T., Mittanck, D.W., Shah, M., Glenn, K.C., Piepenburg, O. Development of a rapid point-of-use DNA test for the screening of Genuity® roundup ready 2 Yield® soybean in seed samples. *Biomed. Res. Int.* 2016:3145921.

Chavda, V.P., Bezbaruah, R., Valu, D., Patel, B., Kumar, A., Prasad, S., Kakoti, B.B., Kaushik, A., Jesawadawala, M. (2023). Adenoviral Vector-Based Vaccine Platform for COVID-19: Current Status. *Vaccines*, 11(2), p.432.

Chen, H., Choi, J., Bailey, S. Cut site selection by the two nuclease domains of the Cas9 RNA-guided endonuclease. *J Biol Chem.* 2014; 289:13284–13294.

Chen, J.S., Ma, E., Harrington, L.B., Da Costa, M., Tian, X., Palefsky, J.M., Doudna, J.A. (2018). CRISPR-Cas12a target binding unleashes indiscriminate single- stranded DNase activity. *Science*, 360(6387), pp.436–439.

Cherian, T., Simoes, E.A.F., Steinhoff, M.C., et al. Bronchiolitis in Tropical South India. *Am J Dis Child.* 1990;144(9):1026–1030.

Cherry, J.D. Clinical practice: croup. *N Engl J Med.* 2008; 358:384–391.

Chertow, D.S. (2018). Next-generation diagnostics with CRISPR. *Science*, 360(6387), 381-382.

Cheung, K.S., Hung, I.FN., Chan, P.PY., Lung, K.C., Tso, E., Liu, R., Ng, Y.Y., Chu, M.Y., Chung, T.WH., Tam, A.R., Yip, C.CY., Leung, K.-H., Yim-Fong Fung, A., Zhang, R.R., Lin, Y., Cheng, H.M., Zhang, A.JX., To, K.KW., Chan, Kwok-H. and Yuen, Kwok-Y. (2020). Gastrointestinal Manifestations of SARS-CoV-2 Infection and Virus Load in Fecal Samples from the Hong Kong Cohort and Systematic Review and Meta-analysis. *Gastroenterology*, [online] 159(1).

Choi, G., Jung, J.H., Park, B.H., Oh, S.J., Seo, J.H., Choi, J.S., Kim, D.H., Seo, T.S. (2016). A centrifugal direct recombinase polymerase amplification (direct-RPA) microdevice for multiplex and real-time identification of food poisoning bacteria. *Lab on a Chip*, 16(12), pp.2309–2316.

Chonmaitree, T., Revai, K., Grady, J.J., Clos, A., Patel, J.A., Nair, S., et al. Viral upper respiratory tract infection and otitis media complication in young children. *Clin Infect Dis.* 2008;46(6):815–23.

Chothia, C. and Lesk, A.M. (1986). The relation between the divergence of sequence and structure in proteins. *The EMBO Journal*, 5(4), pp.823–826.

Chow, B.D.W. and Esper, F.P. (2009). The Human Bocaviruses: A Review and Discussion of Their Role in Infection. *Clinics in Laboratory Medicine*, 29(4), pp.695– 713.

Chow, W.H.A., McCloskey, C., Tong, Y., Hu, L., You, Q., Kelly-Cirino, C., Lee, H.H. (2020). Lateral flow assays (LFAs) combined with isothermal amplification methods for rapid infectious disease diagnostics. *Critical Reviews in Microbiology*, 46(4), 349-370.

Christopherson, C., Sninsky, J.J., Kwok, S. The effects of internal primer template mismatches on RT-PCR: hIV-1 model studies. *Nucleic Acids Res.* 1997; 25:654–658.

Chukwuemeka, P.O., Umar, H.I., Olukunle, O.F., Oretade, O.M., Olowosoke, C.B., Akinsola, E.O., Elabiyi, M.O., Kurmi, U.G., Eigbe, J.O., Oyelere, B.R., Isunu, L.E., Oretade, O.J. (2020). In silico design and validation of a highly degenerate primer pair: a systematic approach. *Journal of Genetic Engineering and Biotechnology*, 18(1).

Clancy, B. and Cauller, L.J. Reduction of background autofluorescence in brain sections following immersion in sodium borohydride. *J Neurosci Methods.* 1998; 83:97–102.

Clayman, G.L., Adams, G.L., Paugh, D.R., Koopmann, C.F. Jr. Intracranial complications of paranasal sinusitis: a combined institutional review. *Laryngoscope* 2021;101234- 239.

Clem, A.S. (January 2011). "Fundamentals of vaccine immunology". *Journal of Global Infectious Diseases*. 3 (1): 73–78.

Clements, M.L. and Murphy, B.R. Development and persistence of local and systemic antibody responses in adults given live attenuated or inactivated Influenza A virus vaccine. *J Clin Microbiol*. 1986; 23:66-72.

Cohen, A. and Biddle, F. (1963) Hemagglutination inhibition: interaction of Influenza viruses with horse serum inhibitor. *Nature* 198:508–509.

Collins, P.L. and Graham, B.S. (2008). Viral and Host Factors in Human Respiratory Syncytial Virus Pathogenesis. *Journal of Virology*, [online] 82(5), pp.2040–2055.

Cooper, G.M. (2016). *DNA Replication*. [online] Nih.gov.

Corman, V. M., Landt, O., Kaiser, M., Molenkamp, R., Meijer, A., Chu, D. K. W., Bleicker, T., Brünink, S., Schneider, J., Schmidt, M. L., Mulders, D. G. J. C., Haagmans, B. L., van der Veer, B., van den Brink, S., Wijsman, L., Goderski, G., Romette, J. L., Ellis, J., Zambon, M., … Drosten, C. (2020). Detection of 2019 novel coronavirus (2019-nCoV) by real-time RT-PCR. *Eurosurveillance*, 25(3), 2000045.

Cox, M.M., Patriarca, P.A., Treanor, J. FluBlok, a recombinant hemagglutinin Influenza vaccine. *Influenza Other Respir. Viruses.* 2008; 2:211–219.

Coyle, K.M. and Kelly, T.H. (2020). *Viral co-infections in patients with respiratory illnesses: Implications for clinical management. Clinical Infectious Diseases*, 71(1), 73- 81.

Crannell, Z. A., Cabada, M. M., Castellanos-Gonzalez, A., & Richards-Kortum, R. (2016). Recombinase polymerase amplification-based assay to diagnose cutaneous leishmaniasis. *Journal of Clinical Microbiology*, 54(12), 3002–3008.

Crannell, Z. A., Rohrman, B., & Richards-Kortum, R. (2014). Equipment-free incubation of recombinase polymerase amplification reactions using body heat. *PLoS One*, 9(11), e112146.

Crannell, Z., Castellanos-Gonzalez, A., Nair, G., Mejia, R., White, A.C., Richards-Kortum, R. Multiplexed Recombinase Polymerase Amplification Assay To Detect Intestinal Protozoa. *Anal. Chem.* 2016, 88, 1610.

Crawford-Miksza, L. and Schnurr, D.P. 1996. Analysis of 15 adenovirus hexon proteins reveals the location and structure of seven hypervariable regions containing serotype-specific residues. *J. Virol.* 70:1836-1844.

Cui, J., Li, F., Shi, Z.L. (2018). Origin and evolution of pathogenic coronaviruses. *Nature Reviews Microbiology*, [online] 17(3), pp.181–192.

Currier, A.W., Jeshurin, M.C., Sampson, V.B. (2021). SARS-CoV-2 Targets and COVID-19 Vaccines. *COVID* 1 608–621.

Daher, R. K., Stewart, G., Boissinot, M., & Bergeron, M. G. (2016). Recombinase Polymerase Amplification for Diagnostic Applications. *Clinical Chemistry*, 62(7), 947–958.

Daher, R.K., Stewart, G., Boissinot, M., Bergeron, M.G. Recombinase polymerase amplification for diagnostic applications. *Clin. Chem.* 2016; 62:947–958.

Darwish, I.A. (2006). Immunoassay Methods and their Applications in Pharmaceutical Analysis: Basic Methodology and Recent Advances. *International journal of biomedical science: IJBS*, [online] 2(3), pp.217–35.

Dasaraju, P.V. and Liu, C. (2014). *Infections of the Respiratory System*. [online] Nih.gov.

De La Escosura-Muñiz, A., Baptista-Pires, L., Serrano, L., Altet, L., Francino, O., Sánchez, A., Merkoçi, A. Magnetic bead/gold nanoparticle double-labeled primers for electrochemical detection of isothermal amplified Leishmania DNA. *Small.* 2016; 12:205–213.

Deng, S., Liang, H., Chen, P., Li, Y., Li, Z., Fan, S., Wu, K., Li, X., Chen, W., Qin, Y., Yi, L., Chen, J. (2022). Viral Vector Vaccine Development and Application during the COVID-19 Pandemic. *Microorganisms*, 10(7), p.1450.

Deveau, H., Garneau, J.E., Moineau, S. CRISPR/Cas system and its role in phage-bacteria interactions. *Annu Rev Microbiol.* 2010; 64:475–493.

Dien Bard, J. and McElvania, E. (2020). Panels and Syndromic Testing in Clinical Microbiology. *Clinics in Laboratory Medicine*, 40(4), pp.393–420.

Dinnes, J., Sharma, P., Berhane, S., van Wyk, S.S., Nyaaba, N., Domen, J., Taylor, M., Cunningham, J., Davenport, C., Dittrich, S., Emperador, D., Hooft, L., Leeflang, M.M., McInnes, M.D., Spijker, R., Verbakel, J.Y., Takwoingi, Y., Taylor-Phillips, S., Van den Bruel, A. and Deeks, J.J. (2022). Rapid, point-of-care antigen tests for diagnosis of SARS-CoV-2 infection. *Cochrane Database of Systematic Reviews*, 2022(7).

Dobrowolski, S.F., Teng, D.H.F... & Ririe, K.M. (2011). FilmArray, an Automated Nested Multiplex PCR System for Multi-Pathogen Detection: Development and Application to Respiratory Tract Infection. *PLoS ONE*, [online] 6(10), p.e26047.

Domnich, A., Orsi, A., Trombetta, C.S., Costa, E., Giulia Guarona, Lucente, M., Ricucci, V., Bruzzone, B. and Giancarlo Icardi (2022). Comparative Diagnostic Accuracy of the STANDARD M10 Assay for the Molecular Diagnosis of SARS-CoV-2 in the Point-of-Care and Critical Care Settings. 11(9), pp.2465–2465.

Dong, Y., Dai, T., Wei, Y., Zhang, L., Zheng, M., Zhou, F.A. (2020). Systematic review of SARS-CoV-2 vaccine candidates. *Signal Transduct. Target. Ther.* 5:237.

Dukes, J.P., King, D.P., Alexandersen, S. Novel reverse transcription loop-mediated isothermal amplification for rapid detection of foot-and-mouth disease virus. *Arch Virol.* 2006; 151:1093 106.

Dumkow, L.E., Worden, L.J., Rao, S.N. (2021). Syndromic diagnostic testing: a new way to approach patient care in the treatment of infectious diseases. *Journal of Antimicrobial Chemotherapy*, 76(Supplement_3), pp. iii4–iii11.

E. Avaniss-Aghajani, Sarkissian, A., Fernando, F. and A. Avaniss-Aghajani (2020). Validation of the Hologic Aptima Unisex and Multitest Specimen Collection Kits Used for Endocervical and Male Urethral Swab Specimens (Aptima Swabs) for Collection of Samples from SARS-CoV-2-Infected Patients. *Journal of Clinical Microbiology*, [online] 58(8).

Echaide, M., Labiano, I., Delgado, M., Fernandez de Lascoiti, A., Ochoa, P., Garnica, M., Ramos, P., Chocarro, L., Fernandez, L., Arasanz, H., et al. Immune Profiling Uncovers Memory T-Cell Responses with a Th17 Signature in Cancer Patients with Previous SARS-CoV-2 Infection Followed by mRNA Vaccination. *Cancers* 2022, *14*, 4464.

Edoardo Ongaro, A., Ndlovu, Z., Sollier, E., Otieno, C., Ondoa, P., Street, A. and Kersaudy-Kerhoas, M. (2022). Engineering a sustainable future for point-of-care diagnostics and single-use microfluidic devices. *Lab on a Chip*, [online] 22(17), pp.3122–3137.

Egerton, R.F. (2016). *Physical Principles of Electron Microscopy: An Introduction to TEM, SEM, and AEM*. 2nd ed. Springer. ISBN: 9783319398774.

Egwuagu, C.E. STAT3 in CD4+ T helper cell differentiation and inflammatory diseases. *Cytokine* 2009, *47*, 149–156.

Ehrhardt, D., et al. (2003) *GFP technology for Live Cell Imaging*, *Current Opinion in Plant Biology*.

Eid, C. and Santiago, J.G. Assay for Listeria monocytogenes cells in whole blood using Isotachophoresis and recombinase polymerase amplification. *Analyst.* 2017; 142:48–54.

ElHefnawi, M., AlAidi, O., Mohamed, N., Kamar, M., El-Azab, I., Zada, S., Siam, R. (2011). Identification of novel conserved functional motifs across most Influenza A viral strains. *Virology Journal*, 8(1).

Engvall, E. (1980). [28] Enzyme immunoassay ELISA and EMIT. In Methods in enzymology (Vol. 70, pp. 419-439). *Academic Press.*

Engvall, E. The ELISA, enzyme-linked immunosorbent assay. *Clin Chem.* 2010 Feb;56(2):319-20.

Erard, V., Huang, M., Ferrenberg, J., Nguy, L., Stevens, T.L., Hackman, R.C., Corey, L., Boeckh, M. (2007). Quantitative Real-Time Polymerase Chain Reaction for Detection of Adenovirus after T Cell–Replete Hematopoietic Cell Transplantation: Viral Load as a Marker for Invasive Disease. *Clinical Infectious Diseases*, 45(8), pp.958–965.

Erben, T., Ossig, R., Naim, H.Y., Schnekenburger, J. What to do with high autofluorescence background in pancreatic tissues – an efficient Sudan black B quenching method for specific immunofluorescence labelling. *Histopathology.* 2016; 69:406–422.

Euler, M., Wang, Y., Heidenreich, D., Patel, P., Strohmeier, O., Hakenberg, S., Niedrig, M. (2012). Recombinase polymerase amplification assay for rapid detection of Rift Valley fever virus. *Journal of Clinical Virology*, 54(4), 308-312.

Euler, M., Wang, Y., Nentwich, O., Piepenburg, O., Hufert, F.T., Weidmann, M. Recombinase polymerase amplification assay for rapid detection of Rift Valley fever virus. *J Clin Virol.* 2012; 54:308–312.

Falsey, A. (2012). Current management of parainfluenza pneumonitis in immunocompromised patients: a review. *Infection and Drug Resistance*, p.121.

Farquharson, M., Harvie, R., McNicol, A.M. (1990) Detection of messenger RNA using a digoxigenin end-labeled oligonucleotide probe. *J Clin Pathol* 43:423–428.

Fehr, A.R. **and Perlman, S.** (2015). Coronaviruses: An Overview of Their Replication and Pathogenesis. *Coronaviruses*, [online] 1282, pp.1–23.

Ferrero, F., Ossorio, M.F., Rial, M.J. (2022). The return of RSV during the COVID- 19 pandemic. *Pediatric Pulmonology*, 57(3), pp.770–771.

Fiore, A.E., et al. Antiviral agents for the treatment and chemoprophylaxis of Influenza—recommendations of the Advisory Committee on Immunization Practices (ACIP) *MMWR Recomm Rep.* 2011;60(1):1–24.

Fishbane, S., Hirsch, J.S., Nair, V. Special Considerations for Paxlovid Treatment Among Transplant Recipients With SARS-CoV-2 Infection. Am J Kidney Dis. 2022 Apr;79(4):480-482.

Focosi, D. (2022). Molnupiravir: From Hope to Epic Fail? *Viruses*, 14(11), p.2560.

Freshney, R.I. (2000). Introduction to basic principles. *Animal cell culture: a practical approach*, (232), 1.

Freshney, R.I. (2016). *Culture of Animal Cells: A Manual of Basic Technique and Specialized Applications*. 7th ed. Wiley-Blackwell.

Frickmann, H., Jungblut, S., Hirche, T.O., Groß, U., Kuhns, M., Zautner, A.E. (2012). The influence of virus infections on the course of COPD. *European Journal of Microbiology & Immunology*, [online] 2(3), pp.176–185.

Frost, H.M., McLean, H.Q., Chow, B.D.W. (2018). Variability in Antibiotic Prescribing for Upper Respiratory Illnesses by Provider Specialty. *The Journal of Pediatrics*, [online] 203, pp.76-85. e8.

Fry, A.M., Lu, X., Chittaganpitch, M., Peret, T., Fischer, J., Dowell, Scott F., Anderson, Larry J., Erdman, D., Olsen, Sonja J. (2007). Human Bocavirus: A Novel Parvovirus Epidemiologically Associated with Pneumonia Requiring Hospitalization in Thailand. *The Journal of Infectious Diseases*, 195(7), pp.1038–1045.

Gao, H., Yao, H., Yang, S., Li, L. From SARS to MERS: evidence and speculation. *Frontiers in Medicine.* 2016; 10:377–382.

Garnett, L., Bello, A., Tran, K.N., Audet, J., Leung, A., Schiffman, Z., Griffin, B.D., Tailor, N., Kobasa, D. and Strong, J.E. (2020). Comparison analysis of different swabs and transport mediums suitable for SARS-CoV-2 testing following shortages. *Journal of Virological Methods*, 285, p.113947.

Gaucherand, P., Massardier, J., Polazzi, S., Duclos, A. (2021). Low levels of respiratory syncytial virus activity in Europe during the 2020/21 season: what can we expect in the coming summer and autumn/winter? *Eurosurveillance*, [online] 26(29).

Geu-Flores, F., Nour-Eldin, H.H., Nielsen, M.T., Halkier, B.A. (2007). USER fusion: a rapid and efficient method for simultaneous fusion and cloning of multiple PCR products. *Nucleic Acids Research*, [online] 35(7), p.e55.

Ghannam, M.G. and Varacallo, M. (2018). *Biochemistry, Polymerase Chain Reaction (PCR)*. [online] Nih.gov.

Ghelichkhani, P. and Esmaeili, M. Prone position in management of COVID-19 patients; a commentary. *Arc Acad Emerg Med.* 2020;8(1).

Golemba, M.D., Moragas, M., Fernández, M.F., Borgnia, D., Ruhle, M., Palladino, M., Arias, A.P., Ruvinsky, S., Bologna, R. and Mangano, A. (2023). Comparison of SARS-CoV-2 viral load in asymptomatic and symptomatic children attended in a referral public pediatric hospital in Argentina. *Revista Argentina de Microbiología*, [online] 55(2), pp.143–149.

Gootenberg, J.S., Abudayyeh, O.O., Kellner, M.J., Joung, J., Collins, J.J., Zhang, F. (2018). Multiplexed and portable nucleic acid detection platform with Cas13, Cas12a, and Csm6. *Science (New York, N.Y.)*, [online] 360(6387), pp.439–444.

Gootenberg, J.S., Abudayyeh, O.O., Lee, J.W., Essletzbichler, P., Dy, A.J., Joung, J., Verdine, V., Donghia, N., Daringer, N.M., Freije, C.A., Myhrvold, C., Bhattacharyya, R.P., Livny, J., Regev, A., Koonin, E.V., Hung, D.T., Sabeti, P.C., Collins, J.J., Zhang, F. (2017). Nucleic acid detection with CRISPR-Cas13a/C2c2. *Science*, [online] 356(6336), pp.438–442.

Gosselin, D., Gougis, M., Baque, M., Navarro, F.P., Belgacem, M.N., Chaussy, D., Bourdat, A.G., Mailley, P., Berthier, J. Screen-printed polyaniline-based electrodes for the

real-time monitoring of loop-mediated isothermal amplification reactions. *Anal. Chem.,* 89 (2017), pp. 10124-10128.

Graf, E.H. and Pancholi, P. Appropriate use and future directions of molecular diagnostic testing. *Curr Infect Dis Rep* 2020; 22: 5.

Gray, G.C. and Erdman, D.D. (2018). Adenovirus Vaccines. *Plotkin's Vaccines*, [online] pp.121-133.e8.

Grayson, S.A., Griffiths, P.S., Perez, M.K., Piedimonte, G. (2016). Detection of airborne respiratory syncytial virus in a pediatric acute care clinic. *Pediatric Pulmonology*, 52(5), pp.684–688.

Greenfeld, K.T. *China syndrome: the true story of the 21st century's first great epidemic.* London, UK: Penguin Books; 2006.

Grohskopf, L.A., Sokolow, L.Z., Broder, K.R., Walter, E.B., Fry, A.M., Jernigan, D.B. Prevention and Control of Seasonal Influenza with Vaccines: Recommendations of the Advisory Committee on Immunization Practices-United States, 2018–2019 Influenza Season. *MMWR Recomm Rep.* 2018; 67:1–20.

Guido, M., Quattrocchi, M., Campa, A., Zizza, A., Grima, P., Romano, A., De Donno, A. (2011). Human metapneumovirus and human bocavirus associated with respiratory infection in Apulian population. *Virology*, 417(1), pp.64–70.

Guido, M., Tumolo, M.R., Verri, T., Romano, A., Serio, F., De Giorgi, M., Donno, A.D., Bagordo, F., Zizza, A. (2016). Human bocavirus: Current knowledge and future challenges. *World Journal of Gastroenterology*, [online] 22(39), p.8684.

Gunatilaka, A.B., Marco, N., Read, G.H., Sweeney, M., Regan, G., Tsang, C., Abdulrahman, L., Ampabathina, S., Spindler, A., Lu, S.S., Schink, E., Gatti, R., Ingersoll, C., Telesca, D. and Weidhaas, J.B. (2022). Viral burden and clearance in asymptomatic COVID-19 Patients. *Open Forum Infectious Diseases*.

Guo, J., Starr, D., Guo, H. (2020). Classification and review of free PCR primer design software. *Bioinformatics*, 36(22-23).

Gutierrez, A.F. and El Sahly, H. Recombinant hemagglutinin protein vaccine: A new option in immunization against Influenza. *Future Virol.* 2015; 10:1057–1067.

Haas, L.E.M., Thijsen, S.F.T., van Elden, L., Heemstra, K.A. (2013). Human Metapneumovirus in Adults. *Viruses*, [online] 5(1), pp.87–110.

Hall, C.B. and Hall, W.J. Chapter 352: croup (acute laryngotracheobronchitis) In: McInerny TK, Adam HM, Campbell DE, DeWitt TG, Foy JM, Kamat DM, editors. *American academy of pediatrics textbook of pediatric care.* 2. Elk Grove Village, IL: American Academy of Pediatrics; 2017.

Hamilton, D.F., Ghert, M., Simpson, A.H.R.W. (2015). Interpreting regression models in clinical outcome studies. *Bone & Joint Research*, [online] 4(9), pp.152–153.

Hammond, J., Leister-Tebbe, H., Gardner, A., et al. Oral Nirmatrelvir for High-Risk, Nonhospitalized Adults with Covid-19. *N Engl J Med*. 2022;386(15):1397-1408.

Hardinge, P. and Murray, J.A.H. (2019). Reduced False Positives and Improved Reporting of Loop-Mediated Isothermal Amplification using Quenched Fluorescent Primers. *Scientific Reports*, [online] 9(1), pp.1–13.

Harlow, E. **and Lane, D.** (1999) *Using Antibodies: A Laboratory Manual*. Cold Spring Harbor, New York.

Harris, J.R. (2007). Negative staining of thinly spread biological samples. *Methods in Molecular Biology (Clifton, N.J.)*, [online] 369, pp.107–142.

Hartley, J.L. (2000). DNA Cloning Using In Vitro Site-Specific Recombination. *Genome Research*, 10(11), pp.1788–1795.

Hay, A.J., Wolstenholme, A.J., Skehel, J.J., Smith, M.H. The molecular basis of the specific anti-Influenza action of amantadine. *EMBO J* 1985; 4:3021-4.

He, S.L. and Green, R. (2013). Northern blotting. Methods in enzymology, 530, 75-87.

He, X., Lau, E.H.Y., Wu, P., Deng, X., Wang, J., Hao, X., Lau, Y.C., Wong, J.Y., Guan, Y., Tan, X., Mo, X., Chen, Y., Liao, B., Chen, W., Hu, F., Zhang, Q., Zhong, M., Wu, Y., Zhao, L. and Zhang, F. (2020). Temporal dynamics in viral shedding and transmissibility of COVID-19. *Nature Medicine*, [online] 26.

Hendley, J.O. and Gwaltney, J.M. (1988). Mechanisms of transmission of rhinovirus infections. *Epidemiologic Reviews*, [online] 10, pp.243–258.

Henry, B.M. and Lippi, G. Poor survival with extracorporeal membrane oxygenation in acute respiratory distress syndrome (ARDS) due to coronavirus disease 2019 (COVID-19): pooled analysis of early reports. *J Crit Care.* 2020; 58:27.

Heymann, P.W., Carper, H.T., Murphy, D.D., Platts-Mills, T.A.E., Patrie, J., McLaughlin, A.P., Erwin, E.A., Shaker, M.S., Hellems, M., Peerzada, J., Hayden, F.G., Hatley, T.K., Chamberlain, R. (2004). Viral infections in relation to age, atopy, and season of admission among children hospitalized for wheezing. *The Journal of Allergy and Clinical Immunology*, [online] 114(2), pp.239–247.

Hill-Cawthorne, G.A., Hudson, L.O., El Ghany, M.F.A., Piepenburg, O., Nair, M., Dodgson, A., Forrest, M.S., Clark, T.G., Pain, A. Recombinations in staphylococcal cassette chromosome mec elements compromise the molecular detection of methicillin resistance in Staphylococcus aureus. *PLoS One.* 2014;9: e101419.

Hirsch, R.E., Zukin, R.S., Nagel, R.L. Intrinsic Fluorescence Emission of Intact Oxy Hemoglobins. *Biochem Biophys Res Commun.* 1980; 93:432–439.

Hoft, D.F., Lottenbach, K.R., Blazevic, A., Turan, A., Blevins, T.P., Pacatte, T.P., Yu, Y., Mitchell, M.C., Hoft, S.G., Belshe, R.B. Comparisons of the Humoral and Cellular Immune Responses Induced by Live Attenuated Influenza Vaccine and Inactivated Influenza Vaccine in Adults. *Clin. Vaccine Immunol.* 2017;24: e00414-16.

Hogg, J. Peripheral lung remodelling in asthma and chronic obstructive pulmonary disease. *Eur Respir J* 2004; 24:893–894.

Holtzman, M.J., Byers, D.E., Benoit, L.A., Battaile, J.T., You, Y., Agapov, E., Park, C., Grayson, M.H., Kim, E.Y., Patel, A.C. (2009). Chapter 5 Immune Pathways for Translating Viral Infection into Chronic Airway Disease. *Advances in immunology*, [online] pp.245–276.

Hooman Hanifehpour, Ashrafi, F., Elham Siasi and Fallahi, S. (2024). Evaluation and comparison of one-step real-time PCR and one-step RT-LAMP methods for detection of SARS-CoV-2. *BMC infectious diseases*, 24(1).

Horvath, P. and Barrangou, R. CRISPR/Cas, the immune system of bacteria and archaea. *Science.* 2010; 327:167–170.

Hou, H., Wang, T., Zhang, B., Luo, Y., Mao, L., Wang, F., Wu, S., Sun, Z. (2020). Detection of IgM and IgG antibodies in patients with coronavirus disease 2019. *Clinical & Translational Immunology*, [online] 9(5).

Housley, D.J., Zalewski, Z.A., Beckett, S.E., Venta, P.J. (2006). Design factors that influence PCR amplification success of cross-species primers among 1147 mammalian primer pairs. *BMC Genomics*, 7(1).

Hsiung, G.D. (1984). Diagnostic virology: from animals to automation. *The Yale Journal of Biology and Medicine*, [online] 57(5), pp.727–733.

Hu, S., Li, M., Zhong, L., Lu, S., Liu, Z., Pu, J., Wen, J., Huang, X. (2015). Development of reverse-transcription loop-mediated isothermal amplification assay for rapid detection and differentiation of dengue virus serotypes 1–4. *BMC Microbiology,* 15(1).

Huang, M., Arnheim, N., Goodman, M.F. Extension of base mispairs by Taq DNA polymerase: implications for single nucleotide discrimination in PCR. *Nucleic Acids Res.* 1992; 20:4567–4573.

Huang, Q., Deng, X., Yan, Z., Cheng, F., Luo, Y., Shen, W., Lei-Butters, D.C.M., Chen, A.Y., Li, Y., Tang, L., Söderlund-Venermo, M., Engelhardt, J.F., Qiu, J. (2012). Establishment of a Reverse Genetics System for Studying Human Bocavirus in Human Airway Epithelia. *PLoS Pathogens*, 8(8), p.e1002899.

Huang, Y. and Liu, Y. (2021). *Hot-start polymerases for enhancing specificity in isothermal amplification. Biotechnology Advances*, 48, 107724.

Huang, Z.B., Xu, Y., Li, L.S., Li, Y.P., Zhang, H., He, Q.H. Development of an immunochromatographic strip test for the rapid simultaneous detection of deoxynivalenol and zearalenone in wheat and maize. *Food Control* 2012, 28, 7–12.

Hui, D.S.C and Zumla, A. Severe acute respiratory syndrome: historical, epidemiologic, and clinical features. *Infect Dis Clin North Am*. 2019; 33(4):869-889.

Hussein, H.A.M., Thabet, A.A., Wardany, A.A., El-Adly, A.M., Ali, M., Hassan, M.E.A., Abdeldayem, M.A.B., Mohamed, A.R.M.A., Sobhy, A., El-Mokhtar, M.A., Afifi, M.M., Fathy, S.M., Sultan, S. (2024). SARS-CoV-2 outbreak: role of viral proteins and genomic diversity in virus infection and COVID-19 progression. *Virology Journal*, 21, Article 75.

Hwang, Y., Lee, S., Lee, J., Kim, H., Park, S. (2021). Development of a lateral flow immunoassay for rapid detection of SARS-CoV-2 antigens and antibodies. *Journal of Clinical Virology*, 137, pp.104760.

Im, K., Mareninov, S., Diaz, M.F.P., Yong, W.H. (2019). An introduction to Performing Immunofluorescence Staining. *Methods in molecular biology (Clifton, N.J.)*, 1897(2), pp.299–311.

Iserte, J.A., Stephan, B.I., Goñi, S.E., Borio, C.S., Ghiringhelli, P.D., Lozano, M.E. (2013). Family-Specific Degenerate Primer Design: A Tool to Design Consensus Degenerated Oligonucleotides. *Biotechnology Research International*, [online] 2013, pp.1–9.

Ison, M.G. (2006). Emerging Infections: Adenovirus Infections in Transplant Recipients. *Clinical Infectious Diseases*, 43(3), pp.331–339.

Ison, M.G., Sharma, A., Shepard, J.A.O., Wain, J.C., Ginns, L.C. (2008). Outcome of Influenza infection managed with oseltamivir in lung transplant recipients. *The Journal of Heart and Lung Transplantation: The Official Publication of the International Society for Heart Transplantation*, [online] 27(3), pp.282–288.

Iwane, M.K., Prill, M.M., Lu, X., Miller, E.K., Edwards, K.M., Hall, C.B., Griffin, M.R., Staat, M.A., Anderson, L.J., Williams, J.V., Weinberg, G.A., Ali, A., Szilagyi, P.G., Zhu, Y., Erdman, D.D. (2011). Human Rhinovirus Species Associated with Hospitalizations for Acute Respiratory Illness in Young US Children. *The Journal of Infectious Diseases*, 204(11), pp.1702–1710.

Jain, S., Self, W.H., Wunderink, R.G., Fakhran, S., Balk, R., Bramley, A.M., Reed, C., Grijalva, C.G., Anderson, E.J., Courtney, D.M., Chappell, J.D., Qi, C., Hart, E.M., Carroll, F., Trabue, C., Donnelly, H.K., Williams, D.J., Zhu, Y., Arnold, S.R., Ampofo,

K. (2015). Community-Acquired Pneumonia Requiring Hospitalization among U.S. Adults. *New England Journal of Medicine*, [online] 373(5), pp.415–427.

James, A. and Macdonald, J. Recombinase polymerase amplification: emergence as a critical molecular technology for rapid, low-resource diagnostics. *Expert. Rev. Mol. Diagn.* 2015, 15, 1475–1489.

Jaroenram, W. and Owens, L. Recombinase polymerase amplification combined with a lateral flow dipstick for discriminating between infectious Penaeus stylirostris densovirus and virus-related sequences in shrimp genome. *J Virol Methods.* 2014; 208:144–151.

Jaroslaw Krzywanski, Sosnowski, M., Grabowska, K., Zylka, A., Lasek, L., Agnieszka Kijo-Kleczkowska (2024). Advanced Computational Methods for Modeling, Prediction and Optimization—A Review. *Materials*, 17(14), pp.3521–3521.

Jarrett, J., Uhteg, K., Forman, M., Hanlon, A., Vargas, C., Carroll, K.C., Valsamakis, A., Mostafa, H.H. (2021). Clinical performance of the GenMark Dx ePlex respiratory pathogen panels for upper and lower respiratory tract infections. 135, pp.104737–104737.

Jartti, T., Hedman, K., Jartti, L., Ruuskanen, O., Allander, T., Söderlund-Venermo, M. (2011). Human bocavirus-the first 5 years. *Reviews in Medical Virology*, 22(1), pp.46–64.

Jauset-Rubio, M., Markéta Svobodová, Mairal, T., McNeil, C., Keegan, N., M.S. El-Shahawi, Bashammakh, A.S., Al-Youbi, A.O., O'Sullivan, C.K. (2016). Aptamer Lateral Flow Assays for Ultrasensitive Detection of β-Conglutin Combining Recombinase Polymerase Amplification and Tailed Primers. *Analytical Chemistry*, 88(21), pp.10701–10709.

Jauset-Rubio, M., Sabaté Del Rio, J., Mairal, T., Svobodová, M., El-Shahawi, M.S., Bashammakh, A.S., Alyoubi, A.O., O'Sullivan, C.K. Ultrasensitive and rapid detection of β-conglutin combining aptamers and isothermal recombinase polymerase amplification. *Anal. Bioanal. Chem.* 2017; 409:143–149.

Jefferson, T., Del Mar, C., Dooley, L., Ferroni, E., Al-Ansary, L., Bawazeer, G. A., … & Rivetti, A. (2011). Physical interventions to interrupt or reduce the spread of respiratory viruses: systematic review. *BMJ*, 339, b3675.

Jeong, H., Kim, J., Lee, K. (2021). *Rapid and sensitive detection of SARS-CoV-2 using a nucleic acid-based isothermal amplification method. Diagnostics*, 11(9), 1643.

Ji, W., Wang, Y., Chen, Z. Human metapneumovirus in children with acute respiratory tract infections in Suzhou, China 2005-2006. *Scand J Infect Dis.* 2009; 41:735–744.

Jiang, F. and Doudna, J.A. CRISPR-Cas9 structures and mechanisms. *Annu Rev Biophys.* 2017; 46:505–529.

Jinek, M., Chylinski, K., Fonfara, I., Hauer, M., Doudna, J.A. A programmable dual-RNA-guided DNA endonuclease in adaptive bacterial immunity. *Science.* 2012; 337:816–821.

Johnson, S.J. and Beese, L.S. Structures of mismatch replication errors observed in a DNA polymerase. *Cell.* 2004; 116:803–816.

Jordan, W.S. Jr. and Oseasohn, R.O. (1954) The use of RDE to improve the sensitivity of the hemagglutination-inhibition test for the serologic diagnosis of Influenza. *J Immunol* 72(3):229–235.

Joshi, S. and Yu, D. (2017). Immunofluorescence. *Basic Science Methods for Clinical Researchers*, pp.135–150.

Joung, J., Ladha, A., Saito, M., Kim, N. G., Woolley, A. E., Segel, M., ... & Zhang, F. (2020). Detection of SARS-CoV-2 with SHERLOCK One-Pot Testing. *New England Journal of Medicine*, 383(15), 1492-1494.

Kaliyappan, K., Palanisamy, M., Govindarajan, R., Duraiyan, J. (2012). Microarray and its applications. *Journal of Pharmacy and Bioallied Sciences*, [online] 4(6), p.310.

Kalsi, S., Valiadi, M., Tsaloglou, M.N., Parry-Jones, L., Jacobs, A., Watson, R., Turner, C., Amos, R., Hadwen, B., Buse, J., Brown, C., Sutton, M., Morgan, H. Rapid and sensitive detection of antibiotic resistance on a programmable digital microfluidic platform. *Lab. Chip.* 2015; 15:3065–3075.

Kapoor, A., Mehta, N., Esper, F., Poljsak-Prijatelj, M., Quan, P.L., Qaisar, N., Delwart, E., Lipkin, W.I. (2010). Identification and Characterization of a New Bocavirus Species in Gorillas. *PLoS ONE*, 5(7), p.e11948.

Karch, C.P. and Burkhard, P. (November 2016). "Vaccine technologies: From whole organisms to rationally designed protein assemblies". *Biochemical Pharmacology*. 120: 1–14.

Kearney, B.J. and Stoecker, C. (2020). *Challenges in Point-of-Care Testing in Low-Resource Settings: A Review of RT-PCR Limitations and Solutions. Diagnostics*, 10(11), 829.

Kersting, S., Rausch, V., Bier, F.F., von Nickisch-Rosenegk, M. Multiplex isothermal solid-phase recombinase polymerase amplification for the specific and fast DNA-based detection of three bacterial pathogens. *Microchim. Acta.* 2014; 181:1715–1723.

Kesebir, D., Vazquez, M., Weibel, C., Shapiro, E.D., Ferguson, D., Landry, M.L., Kahn, J.S. (2006). Human Bocavirus Infection in Young Children in the United States: Molecular Epidemiological Profile and Clinical Characteristics of a Newly Emerging Respiratory Virus. *The Journal of Infectious Diseases*, 194(9), pp.1276–1282.

Khan, M.U., Farman, A., Rehman, A.U., Israr, N., Ali, M.Z.H., Gulshan, Z.A. "Automated System Design for Classification of Chronic Lung Viruses using Non- Linear Dynamic System Features and K-Nearest Neighbour," *2021 Mohammad Ali Jinnah University International Conference on Computing (MAJICC)*, Karachi, Pakistan, 2021, pp. 1-8.

Kim J.Y. and Lee J.L. Development of a multiplex real-time recombinase polymerase amplification (RPA) assay for rapid quantitative detection of Campylobacter coli and jejuni from eggs and chicken products. *Food Control.* 2016; 73:1247–1255.

Kim, J., Biondi, M.J., Feld, J.J., Chan, W.C.W. Clinical validation of quantum dot barcode diagnostic technology. *ACS Nano.* 2016; 10:4742–4753.

Kim, J.Y., Ko, J.-H., Kim, Y., Kim, Y.-J., Kim, J.-M., Chung, Y.-S., Kim, H.M., Han, M.-G., Kim, S.Y. and Chin, B.S. (2020). Viral Load Kinetics of SARS-CoV-2 Infection in First Two Patients in Korea. *Journal of Korean Medical Science*, 35(7).

Kim, V. and Criner, G.J. (2013). Chronic Bronchitis and Chronic Obstructive Pulmonary Disease. *American Journal of Respiratory and Critical Care Medicine*, [online] 187(3), pp.228–237.

Kinloch, N.N., Ritchie, G., Brumme, C.J., Dong, W., Dong, W., Lawson, T., Jones, R.B., Montaner, J.S.G., Leung, V., Romney, M.G., Stefanovic, A., Matic, N., Lowe, C.F. and Brumme, Z.L. (2020). Suboptimal Biological Sampling as a Probable Cause of False-Negative COVID-19 Diagnostic Test Results. *The Journal of Infectious Diseases*, [online] 222(6), pp.899–902.

Kipkorir, V., Cheruiyot, I., Ngure, B., Misiani, M. and Munguti, J. (2020). Prolonged SARS-Cov-2 RNA Detection in Anal/Rectal Swabs and Stool Specimens in COVID-19 Patients After Negative Conversion in Nasopharyngeal RT-PCR Test. *Journal of Medical Virology*.

Kivekäs, I. and Rautiainen, M. (2018). Epiglottitis, Acute Laryngitis, and Croup. *Infections of the Ears, Nose, Throat, and Sinuses*, pp.247–255.

Klein, D., Leutenegger, C.M., Bahula, C., Gold, P., Hofmann-Lehmann, R., Salmons, B., Lutz, H., Gunzburg, W.H. Influence of preassay and sequence variations on viral load determination by a multiplex real-time reverse transcriptase-polymerase chain reaction for feline immunodeficiency virus. *J Acquir Immune Defic Syndr.* 2001; 26:8–20.

Klock, H.E. and Lesley, S.A. (2009). The Polymerase Incomplete Primer Extension (PIPE) Method Applied to High-Throughput Cloning and Site-Directed Mutagenesis. *Methods in Molecular Biology*, pp.91–103.

Klungthong, C., Chinnawirotpisan, P., Chitpayamongkol, W., et al. (2010). "The impact of primer-template mismatches on the sensitivity of Influenza A/H1N1/2009 detection." *Journal of Virological Methods*, 163(1), 1-7.

Kociolek, L.K., Muller, W.J., Yee, R., Bard, J.D., Brown, C.A., Revell, P.A., Wardell, H., Savage, T.J., Jung, S., Dominguez, S., Parikh, B.A., Jerris, R.C., Kehl, S.C., Campigotto, A., Bender, J.M., Zheng, X., Muscat, E., Linam, M., Abuogi, L. and Smith, C. (2020). Comparison of Upper Respiratory Viral Load Distributions in Asymptomatic and Symptomatic Children Diagnosed with SARS-CoV-2 Infection in Pediatric Hospital Testing Programs. *Journal of Clinical Microbiology*, [online] 59(1).

Kohl, T.O. and Ascoli, C.A. Direct Competitive Enzyme-Linked Immunosorbent Assay (ELISA). Cold Spring Harb Protoc. 2017 Jul 05;2017(7):pdb. prot093740.

Kolm, I.E., O'Brien, A., McCormick, A. (2019). *Development of a rapid lateral flow immunoassay for the detection of respiratory syncytial virus in clinical specimens. Journal of Clinical Microbiology*, 57(6), e00122-19.

Kolosova, A.Y., De Saeger, S., Sibanda, L., Verheijen, R., Van Peteghem, C. Development of a colloidal gold-based lateral-flow immunoassay for the rapid simultaneous detection of zearalenone and deoxynivalenol. Anal. Bioanal. Chem. 2007, 389, 2103–2107.

Koo, K.M., Wee, E.J.H., Trau, M. (2017). High-speed biosensing strategy for non-invasive profiling of multiple cancer fusion genes in urine. *Biosensors and Bioelectronics*, 89, pp.715–720.

Koo, K.M., Wee, E.J.H., Trau, M. Colorimetric TMPRSS2-ERG gene fusion detection in prostate cancer urinary samples via recombinase polymerase amplification. *Theranostics.* 2016; 6:1415–1424.

Koonin, E.V. and Makarova, K.S. CRISPR-Cas: an adaptive immunity system in prokaryotes. *F1000 Biol Rep.* 2009; 1:95.

Koonin, E.V., Makarova, K.S., Zhang, F. Diversity, classification, and evolution of CRISPR-Cas systems. *Curr Opin Microbiol.* 2017; 37:67–78.

Koupaei, M., Shadab Mehr, N., Mohamadi, M. H., Asadi, A., Abbasimoghaddam, S., Shekartabar, A., et al. (2022). Clinical symptoms, diagnosis, treatment, and outcome of COVID-19-associated encephalitis: a systematic review of case reports and case series. *J. Clin. Lab. Anal* 36: e24426.

Kovpak, A., Piniaeva, A.N., Gerasimov, O.A., Tcelykh, I.O., Ermakova, M.Y., Zyrina, A.N., Danilov, D.V., Yury Ivin, Kozlovskaya, L.I., Ishmukhametov, A.A. (2022). Methodology of Purification of Inactivated Cell-Culture-Grown SARS-CoV-2 Using Size-Exclusion Chromatography. *Vaccines*, [online] 10(6), pp.949–949.

Kralik, P. and Ricchi, M. A basic guide to real time PCR in microbial diagnostics: definitions, parameters, and everything. *Front Microbiol*. 2017; 8:108.

Krammer, F., Fouchier, R.A.M., Eichelberger, M.C., Webby, R.J., Shaw-Saliba, K., Wan, H., Wilson, P.C., Compans, R.W., Skountzou, I., Monto, A.S. (2018). NAction!

How Can Neuraminidase-Based Immunity Contribute to Better Influenza Virus Vaccines? *mBio*, [online] 9(2).

Krõlov, K., Frolova, J., Tudoran, O., Suhorutsenko, J., Lehto, T., Sibul, H., Mäger, I., Laanpere, M., Tulp, I., Langel, Ü. Sensitive and rapid detection of Chlamydia trachomatis by recombinase polymerase amplification directly from urine samples. *J. Mol. Diagn.* 2014, 16, 127–135.

Kubista, M., Andrade, J. M., Bengtsson, M., Forootan, A., Jonak, J., Lind, K., et al. (2006). The real-time polymerase chain reaction. *Mol. Aspects Med.* 27, 95–125.

Kucirka, L.M., Lauer, S.A., Laeyendecker, O., Boon, D. and Lessler, J. (2020). Variation in False-Negative Rate of Reverse Transcriptase Polymerase Chain Reaction–Based SARS-CoV-2 Tests by Time Since Exposure. *Annals of Internal Medicine*, 173(4).

Kunze, A., Dilcher, M., Abd El Wahed, A., Hufert, F., Niessner, R., Seidel, M. On- chip isothermal nucleic acid amplification on flow-based chemiluminescence microarray analysis platform for the detection of viruses and bacteria. *Anal. Chem.* 2016; 88:898–905.

Kwok, S., Kellogg, D.E., McKinney, N., Spasic, D., Godal, L., Levenson, C., Sninsky, J.J. Effects of primer-template mismatches on the polymerase chain reaction: human immunodeficiency virus type 1 model studies. *Nucleic Acids Res.* 1990; 18:999– 1005.

LaBarre, P., Hawkins, K.R., Gerlach, J., Wilmoth, J., Beddoe, A., Singleton, J., Weigl, B.H. (2011) 'A simple, inexpensive device for nucleic acid amplification without electricity—toward instrument-free molecular diagnostics in low-resource settings', *PLoS ONE*, 6(5), e19738.

Ladner, R.C. (2007). Mapping the Epitopes of Antibodies. *Biotechnology and Genetic Engineering Reviews*, 24(1), pp.1–30.

Lam, C. and Patel, P. (2022). *Nirmatrelvir/Ritonavir*. [online] PubMed.

Land, K. J., Boeras, D. I., Chen, X. S., Ramsay, A. R., & Peeling, R. W. (2019). REASSURED diagnostics to inform disease control strategies, strengthen health systems and improve patient outcomes. *Nature Microbiology*, 4(1), 46–54.

Landolt, G.A., Townsend, H.G.G., Lunn, D.P. (2014). *Chapter 13 - Equine Influenza Infection*. [online] ScienceDirect.

Landry, M.L. and Hsiung, G.D. (2000). *Clinical Virology Manual*. 3rd ed. ASM Press.

Lang, M. and Orgogozo, V. (2011). Identification of homologous gene sequences by PCR with degenerate primers. *Methods in Molecular Biology (Clifton, N.J.)*, [online] 772, pp.245–256.

Lankester, A.C., Tol, van, Claas, J., Vossen, J.M., Kroes, M. (2002). Quantification of Adenovirus DNA in Plasma for Management of Infection in Stem Cell Graft Recipients. *Clinical infectious diseases/Clinical infectious diseases (Online. University of Chicago. Press)*, [online] 34(6), pp.864–867.

Lassaunière, R., Frische, A., Harboe, Z.B. (2020). *Evaluation of commercial SARS- CoV-2 rapid serological tests. Clinical Microbiology and Infection*, 26(8), 968-974.

Lattanzio, V.M.T., Nivarlet, N., Lippolis, V., Gatta, S.D., Huet, A.C., Delahaut, P., Granier, B., Visconti, A. Multiplex dipstick immunoassay for semi-quantitative determination of Fusarium mycotoxins in cereals. *Anal. Chim. Acta* 2012, 718, 99–108.

Lau, H.Y., Wang, Y., Wee, E.J.H., Botella, J.R., Trau, M. Field demonstration of a multiplexed point-of-care diagnostic platform for plant pathogens. *Anal. Chem.* 2016; 88:8074–8081

Lau, H.Y., Wu, H., Wee, E.J.H., Trau, M., Wang, Y., Botella, J.R. Specific and sensitive isothermal electrochemical biosensor for plant pathogen DNA detection with colloidal gold nanoparticles as probes. *Sci. Rep.* 2017; 7:38896.

Lau, S.K. P., Yip, Cyril C. Y., Que, T., Lee, Rodney A., Au-Yeung, Rex K. H., Zhou, B., So, L., Lau, Y., Chan, K., Woo, Patrick, C.Y., Yuen, K. (2007). Clinical and Molecular Epidemiology of Human Bocavirus in Respiratory and Fecal Samples from Children in Hong Kong. *The Journal of Infectious Diseases*, 196(7), pp.986–993.

Lau, Y. L. et al. (2021). A rapid and portable recombinase polymerase amplification assay for African swine fever virus. *Veterinary Microbiology*, 254, 108995.

Lau, Y.L., Ismail, I B., Mustapa, N.I.B., Lai, M.Y., Tuan Soh, T.S., Haji Hassan, A. (2021). Development of a reverse transcription recombinase polymerase amplification assay for rapid and direct visual detection of Severe Acute Respiratory Syndrome Coronavirus 2 (SARS-CoV-2). *PLOS ONE*, 16(1), e0245164.

Lau, Y.L., Ismail, I. binti, Mustapa, N.I. binti, Lai, M.Y., Tuan Soh, T.S., Haji Hassan, A., Peariasamy, K.M., Lee, Y.L., Abdul Kahar, M.K.B., Chong, J. and Goh, P.P. (2021). Development of a reverse transcription recombinase polymerase amplification assay for rapid and direct visual detection of Severe Acute Respiratory Syndrome Coronavirus 2 (SARS-CoV-2). *PLOS ONE*, 16(1), p.e0245164.

Lau, Y.L., Ismail, I.B., Mustapa, N.I., Lai, M.Y., Tuan Soh, T.S., Annan, W.F. (2020). Real-time reverse transcription recombinase polymerase amplification for rapid detection of SARS-CoV-2. *PLoS One*, 15(11), e0241433.

Lee, C.S., Bishop, E.S., Zhang, R., Yu, X., Farina, E.M., Yan, S., Zhao, C., Zeng, Z., Shu, Y., Wu, X., et al. Adenovirus-mediated gene delivery: Potential applications for gene and cell-based therapies in the new era of personalized medicine. *Genes Dis.* 2017; 4:43–63.

Lee, J., Chung, J., Han, T., Song, M., Hwang, E. (2007). Detection of Human Bocavirus in Children Hospitalized because of Acute Gastroenteritis. *The Journal of Infectious Diseases*, 196(7), pp.994–997.

Lee, J., Eun Hwa Choi, Hoan Jong Lee (2010). Comprehensive serotyping and epidemiology of human adenovirus isolated from the respiratory tract of Korean children over 17 consecutive years (1991–2007). *Journal of Medical Virology*, 82(4), pp.624–631.

Lee, J.T., Yang, Q., Gribenko, A., Perrin, B.S., Zhu, Y., Cardin, R., Liberator, P.A., Anderson, A.S., Hao, L. Genetic Surveillance of SARS-CoV-2 M^{pro} Reveals High Sequence and Structural Conservation Prior to the Introduction of Protease Inhibitor Paxlovid. mBio. 2022 Aug 30;13(4): e0086922.

Lemiengre, M.B., van Driel, M.L., Merenstein, D., Liira, H., Mäkelä, M., De Sutter, A.I. Antibiotics for acute rhinosinusitis in adults. Cochrane Database Syst Rev. 2018 Sep 10;9(9):CD006089.

Lenharo, M. (2023). GISAID in crisis: can the controversial COVID genome database survive? *Nature*, [online] 617(7961), pp.455–457.

Lerner, D.N., Choi, S.S., Zalzal, G.H., Johnson, D.L. Intracranial complications of sinusitis in childhood. *Ann Otol Rhinol Laryngol* 2021;104288- 293

Levin, J.D., Fiala, D., Samala, M.F., Kahn, J.D., Peterson, R.J. (2006). Position-dependent effects of locked nucleic acid (LNA) on DNA sequencing and PCR primers. *Nucleic Acids Research*, 34(20), pp. e142–e142.

Levine, E.M., Becker, Y., Boone, C.W., Eagle, H. (1965). "Contact inhibition, macromolecular synthesis, and polyribosomes in cultured human diploid fibroblasts". *Proceedings of the National Academy of Sciences of the United States of America*, 53(2), pp.350–356.

Li, C., Wen, A., Shen, B., Lu, J., Huang, Y., Chang, Y. (2011). FastCloning: a highly simplified, purification-free, sequence- and ligation-independent PCR cloning method. *BMC Biotechnology*, 11(1), p.92.

Li, J. and Macdonald, J. Multiplex lateral flow detection and binary encoding enables a molecular colorimetric 7-segment display. *Lab Chip* 2016, 16, 242–245.

Li, J., Macdonald, J., & von Stetten, F. (2019). Review: Barriers to the adoption of isothermal nucleic acid amplification technologies in clinical diagnostics. *Chemical Society Reviews*, 48(2), 422–436.

Li, J., Macdonald, J., von Stetten, F. (2018). Review: a comprehensive summary of a decade development of the recombinase polymerase amplification. *Analyst* 144 (1), 31– 67.

Li, M.Z. and Elledge, S.J. (2007). Harnessing homologous recombination in vitro to generate recombinant DNA via SLIC. *Nature methods*, [online] 4(3), pp.251–6.

Li, S., Fang, M., Zhou, B., Ni, H., Shen, Q., Zhang, H., et al. Simultaneous detection and differentiation of dengue virus serotypes 1–4, Japanese encephalitis virus, and West Nile virus by a combined reverse-transcription loop-mediated isothermal amplification assay. *Virol J.* 2011; 8:360.

Li, X. and Ma, X. Acute respiratory failure in COVID-19: is it "typical" ARDS? Crit Care. 2020;24(1):1–5.

Li, Y. and Zhang, Y. (2021). *Coinfection of respiratory viruses and the risk of severe disease. Influenza and Other Respiratory Viruses*, 15(5), 598-606.

Li, Y., Shi, J., Xia, J., Duan, J., Chen, L., Yu, X., Lan, W., Ma, Q., Wu, X., Yuan, Y., Gong, L., Yang, X., Gao, H. and Wu, C. (2020). Asymptomatic and Symptomatic Patients With Non-severe Coronavirus Disease (COVID-19) Have Similar Clinical Features and Virological Courses: A Retrospective Single Center Study. *Frontiers in Microbiology*, 11.

Li, Z., Zhang, X., Chen, M. (2018). *Development and evaluation of a rapid RT-RPA assay for detection of Zika virus. Journal of Virological Methods*, 259, 94-100.

Lieber, M.R. The mechanism of double-strand DNA break repair by the nonhomologous DNA end-joining pathway. *Annu Rev Biochem.* 2010; 79:181–211.

Liljander, A., Yu, M., O'Brien, E., Heller, M., Nepper, J.F., Weibel, D.B., Gluecks, I., Younan, M., Frey, J., Falquet, L., Jores, J. Field-applicable recombinase polymerase amplification assay for rapid detection of mycoplasma capricolum subsp. Capripneumoniae. *J. Clin. Microbiol.* 2015; 53:2810–2815.

Lillis, L. et al. (2016). Factors influencing recombinase polymerase amplification (RPA) assay outcomes at point of care. *Molecular and Cellular Probes*, 30(2), 74–78.

Lillis, L., Lehman, D., Singhal, M.C., Cantera, J., Singleton, J., Labarre, P., Toyama, A., Piepenburg, O., Parker, M., Wood, R., Overbaugh, J., Boyle, D.S. Non- instrumented incubation of a recombinase polymerase amplification assay for the rapid and sensitive detection of proviral HIV-1 DNA. *PLoS One.* 2014;9: e108189.

Lillis, L., Siverson, J., Lee, A., Cantera, J., Parker, M., Piepenburg, O., Lehman, D.A., Boyle, D.S. Factors influencing Recombinase polymerase amplification (RPA) assay outcomes at point of care. *Mol. Cell. Probes.* 2016; 30:74–78.

Limberis, J.D. and Metcalfe, J.Z. (2023). primerJinn: a tool for rationally designing multiplex PCR primer sets for amplicon sequencing and performing in silico PCR. *BMC Bioinformatics*, 24(1).

Lin, X., et al. Fast and parallel detection of four ebola virus species on a microfluidic- chip-based portable reverse transcription loop-mediated isothermal amplification system. *Micromachines* 10 (2019).

Linden, D., Guo-Parke, H., Coyle, P.V., Fairley, D., McAuley, D.F., Taggart, C.C., Kidney, J. (2019). Respiratory viral infection: a potential 'missing link' in the pathogenesis of COPD. *European Respiratory Review*, [online] 28(151).

Lindsay, M.I., Herrmann, E.C., Morrow, G.W., Brown, A.L. (1970). Hong Kong Influenza: clinical, microbiologic, and pathologic features in 127 cases. *JAMA: The Journal of the American Medical Association*, 214(10), pp.1825–1832.

Liu, D.X., Liang, J.Q., Fung, T.S. (2020). Human Coronavirus-229E, -OC43, -NL63, and -HKU1. *Reference Module in Life Sciences*.

Liu, J., Nian, Q.G., Li, J., Hu, Y., Li, X.F., Zhang, Y., et al. Development of reverse-transcription loop mediated isothermal amplification assay for rapid detection of novel avian Influenza A (H7N9) virus. *BMC Microbiol.* 2014; 14:271.

Liu, S. and Lee, J. (2014) 'Cell disruption and protein recovery using high-pressure homogenization and centrifugation', *Biotechnology Advances*, 32(3), pp. 491-503.

Liu, Y., Lei, T., Liu, Z., Kuang, Y., Lyu, J., Wang, Q. A novel technique to detect EGFR mutations in lung cancer, Int. *J. Mol. Sci.* 2016;17:792.

Liu, Y., Wang, Y., Wang, Y., Mai, H., Chen, Y., Zhang, Y., Ji, Y., Cong, X., Gao, Y. (2023). Phylogenetic analysis of HA and NA genes of Influenza A viruses in immunosuppressed inpatients in Beijing during the 2018–2020 Influenza seasons. *Virology Journal*, 20(1).

Lobato, I.M. and O'Sullivan, C.K. (2018). Recombinase polymerase amplification: Basics, applications and recent advances. *TrAC Trends in Analytical Chemistry*, [online] 98, pp.19–35.

Lohman, G.J., Zhang, Y., Zhelkovsky, A.M., Cantor, E J., Evans, T.C., Jr. (2014). Efficient DNA Ligation in DNA-RNA Hybrid Helices by Chlorella Virus DNA Ligase. *Nucleic Acids Res*. 42, 11846 11846.

Lonberg, N. Fully human antibodies from transgenic mouse and phage display platforms. *Curr. Opin. Immunol.* 2008, *20*, 450–459.

Londoño, M.A., Harmon, C.L., Polston, J.E. (2016). Evaluation of recombinase polymerase amplification for detection of begomoviruses by plant diagnostic clinics. *Virology Journal*, 13(1).

Loo, J.F.C., Lau, P.M., Ho, H.P., Kong, S.K. An aptamer-based bio-barcode assay with isothermal recombinase polymerase amplification for cytochrome-c detection and anti-cancer drug screening. *Talanta.* 2013; 115:159–165.

Louten, J. (2016). Detection and Diagnosis of Viral Infections. *Essential Human Virology*, [online] pp.111–132.

Lynch, J., Fishbein, M., Echavarria, M. (2011). Adenovirus. *Seminars in Respiratory and Critical Care Medicine*, 32(04), pp.494–511.

Madeley, C. R., & Peiris, J. S. M. (2002). Methods in virus diagnosis: the art and the science. *Journal of Clinical Virology*, 25(1), 7–12.

Mahony, J. B. (2008). Detection of respiratory viruses by molecular methods. *Clinical Microbiology Reviews*, 21(4), 716–747.

Makarova, K.S., Haft, D.H., Barrangou, R., Brouns, S.J., Charpentier, E. Evolution and classification of the CRISPR-Cas systems. *Nat Rev Microbiol.* 2011; 9:467–477.

Malhotra, B., Hasan, M.R., Sathi, K.S., Hossain, M.S., Rahman, S.M.A., Bhuiyan, A. (2017). Evaluation of degenerate primers for detection of novel human coronaviruses. *Journal of Clinical Virology*, 97, 16-21.

Mali, P., Yang, L., Esvelt, K.M., Aach, J., Guell, M. RNA-guided human genome engineering via Cas9. *Science.* 2013; 339:823–826.

Mardiana, M., et al. (2022). *A comparison of extraction methods for detection of SARS-CoV-2 RNA from saliva samples using RT-PCR. Journal of Virological Methods*, 300, 114433.

Marks, K.M. **and Nolan, G.P.** (2006). Chemical labeling strategies for cell biology. *Nature Methods*, 3(8), pp.591–596.

Martin, E.T., Taylor, J., Kuypers, J., Magaret, A., Wald, A., Zerr, D., Englund, J.A. (2009). Detection of Bocavirus in Saliva of Children with and without Respiratory Illness. *Journal of clinical microbiology*, [online] 47(12), pp.4131–4132.

Martonik, D., Parfieniuk-Kowerda, A., Rogalska, M., Flisiak, R. The Role of Th17 Response in COVID-19. *Cells* 2021, *10*, 1550.

Marx, A., Torok, T., Holman, R., et al. Pediatric hospitalizations for croup (laryngotracheobronchitis): biennial increases associated with human parainfluenza virus 1 epidemics. *J Infect Dis.* 1997; 176:1423–1427.

Marzieh Soheili, Sorour Khateri, Farhad Moradpour, Pardis Mohammadzedeh, Mostafa Zareie, Mahdavi, M., Manifar, S., Hamed Gilzad Kohan, Moradi, Y. (2023). The efficacy and effectiveness of COVID-19 vaccines around the world: a mini- review and meta-analysis. *The efficacy and effectiveness of COVID-19 vaccines around the world: a mini-review and meta-analysis*, 22(1).

Mastroianni, F., Guida, P., Bellanova, G., Valentina De Nicolo, E., Righetti, G., Formoso, M., Celani, F. SARS-CoV-2 antibody response after BNT162b2 mRNA vaccine in healthcare workers: Nine-month of follow-up. *Vaccine X* 2022, *11*, 100175.

Maziarz, R.T., Sridharan, P., Slater, S., Meyers, G., Post, M., Erdman, D.D., Teresa, C.T., Peret and Taplitz, R.A. (2009). Control of an Outbreak of Human Parainfluenza Virus 3 in Hematopoietic Stem Cell Transplant Recipients. *Biology of Blood and Marrow Transplantation*, [online] 16(2), pp.192–198.

McBride, R. **and Fielding, B.** (2012). The Role of Severe Acute Respiratory Syndrome (SARS)- Coronavirus Accessory Proteins in Virus Pathogenesis. *Viruse*s, 4(11), pp.2902–2923.

McDonald, J. (2020). *A Guide to Moderna's COVID-19 Vaccine*. [online] FactCheck.org.

McLean, G.R. (2014). Developing a vaccine for human rhinoviruses. *Journal of Vaccines & Immunization*, 2(3), pp.16–20.

Meherali, S., Campbell, A., Hartling, L., Scott, S. Understanding Parents' Experiences and Information Needs on Pediatric Acute Otitis Media: A Qualitative Study. *J Patient Exp.* 2019 Mar;6(1):53-61.

Mekuria, T. A., Zhang, S., Eastwell, K.C. Rapid and sensitive detection of little cherry virus 2 using isothermal reverse transcription-recombinase polymerase amplification. *J. Virol. Methods* 2014, 205, 24–30.

Middleton, D.B. Pharyngitis. *Prim Care.* 1996; 23:719-39.

Moghadami, M. (2017). A Narrative Review of Influenza: A Seasonal and Pandemic Disease. *Iranian Journal of Medical Sciences*, [online] 42(1), pp.2–13.

Mohn, K.G., Brokstad, K.A., Pathirana, R.D., et al. Live attenuated Influenza vaccination in children induces B-cell responses in tonsils. *J Infect Dis*. 2016;214(5):722–731.

Monaghan, N.P. Emerging infections–implications for dental care. *British Dental Journal*. 2016;221(1):13–15.

Mondal, D., Ghosh, P., Khan, M.A.A., Hossain, F., Böhlken-Fascher, S., Matlashewski, G., Kroeger, A., Olliaro, P., Abd El Wahed, A. Mobile suitcase laboratory for rapid detection of Leishmania donovani using recombinase polymerase amplification assay. *Parasit. Vectors.* 2016; 9:281.

Mori, I., Kazuya Nakakuki and Kimura, Y. (1996). Temperature-Sensitive Parainfluenza Type 1 Vaccine Virus Directly Accesses the Central Nervous System by Infecting Olfactory Neurons. *Journal of general virology*, 77(9), pp.2121–2124.

Morris, J.A., Blount, R.E., Jr, Savage, R.E. Recovery of cytopathogenic agent from chimpanzees with coryza. *Proc Soc Exp Biol Med.* 1956; 92:544–549.

Morris, R.G., Arends, M.J., Bishop, P.E., et al. (1990) Sensitivity of digoxigenin and biotin-labeled probes for detection of human papillomavirus by in situ hybridization. J Clin Pathol 43: 800–805.

Morshed, M., Jassem, A., Luk, D., Cheong, A., Krajden, M. and Sekirov, I. (2024). Clinical utility and interpretive guidance for SARS-CoV-2 serological testing. *Clinical Microbiology Newsletter*, [online] 45(24), pp.209–218.

Moscona, A. (2005). Neuraminidase Inhibitors for Influenza. *New England Journal of Medicine*, [online] 353(13), pp.1363–1373.

Mozgovoj, M., Merceder Dieder Graham, Ferrufino, C., Blanc, S., Adriana Fernandez Souto, Pillof, M. and Jose, M. (2023). Viral load in symptomatic and asymptomatic patients infected with SARS-CoV-2. What have we learned? *Journal of Clinical Virology Plus*, 3(4), pp.100166–100166.

Murray, K., Selleck, P., Hooper, P., Hyatt, A., Gould, A., Gleeson, L., Westbury, H., Hiley, L., Selvey, L., Rodwell, B., Ketterer, P. A morbillivirus that caused fatal disease in horses and humans *Science* 1995. 268 94–97.

Musuuza, J.S., Watson, L., Parmasad, V., Putman-Buehler, N., Christensen, L. and Safdar, N. (2021). Prevalence and outcomes of co-infection and superinfection with SARS-CoV-2 and other pathogens: A systematic review and meta-analysis. *PLOS ONE*, 16(5), p.e0251170.

Nagamine, K., Hase, T., Notomi, T. Accelerated reaction by loop-mediated isothermal amplification using loop primers. *Mol. Cell. Probes.* 2002; 16:223–229.

Nguyen, T.C., Kathia Zaleta-Rivera, Huang, X., Dai, X., Zhong, S. (2018). RNA, Action through Interactions. *Trends in Genetics*, 34(11), pp.867–882.

Nilsson, M., Antson, D.O., Barbany, G., Landegren, U. (2001). RNA-Templated DNA Ligation for Transcript Analysis. *Nucleic Acids Res.* 29, 578–581.

Nobusawa, E. and Sato, K. (2006). Comparison of the Mutation Rates of Human Influenza A and B Viruses. *Journal of Virology*, [online] 80(7), pp.3675–3678.

Noguera, P., Posthuma-Trumpie, G.A., van Tuil, M., van der Wal, F.J., de Boer A., Moers, A.P.H.A., van Amerongen, A. Carbon nanoparticles in lateral flow methods to detect genes encoding virulence factors of Shiga toxin-producing Escherichia coli. *Anal. Bioanal. Chem.* 2011, 399, 831 838.

Noor, R. and Maniha, S.M. (2020). A brief outline of respiratory viral disease outbreaks: 1889–till date on the public health perspectives. *VirusDisease*, 31(4), pp.441–449.

Notomi, T., Okayama, H., Masubuchi, H., Yonekawa, T., Watanabe, K., Amino, N., Hase, T. Loop mediated isothermal amplification of DNA. *Nucleic Acids Res.,* 28 (2000), p. e63.

Notomi, T., Okayama, H., Masubuchi, H., Yonekawa, T., Watanabe, K., Amino, N., & Hase, T. (2000). Loop-mediated isothermal amplification of DNA. *Nucleic Acids Research*, 28(12), e63.

Nuovo, G.J., Gorgone, G., MacConnell, P., Margiotta, M., Gorevic, P.D. (1992). In situ localization of PCR-amplified human and viral cDNAs. *Genome Research*, 2(2), pp.117–123.

Nuwarda, R.F., Alharbi, A.A., Kayser, V. (2021). An Overview of Influenza Viruses and Vaccines. *Vaccines*, 9(9), p.1032.

Odell, I.D. and Cook, D. (2013). Immunofluorescence Techniques. *Journal of Investigative Dermatology*, 133(1), pp.1–4.

Ogawa, M., Mutsuga, N., Tsurudome, M., Kawano, M., Matsumura, H., Kusagawa, S., Komada, H., Nishio, M., Ito, Y. (1992). Nucleotide Sequence Analysis of the Simian Virus 41 Gene Encoding the Large (L) Protein and Construction of a Phylogenetic Tree for the L Proteins of Paramyxoviruses. *Journal of General Virology*, 73(10), pp.2743–2750.

Olivier, B. and Walter, W. (1998) A simplified in situ hybridization protocol using non-radioactively labeled probes to detect abundant and rare mRNAs on tissue sections. *Biochemica* 1:10–16.

Olsen, M.A., Shuck, K.M., Sambol, A.R., Flor, S.M., O'Brien, J., Cabrera, B.J. (1993). Isolation of seven respiratory viruses in shell vials: a practical and highly sensitive method. *J. Clin. Microbiol*. 31, 422–425.

Otter, J.A., Donskey, C., Yezli, S., Douthwaite, S., Goldenberg, S.D., Weber, D.J. Transmission of SARS and MERS coronaviruses and Influenza virus in healthcare settings: the possible role of dry surface contamination. *Journal of Hospital Infection*. 2016; 92(3):235–250.

Palese, P. and Compans, R.W. Inhibition of Influenza virus replication in tissue culture by 2-deoxy-2,3-dehydro-N-trifluoroacetylneuraminic acid (FANA): mechanism of action. *J Gen Virol* 1976; 33:159- 63.

Panda, S., Mohakud, N.K., Pena, L., Kumar, S. (2014). Human metapneumovirus: review of an important respiratory pathogen. *International Journal of Infectious Diseases*, [online] 25, pp.45–52.

Panning, M., Eickmann, M., Landt, O., Monazahian, M., Ölschläger, S., Baumgarte, S., ... & Drosten, C. (2007). Detection of influenza A(H5N1) virus by real-time reverse-transcription PCR. *Euro Surveillance*, 12(5), 717.

Papenburg, J. and Boivin, G. The distinguishing features of human metapneumovirus and respiratory syncytial virus. *Rev Med Virol.* 2010; 20:245–260.

Pappas, D.E., Hendley, J.O., Hayden, F.G., Winther, B. (2008). Symptom Profile of Common Colds in School-Aged Children. *Pediatric Infectious Disease Journal*, 27(1), pp.8–11.

Pardue, M.L. and Gall, J.G. (1969). Molecular Hybridization of Radioactive DNA to the DNA of Cytological Preparations. *Proceedings of the National Academy of Sciences*, [online] 64(2), pp.600–604.

Parida, M., Sannarangaiah, S., Dash, P. K., Rao, P. V. L., & Morita, K. (2008). Loop mediated isothermal amplification (LAMP): a new generation of innovative gene amplification technique; perspectives in clinical diagnosis of infectious diseases. *Reviews in Medical Virology*, 18(6), 407–421.

Parida, M., Sannarangaiah, S., Dash, P.K., Rao, P.V., Morita, K. Loop mediated isothermal amplification (LAMP): A new generation of innovative gene amplification technique; perspectives in clinical diagnosis of infectious diseases. *Rev. Med. Virol.* 2008; 18:407–421.

Patel, P., Abd El Wahed, A., Faye, O., Prüger, P., Kaiser, M., Thaloengsok, S., Ubol, S., Sakuntabhai, A., Leparc-Goffart, I., Hufert, F.T., Sall, A.A., Weidmann, M. and Niedrig, M. (2016). A Field-Deployable Reverse Transcription Recombinase Polymerase Amplification Assay for Rapid Detection of the Chikungunya Virus. *PLOS Neglected Tropical Diseases*, 10(9), p. e0004953.

Patriquin, G., Davis, I., Heinstein, C., MacDonald, J., Hatchette, T.F. and LeBlanc, J.J. (2020). Exploring alternative swabs for use in SARS-CoV-2 detection from the oropharynx and anterior nares. *Journal of Virological Methods*, 285, p.113948.

Peeling, R. W., Holmes, K. K., Mabey, D., & Ronald, A. (2006). Rapid tests for sexually transmitted infections (STIs): the way forward. *Sexually Transmitted Infections*, 82(suppl 5), v1–v6.

Peteranderl, C., Schmoldt, C., Herold, S. (2016). Human Influenza Virus Infections. *Seminars in Respiratory and Critical Care Medicine*, 37(04), pp.487–500.

Piepenburg O., Williams C.H., Stemple D.L., Armes N.A. DNA detection using recombination proteins. *PLoS Biol.* 2006; 4:1115–1121.

Piepenburg, O., Williams, C. H., Stemple, D. L., & Armes, N. A. (2006). DNA detection using recombination proteins. *PLoS Biology*, 4(7), e204.

Piña, R., Santos-Díaz, A.I., Orta-Salazar, E., Aguilar-Vazquez, A.R., Mantellero, C.A., Acosta-Galeana, I., Estrada-Mondragon, A., Prior-Gonzalez, M., Martinez- Cruz, J.I., Rosas-Arellano, A. (2022). Ten Approaches That Improve Immunostaining: A Review of the Latest Advances for the Optimization of Immunofluorescence. *International Journal of Molecular Sciences*, 23(3), p.1426.

Pinsky, B.A. and Hayden, R.T. (2019). Cost-Effective Respiratory Virus Testing. *Journal of Clinical Microbiology*, 57(9).

Pitkäranta, A., Arruda, E., Malmberg, H., Hayden, F.G. (1997). Detection of rhinovirus in sinus brushings of patients with acute community-acquired sinusitis by reverse transcription-PCR. *Journal of clinical microbiology*, 35(7), pp.1791–1793.

Plotkin, S.A., Orenstein, W.A., Offit, P.A., Edwards, K.M. (2018). *Plotkin's Vaccines* (7th ed.). Elsevier.

Poitras, S., Wood, K.S., Savard, J., Dervin, G.F., Beaule, P.E. Predicting early clinical function after hip or knee arthroplasty. *Bone Joint Res* 2015; 4:145–151.

Poje, J.E., Kastratovic, T., Macdonald, A.R., Guillermo, A.C., Troetti, S.E., Jabado, O. J., Fanning, M.L., Stefanovic, D., Macdonald, J. Visual displays that directly interface

and provide read-outs of molecular states via molecular graphics processing units. *Angew. Chem., Int. Ed. Engl.* 2014, 53, 9222–9225.

Pollard, A.J. and Bijker, E.M. (February 2021). "A guide to vaccinology: from basic principles to new developments". *Nature Reviews. Immunology*. 21 (2): 83–100.

Poritz, M.A., Blaschke, A.J., Byington, C.L., Meyers, L., Nilsson, K., Jones, D.E., Thatcher, S.A., Robbins, T., Lingenfelter, B., Amiott, E., Herbener, A., Daly, J.,

Pritzker, K. (2021). Impact of the COVID-19 pandemic on Molecular Diagnostics. *Expert Review of Molecular Diagnostics*, pp.1–3.

Protasova, I.N., Per'yanova, O.V., Podgrushnaya, T.S. [Acute otitis media in the children: etiology and the problems of antibacterial therapy]. *Vestn Otorinolaringol.* 2017;82(2):84-89.

Quan, J. and Tian, J. (2009). Circular Polymerase Extension Cloning of Complex Gene Libraries and Pathways. *PLoS ONE*, 4(7), p.e6441.

Rahmani, A., Dini, G., Leso, V., Montecucco, A., Vitturi, B.K., Ivo Iavicoli and Durando, P. (2022). Duration of SARS-CoV-2 shedding and infectivity in the working age population: a systematic review and meta-analysis. *La Medicina del lavoro*, [online] 113(2), pp.e2022014–e2022014.

Ramos-Vara, J.A. (2005). Technical aspects of immunohistochemistry. *Veterinary Pathology*, 42(4), pp.405-426.

Ran, F.A., Hsu, P.D., Wright, J., Agarwala, V., Scott, D.A. Genome engineering using the CRISPR-Cas9 system. *Nat Protoc.* 2013; 8:2281–2308.

Rappo, U., Schuetz, A.N., Jenkins, S.G., Calfee, D.P., Walsh, T.J., Wells, M.T., Hollenberg, J.P., Glesby, M.J. (2016). Impact of Early Detection of Respiratory Viruses by Multiplex PCR Assay on Clinical Outcomes in Adult Patients. *Journal of Clinical Microbiology*, 54(8), pp.2096–2103.

Regamey, N., Frey, U., Deffernez, C., Latzin, P., Kaiser, L. and Group, on behalf of the S.P.R.R. (2007). Isolation of Human Bocavirus from Swiss Infants with Respiratory Infections. *The Pediatric Infectious Disease Journal*, [online] 26(2), p.177.

Regunath, H. and Oba, Y. (2023). *Community-Acquired Pneumonia*. [online] PubMed.

Reich, N. (2023). *A modeler's primer for working with SARS-CoV-2 genomic data.* [online] Nicholas Reich: Biostatistics and Infectious Disease Epidemiology.

Richter, M., Piwocka, O., Musielak, M., Piotrowski, I., Suchorska, W.M., Trzeciak, T. (2021). From Donor to the Lab: A Fascinating Journey of Primary Cell Lines. *Frontiers in Cell and Developmental Biology*, 9.

Rihkanen, H., Rönkkö, E., Nieminen, T., et al. Respiratory viruses in laryngeal croup of young children. *J Pediatr.* 2008;152(5):661–665.

Rodino, K.G., Espy, M.J., Buckwalter, S.P., Walchak, R.C., Germer, J.J., Fernholz, E., Boerger, A., Schuetz, A.N., Yao, J.D. and Binnicker, M.J. (2020). Evaluation of saline, phosphate buffered saline and minimum essential medium as potential alternatives to viral transport media for SARS-CoV-2 testing. *Journal of Clinical Microbiology*.

Rogers, A.A., Baumann, R.E., Borillo, G.A., Kagan, R.M., Batterman, H.J., Galdzicka, M. and Marlowe, E.M. (2020). Evaluation of Transport Media and Specimen Transport Conditions for the Detection of SARS-CoV-2 Using Real Time Reverse Transcription PCR. *Journal of Clinical Microbiology*.

Rohland, N. and Reich, D. (2012) 'Cost-effective, high-throughput DNA sequencing libraries for multiplexed target capture', *Genome Research*, 22(5), pp. 939-946.

Rohrman, B. and Richards-Kortum, R. Inhibition of recombinase polymerase amplification by background DNA: a lateral flow-based method for enriching target DNA. *Anal. Chem.* 2015; 87:1963–1967.

Roingeard, P., Raynal, P.I., Eymieux, S., Blanchard, E. (2018). Virus detection by transmission electron microscopy: Still useful for diagnosis and a plus for biosafety. *Reviews in Medical Virology*, 29(1), p.e2019.

Romijn, H.J., van Uum, J.F.M., Breedijk, I., Emmering, J., Radu, I., Pool, C.W. (1999). Double Immunolabeling of Neuropeptides in the Human Hypothalamus as Analyzed by Confocal Laser Scanning Fluorescence Microscopy. *Journal of Histochemistry & Cytochemistry*, 47(2), pp.229–235.

Rose, T.M., Henikoff, J.G., Henikoff, S. CODEHOP (COnsensus-DEgenerate Hybrid Oligonucleotide Primer) PCR primer design. Nucleic Acids Res. 2003, 31: 3763-3766.

Rosser, A., Rollinson, D., Forrest, M., Webster, B.L. Isothermal recombinase polymerase amplification (RPA) of Schistosoma haematobium DNA and oligochromatographic lateral flow detection. *Parasit. Vectors.* 2015, 8, 446.

Rotbart, H. Enteroviruses. In: Katz SL, Gershon AA, Hotez PJ, Krugman S, eds. Krugman's Infectious diseases of children. 10th ed. St. Louis: Mosby, 1998;81–97.

Ruangrong Cheepsattayakorn, A.C. (2013). Novel Avian Flu A (H7N9): Clinical and Epidemiological Aspects, and Management. *Virology & Mycology*, 02(03).

Ruijter, J.M., Ramakers, C., Hoogaars, W.M.H., et al. Amplification efficiency: linking baseline and bias in the analysis of quantitative PCR data. *Nucleic Acids Res*. 2009; 37(6): e45.

Ruis, T., et al. (2020). *Impact of the COVID-19 pandemic on seasonal respiratory virus testing in the UK. The Lancet Regional Health - Europe*, 2, 100024.

Ruiz, C., Huang, J., Giardina, S.F., Feinberg, P.B., Mirza, A.H., Bacolod, M.D., et al. (2020). Single-Molecule Detection of Cancer Mutations Using a Novel PCR-LDR- qPCR *Assay. Hum. Mutat*. 41, 1051–1068.

Rusling, J.F., Kumar, C.V., Gutkind, J.S., Patel, V. Measurement of biomarker proteins for point of-care early detection and monitoring of cancer. *Analyst* 2010, 135, 2496–2511.

Russell, J.N., Clements, J.E., Gama, L. (2013). Quantitation of Gene Expression in Formaldehyde-Fixed and Fluorescence-Activated Sorted Cells. *PLoS ONE*, 8(9), p.e73849.

Sabaté del Río, J., Steylaerts, T., Henry, O.Y.F., Bienstman, P., Stakenborg, T., Van Roy, W., O'Sullivan, C.K. Real-time and label-free ring-resonator monitoring of solid-phase recombinase polymerase amplification. *Biosens. Bioelectron.* 2015; 73:130–137.

Sanchez, A.O., Ochoa, A.R., Mahoney, R.E., McDaniel, J.S., Asin, S.N., Yuan, T.T. (2021). Comparison of next generation diagnostic systems (NGDS) for the detection of SARS-CoV-2. *Journal of Clinical Laboratory Analysis*, 36(1), e24285.

Sandkovsky, U., Vargas, L., Florescu, D.F. (2014). Adenovirus: Current Epidemiology and Emerging Approaches to Prevention and Treatment. *Current Infectious Disease Reports*, 16(8).

Santiago-Felipe, S., Tortajada-Genaro, L.A., Morais, S., Puchades, R., Maquieira, Á. One-pot isothermal DNA amplification- hybridisation and detection by a disc-based method. *Sensor. Actuator. B Chem.* 2014; 204:273–281.

Santiago-Felipe, S., Tortajada-Genaro, L.A., Puchades, R., Maquieira, A. Recombinase polymerase and enzyme-linked immunosorbent assay as a DNA amplification-detection strategy for food analysis. *Anal. Chim. Acta.* 2014; 811:81–87.

Santos, R., Silva, A., Almeida, N., Costa, P. (2022). Primer design for SARS-CoV-2: A comprehensive approach to detect and differentiate variants. *Journal of Virological Methods*, 301, 114-123.

Saraya, T., Kurai, D., Ishii, H., Ito, A., Sasaki, Y., Niwa, S., Kiyota, N., Tsukagoshi, H., Kozawa, K., Goto, H., Takizawa, H. (2014). Epidemiology of virus-induced asthma exacerbations: with special reference to the role of human rhinovirus. *Frontiers in Microbiology*, 5.

Schilder, A.G., Chonmaitree, T., Cripps, A.W., Rosenfeld, R.M., Casselbrant, M.L., Haggard, M.P., Venekamp, R.P. Otitis media. *Nat Rev Dis Primers.* 2016 Sep 08;2(1):16063.

Schildgen, O. (2013). Human Bocavirus: Lessons Learned to Date. *Pathogens*, 2(1), pp.1–12.

Schnell, S.A., Staines, W.A., Wessendorf, M.W. Reduction of Lipofuscin— like Autofluorescence in Fluorescently Labeled Tissue. *J Histochem Cytochem.* 1999; 47:719–730.

Schotsaert, M. and García-Sastre, A. (2016). A High-Resolution Look at Influenza Virus Antigenic Drift. *The Journal of Infectious Diseases*, [online] 214(7), pp. 982– 982.

Segal, A.O., Crighton, E.J., Rym. M. Croup hospitalizations in Ontario: a 14-year time-series analysis. *Pediatrics.* 2005;116(1):51–55.

Shah, K. and Maghsoudlou, P. Enzyme-linked immunosorbent assay (ELISA): the basics. Br J Hosp Med (Lond). 2016 Jul;77(7):C98-101.

Shaikh, N.I., Kumar, S., Choudhary, S., Sethi, R.S. (2024). Biotechnological approaches in disease diagnosis and management of goats. [online] Academic Press, pp.553–568.

Sharma, A., Bhatt, N.S., St Martin, A., Abid, M.B., Bloomquist, J., Chemaly, R.F., Dandoy, C., Gauthier, J., Gowda, L., Perales, M.-A., Seropian, S., Shaw, B.E., Tuschl, E.E., Zeidan, A.M., Riches, M.L., Shah, G.L. (2021). Clinical characteristics and outcomes of COVID-19 in haematopoietic stem-cell transplantation recipients: an observational cohort study. *The Lancet Haematology*, 8(3), pp. e185–e193.

Sharma, L., Rebaza, A., Dela Cruz, C.S. (2019). When 'B' becomes 'A': the emerging threat of Influenza B virus. *European Respiratory Journal*, 54(2), p.1901325.

Shim, W.B., Dzantiev, B.B., Eremin, S.A., Chung, D.H. One-step simultaneous immunochromatographic strip test for multianalysis of ochratoxin a and zearalenone. *J. Microbiol. Biotechnol.* 2009, 19, 83–92.

Shin, Y., Perera, A.P., Kim, K.W., Park, M.K. Real-time, label-free isothermal solid-phase amplification/detection (ISAD) device for rapid detection of genetic alteration in cancers. *Lab. Chip.* 2013; 13:2106–2114.

Shin, Y., Perera, A.P., Tang, W.Y., Fu, D.L., Liu, Q., Sheng, J.K., Gu, Z., Lee, T.Y., Barkham, T., Kyoung Park, M. A rapid amplification/detection assay for analysis of Mycobacterium tuberculosis using an isothermal and silicon bio-photonic sensor complex, Biosens. *Bioelectron.* 2015; 68:390–396.

Shuman, S. (1991). Recombination mediated by vaccinia virus DNA topoisomerase I in Escherichia coli is sequence specific. *Proceedings of the National Academy of Sciences*, 88(22), 10104-10108.

Shuman, S. (1991). Site-specific interaction of vaccinia virus topoisomerase I with duplex DNA. Minimal DNA substrate for strand cleavage in vitro. *The Journal of biological chemistry*, [online] 266(17).

Shuman, S. (1992). DNA strand transfer reactions catalyzed by vaccinia topoisomerase I. *The Journal of Biological Chemistry*, [online] 267(12), pp.8620–8627.

Siegrist, J. (2024). NMR Chemical Shifts of Impurities Charts. *Merck*, [online] 1(1).

Simasek, M. and Blandino, D.A. Treatment of the common cold. Am Fam Physician. 2007 Feb 15;75(4):515-20.

Simões, E.A.F. (1999). Respiratory syncytial virus and subsequent lower respiratory tract infections in developing countries: A new twist to an old virus. *The Journal of Pediatrics*, 135(6), pp.657–661.

Simões, E.A.F. (2022). The Burden of Respiratory Syncytial Virus Lower Respiratory Tract Disease in Infants in the United States: A Synthesis. *The Journal of Infectious Diseases*, 226(Supplement_2), pp. S143–S147.

Simões, J., Sales Luís, J., Tilley, P. (2019). Contribution of lung function tests to the staging of severe equine asthma syndrome in the field. *Research in Veterinary Science*, 123, pp.112–117.

Simpson, R.T. and Richardson, C.C. (1985). Enzymes involved in DNA replication. *Annual Review of Biochemistry*, 54, 477–530.

Singanayagam, A., Hakki, S., Dunning, J., Madon, K.J., Crone, M.A., Koycheva, A., Derqui-Fernandez, N., Barnett, J.L., Whitfield, M.G., Varro, R., Charlett, A., Kundu, R., Fenn, J., Cutajar, J., Quinn, V., Conibear, E., Barclay, W., Freemont, P.S., Taylor, G.P. and Ahmad, S. (2021). Community transmission and viral load kinetics of the SARS-CoV-2 delta (B.1.617.2) variant in vaccinated and unvaccinated individuals in the UK: a prospective, longitudinal, cohort study. *The Lancet Infectious Diseases*, [online] 22(2).

Singanayagam, A., Joshi, P.V., Mallia, P., Johnston, S.L. Viruses exacerbating chronic pulmonary disease: the role of immune modulation. *BMC Med.* 2012 Mar 15; 10:27.

Singer, R.H, and Ward, D.C. (1982) Actin gene expression visualized in chicken muscle tissue culture by using in situ hybridization with a biotinated nucleotide analog. *Proc Natl Acad Sci USA* 79:7331–7335.

Sleight, S.C. and Sauro, H.M. (2013). BioBrick™ Assembly Using the In-Fusion PCR Cloning Kit. *Humana Press eBooks*, pp.19–30.

Smith, C.J. and Osborn, A.M. Advantages and limitations of quantitative PCR (Q- PCR)-based approaches in microbial ecology. FEMS Microbiol Ecol. 2009 Jan;67(1):6- 20.

Smith, S., Vigilant, L., Morin, P.A. The effects of sequence length and oligonucleotide mismatches on 5′ exonuclease assay efficiency. *Nucleic Acids Res.* 2002; 20:43–49.

Song, J.Z., Mauk, M.G., Hackett, B.A., Cherry, S., Bau, H.H., Liu, C.C. Instrument- free point-of-care molecular detection of Zika virus. *Anal. Chem.,* 88 (2016), pp. 7289- 7294.

Soroka, M., Wasowicz, B., Rymaszewska, A. (2021). Loop-Mediated Isothermal Amplification (LAMP): The Better Sibling of PCR? *Cells,* [online] 10(8), p.1931.

Srinivasan, P. (2020). *Statistical Data Exploration - Interpreting P-Value and R Squared Score.* [online] Analytics Vidhya.

Sritong, N., Sala de Medeiros, M., Basing, L.A. and Linnes, J.C. (2023). Promise and perils of paper-based point-of-care nucleic acid detection for endemic and pandemic pathogens. *Lab on a Chip*, 23(5), pp.888–912.

Stadhouders, R., Pas, S.D., Anber, J., Voermans, J., Mes, T.H.M., Schutten, M. The effect of primer-template mismatches on the detection and quantification of nucleic acids using the 5′ nuclease assay. *J Mol Diagn*. 2010; 12(1): 109-117.

Stafylaki, D., Maraki, S., Vaporidi, K., Georgopoulos, D., Kontoyiannis, D.P., Kofteridis, D.P., Georgios, C. (2022). Impact of Molecular Syndromic Diagnosis of Severe Pneumonia in the Management of Critically Ill Patients. *Microbiology spectrum*, 10(5).

Stensballe, L.G., Devasundaram, J.K., Simões, E.A. (2003). Respiratory syncytial virus epidemics: the ups and downs of a seasonal virus. *The Pediatric Infectious Disease Journal*, [online] 22(2 Suppl), pp. S21-32.

Sterchi, D.L. (2008). Molecular Pathology—In Situ Hybridization. *Theory and Practice of Histological Techniques*, pp.537–558.

Subramony, A., Zachariah, P., Krones, A., et al. Impact of multiplex polymerase chain reaction testing for respiratory pathogens on healthcare resource utilization for pediatric inpatients. *J Pediatr* 2016; 173: 196–201.

Summeren, J. van, Meijer, A., Aspelund, G., Casalegno, J.S., Erna, G., Hoang, U., Lina, B., Lyon, V. study group in, Lusignan, S. de, Teirlinck, A.C., Thors, V., Paget, J., Lyon, V. study group in, Lyon, V. study group in, Ouziel, A., Tardy, J., Sun, Y., Yu, H., Zheng, D., Cao, Q., Wang, Y., Harris, D., Wang, Y. Sudan Black B Reduces Autofluorescence in Murine Renal Tissue. *Arch Pathol Lab Med.* 2011; 135:1335–1342.

Supriya, R., Gao, Y., Gu, Y., Baker, J.S. Role of Exercise Intensity on Th1/Th2 Immune Modulations During the COVID-19 Pandemic. *Front. Immunol.* 2021, *12*, 761382.

Suwancharoen, D., Sittiwicheanwong, B., Wiratsudakul, A. Evaluation of loop- mediated isothermal amplification method (LAMP) for pathogenic Leptospira spp.detection with leptospires isolation and real-time PCR. *J. Vet. Med. Sci.,* 78 (2016), pp. 1299-1302.

Suzuki, H., Chen, G.M., Hung, T., Beards, G.M., Brown, G., Flewett, T.H. (1987). Effects of two negative staining methods on the Chinese atypical rotavirus. *Archives of virology*, 94(3-4), pp.305–308.

Swayne, D.E., Suarez, D.L., Sims, L.D. (2013) Influenza. In: Swayne D (ed) Diseases of poultry, 13th edn. *Blackwell, Ames, IA*, pp 181–218.

Sykes, A., Mallia, P., Johnston, S.L. (2007). Diagnosis of Pathogens in Exacerbations of Chronic Obstructive Pulmonary Disease. *Proceedings of the American Thoracic Society*, 4(8), pp.642–646.

Szántó-Egész, R., Jánosi, A., Mohr, A., Szalai, G., Szabó, E.K., Micsinai, A., Sipos, R., Rátky, J., Anton, I., Zsolnai, A. Breed-specific detection of mangalica meat in food products. *Food. Anal. Method.* 2016, 889–894.

Tan, L., Lemey, P., Houspie, L., Viveen, M.C., Jansen, N.J.G., van Loon, A.M.,

Tang, Y.W., Schmitz, J.E., Persing, D.H., Stratton, C.W. (2020). The Laboratory Diagnosis of COVID-19 Infection: Current Issues and Challenges. *Journal of Clinical Microbiology*, 58(6).

Taubenberger, J.K. and Morens, D.M. (2006). 1918 Influenza: The Mother of All Pandemics. *Emerging Infectious Diseases*, [online] 12(1), pp.15–22.

Taubenberger, J.K. and Morens, D.M. (2008). The Pathology of Influenza Virus Infections. Annual Review of Pathology: Mechanisms of Disease, [online] 3(1), pp.499–522.

Teo, A.K.J., Choudhury, Y., Tan, I.B., Cher, C.Y., Chew, S.H., Wan, Z.Y., Cheng, L.T.E., Oon, L.L.E., Tan, M.H., Chan, K.S. and Hsu, L.Y. (2021). Saliva is more sensitive than nasopharyngeal or nasal swabs for diagnosis of asymptomatic and mild COVID-19 infection. *Scientific Reports*, 11(1).

Tewawong, N., Prachayangprecha, S., Vichiwattana, P., Korkong, S., Klinfueng, S., Vongpunsawad, S., et al. Assessing antigenic drift of seasonal Influenza A(H3N2) and A(H1N1) pdm09 viruses. PLoS ONE. 2015;10(10): e0139958.

Thermofisher (n.d.). *Tm Calculator - US.* [online] www.thermofisher.com. Available at: https://www.thermofisher.com/uk/en/home/brands/thermo-scientific/molecular-biology/molecular-biology-learning-center/molecular-biology-resource-library/thermo-scientific-web-tools/tm-calculator.html.

Thermofisher.com. (2024). *TOPO™ TA Cloning™ Kit for Sequencing, with One Shot™ TOP10 Chemically Competent* E. coli. [online] Available at: https://www.thermofisher.com/order/catalog/product/K457540.

Thi, V.L.D., Herbst, K., Boerner, K., Meurer, M., Kremer, L.P., Kirrmaier, D., Freistaedter, A., Papagiannidis, D., Galmozzi, C., Stanifer, M.L., Boulant, S., Klein, S., Chlanda, P., Khalid, D., Miranda, I.B., Schnitzler, P., Kräusslich, H.-G., Knop, M. and Anders, S. (2020). A colorimetric RT-LAMP assay and LAMP-sequencing for detecting SARS-CoV-2 RNA in clinical samples. *Science Translational Medicine*, [online] 12(556).

Thomas, M. and Bomar, P.A. (2022). *Upper respiratory tract infection*. [online] National Library of Medicine.

Tian, L., Sato, T., Niwa, K., Kawase, M., Tanner, A.C., Takahashi, N. Rapid and sensitive PCR dipstick DNA chromatography for multiplex analysis of the oral microbiota. *Biomed. Res. Int.* 2014, 2014, 180323.

Tille, P. (2017). *Bailey & Scott's Diagnostic Microbiology*. 14th ed. Mosby. ISBN: 9780323354820.

Tolar, B.B., Wilhelms, D.B., Musser, J.M. (2019). *Evaluation of a high-fidelity polymerase for accurate RPA-based detection of pathogens. Journal of Molecular Diagnostics*, 21(4), 672-682.

Tombuloglu, H., Sabit, H., Al-Khallaf, H., Kabanja, J.H., Alsaeed, M., Al-Saleh, N., Al-Suhaimi, E. (2022). Multiplex real-time RT-PCR method for the diagnosis of SARS-CoV-2 by targeting viral N, RdRP and human RP genes. *Scientific Reports*, 12(1).

Tomita, N., Mori, Y., Kanda, H., Notomi, T. (2008). Loop-mediated isothermal amplification (LAMP) of gene sequences and simple visual detection of products. *Nature Protocols*, 3(5), 877-882.

Tomlinson, J. (2012). In-Field Diagnostics Using Loop-Mediated Isothermal Amplification. *Methods in molecular biology*, pp.291–300.

Tortajada-Genaro, L.A., Santiago-Felipe, S., Amasia, M., Russom, A., Maquieira, Á. Isothermal solid-phase recombinase polymerase amplification on microfluidic digital versatile discs (DVDs) *RSC Adv.* 2015;5:29987–29995.

Tozer, S.J., Lambert, S.B., Whiley, D.M., Bialasiewicz, S., Lyon, M.J., Nissen, M.D., Sloots, T.P. (2009). Detection of human bocavirus in respiratory, fecal, and blood samples by real-time PCR. *Journal of Medical Virology*, 81(3), pp.488–493.

Trapnell, B.C., Carey, B.C., Uchida, K., Suzuki, T. Pulmonary alveolar proteinosis, a primary immunodeficiency of impaired GM-CSF stimulation of macrophages. *Curr Opin. Immunol.* 2009, *21*, 514–521.

Treanor, J. Influenza vaccine--outmaneuvering antigenic shift and drift. *N. Engl. J. Med*. 2004; 350:218–220.

Treanor, J.J., Wilkinson, B.E., Masseoud, F., Hu-Primmer, J., Battaglia, R., O'Brien, D., Wolff, M., Rabinovich, G., Blackwelder, W., Katz, J.M. Safety and immunogenicity of a recombinant hemagglutinin vaccine for H5 Influenza in humans. *Vaccine.* 2001; 19:1732–1737.

Trevethan R. Sensitivity, Specificity, and Predictive Values: Foundations, Pliabilities, and Pitfalls in Research and Practice. Front Public Health. 2017; 5:307.

Tsaloglou, M.N., Watson, R.J., Rushworth, C.M., Zhao, Y., Niu, X., Sutton, J.M., Morgan, H. Real-time microfluidic recombinase polymerase amplification for the toxin B gene of Clostridium difficile on a SlipChip platform. *Analyst.* 2015; 140:258264.

Turner, D.H. and Mathews, D.H. (2010) 'Nearest-neighbor thermodynamic parameters and revised helix initiation parameters for RNA', *Biochemistry*, 49(20), pp. 3735-3739.

Tyrrell, D.A.J. **and Almeida, J.D.** (1967). Direct electron-microscopy of organ cultures for the detection and characterization of viruses. *Archiv für die gesamte Virusforschung*, 22(3-4), pp.417–425.

Tzotzos, S.J., Fischer, B., Fischer, H., Zeitlinger, M. Incidence of ARDS and outcomes in hospitalized patients with COVID-19: a global literature survey. *Crit Care.* 2020;24(1):1–4.

Ubukata, K., Morozumi, M., Sakuma, M., Adachi, Y., Mokuno, E., Tajima, T., Iwata, S. AOM Surveillance Study Group. Genetic characteristics and antibiotic resistance of Haemophilus Influenzae isolates from pediatric patients with acute otitis media after introduction of 13-valent pneumococcal conjugate vaccine in Japan. *J Infect Chemother*. 2019 Sep;25(9):720-726.

Ubukata, K., Morozumi, M., Sakuma, M., Takata, M., Mokuno, E., Tajima, T., Iwata, S. AOM Surveillance Study Group. Etiology of Acute Otitis Media and Characterization of Pneumococcal Isolates After Introduction of 13-Valent Pneumococcal Conjugate Vaccine in Japanese Children. *Pediatr Infect Dis J.* 2018 Jun;37(6):598-604.

UK Health Security Agency. (2023). Surveillance of Influenza and other seasonal respiratory viruses in the UK, winter 2022 to 2023. Retrieved from GOV.UK.

Ullman, E.F. (2013). Homogeneous Immunoassay. In: D. Wild, ed. *The Immunoassay Handbook*. 4th ed. Elsevier, pp.76-77.

Usonis, V., Jackowska, T., Petraitiene, S., Sapala, A., Neculau, A., Stryjewska, I., Devadiga, R., Tafalla, M., Holl, K. Incidence of acute otitis media in children below 6 years of age seen in medical practices in five East European countries. *BMC Pediatr.* 2016 Jul 26; 16:108.

Vainionpää, R. and Leinikki, P. (2008). Diagnostic Techniques: Serological and Molecular Approaches. *Encyclopedia of Virology*, [online] pp.29–37.

Valiadi, M., Kalsi, S., Jones, I.G.F., Turner, C., Sutton, J.M., Morgan, H. Simple and rapid sample preparation system for the molecular detection of antibiotic resistant pathogens in human urine. *Biomed. Microdevices.* 2016; 18:1–10.

Valleron, A.J., Cori, A., Valtat, S., Meurisse, S., Carrat, F., Boëlle, P.Y. (2010). Transmissibility and geographic spread of the 1889 Influenza pandemic. *Proceedings of the National Academy of Sciences of the United States of America*, [online] 107(19), pp.8778–8781.

Van Benten, I., Koopman, L., Niesters, B., Hop, W., Van Middelkoop, B., De Waal, L., Van Drunen, K., Osterhaus, A., Neijens, H., Fokkens, W. (2003). Predominance of rhinovirus in the nose of symptomatic and asymptomatic infants. *Pediatric Allergy and Immunology*, 14(5), pp.363–370.

van den Hoogen, B.G., de Jong, J.C., Groen, J., Kuiken, T., de Groot, R., Fouchier, R.A.M., Osterhaus, A.D.M.E. (2001). A newly discovered human pneumovirus isolated from young children with respiratory tract disease. *Nature Medicine*, 7(6), pp.719–724.

van Doorn, A.S., Meijer, B., Frampton, C.M.A., Barclay, M.L. and de Boer, N.K.H. (2020). Systematic review with meta-analysis: SARS-CoV-2 stool testing and the potential for faecal-oral transmission. *Alimentary Pharmacology & Therapeutics*.

Van Vooren, S., Grayson, J., Van Ranst, M., Dequeker, E., Laenen, L., Janssen, R., Gillet, L., Bureau, F., Coppieters, W., Devos, N., Hengchen, B., Wattiau, P., Méhauden, S., Verlinden, Y., Van Baelen, K., Pattery, T., Valentin, J.-P., Janssen, K., Geraerts, M., Smeraglia, J. (2022). Reliable and Scalable SARS-CoV-2 qPCR Testing at a High Sample Throughput: Lessons Learned from the BelgianInitiative. *Life*, [online] 12(2), p.159.

Vaselli, N.M., Wega Setiabudi, Subramaniam, K., Adams, E.R., Turtle, L., Miren Iturriza-Gómara, Solomon, T., Cunliffe, N.A., French, N., Hungerford, D., Turtle, L., Hungerford, D., Subramaniam, K., Vivancos, R., Gabbay, M., Buchan, I., Carrol, E.D., Miren Iturriza-Gómara, Solomon, T. and Cunliffe, N.A. (2021). Investigation of SARS-CoV-2 faecal shedding in the community: a prospective household cohort study (COVID-LIV) in the UK. *BMC Infectious Diseases*, 21(1).

Vetter, V., Denizer, G., Friedland, L.R., Krishnan, J., Shapiro, M. (March 2018). "Understanding modern-day vaccines: what you need to know". *Annals of Medicine*. 50 (2): 110–120.

Viegas, M.S., Martins, T.C., Seco, F., do Carmo, A. An improved and cost— effective methodology for the reduction of autofluorescence in direct immunofluorescence studies on formalin— fixed paraffin— embedded tissues. *Eur J Histochem.* 2007; 51:59–66.

Vira, H., Bhat, V., Chavan, P. Diagnostic molecular microbiology and its applications: current and future perspectives. *Clin Microbiol Infect Disease*. 2016;1(1):20–31.

Vrtis, K.B., Bei, Y., Lund, S., Chuzel, L., Zhang, Y., Tanner, N.A., Ong, J.L., Patton, G.C. (2023). Enhanced Rolling Circle Amplification Performance with a Newly Engineered phi29 DNA Polymerase. *New England Biolabs*.

Walsh, E.E., Gonzalo Pérez Marc, Zareba, A.M., Falsey, A.R., Jiang, Q., Patton, M., Polack, F.P., Conrado Llapur, Doreski, P.A., Kumar Ilangovan, Rämet, M., Fukushima, Y., Hussen, N., Bont, L.J., Cardona, J., DeHaan, E., Giselle Castillo Villa, Marinela Ingilizova, Eiras, D., Tarek Mikati (2023). Efficacy and Safety of a Bivalent RSV Prefusion F Vaccine in Older Adults. *The New England Journal of Medicine*, 388(16), pp.1465–1477.

Walsh, K.A., Jordan, K., Clyne, B., Rohde, D., Drummond, L., Byrne, P., Ahern, S., Carty, P.G., O'Brien, K.K., O'Murchu, E., O'Neill, M., Smith, S.M., Ryan, M. and Harrington, P. (2020). SARS-CoV-2 detection, viral load and infectivity over the course of an infection. *Journal of Infection*, 81(3), pp.357–371.

Waman, V.P., Kolekar, P.S., Kale, M.M., Kulkarni-Kale, U. (2014). Population Structure and Evolution of Rhinoviruses. *PLoS ONE*, 9(2), p.e88981.

Wand, O., Breslavsky, A., Bar-Shai, A., Levy, C., Maayan, S., Rimler, A., Zwahra, M., Cohen-Hagai, K., Harish, A., Zacks, N., et al. One-year dynamics of antibody titers after three doses of SARS-CoV-2 BNT162b2 vaccine. *Vaccine* 2023, *41*, 871–874.

Wang, J., Koo, K., Wee, E.J.H., Wang, Y., Trau, M. Nanoplasmonic label-free surface-enhanced Raman scattering strategy for non-invasive cancer genetic subtyping in patient samples. *Nanoscale.* 2017; 9:3496–3503.

Wang, K., Wang, W., Yan, H., Ren, P., Zhang, J., Shen, J., Deubel, V. (2010). Correlation between bocavirus infection and humoral response, and co-infection with other respiratory viruses in children with acute respiratory infection. *Journal of Clinical Virology*, 47(2), pp.148–155.

Wang, P., Ma, C., Zhang, X., Chen, L., Yi, L., Liu, X., Lu, Q., Cao, Y., Gao, S. (2021). A ligation/recombinase polymerase amplification assay for rapid detection of SARS-CoV-2. *Frontiers in Cellular and Infection Microbiology*, 11, 680728.

Wang, W., Xu, Y., Gao, R., Lu, R., Han, K., Wu, G. and Tan, W. (2020). Detection of SARS-CoV-2 in Different Types of Clinical Specimens. *JAMA*, 323(18), pp.1843–1844.

Wang, X., Zhao, P., Yang, X., Li, J., Zhang, J., Zhang, X., Zeng, Z., Dong, J., Gao, S., Lu, C. (2019) 'Rapid and Sensitive Recombinase Polymerase Amplification Combined with Lateral Flow Strip for Detection of African Swine Fever Virus'. *Frontiers in Microbiology*, 10, 1004.

Wang, Y. et al. (2020). Rapid and sensitive detection of SARS-CoV-2 RNA using reverse transcription-recombinase polymerase amplification. *Analytical Chemistry*, 92(14), 9446–9449.

Wang, Y., et al. (2023). *An improved TOPO cloning method for high-efficiency construction of expression vectors. Molecular Biology Reports*, 50(3), 2449-2456.

Wang, Y., Zhang, Z., Shang, L., Gao, H., Du, X., Li, F., Gao, Y., Qi, G.-Y., Guo Wei-yuan, Qu, Z., Dong, T. (2021). Immunological Study of Reconstructed Common Ancestral Sequence of Adenovirus Hexon Protein. *Frontiers in Microbiology*, 12.

Warnatsch, A. (2013). Impact of proteasomal immune adaptation on the early immune response to viral infection.

Webster, R.G. Wet markets-a continuing source of severe acute respiratory syndrome and Influenza? *The Lancet.* 2004; 363:234–236.

Wee, E.J.H. and Trau, M. Simple isothermal strategy for multiplexed, rapid, sensitive, and accurate miRNA detection. *ACS Sensor.* 2016;1(6):670–675.

Wee, E.J.H., Ha, Ngo T., Trau, M. A simple bridging flocculation assay for rapid, sensitive, and stringent detection of gene specific DNA methylation. *Sci. Rep.* 2015; 5:15028.

Wee, E.J.H., Lau, H.Y., Botella, J.R., Trau, M. Re-purposing bridging flocculation for on-site, rapid, qualitative DNA detection in resource-poor settings. *Chem. Commun.* 2015; 51:5828–5831.

Wee, E.J.H., Ngo, T.H., Trau, M. Colorimetric detection of both total genomic and loci-specific DNA methylation from limited DNA inputs. *Clin. Epigenetics.* 2015; 7:65.

Weiss, A., Jellingsø, M. and Sommer, M.O.A. (2020). Spatial and temporal dynamics of SARS-CoV-2 in COVID-19 patients: A systematic review and meta-analysis. *EBioMedicine*, 58, p.102916.

Weterings, E. and Chen, D.J. The endless tale of non-homologous end-joining. *Cell Res.* 2008; 18:114–124.

Whiley, D.M. and Sloots, T.P. Sequence variation in primer targets affects the accuracy of viral quantitative PCR. *J Clin Virol.* 2005; 34:104–107.

Whittington, N.C. and Wray, S. (2017). Suppression of Red Blood Cell Autofluorescence for Immunocytochemistry on Fixed Embryonic Mouse Tissue. *Current Protocols in Neuroscience*, [online] 81(1).

Widders, A., Broom, A. and Broom, J. (2020). SARS-CoV-2: The viral shedding vs infectivity dilemma. *Infection, Disease & Health*.

Wiertz, E., van Bleek, G.M., Martin, D.P., Coenjaerts, F.E. 2012. Genetic variability among complete human respiratory syncytial virus subgroup A genomes: bridging molecular evolutionary dynamics and epidemiology. *PLoS One* **7**: e51439.

Winn, W.C. and Koneman, E.W. (2006). *Koneman's Color Atlas and Textbook of Diagnostic Microbiology.* Philadelphia, PA: Lippincott Williams & Wilkins.

Winokur, P., Gayed, J., Fitz-Patrick, D., Thomas, S.J., Diya, O., Lockhart, S., Xu, X., Zhang, Y., Bangad, V., Schwartz, H.I., et al. Bivalent Omicron BA.1-Adapted BNT162b2 Booster in Adults Older than 55 Years. *N. Engl. J. Med.* 2023, *388*, 214– 227.

Wohlfart, C. 1988. Neutralization of adenoviruses: kinetics, stoichiometry, and mechanisms. *J. Virol*. 62:2321-2328.

Woloshin, S., Patel, N. and Kesselheim, A.S. (2020). False Negative Tests for SARS-CoV-2 Infection — Challenges and Implications. *New England Journal of Medicine*, 383(6).

Wong, S.S. and Webby, R.J. Traditional and new Influenza vaccines. *Clin. Microbiol. Rev.* 2013; 26:476–492.

World Health Organization (WHO). (2010). Evolution of H5N1 avian Influenza viruses in Asia. *Emerging Infectious Diseases*, 16(4), 569-575.

World Health Organization (WHO). (2014). Influenza (Seasonal). Available at: https://www.who.int/news-room/fact-sheets/detail/Influenza-(seasonal).

World Health Organization (WHO). (2020). *Diagnostic testing for SARS-CoV-2: interim guidance, 11 September 2020*. Available at: https://apps.who.int/iris/handle/10665/334254.

Worrall, G. (2008). Acute bronchitis. *Canadian Family Physician*, [online] 54(2), pp.238–239.

Wozniak, T.M., Barnsley, L., Glass, K. (2020). Early detection of respiratory viruses: Impact on disease transmission and prevention strategies. *Epidemiology & Infection*, 148, e105.

Wrammert, J., Smith, K., Miller, J., et al. Rapid cloning of high-affinity human monoclonal antibodies against Influenza virus. *Nature*. 2008; 453:667-71.

Wu, C., Chen, X., Cai, Y., Zhou, X., Xu, S., Huang, H., et al. Risk factors associated with acute respiratory distress syndrome and death in patients with coronavirus disease 2019 pneumonia in Wuhan, China. *JAMA Intern Med.* 2020;180(7):934–43.

Wu, F., Zhao, S., Yu, B., Chen, Y.-M., Wang, W., Song, Z.-G., Hu, Y., Tao, Z.-W., Tian, J.-H., Pei, Y.-Y., Yuan, M.-L., Zhang, Y.-L., Dai, F.-H., Liu, Y., Wang, Q.-M., Zheng, J.-J., Xu, L., Holmes, E.C. and Zhang, Y.-Z. (2020). A new coronavirus associated with human respiratory disease in China. *Nature*, 579(7798), pp.265–269.

Wu, H., Zhao, P., Yang, X., Li, J., Zhang, J., Zhang, X., Zeng, Z., Dong, J., Gao, S., Lu, C. (2017) ‘A Recombinase Polymerase Amplification and Lateral Flow Strip Combined

Method That Detects Salmonella enterica Serotype Typhimurium With No Worry of Primer-Dependent Artifacts'. *Frontiers in Microbiology*, 8, 1015.

Wu, S. et al. (2024). Advances in Virus Detection Techniques Based on Recombinant Polymerase Amplification. *Molecules*, 29(20), 4972.

Wu, S., Yu, W., Fu, X., Yu, X., Ye, Z., Zhang, M., Qiu, Y., Ma, B. (2024). Advances in Virus Detection Techniques Based on Recombinant Polymerase Amplification. Molecules, [online] 29(20), pp.4972–4972.

Xia, X., Yu, Y., Weidmann, M., Pan, Y., Yan, S., Wang, Y. Rapid detection of shrimp white spot syndrome virus by real time, isothermal recombinase polymerase amplification assay. *PLoS One.* 2014;9: e104667.

Xu, J., Zhang, Y., Zhao, L., Li, X., Wang, Y. (2016). Community-acquired pneumonia in adults: Clinical practice guidelines by the Chinese Thoracic Society, Chinese Medical Association. *Clinical Respiratory Journal*, 10(6), 1201-1220.

Xu, R., Ekiert, D.C., Krause, J.C., Hai, R., Crowe, J.E., Wilson, I.A. (2010). Structural Basis of Preexisting Immunity to the 2009 H1N1 Pandemic Influenza Virus. *Science*, [online] 328(5976), pp.357–360.

Xu, Y., Liu, Y., Wu, Y., Xia, X., Liao, Y., Li, Q. Fluorescent probe-based lateral flow assay for multiplex nucleic acid detection. *Anal. Chem.* 2014, 86, 5611–5614.

Yamanaka, E.S., Tortajada-Genaro, L.A., Maquieira, Á. Low-cost genotyping method based on allele-specific recombinase polymerase amplification and colorimetric microarray detection. *Microchim. Acta.* 2017; 184:1453–1462.

Yan, D., Zhang, X., Chen, C., Jiang, D., Liu, X., Zhou, Y., Huang, C., Zhou, Y., Guan, Z., Ding, C., Chen, L., Lan, L., Fu, X., Wu, J., Li, L. and Yang, S. (2021). Characteristics of Viral Shedding Time in SARS-CoV-2 Infections: A Systematic Review and Meta-Analysis. *Frontiers in Public Health*, [online] 9.

Yan, L., Zhou, J., Zheng, Y., Gamson, A. S., Roembke, B. T., Nakayama, S., et al. (2014). Isothermal amplified detection of DNA and RNA. *Mol. Biosyst.* 10 (5), 970–1003.

Yang, S. and Rothman, R.E. (2004). PCR-based diagnostics for infectious diseases, uses, limitations, and future applications in acute-care settings. *Lancet Infect. Dis*. 4, 337–348.

Yang, Y., Qin, X., Sun, Y., Cong, G., Li, Y., Zhang, Z. Development of Isothermal Recombinase Polymerase Amplification Assay for Rapid Detection of Porcine Circovirus Type 2. *Biomed Res Int* 2017, 2017, 8403642.

Yang, Y., Qin, X., Wang, G., Jin, J., Shang, Y., Zhang, Z. Development of an isothermal amplification-based assay for rapid visual detection of an Orf virus. *Virol. J.* 2016, 13, 46.

Yao, S., Hart, D.J., An, Y. Recent advances in universal TA cloning methods for use in function studies. *Protein Eng Des Sel.* 2016;29(11):551–556.

Yeh, E.C. and Lee, L.P. One-step digital plasma separation for molecular diagnostics. *17th Int. Conf. Miniaturized Syst. Chem. Life Sci.* 2013:1323–1325.

Yin, K., Ding, X., Li, Z., Zhao, H., Cooper, K., Liu, C. (2021). A CRISPR-Cas13a-based specific enhancer for more sensitive detection of SARS-CoV-2 infection. *EClinicalMedicine*, 32, 100770.

Yüce, M., Filiztekin, E., & Özkaya, K. G. (2021). COVID-19 diagnosis—a review of current methods. *Biosensors and Bioelectronics*, 172, 112752.

Zaraket, H., Hurt, A.C., Clinch, B., Barr, I., Lee, N. (2021). Burden of Influenza B virus infection and considerations for clinical management. *Antiviral Research*, 185, p.104970.

Zeng, D., Jiao, J., Mo, T. (2024). Combination of nucleic acid amplification and CRISPR/Cas technology in pathogen detection. *Frontiers in microbiology*, 15.

Zetsche, B., Gootenberg, Jonathan S., Abudayyeh, Omar O., Slaymaker, Ian M., Makarova, Kira S., Essletzbichler, P., Volz, Sara E., Joung, J., van der Oost, J., Regev, A., Koonin, Eugene V., Zhang, F. (2015). Cpf1 Is a Single RNA-Guided Endonuclease of a Class 2 CRISPR-Cas System. *Cell*, 163(3), pp.759–771.

Zhang, Y., Odiwuor, N., Xiong, J., Mwaliko, C., Tanner, N.A. (2020). Rapid molecular detection of SARS-CoV-2 (COVID-19) virus RNA using colorimetric LAMP. *medRxiv*, 1-8.

Zhang, Y., Werling, U., Edelmann, W. (2012). SLiCE: a novel bacterial cell extract- based DNA cloning method. *Nucleic Acids Research*, [online] 40(8), pp. e55–e55.

Zhang, Y., Wu, S., Zhang, Y., Huang, Z. (2021). *Development of a reverse transcription recombinase polymerase amplification assay for rapid detection of SARS- CoV-2. Frontiers in Microbiology*, 12, Article 655307.

Zhao, S., Lin, Q., Ran, J., Musa, S.S., Yang, G., Wang, W., Lou, Y., Gao, D., Yang, L., He, D., Wang, M.H. (2020). Preliminary estimation of the basic reproduction number of novel coronavirus (2019-nCoV) in China, from 2019 to 2020: A data-driven analysis in the early phase of the outbreak. *International Journal of Infectious Diseases*, 92.

Zhou, C., Zhang, T., Ren, H., Sun, S., Yu, X., Sheng, J., Shi, Y. and Zhao, H. (2020). Impact of age on duration of viral RNA shedding in patients with COVID-19. *Aging*.

Zhou, R., Li, F., Chen, F., Liu, H., Zheng, J., Lei, C. and Wu, X. (2020). Viral dynamics in asymptomatic patients with COVID-19. *International Journal of Infectious Diseases*, 96, pp.288–290.

Zuin, M., Gentili, V., Cervellati, C., Rizzo, R. and Zuliani, G. (2021). Viral Load Difference between Symptomatic and Asymptomatic COVID-19 Patients: Systematic Review and Meta-Analysis. *Infectious Disease Reports*, 13(3), pp.645–653.

Zumla, A., Hui, D.S., Perlman, S. (2016). "Middle East respiratory syndrome." *The Lancet*, 386(9997), 995-1007.

Zuurbier, R.P., Korsten, K., Verheij, T.J.M., Butler, C., Adriaenssens, N., Coenen, S., Gruselle, O., Vantomme, V., van Houten, M.A., Bont, L.J., Wildenbeest, J.G., Zuurbier, R., Korsten, K., Verheij, T., van Houten, M., Bont, L., Wildenbeest, J., Adriaenssens, N., Coenen, S., Butler, C. (2022). Performance Assessment of a Rapid Molecular Respiratory Syncytial Virus Point-of-Care Test: A Prospective Community Study in Older Adults. *The Journal of Infectious Diseases*, [online] 226(Supplement_1), pp. S63–S7.

Chapter 9: Appendix

9.1. Raw data for SARS-CoV-2 NHS Sample Collection

Sample ID	Date of Sample Collection	Sample Type	RT-PCR Cumulative Results	LAMP Cumulative Results	RT-RPA Results	RT-RPA Tt Values	Discrepancy
1	29-Apr ‘21	NP Swab	+	+	+	N/A	Non-discrepancy
2	29-Apr ‘21	NP Swab	+	+	+	1.08	Non-discrepancy
3	29-Apr ‘21	NP Swab	+	+	+	28.70	Non-discrepancy
4	29-Apr ‘21	NP Swab	+	+	+	N/A	Non-discrepancy
5	29-Apr ‘21	NP Swab	+	+	+	N/A	Non-discrepancy
6	29-Apr ‘21	NP Swab	+	+	+	5.57	Non-discrepancy
7	29-Apr ‘21	NP Swab	+	+	+	31.10	Non-discrepancy
8	29-Apr ‘21	NP Swab	+	+	+	5.09	Non-discrepancy
9	29-Apr ‘21	NP Swab	+	+	+	27.25	Non-discrepancy
10	29-Apr ‘21	NP Swab	+	+	+	21.62	Non-discrepancy
12	29-Apr ‘21	NP Swab	+	-	+	6.43	Non-discrepancy
13	29-Apr ‘21	NP Swab	+	+	+	3.96	Non-discrepancy
14	29-Apr ‘21	NP Swab	+	+	+	2.27	Non-discrepancy
15	29-Apr ‘21	NP Swab	-	-	-	N/A	Non-discrepancy
16	29-Apr ‘21	NP Swab	+	+	+	4.13	Non-discrepancy
17	39-Apr ‘21	NP Swab	+	+	+	N/A	Non-discrepancy
18	30-Apr ‘21	NP Swab	+	-	+	N/A	Non-discrepancy
19	30-Apr ‘21	NP Swab	-	-	-	11.68	Non-discrepancy
20	1-May ‘21	NP Swab	+	+	+	7.89	Non-discrepancy
21	1-May ‘21	NP Swab	+	+	+	31.83	Non-discrepancy
22	1-May ‘21	NP Swab	+	+	+	34.11	Non-discrepancy
23	1-May ‘21	NP Swab	+	+	+	21.33	Non-discrepancy
24	1-May ‘21	NP Swab	+	+	+	N/A	Non-discrepancy
25	1-May ‘21	NP Swab	+	+	+	28.93	Non-discrepancy
26	3-May ‘21	NP Swab	+	-	+	N/A	Non-discrepancy
27	3-May ‘21	NP Swab	+	+	+	8.47	Non-discrepancy
28	3-May ‘21	NP Swab	+	+	+	24.40	Non-discrepancy
29	3-May ’21	NP Swab	+	+	+	N/A	Non-discrepancy
30	4-May ‘21	NP Swab	+	+	+	32.06	Non-discrepancy
31	5-May ‘21	NP Swab	-	-	-	N/A	Non-discrepancy
32	5-May ‘21	NP Swab	+	-	+	1.31	Non-discrepancy
34	5-May ‘21	NP Swab	-	-	-	N/A	Non-discrepancy
35	5-May ‘21	NP Swab	+	+	+	N/A	Non-discrepancy
36	8-May ‘21	NP Swab	+	+	+	1.07	Non-discrepancy
37	8-May ‘21	NP Swab	+	+	+	N/A	Non-discrepancy
39	8-May ‘21	NP Swab	-	+	-	N/A	Non-discrepancy
40	8-May ‘21	NP Swab	-	+	-	N/A	Non-discrepancy
41	8-May ‘21	NP Swab	+	+	-	N/A	Discrepancy
42	8-May ‘21	NP Swab	+	+	+	7.54	Non-discrepancy
44	8-May ‘21	NP Swab	+	+	+	27.12	Non-discrepancy
45	8-May ‘21	NP Swab	+	+	+	1.04	Non-discrepancy
46	8-May ‘21	NP Swab	+	+	+	20.72	Non-discrepancy
48	9-May ‘21	NP Swab	-	-	+	N/A	Discrepancy
50	9-May ‘21	NP Swab	-	-	-	35.24	Non-discrepancy

51	9-May ‘21	NP Swab	-	+	+	20.99	Discrepancy
52	9-May ‘21	NP Swab	-	+	+	18.67	Discrepancy
53	9-May ‘21	NP Swab	-	+	-	N/A	Non-discrepancy
54	10-May ‘21	NP Swab	+	+	+	N/A	Non-discrepancy
55	10-May ‘21	NP Swab	-	-	-	N/A	Non-discrepancy
56	10-May ‘21	NP Swab	-	-	-	N/A	Non-discrepancy
57	10-May ‘21	NP Swab	+	+	+	37.04	Non-discrepancy
58	10-May ‘21	NP Swab	+	+	+	11.30	Non-discrepancy
59	10-May ‘21	NP Swab	-	-	-	N/A	Non-discrepancy
60	11-May ‘21	NP Swab	+	+	+	23.06	Non-discrepancy
61	11-May ‘21	NP Swab	+	+	+	20.78	Non-discrepancy
62	13-May ‘21	NP Swab	-	-	-	36.05	Non-discrepancy
63	13-May ‘21	NP Swab	+	+	+	N/A	Non-discrepancy
64	13-May ‘21	NP Swab	+	+	+	32.40	Non-discrepancy
66	13-May ‘21	NP Swab	-	+	-	N/A	Non-discrepancy
67	13-May ‘21	NP Swab	-	+	-	N/A	Non-discrepancy
69	13-May ‘21	NP Swab	+	+	+	21.59	Non-discrepancy
70	13-May ‘21	NP Swab	+	-	+	8.11	Non-discrepancy
71	13-May ‘21	NP Swab	+	+	+	39.24	Non-discrepancy
72	13-May ‘21	NP Swab	+	+	+	31.79	Non-discrepancy
74	15-May ‘21	NP Swab	-	-	-	N/A	Non-discrepancy
75	15-May ‘21	NP Swab	-	+	-	N/A	Non-discrepancy
76	16-May ‘21	NP Swab	-	+	-	N/A	Non-discrepancy
77	16-May ‘21	NP Swab	-	-	-	N/A	Non-discrepancy
78	16-May ‘21	NP Swab	-	+	-	N/A	Non-discrepancy
79	16-May ‘21	NP Swab	-	-	-	N/A	Non-discrepancy
81	16-May ‘21	NP Swab	+	-	+	N/A	Non-discrepancy
82	18-May ‘21	NP Swab	-	+	-	37.96	Non-discrepancy
83	19-May ‘21	NP Swab	+	+	+	22.36	Non-discrepancy
85	19-May ‘21	NP Swab	-	-	-	36.39	Non-discrepancy
86	19-May ‘21	NP Swab	-	-	-	N/A	Non-discrepancy
87	19-May ‘21	NP Swab	-	-	-	N/A	Non-discrepancy
88	19-May ‘21	NP Swab	+	+	+	37.00	Non-discrepancy
90	20-May ‘21	NP Swab	+	+	+	37.21	Non-discrepancy
93	20-May ‘21	NP Swab	-	+	-	8.35	Non-discrepancy
94	20-May ‘21	NP Swab	-	-	-	N/A	Non-discrepancy
95	26-May ‘21	NP Swab	-	-	-	13.12	Non-discrepancy
97	26-May ‘21	NP Swab	-	+	-	38.94	Non-discrepancy
99	26-May ‘21	NP Swab	-	-	-	N/A	Non-discrepancy
100	26-May ‘21	NP Swab	-	-	-	N/A	Non-discrepancy
101	26-May ‘21	NP Swab	-	-	-	26.91	Non-discrepancy
102	26-May ‘21	NP Swab	-	+	+	29.56	Discrepancy
103	26-May ‘21	NP Swab	-	+	-	11.93	Non-discrepancy
104	26-May ‘21	NP Swab	-	+	-	40.19	Non-discrepancy
105	26-May ‘21	NP Swab	-	+	-	N/A	Non-discrepancy
106	26-May ‘21	NP Swab	-	-	-	N/A	Non-discrepancy
107	26-May ‘21	NP Swab	-	-	-	20.49	Non-discrepancy
109	26-May ‘21	NP Swab	-	-	-	10.88	Non-discrepancy
110	26-May ‘21	NP Swab	-	-	-	8.42	Non-discrepancy
111	26-May ‘21	NP Swab	-	-	-	N/A	Non-discrepancy
112	26-May ‘21	NP Swab	-	-	-	N/A	Non-discrepancy
113	26-May ‘21	NP Swab	-	-	-	1.03	Non-discrepancy
114	26-May ‘21	NP Swab	-	-	-	N/A	Non-discrepancy
115	26-May ‘21	NP Swab	-	+	+	28.02	Discrepancy
116	26-May ‘21	NP Swab	-	+	-	N/A	Non-discrepancy
117	26-May ‘21	NP Swab	-	+	-	N/A	Non-discrepancy
118	26-May ‘21	NP Swab	-	+	-	N/A	Non-discrepancy

120	26-May ‘21	NP Swab	-	+	-	N/A	Non-discrepancy
121	26-May ‘21	NP Swab	-	+	-	N/A	Non-discrepancy
122	26-May ’21	NP Swab	-	-	-	20.14	Non-discrepancy
123	26-May ‘21	NP Swab	-	+	+	15.52	Discrepancy
124	26-May ‘21	NP Swab	-	-	-	18.83	Non-discrepancy
125	26-May ‘21	NP Swab	-	+	-	N/A	Non-discrepancy
126	26-May ‘21	NP Swab	-	-	-	N/A	Non-discrepancy
127	26-May ‘21	NP Swab	-	-	-	N/A	Non-discrepancy
128	26-May ‘21	NP Swab	-	+	-	N/A	Non-discrepancy
129	26-May ‘21	NP Swab	-	-	-	N/A	Non-discrepancy
130	26-May ‘21	NP Swab	-	+	-	N/A	Non-discrepancy
131	26-May ‘21	NP Swab	-	-	-	N/A	Non-discrepancy
132	26-May ‘21	NP Swab	-	-	-	N/A	Non-discrepancy
133	26-May ‘21	NP Swab	-	+	-	N/A	Non-discrepancy
134	26-May ‘21	NP Swab	-	+	-	30.05	Non-discrepancy
136	26-May ‘21	NP Swab	-	-	-	29.99	Non-discrepancy
138	26-May ‘21	NP Swab	-	+	-	N/A	Non-discrepancy
139	26-May ‘21	NP Swab	-	-	-	N/A	Non-discrepancy
140	26-May ‘21	NP Swab	-	-	-	N/A	Non-discrepancy
141	26-May ‘21	NP Swab	-	-	-	N/A	Non-discrepancy
148	26-May ‘21	NP Swab	+	+	+	28.43	Non-discrepancy
150	26-May ‘21	NP Swab	-	-	+	N/A	Discrepancy
151	26-May ‘21	NP Swab	+	+	+	31.58	Non-discrepancy